



University  
of Glasgow

Scott, Rebecca Wilson (2010) *LIM kinase regulation of cell motility and invasion*. PhD thesis.

<http://theses.gla.ac.uk/2247/>

Copyright and moral rights for this thesis are retained by the author

A copy can be downloaded for personal non-commercial research or study, without prior permission or charge

This thesis cannot be reproduced or quoted extensively from without first obtaining permission in writing from the Author

The content must not be changed in any way or sold commercially in any format or medium without the formal permission of the Author

When referring to this work, full bibliographic details including the author, title, awarding institution and date of the thesis must be given

# **LIM Kinase regulation of cell motility and invasion**

Rebecca Wilson Scott

A thesis submitted to the University of Glasgow for the degree of  
Doctor of Philosophy

October 2009

Beatson Institute for Cancer Research  
Garscube Estate  
Switchback Road  
Glasgow G61 1BD

## Abstract

This thesis describes how both LIM Kinase 1 and LIM Kinase 2 are important regulators of cell invasion. Chapter 3 presents data that shows that inhibition of LIMK function blocks the collective invasion of MDA MB 231 breast carcinoma cells in a three-dimensional matrix. Although LIMK was not required for cell motility in two dimensions, a novel role for LIMK in both extracellular matrix degradation and deformation activities was shown in three dimensions in Chapter 4. Consistent with matrix remodeling being a requirement for path generation by leading cells in collective invasion, LIMK activity was also shown to be required by leading cells in MDA MB 231 collective invasion. However, it was also discovered that LIMK activity was not required for path following by MDA MB 231 cells. The importance of Cofilin activity as a conduit of LIMK activity during invasion was investigated in Chapter 5, as well as potential novel protein interactions of Cofilin. The identification of novel substrates of LIMK was attempted in Chapter 6, leaving prospective routes of investigation to further elucidate the roles of LIMK1 and LIMK2 in cells.

The main findings presented in this thesis reveal a requirement for LIMK activity in the path generation function of leading cells in collective invasion. Given that individual invading cells must generate their own paths, these results lend support to the continued development of LIMK inhibitors to counter tumor cell invasion and metastasis.

# Table of Contents

1	Introduction .....	13
1.1	Introduction to LIM Kinases .....	14
1.2	LIM Kinase protein organisation .....	19
1.3	Activation and regulation.....	23
1.4	Cell biological functions .....	33
1.5	Tissue distribution .....	36
1.6	LIMK in development and disease .....	37
1.6.1	Genetic deletion.....	37
1.6.2	Cancer cell metastasis.....	38
1.7	Cancer Metastasis.....	39
1.8	Individual cell invasion.....	40
1.9	Collective cell invasion .....	41
1.10	Role of the actin cytoskeleton in invasion .....	44
1.11	Invadopodia.....	46
2	Materials and Methods.....	48
2.1	Chemicals and Reagents .....	48
2.2	Bacterial techniques .....	48
2.2.1	Reagents .....	48
2.2.2	Enzymes and kits .....	48
2.2.3	Bacterial strains .....	49
2.2.4	Bacterial Transformation and culture.....	49
2.2.5	Small-scale plasmid DNA preparation .....	50
2.2.6	Large-scale plasmid DNA preparation .....	50
2.2.7	Quantification of DNA .....	50
2.2.8	Plasmids.....	50
2.2.9	Cloning protocols.....	51
2.2.10	Generation of fragments by PCR.....	52
2.2.11	Annealing oligonucleotides .....	53
2.2.12	Cloning .....	53
2.2.13	PCR directly from Bacteria .....	53
2.2.14	Mutagenesis .....	54
2.2.15	Sequencing .....	55
2.2.16	Primers.....	56
2.2.17	Recombinant protein preparation .....	56
2.3	Mammalian cell culture techniques .....	58
2.3.1	Reagents .....	58
2.3.2	Growth conditions.....	60
2.3.3	Transfection with siRNA.....	60
2.3.4	Transient transfection with plasmid DNA.....	61
2.3.5	Nucleofection .....	62
2.3.6	Retrovirus Production.....	62
2.3.7	Retrovirus Transduction .....	63
2.3.8	TAT (PTD) proteins.....	63
2.3.9	Wound healing .....	63
2.3.10	Inverse Invasion assay .....	64
2.3.11	Gelatin Degradation Assay .....	65
2.3.12	Cell derived Matrix (CDM).....	66
2.4	Methods in Protein Extraction and Analysis .....	68

2.4.1	Reagents .....	68
2.4.2	Whole cell extracts .....	69
2.4.3	mRNA preparation.....	69
2.4.4	cDNA synthesis .....	70
2.4.5	qPCR.....	70
2.4.6	Protein quantification: BCA Assay .....	71
2.4.7	SDS-PAGE .....	71
2.4.8	Western blots .....	72
2.4.9	Immunoprecipitation .....	72
2.4.10	Antibodies .....	73
2.5	Kinase activity.....	73
2.5.1	Buffers and reagents.....	73
2.5.2	In Vitro Kinase assay .....	74
2.5.3	IP-Kinase Assay.....	75
2.5.4	Pep-Scan Peptide Array .....	76
2.6	F-actin severing assays.....	76
2.6.1	Buffers .....	77
2.6.2	F-actin preparation .....	77
2.6.3	Pyrene labelling .....	77
2.6.4	F-actin Severing .....	77
2.7	Zymography.....	78
2.7.1	Buffers and Reagents .....	78
2.7.2	Zymography - Gelatinase activity.....	78
2.8	Immunofluorescent microscopy .....	79
2.8.1	Reagents .....	79
2.8.2	Fixing and staining cells on glass for microscopy .....	79
2.8.3	Fixing and staining cells for 3D Confocal imaging.....	80
2.8.4	Time-lapse microscopy .....	80
3	Requirement of LIMK in cancer cell motility and invasion.....	81
3.1	Chapter Summary .....	81
3.2	Results .....	81
3.2.1	LIMK knock down by siRNA in MDAMB231 cells .....	81
3.2.2	Knockdown of LIMK induces changes in the actin cytoskeleton ....	84
3.2.3	Initial observations suggest LIM Kinases are important in cell motility.	88
3.2.4	Knockdown of LIMK has little effect on cell motility in 2D on plastic.	91
3.2.5	Knockdown of LIMK has no effect on cell motility on CDM. ....	96
3.2.6	LIMK is a requirement of cell invasion into 3D matrix.....	97
3.2.7	Cell morphology in 3D following loss of LIMK .....	107
3.2.8	Is LIMK a driver of cell motility or invasion? .....	111
3.3	Conclusions .....	126
4	LIM Kinase regulation of invasion .....	128
4.1	Chapter summary .....	128
4.2	Results .....	128
4.2.1	Knock down of LIM Kinase reduces functional invadopodia formation and gelatin degrading activity in MDAMB231 cells .....	128
4.2.2	Knockdown of LIMK reduces levels of secreted active MMP9.....	137
4.2.3	Knockdown of LIMK has no effect on MMP9 transcription.....	138
4.2.4	LIMK is required for optimal collagenase activity in 3D.....	141
4.2.5	LIMK is important in cells 'leading' invasion.....	143
4.3	Conclusion.....	146
5	Cofilin phosphorylation and invasion.....	147

5.1	Chapter Summary .....	147
5.1.1	PTD Flag Cofilin1 .....	147
5.1.2	In Vitro activity of PTD Cofilins .....	151
5.1.3	Increased levels of Wild Type Cofilin do not affect cell motility in 2D .....	152
5.1.4	3D Invasiveness is altered by disruption of the Cofilin phosphorylation balance .....	157
5.2	Conclusions .....	159
6	Identification of Novel LIMK1 substrates .....	161
6.1	Chapter Summary .....	161
6.2	LIMK1 phosphorylates Cofilin1 on Serine 3 and potentially Serine 8 ..	161
6.3	Peptide Array .....	162
6.3.1	Proto-oncogene tyrosine kinase c- ROS (Kros) .....	165
6.3.2	Fibrinogen alpha chain (FIBA) .....	165
6.3.3	Lysozyme C .....	168
6.3.4	Glutamate Receptor 2 (GLR2) .....	168
6.3.5	LIMK1 does not phosphorylate peptides in vitro .....	171
6.4	Kestrel approach to novel substrate identification. ....	174
6.4.1	Ef1 $\alpha$ 2 .....	174
6.5	Conclusions and Discussion .....	175
7	Discussion .....	178
7.1	Chapter Summary .....	178
7.2	Requirement for LIMK in cell motility and Invasion .....	178
7.3	Role for LIMK in motility and invasion .....	179
7.3.1	LIMK levels important for invasion .....	180
7.3.2	Cofilin regulation .....	181
7.3.3	LIMK inhibition impairs matrix degradation .....	181
7.4	LIMK is required in leading path-generating cells for collective invasion .....	183
7.5	Investigations into novel substrates of LIMK .....	184
7.6	Final conclusions .....	185
8	References .....	188

## List of Tables

Table 1 Plasmids .....	50
Table 2 Oligonucleotides and Primers .....	56
Table 3 siRNA duplex sequences .....	60
Table 4 Acrylamide gel recipe .....	71
Table 5 Table of primary antibodies.....	73

## List of Figures

Figure 1.1 Phylogenetic dendrogram of LIMK1 and LIMK2 across species.....	15
Figure 1.2 LIM Kinases phosphorylate and inactivate Cofilin. ....	18
Figure 1.3 LIM Kinase structure and homology.....	21
Figure 1.4 Relationship of LIMK kinase with members of the Tyrosine Kinase-Like family. ....	22
Figure 1.5 LIMK is a convergence point for upstream signals.....	25
Figure 1.6 LIM Kinase modifications. ....	26
Figure 1.7 Regulation of LIMK nuclear/cytoplasmic localisation. ....	27
Figure 1.8 LIMK Inhibitors. ....	32
Figure 1.9-Mesenchymal vs. Amoeboid invasion. ....	42
Figure 1.10- Individual vs. Collective invasion.....	43
Figure 1.11 Actin cycling at the leading edge.....	45
Figure 1.12 Schematic view of signalling pathways that lead to actin organisation at invadopodia or podosomes. ....	47
Figure 3.3.1-siRNA of LIMK1 and LIMK2 in MDAMB231 and effect on proliferation. ....	83
Figure 3.3.2-MDAMB231 morphology on glass. ....	85
Figure 3.3.3-BT549 morphology on glass.....	86
Figure 3.3.4-BE morphology on glass. ....	87
Figure 3.3.5-MDAMB231 wound healing assay. ....	90
Figure 3.3.6-Motility of MDAMB231 using the Oris cell migration assay.....	93
Figure 3.3.7-Motility of BT549 using the Oris cell migration assay.....	94
Figure 3.3.8- BE wound healing and motility on plastic. ....	95
Figure 3.3.9-MDAMB231 Motility on Cell Derived Matrix mapped. ....	98
Figure 3.3.10-MDAMB231 Motility on Cell Derived Matrix quantified.....	99
Figure 3.3.11-Timeline of MDAMB231 motility on CDM, LIMK knockdown cells refract more than controls. ....	100
Figure 3.3.12-Inverse invasion assay.....	102
Figure 3.3.13-Loss of LIMK reduces MDAMB231 3D Invasion.....	103
Figure 3.3.14-Quantification of MDAMB231 loss of Invasion following knockdown of LIM Kinases.....	104
Figure 3.3.15-Quantification of BT549 loss of Invasion following knockdown of LIM Kinases.....	105
Figure 3.3.16 Quantification of BE loss of Invasion following knockdown of LIM Kinases.....	106
Figure 3.3.17-3D morphology of MDAMB231 cells invading into matrigel.....	108
Figure 3.3.18-MDAMB231 cells lose the ability to invade in tracks following LIMK knockdown. ....	109
Figure 3.3.19-3D F-actin staining and invasion of MDAMB231 is reduced by LIMK inhibitor. ....	112
Figure 3.3.20- F-actin staining of MDAMB231 in 3D is reduced by siRNA knockdown of LIM Kinases in the invasive population of cells.....	113
Figure 3.3.21-F-actin staining in 3D is reduced by siRNA knockdown of LIM Kinases in the non invasive population of cells. ....	114
Figure 3.3.22-Conditional activation of LIMK:ER by 4-Hydroxytamoxifen.....	117
Figure 3.3.23-NIH3T3 Express LIMK:ER, exhibiting a very subtle phenotype following induction with 4HT. ....	118
Figure 3.3.24-SAOS express LIMK:ER but do not exhibit a consistent phenotype following induction with 4HT. ....	119

Figure 3.3.25-SAOS express LIMK:ER but do not exhibit a consistent phenotype following induction with 4HT. ....	120
Figure 3.3.26-LIMK:ER activity in vitro, optimisation of kinase assays.....	122
Figure 3.3.27- Identification of optimal dose and timeframe in which to assess LIMK:ER activity in cells. ....	123
Figure 3.28-Increased levels of LIMK reduces 3D invasion of MDAMB231 cells..	125
Figure 4.4.1-F-actin rich invadopodia of MDAMB231 degrade FITC labelled gelatin matrices. ....	131
Figure 4.4.2-Knock-down of LIM Kinase 1 and 2 by siRNA reduces invadopodia formation.....	132
Figure 4.4.3-Inhibition of LIMK1 and 2 by CRT101106 reduces invadopodia formation.....	133
Figure 4.4.4-Inhibition of LIMK reduces the percentage of cells making invadopodia. ....	134
Figure 4.4.5-ImageJ method for analysis of invadopodia. ....	135
Figure 4.4.6-Quantification of gelatin degradation following LIM Kinase inhibition by CRT101106 or knockdown by siRNA. ....	136
Figure 4.4.7-Knockdown of LIM Kinases reduces MMP9 activity in MDAMB231 ..	139
Figure 4.4.8-Effects of LIM Kinase Knockdown on MMP RNA levels .....	140
Figure 4.4.9-Knockdown of LIMK reduces Collagenase activity in 3D .....	142
Figure 4.4.10-Cells leading collective invasion require LIMK .....	144
Figure 4.4.11-Loss of leading 'tip' position during invasion by cells following LIMK knockdown. ....	145
Figure 5.5.1-PTD, an optimised TAT protein. ....	149
Figure 5.5.2-PTD Cofilin purification and cell permeability. ....	150
Figure 5.5.3-Localisation of PTD FLAG Cofilin in MDAMB231 cells. ....	153
Figure 5.5.4-In Vitro F-actin severing activity of PTD Cofilin .....	154
Figure 5.5.5-Motility in 2D following an increase in cellular levels of Cofilin. .	155
Figure 5.5.6- Quantification of motility in 2D following an increase in cellular levels of Cofilin .....	156
Figure 5.5.7-Disruption of the Cofilin balance reduces cell invasion. ....	158
Figure 6.6.1- LIMK1 phosphorylates Cofilin 1 predominantly on Serine 3. ....	163
Figure 6.6.2- Pepscan Peptide Array. ....	164
Figure 6.6.3- c-ROS peptide is not phosphorylated by LIMK1 <i>in vitro</i> .....	166
Figure 6.6.4- Fibrinogen alpha chain peptide is not phosphorylated by LIMK1 <i>in vitro</i> .....	167
Figure 6.6.5- LYC does not appear to be phosphorylated by LIMK1. ....	169
Figure 6.6.6- GLR2 does not appear to be phosphorylated by LIMK1.....	170
Figure 6.6.7- Hypothesised mechanism by which peptides may be phosphorylated by LIMK1. ....	172
Figure 6.6.8- LIMK does not phosphorylate Cofilin Peptides in vitro. ....	173
Figure 6.6.9- Kestrel screening for novel substrates.....	176
Figure 6.6.10-Ef1a2 kinase assay.....	177
Figure 7.1 Novel understanding of LIMK Role in cell invasion .....	187

## List of accompanying material

*Supplementary CD to compliment figures as required.*

Figure 3.17 part B.

Figure 3.28 part C.

## Abbreviations

ATP	Adenosine 5'-triphosphate
Cof	Cofilin
DMEM	Dulbeccos Modified Eagles Medium
DMSO	Dimethyl Sulphoxide
dNTPs	Deoxy nucleotide-5'-triphosphate
ECL	Enhanced chemiluminescence
ECM	Extracellular Matrix
EDTA	Ethylene diamine triacetic acid
EGF	Epidermal growth factor
EGFP	Enhanced green fluorescent protein
EtBr	Ethidium Bromide
FBS	Foetal bovine serum
GST	Glutathione S-transferase
GTP	Guanosine triphosphate
HRP	Horseradish peroxidase
IgG	Immunoglobulin G
Kb	Kilobase
KDa	Kilodalton
LIM	Lin11, Isl-1, Mec-3 domain
LIMK	LIMK1 and LIMK2
LIMK1	LIM kinase 1
LIMK2	LIM kinase 2
Min	Minute(s)
MMP	Matrix metalloprotease
mRNA	Messenger ribonucleic acid
NP-40	Nonidet (non ionic detergent) P-40
NT	Non-targeting
OD	Optical density
p	Phospho-
PAGE	Polyacrylamide gel electrophoresis
PBS	Phosphate buffered saline
pCofilin	Phospho-Cofilin
PCR	Polymerase chain reaction
PDZ	PSD95, DlgA, zo-1 domain
PIP2	Phosphatidylinositol (4,5)-bisphosphate
RNA	Ribonucleic acid
RNAi	Ribonucleic acid interference
RT-PCR	Reverse transcription polymerase chain reaction
siRNA	Short interfering ribonucleic acid
TAE	Tris acetate EDTA
TBS	Tris buffered saline
TBST	Tris buffered saline - Tween 20
TE	Tris-EDTA
Tiff	Telomerase-immortalised fibroblast
Tris	2-amino-(hydroxymethyl)propane-1, 3-diol
Tween 20	Polyoxyethylene sorbitan monolaurate
U	Units
V	Volts
WT	Wild type

## Acknowledgements

First, and foremost, I would like to express my gratitude to Mike Olson, for his excellent supervision and support throughout my PhD. I would like to thank my Advisor Walter Kolch for his encouragement, and to give a special thanks to Dan for his guidance, reagents and patience in teaching me ‘the way of Dan’.

Thanks to all R17 members, past and present, and to all the lovely friends I have made at the Beatson for their help, support and fantastic baking skills. A big thank you to all of the support staff throughout the Beatson Institute for their invaluable help, especially Margaret and Tom for teaching me everything I know about microscopy.

Finally, I am extremely grateful to the Director, Karen Vousden, for giving me this opportunity, and to CRUK for their generous support.

## Author's Declaration

I am the sole author of this thesis. The work presented in this thesis is entirely my own unless otherwise stated.

# 1 Introduction

Cancer cell metastasis, the process by which cancer cells move away from a primary tumour mass, accounts for 90% of human cancer deaths (Hanahan & Weinberg, 2000). A multistage process, cancer cell metastasis involves localised invasion into surrounding tissue, intravasation from the original tissue, transit in either of the circulatory systems (lymph or blood), extravasation into new tissue, and colonisation of a new metastatic site (Olson & Sahai, 2008). The ability of metastatic cells to invade is determined by their ability to reorganize the actin-myosin cytoskeleton and cell morphology, and remodel the extracellular matrix (ECM) to facilitate movement.

Rho GTPases have a long established role in the regulation of cell morphology, motility and invasion (Hall, 2005). One approach to further understanding and therapeutically targeting metastasis is to identify the elements of Rho GTPase signaling and actin-myosin regulation required for cancer cell invasion; with the aim of developing inhibitors that could be useful in suppressing metastatic spread. The LIM kinases 1 and 2 (LIMK1 and LIMK2) are activated downstream of the Rho-ROCK, Rac-PAK and Cdc42-MRCK pathways, thereby acting as a convergence point for the signaling pathways that regulate the actin cytoskeleton (Scott & Olson, 2007). LIM kinases may therefore provide a vulnerable point in actin regulation which when targeted could result in inhibition of invasion, independent of the upstream signaling pathway utilised.

The work in this thesis aimed to determine the role of LIMK in motility and invasion, and validate LIMK as a target for cancer therapeutics. The introduction to this thesis describes previous literature relevant to the data presented within, relating to LIM Kinases and the field of cancer cell motility and invasion.

## 1.1 Introduction to LIM Kinases

The LIM-kinase protein family has two highly-related members, LIM kinase 1 (LIMK1) and LIM kinase 2 (LIMK2), which are encoded by separate genes located on human chromosomes 7q11.23 and 22q12.2 respectively. The LIMK1 gene spans 39,499 base pairs with 16 exons. Alternative splicing results in the generation of two LIMK1 mRNAs, one encoding the full-length protein (GenBank NM\_002314) while the second has a 61 base deletion that results in the production of a truncated protein lacking the carboxyl-terminal kinase domain (<http://www.ncbi.nlm.nih.gov/entrez/viewer.fcgi?val=8051616&itemID=2&view=gbwithparts>). The LIMK2 gene spans 68,617 base pairs, comprising 19 potential exons. Alternative splicing results in three LIMK2 isoforms; variant 1 (GenBank NM\_001031801) is the largest protein, 2a (GenBank NM\_005569) differs in both the 5' and 3' untranslated regions (UTR) and coding sequences resulting in the production of a smaller protein with distinct amino- and carboxyl termini, and 2b (GenBank NM\_016733) differs in the 3' UTR and coding sequences to generate a protein identical to variant 1 at the amino-terminus and to 2a in the carboxyl terminus. Functional differences between the various isoforms have not been determined, although there is some data indicating that their expression may vary in different tissues. To date, LIM Kinase homologues have been identified in a variety of species (Figure 1.1) including; humans (Mizuno et al, 1994);(Nunoue et al, 1995); (Okano et al, 1995), mice (with mouse LIMK1 initially named Kiz-1(Bernard et al, 1994)), rats (Nunoue et al, 1995) and chicken(Koshimizu et al, 1997), with related LIMK1 homologues also expressed in more distantly related species such as; *Xenopus laevis* (XLIMK;(Takahashi et al, 1997)), *Drosophila melanogaster* (DLIMK;(Ohashi et al, 2000a)) and the African malaria mosquito *Anopheles gambiae*. The majority of research reported in the literature has focused on LIMK1, likely due to the fact that it was isolated first, in fact many reports use the generic term "LIMK" without defining the kinase to which it refers. In this thesis, references to LIMK imply both kinases, specific reference to either one will be made where differences between the two proteins have been established, or where only one of the LIM kinases has been investigated.

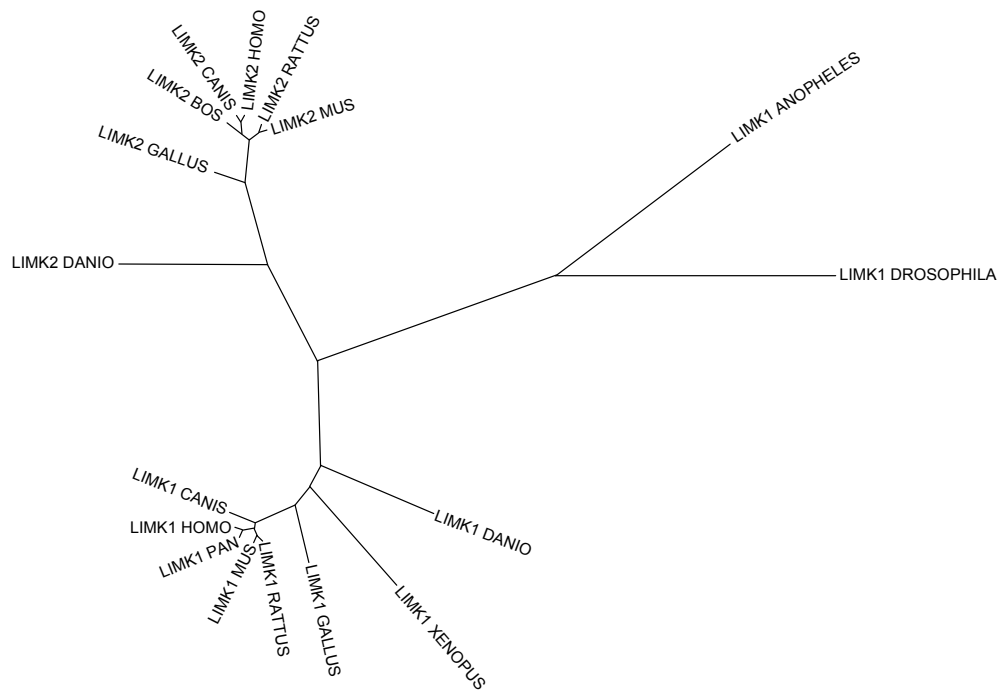


**Figure 1.1 Phylogenetic dendrogram of LIMK1 and LIMK2 across species.**

Protein sequences of LIMK1 and LIMK2 from a number of species were aligned using the MultAlin multiple sequence alignment program (Corpet, 1988). For brevity, only genus names are indicated on the diagram for *Homo sapiens*, *Pan troglodytes*, *Canis familiaris*, *Mus musculus*, *Rattus norvegicus*, *Bos taurus*, *Gallus gallus*, *Drosophila melanogaster*, *Xenopus laevis*, *Anopheles gambiae*, *Danio rerio*. The LIMK present in the representative Insectae species is most similar to LIMK1.

The most extensively characterised substrates of LIMK are Cofilin1 (also known as non-muscle Cofilin, found on human chromosome 11q13), Cofilin2 (a.k.a. muscle Cofilin, chromosome 14q12) and destrin (also known as actin depolymerizing factor or ADF, chromosome 20p12.1). Similar to the ambiguous use of the term “LIMK” in some publications, the substrates are often generically referred to as “Cofilin” without precise identification of which of the three proteins is actually being studied. Although this may not be a major problem, there are indications that each of the three proteins may have different biochemical properties which may have significant implications upon the regulation of actin dynamics in specific cell types (Vartiainen et al, 2002). In this review, I will use the generic term “Cofilin” except where specific differences between the proteins have been determined. In addition to Cofilin proteins, recent research has identified the nuclear transcription factors CREB (Yang et al, 2004a) and Nurr1 (Sacchetti et al, 2006) as putative LIMK substrates in neurons. Although not as well validated as Cofilin proteins as bona fide LIMK substrates, given that both LIMK1 and LIMK2 undergo nuclear/cytoplasmic shuttling in certain circumstances and the previous suggestion of nuclear LIMK targets (e.g. (Roovers et al, 2003)), the identification of these proteins as LIMK substrates should be given due consideration.

The Cofilin proteins were originally identified on the basis of their ability to depolymerise filamentous actin (F-actin) in vitro (reviewed in reference (Bamburg, 1999)). As well as depolymerising actin in vitro, it has been proposed that a primary function of Cofilin in vivo is to sever F-actin filaments to generate barbed ends that can serve as de novo actin nucleation sites (Ghosh et al, 2004) (Lorenz et al, 2004). LIMK plays a central role in the regulation of the actin cytoskeleton by phosphorylating Cofilin on Serine 3 and inactivating its actin severing activity (Amano et al, 2001; Maekawa et al, 1999; Ohashi et al, 2000a; Sumi et al, 1999), altering the rate of actin depolymerisation and/or barbed end formation (Figure 1.2). Some researchers in the field see Cofilin's role in actin dynamics as a recycling protein, and those that see Cofilin as a promoter of actin nucleation (Condeelis, 2001; Cramer 1999). I believe Cofilin is both of these things as actin nucleation is dependent upon free barbed ends to act as nuclei, Arp2/3 prefers barbed ends to bind to and thus it can amplify the nucleation activity of Arp2/3 (Des Marais et al, 2004). Although Cramer might suggest that

Cofilin merely mediates the depolymerisation of actin filaments to provide actin monomers for ongoing filament assembly, such as in migrating chick embryos, I believe both the nucleation and recycling qualities of Cofilin are important for cell motility and invasion (Cramer, 1999). Actin monomers are required for filament assembly as well as the new barbed end sites for actin nucleation, both are provided by Cofilin (Cramer, 1999).

Although Cofilin is the principal LIMK substrate (Arber et al, 1998; Yang et al, 1998b) (Takahashi et al, 2001), other kinases have also been reported to phosphorylate Cofilin such as TESK1 (Toshima et al, 2001a), TESK2 (Toshima et al, 2001b) and NRK/NESK (Nakano et al, 2003), indicating that Cofilin may be a significant point of upstream signal integration. The function LIMK manifests in cytoskeleton dynamics makes it an interesting prospective target for anti-metastatic drug development, given that a role for LIMK in cancer metastasis has been proposed (Davila et al, 2003) (Yoshioka et al, 2003) (Suyama et al, 2004). Disruption of LIMK signalling has also been associated with the human genetic condition Williams syndrome (Hoogenraad et al, 2004), which results in a range of developmental abnormalities, and has more recently been proposed to have a role in primary pulmonary hypertension (Foletta et al, 2003) and the formation of intracranial aneurysms (Akagawa et al, 2006). The association of LIMK with a variety of human diseases emphasises the critical importance of proper dynamic regulation of actin cytoskeletal structures.

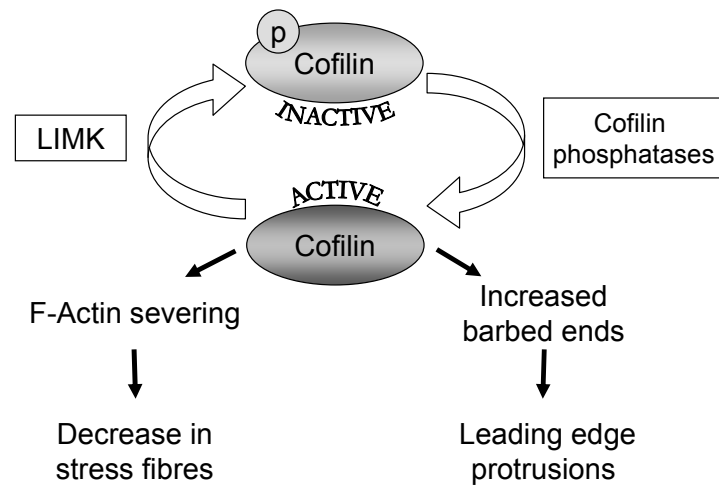


**Figure 1.2 LIM Kinases phosphorylate and inactivate Cofilin.**

LIMK1 and LIMK2 phosphorylate and inactivate members of the Cofilin protein family (Cofilin1, Cofilin2 and actin depolymerising factor/destrin), which results in reorganisation of the cytoskeleton. LIMK increases stress fibre and focal adhesion formation by reducing actin depolymerisation. LIMK initiated changes in F-actin severing also leads to reduced barbed end formation and leading edge protrusions.

## 1.2 LIM Kinase protein organisation

LIM kinases have a unique organization of signalling domains, with two amino-terminal LIM domains (each containing double zinc finger motifs), adjacent PDZ and proline serine (P/S) rich regions, followed by a carboxyl-terminal kinase domain (Figure 1.3). The LIM domains have been shown to play an important role in regulating kinase activity (Nagata et al, 1999) (Tomiyoshi et al, 2004) and likely also contribute to LIMK function by acting as sites of protein:protein (Hiraoka et al, 1996) and possibly protein:DNA interactions (Nishiya et al, 1998), although a direct demonstration of DNA binding activity of these LIM domains has not been reported. LIMK1 and LIMK2 have 50% overall identity, with 70% identity in the kinase domain (Mizuno et al, 1994) (Nunoue et al, 1995). The regulatory LIM domains are also 50% identical when compared between kinases, with 20% identity between LIM domains within each kinase including complete conservation of the zinc-binding Cys and His residues. The PDZ domains are almost as well conserved as the LIM domains between kinases with just under 50% identity. Although perhaps best known as a protein:protein interaction domain, the PDZ of LIMK influences nuclear/cytoplasmic shuttling with two leucine-rich nuclear export signals (Yang et al, 1998a; Yang & Mizuno, 1999). Translocation into the nucleus is driven by nuclear localization signals, one of which is found between the PDZ and kinase domains in both LIMK1 and LIMK2 and a second being found only in the kinase domain of LIMK2 (Goyal et al, 2006). The presence of both nuclear export and nuclear import sequences suggests that nuclear/cytoplasmic shuttling might be a regulated process and that LIMK may have active functions in the nucleus.

Primary sequence analysis does not make it immediately clear whether LIMK is likely to be a serine/threonine or tyrosine kinase. Given that the diagnostic sequence motif for a serine/threonine kinase is DLKXXN and for a tyrosine kinase is DLAARN or DLRAAN (Hanks et al, 1988), the presence of a less than diagnostic DLNSHN motif in the kinase VIB subdomain has resulted in LIMK being grouped in the Tyrosine Kinase-Like (TKL) subfamily along with others such as the next most closely related TESK kinases (Figure 1.4).

Early characterization described LIMK1 as a strict threonine/serine kinase (Nunoue et al, 1995; Okano et al, 1995) although tyrosine autophosphorylation has also been reported (Proschel et al, 1995). Although the related Cofilin1, Cofilin2 and destrin proteins were initially reported to be the only physiological substrates, the identification of CREB (Yang et al, 2004b) and Nurr1 (Sacchetti et al, 2006) as LIMK substrates and the ability of LIMK to phosphorylate myelin basic protein and histone in vitro suggests that LIMK may be more promiscuous than previously thought and that there may be additional in vivo substrates.

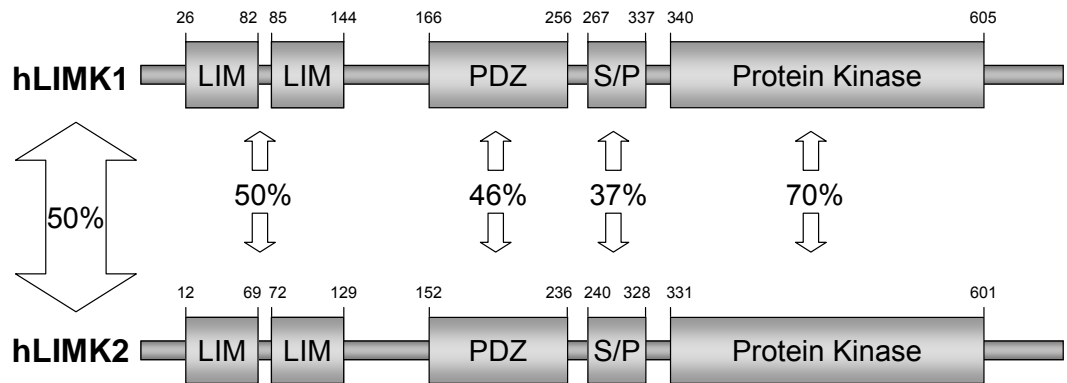


**Figure 1.3 LIM Kinase structure and homology.**

LIMK1 and LIMK2 share 50% overall identity. LIMK1 and LIMK2 consist of 2 amino-terminal LIM domains, adjacent PDZ and proline/serine rich regions, followed by a carboxyl-terminal protein kinase domain, with the identities between homologous domains indicated.

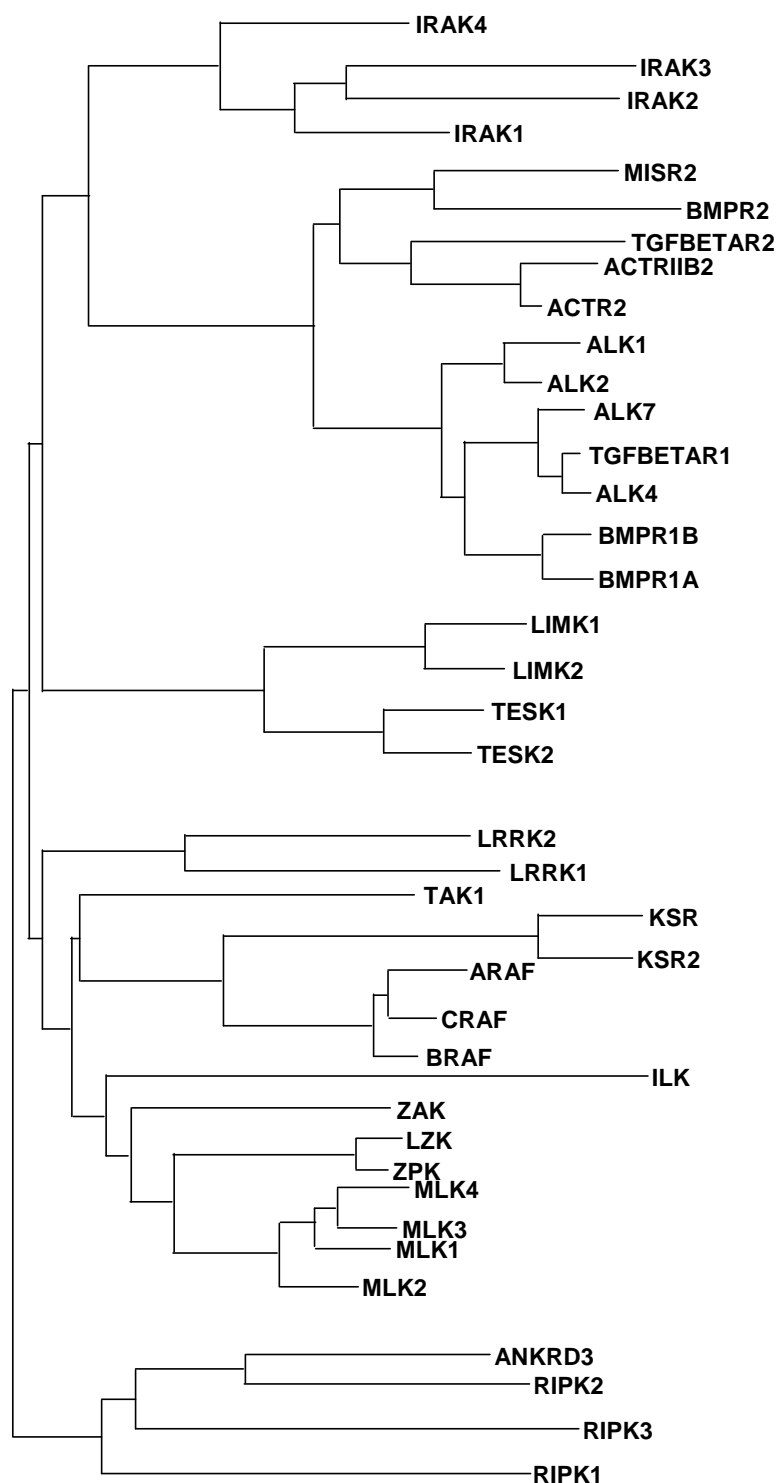


**Figure 1.4 Relationship of LIMK kinase with members of the Tyrosine Kinase-Like family.** Protein sequences of human LIMK1 and LIMK2 kinase domains were aligned with the kinase domains of other members of the Tyrosine Kinase-Like family using the MultAlin multiple sequence alignment program (Corpet, 1988). The most closely related kinases to LIMK1 and LIMK2 are TESK1 and TESK2, which also share the ability to act as Cofilin kinases, suggesting that there may be some degree of functional redundancy between these proteins.

### 1.3 Activation and regulation

In addition to the possible function of the LIM and PDZ domains in mediating protein:protein interactions, they are also involved in regulating LIMK activity. Deletion, or mutation of conserved Cysteine residues, of the LIM domains results in significantly increased kinase activity in vitro and deletion of both LIM and PDZ domains results in further kinase activation (Nagata et al, 1999). In addition, purified recombinant LIM domains interact with the kinase domain and result in dose-dependent inhibition of in vitro kinase activity, consistent with a role of the LIM domains in regulating LIMK activity via direct protein interaction (Nagata et al, 1999).

Similar to many other kinases, phosphorylation in the activation loop results in increased LIMK activity. Both LIMK1 and LIMK2 are phosphorylated by the Rho effector ROCK on conserved threonine residues, Thr-508 in LIMK1 and Thr-505 in LIMK2, and these phosphorylation events are required for activation above basal levels (Figure 1.5 and Figure 1.6) (Amano et al, 2001; Ohashi et al, 2000b; Sumi et al, 2001a). Pak1 (shown to work on LIMK1; (Edwards et al, 1999)), Pak4 (LIMK1; (Dan et al, 2001)) and the myotonic dystrophy kinase-related Cdc42-binding kinase (MRCK $\alpha$ ; LIMK1 and LIMK2; (Sumi et al, 2001b)) have each been reported to phosphorylate and activate the indicated form of LIMK. In addition, data consistent with a similar role for Pak2 in regulating LIMK activity has been reported (Misra et al, 2005; Wu et al, 2003). Therefore, LIMK acts to integrate signals from a number of upstream pathways in regulating the actin cytoskeleton.

Transphosphorylation also appears to regulate LIMK activity in two ways. Firstly, unphosphorylated LIMK1 is relatively unstable with a half life of ~4 hours, association with Hsp90 promotes homodimerization and transphosphorylation leading to the production of stable LIMK1 dimers (Li et al, 2006). Secondly, transphosphorylation at numerous sites in the kinase domain elevates LIMK1 specific activity (Li et al, 2006). The region of the LIMK1 kinase domain that interacts with Hsp90 was identified by homology with ErbB-2 as being between amino acids 387-402, with a critical amino acid for this interaction determined to be Proline 394 (Figure 1.6). Treatment of cells with Hsp90 inhibitors such as

17AAG reduced LIMK1 and LIMK2 levels, and led to decreased levels of phospho-Cofilin, suggesting that Hsp90 regulates the activity of both kinases and that the LIMK-Hsp90 interaction is important for the regulation of actin cytoskeletal structures.

Although LIMK1 was reported to autophosphorylate when expressed in bacteria (Proschel et al, 1995), it was suggested that because the sequence surrounding Thr508 in the LIMK1 activation loop was very different from the sequence adjacent to Ser3 in Cofilin, trans-autophosphorylation of the activation loop was unlikely (Edwards & Gill, 1999). Autophosphorylation of LIMK1 was exclusively on Serine and Tyrosines, indicating that Thr508 was not a substrate (Proschel et al, 1995). In addition, a recent report showed that a T508V LIMK1 mutant autophosphorylated to the same extent as wild-type when corrected for enzyme activity (Kobayashi et al, 2006). These results indicated that autophosphorylation does occur but is unlikely to be at the activation loop Threonine. To date, the sites of autophosphorylation, and how they may regulate LIMK activity or function, have not been determined.

Proteins regulated by phosphorylation are typically reverted to their basal unphosphorylated state by phosphatases. One phosphatase that has been found to dephosphorylate and inactivate LIMK1 is slingshot 1 (SSH1) (Soosairajah et al, 2005), which previously had been identified as a Cofilin phosphatase (Niwa et al, 2002)(Figure 1.5 and Figure 1.8).

SSH1 bound directly to the kinase domain where it catalysed the dephosphorylation of Threonine 508, as well as autophosphorylated Serine residues, resulting in reduced LIMK1 phosphorylation of Cofilin. LIMK1 was a better substrate for SSH1 than was LIMK2, suggesting that there may be differential regulation of these two kinases. The activity of SSH1 is dependent on binding to F-actin and is negatively regulated by PAK4 mediated phosphorylation. These results indicate that kinases such as PAK4, and possibly others including ROCK and MRCK $\alpha$ , increase LIMK1 activity both by direct phosphorylation and by inhibition of the LIMK1 dephosphorylating activity of SSH1. In addition, low levels of F-actin in the cell, either globally or locally, would reduce SSH1 activity thereby favouring the activation of LIMK1 and increasing phospho-Cofilin levels.

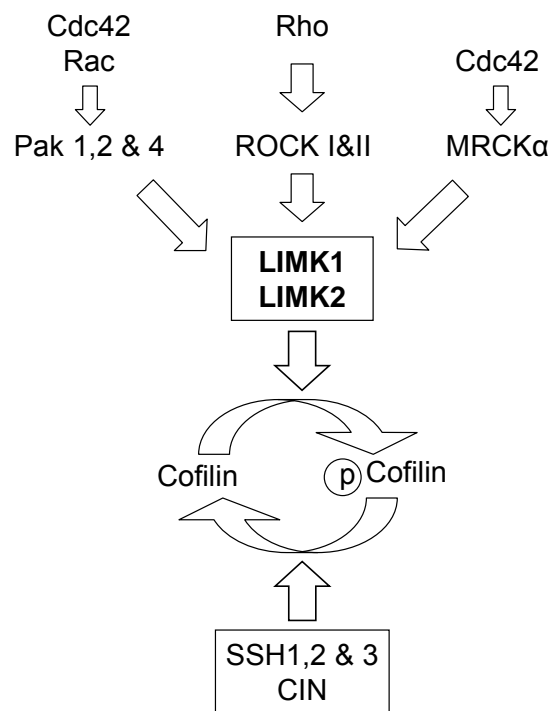


**Figure 1.5 LIMK is a convergence point for upstream signals.**

LIMK1 and LIMK2 integrate signals from a number of Rho GTPase family signalling pathways to regulate the actin cytoskeleton. Both ROCK I and II have been shown to phosphorylate and activate LIMK and a similar role in LIMK regulation has been identified for PAK1, 2 and 4 and MRCK $\alpha$ . Cofilin phosphatases such as SSH and CIN counteract the phosphorylation and inactivation of Cofilin.

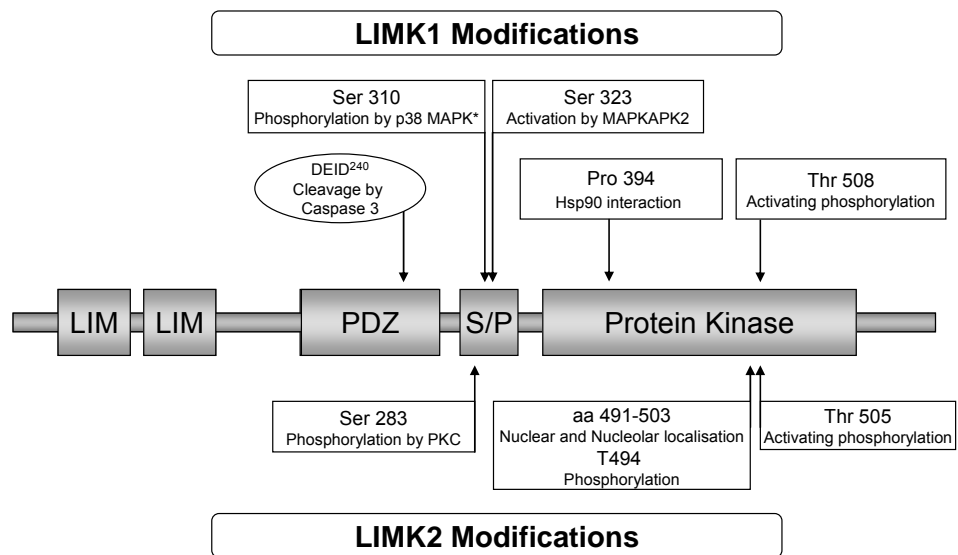


**Figure 1.6 LIM Kinase modifications.**

LIMK1 and LIMK2 are modified by a variety of proteins, which alter kinase activity or subcellular localisation. Sites of phosphorylation or proteolysis for LIMK1 (above) and LIMK2 (below) are indicated.

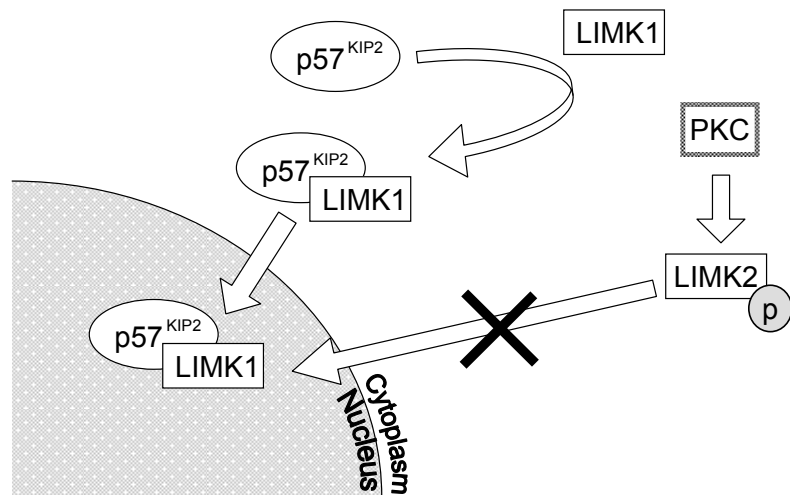


**Figure 1.7 Regulation of LIMK nuclear/cytoplasmic localisation.**

Nuclear import of LIMK1 can be influenced by association with the cyclin dependent kinase inhibitor p57KIP2. Once associated, the LIMK1:p57KIP2 complex is translocated from the cytoplasm to the nucleus where it appears to be sequestered. LIMK2 nuclear localisation can be inhibited through phosphorylation of residues within nuclear localisation sequences by PKC.

LIMK1 has also been reported to be activated by MAPKAPK2 in VEGF-stimulated endothelial cells, by phosphorylation at Serine 323 between the PDZ and kinase domains (Kobayashi et al, 2006) (Figure 1.6). Unlike the more well characterised mechanisms of kinase-induced LIMK activation, phosphorylation of Threonine 508 was not required for LIMK1 activation by VEGF or by kinases upstream of MAPKAPK2 including MKK6 or p38. Although p38 was capable of directly phosphorylating LIMK on Serine 310, there was no effect on kinase activity, therefore the role of p38 in LIMK regulation works via MAPKAPK2 (Fig. 1.6). The proposed mechanism to explain the positive effect of Serine 323 phosphorylation on kinase activity is that the autoinhibitory amino-terminal domains are displaced from binding to the kinase domain, however, direct experimental evidence confirming this hypothesis has not yet been reported.

In addition to activation loop phosphorylation contributing to LIMK activity, an insert region consisting of 11 basic amino acids amino-terminal to Thr508 appears to be necessary for LIMK-induced effects on actin structures in cells, but not for kinase activity in vitro, suggesting that this activation loop region might be involved in substrate recognition (Edwards & Gill, 1999). Phosphorylation on residues outside the kinase domain have been shown to regulate the biological function of LIMK by influencing nuclear/cytoplasmic shuttling. Phosphorylation of LIMK2 by protein kinase C at Serine 283 alone (Goyal et al, 2005), or in combination with Threonine 494 phosphorylation has been reported to prevent nuclear import in endothelial cells by inhibiting the function of nuclear import sequences (Goyal et al, 2006) (Figure 1.6 and Figure 1.7).

Nuclear import of LIMK1 is also influenced by association with the cyclin-dependent kinase (CDK) inhibitor p57KIP2 (Yokoo et al, 2003). The LIMK1:p57KIP2 interaction results in translocation of LIMK1 from the cytoplasm to the nucleus where the complex then appears to be anchored, possibly due to the masking of LIMK nuclear export signals (Figure 1.7). The central portion of p57KIP2, which is unique among CDK inhibitors, associates with the LIM domains. Consistent with a role in LIMK regulation through subcellular localization, p57KIP2 binding did not inhibit LIMK1 kinase activity, although transfection of p57KIP2, but not the related CDK inhibitor p27KIP1, resulted in a reduction in LIMK1-induced stress fibres (Yokoo et al, 2003). It is also possible that LIMK1 is performing a specific role within the nucleus, consistent with its ability to

phosphorylate the transcription factors CREB (Yang et al, 2004a) and Nurr1 (Sacchetti et al, 2006). The effects of p57KIP2 on LIMK1 and consequently on the actin cytoskeleton is reminiscent of the inhibition of ROCK by the CDK inhibitor p21Waf1/Cip1 (Lee & Helfman, 2004) (Tanaka et al, 2002). These data are consistent with the increasingly clear role of cell cycle regulatory proteins in the regulation of the actin cytoskeleton (Besson et al, 2004).

The polarity protein Par-3 ordinarily plays an important role in the proper assembly of tight junctions in mammalian epithelial cells (Chen & Macara, 2005) and the specification of epithelial apical-basal polarity (Hurd et al, 2003). Reduction in Par-3 levels by siRNA-mediated knockdown resulted in a substantial increase in Cofilin Serine 3 phosphorylation, while overexpression of Par-3 reduced lysophosphatidic acid stimulation of Cofilin phosphorylation, suggesting that Par-3 might influence the activity of a Cofilin kinase or phosphatase (Chen & Macara, 2006). The elevated Cofilin phosphorylation observed when Par-3 was knocked down could be reversed by treatment with a reported activator of the Cofilin phosphatase slingshot, Neuregulin-1 $\beta$  (Nagata-Ohashi et al, 2004), consistent with the target of Par-3 not being a phosphatase. Instead, a carboxyl-terminal fragment of Par-3 was found to interact with LIMK2 (but not LIMK1) in a LIM domain dependent manner (Chen & Macara, 2006) (Figure 1.8). The association between Par-3 and LIMK2 inhibits kinase activity in vitro without affecting LIMK1 activity. Knockdown of LIMK2, or expression of a non-phosphorylatable Cofilin, reversed the loss of tight junctions in MDCK canine kidney epithelial cells induced by Par-3 knockdown, indicating that the inhibition of LIMK2 and consequent inactivation of Cofilin is a critical action of Par-3 in regulating tight junctions.

The *lats* gene was first identified as a tumour suppressor in *Drosophila*, and the two mammalian homologues that have been identified are also believed to function similarly. Mice deleted for the *lats1* gene develop a limited spectrum of cancers (St John et al, 1999) while the human *LATS1* gene is lost in sporadic cases of sarcoma (Hisaoka et al, 2002) and breast cancer (Morinaga et al, 2000). In an attempt to further characterize the downstream signalling events, a suppressor screen was undertaken in *lats*-overexpressing flies (Yang et al, 2004a). The *Drosophila* Cofilin homologue *twinstar* was identified as a dominant suppressor, although further analysis revealed that *lats* and *twinstar* did not

interact directly. Instead, mammalian Lats1 and LIMK1 were found to interact, resulting in inhibition of kinase activity (Figure 1.8).

Overexpression of LIMK1 has been reported to result in defective cytokinesis and the production of multinucleate cells, suggesting that LIMK1 may play an important role in cell division (Amano et al, 2002). Consistent with LATS1 being a regulator of LIMK1 in vivo, co-expression of LATS1 with LIMK1 reversed the cytokinesis defect induced by LIMK1 overexpression, while knockdown or genetic deletion of LATS1 resulted in significant levels of multinucleate cells being produced (Yang et al, 2004a). Therefore, it appears that LATS1 plays a significant role in cell division, acting via LIMK1-mediated regulation of actin cytoskeletal structures.

Normal cell morphology is influenced by the actin cytoskeleton, in addition, the morphological responses observed during apoptosis are due to profound alterations in cytoskeletal architecture. Playing a central and critical role in the cell contraction and membrane blebbing that occur during apoptosis is ROCK I, which undergoes caspase-mediated proteolysis resulting in the generation of an active kinase fragment (Coleman et al, 2001; Croft et al, 2005; Sebbagh et al, 2001). Similarly, LIMK1 has been found to be cleaved at a caspase 3 type site DEID (amino acids 237-240) to generate a constitutively active fragment during apoptosis (Tomiyoshi et al, 2004)(Figure 1.6). The cleavage site is conserved in vertebrate LIMK1 homologues, but is not present in LIMK2. The truncated LIMK1 has elevated kinase activity in vitro and when expressed in cells results in membrane blebbing. Knockdown of LIMK1 by siRNA partially reduced Cofilin phosphorylation and membrane blebbing in Fas ligand treated cells, suggesting that although LIMK1 is the only reported Cofilin kinase found to be activated by caspase cleavage, additional pathways might lead to Cofilin phosphorylation and actin rearrangements in apoptotic cells (e.g. cleaved ROCK I > LIMK2 > Cofilin). Consistent with this possibility, overexpression of LIMK2 resulted in plasma membrane blebbing, which was dependent on ROCK-mediated phosphorylation of the activation loop Threonine 505 (Amano et al, 2001). The role of LIMK1 cleavage during apoptosis may be to amplify ROCK I induced effects on the actin cytoskeleton that result in membrane blebbing.

Proteolysis of LIMK1 has also been shown to occur via the proteasome-mediated degradation in neuronal cells (Tursun et al, 2005). The RING finger E3 ubiquitin ligase Rnf6 is expressed at high levels in the axons of developing neurons during mouse embryogenesis, and can influence axon outgrowth of cultured hippocampal neurons. Rnf6 binds to and catalyzes the polyubiquitination of LIMK1, which leads to its degradation by the proteasome. Changes to axon outgrowth of cultured neurons were reciprocally regulated by LIMK1 and Rnf6, indicating that the two proteins are functionally linked (Figure 1.8). LIMK1 protein levels are also regulated in the brain by the microRNA miR-134, which binds to the 3' UTR of the LIMK1 mRNA and blocks translation during synapse development (Schratt et al, 2006)(Figure 1.8). Therefore, in addition to phosphorylation/dephosphorylation, LIMK activity may be regulated via the modulation of protein levels, further research will reveal whether these mechanisms also contribute to actin regulation in additional cell types.

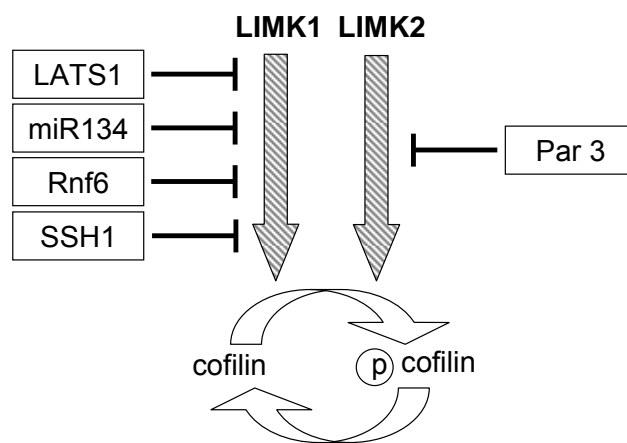


**Figure 1.8 LIMK Inhibitors.**

LATS1, miR134, Rf6 and SSH1 have each been shown to inhibit LIMK1 activity by different mechanisms as described in the text, reducing its ability to phosphorylate Cofilin. Par 3 has been shown to specifically inhibit LIMK2 kinase activity.

## 1.4 Cell biological functions

The most well characterised function of LIMK is the phosphorylation and consequent deactivation of Cofilin family proteins, which results in reorganisation of the actin cytoskeleton. A model describing the role of LIMK-mediated Cofilin phosphorylation on actin dynamics is found in Figure 1.2.

Given the importance of the actin cytoskeleton, it is perhaps not surprising that the LIM kinases play central roles in numerous biological processes, particularly in the regulation of cell morphology and motility. Additional more specialized activities also appear to be influenced by LIMK, for example, internalisation of fluorescently-labelled EGF into invasive tumour cells that over-expressed LIMK1 was markedly lower than mock transfected control cells (Nishimura et al, 2004), while over-expression of a dominant-negative LIMK1 or a non-phosphorylatable Cofilin restored EGF internalization in MDA-MB-231 cells that have elevated levels of endogenous LIMK1 (Nishimura et al, 2006).

Although LIMK is likely to contribute significantly to the morphology of numerous cell types, it is in the regulation of neuronal morphology and neuritogenesis where LIMK is particularly important. Some of the most compelling data comes from the *limk1* knockout mouse, in which neurons had reduced or absent growth cones and abnormal dendrite morphology (Meng et al, 2002). Genetic deletion of *limk2* did not affect neuronal morphology, but the double *limk1 limk2* knockout had a more pronounced neuronal phenotype than the single *limk1* deletion (Meng et al, 2004). Consistent with these results, expression of wild-type LIMK1 in cultured hippocampal pyramidal neurons induced growth cone formation and neuritogenesis at early time points (Rosso et al, 2004). However, at longer time points, LIMK1 expression led to retraction of growth cones and neurites, ultimately resulting in axon retraction. These results are similar to other studies reporting a role for LIMK in the retraction of growth cones and neurites (Endo et al, 2003) (Aizawa et al, 2001; Heredia et al, 2006). The seemingly contradictory conclusions of both positive and negative roles of LIMK in the regulation of neuronal morphology likely reflect a requirement for precise temporal and spatial LIMK regulation for proper development and maintenance of neuronal cytoarchitecture. Extrinsic factors that affect neuronal morphology include:

bone morphogenetic protein (BMP) 7, which acts via the BMP type II receptor (BMPRII) to activate LIMK1 and induce dendritogenesis (Lee-Hoeflich et al, 2004), Semaphorin 3A which activates LIMK1 to induce growth cone collapse (Aizawa et al, 2001) and fibrillar amyloid beta which activates LIMK to induce reorganization of actin filaments and neurite deformation (Heredia et al, 2006). The requirement for precise control of LIMK activity in the nervous system is reflected by additional layers of regulation including microRNA modulation of translation (Schratt et al, 2006) and proteasome-mediated degradation of LIMK1 (Tursun et al, 2005).

Cell cycle regulation appears to be influenced by LIMK at several points. In early stages of the cell cycle, it has been reported that LIMK2 mediates the ROCK-induced induction of cyclin A2 in fibroblasts (Croft & Olson, 2006). At later stages of the cell cycle, LIMK regulation of Cofilin is reported to contribute significantly to mitosis and cytokinesis. In cells synchronized in S phase by a double thymidine block, LIMK1 became hyperphosphorylated and activated in prometaphase and metaphase, gradually returning to basal levels of phosphorylation and activity as cells entered telophase and cytokinesis (Amano et al, 2002; Sumi et al, 2002). Cofilin phosphorylation mirrored the effects on LIMK1, with increased phosphorylation during prometaphase and metaphase, with a gradual return to basal levels during telophase and cytokinesis (Amano et al, 2002; Sumi et al, 2002). Interestingly, the increased LIMK1 activity could be blocked by the broad specificity cyclin-dependent kinase inhibitor Roscovitine, suggesting that CDKs may activate LIMK1 (Sumi et al, 2002). Consistent with these findings, SSH1 activity was decreased during early mitosis and returned to basal levels during telophase and cytokinesis (Kaji et al, 2003). Overexpression of LIMK1 or a phosphatase-inactive SSH1 resulted in increased levels of phospho-Cofilin and the production of multi-nucleated cells, an effect that could be rescued by overexpression of Cofilin in the case of inactive SSH1 (Amano et al, 2002; Kaji et al, 2003). In contrast, partial reduction of LIMK1 levels resulted in a G2/M cell cycle block (Davila et al, 2003). During interphase and prophase, LIMK1 was found associated with cell-cell adhesion sites, localizing at the spindle poles from prophase to metaphase (Sumi et al, 2006). LIMK1 disappears from these regions during late anaphase and appears again at the contractile ring and cleavage furrow during cytokinesis, where SSH1 was also found to accumulate

(Kaji et al, 2003). These results indicate that the effects on Cofilin phosphorylation during mitosis likely result from the concerted regulation of kinase and phosphatase activities, which together contribute to the processes of mitosis and cytokinesis.

In contrast to LIMK1, the activity of LIMK2 did not change after cells were released from an S phase cell cycle block (Sumi et al, 2006). However, when cells were treated with nocodazole or taxol to disrupt microtubules and induce an M-phase block, LIMK2 was activated suggesting that LIMK2 might be responsive to a spindle checkpoint. During prophase and prometaphase LIMK2 is concentrated at the centrosomes, associating with mitotic spindle microtubules during metaphase and early anaphase. As cells progress through late anaphase and telophase, LIMK2 localized at the spindle midzone where it was seen to co-localise with midzone microtubules. The distinct subcellular localization and activities displayed by LIMK1 and LIMK2 during the late stages of the cell cycle suggest that the two related kinases likely have different functions in mitosis and cytokinesis (Amano et al, 2002; Sumi et al, 2006; Yang et al, 2004a).

The regulation of gene transcription by the serum response factor (SRF) has been shown to be influenced by LIMK (Geneste et al, 2002; Sotiropoulos et al, 1999). By modulating the ratio of G-actin to F-actin through its actions on Cofilin, LIMK influences the nuclear translocation of the actin-binding SRF co-factor MAL (Miralles et al, 2003). When released from G-actin in the cytoplasm, MAL associates with SRF to promote the transcription of SRF target genes including vinculin, *cyr61* and SRF itself.

Identification of the transcription factors CREB (Yang et al, 2004a) and Nurr1 (Sacchetti et al, 2006) as LIMK1 substrates suggests that there may also be a direct link through LIMK to transcriptional regulation. In the case of CREB, which regulates expression of numerous “cyclin-AMP responsive” genes by binding to gene promoter cAMP-response elements, LIMK1 activation by basic fibroblast growth factor in immortalized hippocampal progenitor cells led to increased CREB phosphorylation and CREB-responsive promoter activity (Yang et al, 2004a). Nurr1 is an orphan member of the nuclear receptor family that regulate gene transcription via hormone response elements in promoter sequences. Purification of Nurr1 binding proteins from immortalized CSM14.1 mesencephalic

neurons identified LIMK1, further analysis revealed that LIMK1 phosphorylated Nurr1 leading to diminished transcriptional activity from a promoter/reporter construct (Sacchetti et al, 2006). The effects of LIMK1 were in opposition to the enhanced transcription induced by activated ERK2. The interaction of full-length LIMK1 with Nurr1 could be recapitulated with isolated LIM or kinase domains. Given that Nurr1 and LIMK1 each interact with p57Kip2 (Joseph et al, 2003; Yokoo et al, 2003), and both LIMK1 and p57Kip2 negatively regulate Nurr1 transcription activity, it is tempting to speculate that there might be a functional relationship between these three proteins. In addition to these, the microtubule bundling protein p25/TPPP has recently been identified as a novel substrate of LIMK (Acevedo et al, 2007). Future experiments will validate CREB and Nurr1 as LIMK targets, to reveal whether these additional substrates are cell-type specific, and potentially lead to the identification of further novel LIMK substrates.

## 1.5 Tissue distribution

Early studies on LIMK tissue distribution made use of RNA-based methodologies such as Northern blotting (Ikebe et al, 1998; Koshimizu et al, 1997; Mizuno et al, 1994) (Cheng & Robertson, 1995; Nunoue et al, 1995), RNase protection (Nomoto et al, 1999), RT-PCR (Ikebe et al, 1998) and in situ hybridization (Mori et al, 1997; Proschel et al, 1995) (Cheng & Robertson, 1995). Although these studies generally report widespread distribution of LIMK1 and LIMK2, the existence of multiple splice forms, which wasn't necessarily recognized in early studies, could complicate interpretation. As noted above, additional factors regulate LIMK protein stability and translation, meaning that mRNA expression does not necessarily reflect protein levels. Recent studies have made use of specific monoclonal antibodies to determine the patterns of LIMK1 and LIMK2 expression. LIMK1 was found to be expressed widely in embryonic and adult tissues, with notably high expression in the brain, kidney, lung, stomach and testis (Foletta et al, 2004). Similarly, LIMK2 was found to be expressed in almost all embryonic and adult tissues examined, with the exceptions of glial cells, kidney glomeruli and the testis, save for elongated spermatids (Acevedo et al, 2006). However, given that a testis-specific form of LIMK2 has been described (LIMKt) that lacks the amino-terminal LIM domains and half of the PDZ domain (Ikebe et al, 1998),

it is possible that a testis-specific form of LIMK2 which lacks the monoclonal anti-LIMK2 antibody epitope, is expressed in the spermatogonia, Sertoli cells, and primary and secondary spermatocytes (Acevedo et al, 2006).

## **1.6 LIMK in development and disease**

### ***1.6.1 Genetic deletion***

Despite the wide distribution of LIMK1 and LIMK2 expression, deletion of either gene resulted in relatively mild phenotypes in mice. Deletion of *limk1* led to abnormalities in synaptic structure and spine development most likely due to aberrant regulation of the actin cytoskeleton, and manifested behavioural alterations, such as a deficit in re-learning spatial information, similar to those observed in the human disorder Williams syndrome (Meng et al, 2002). Williams syndrome is a rare genetic disorder characterized by mild to moderate mental retardation or learning difficulties, with the most significant medical problem being cardiovascular disease caused by narrowed arteries (Meyer-Lindenberg et al, 2006). The syndrome has been mapped to deletion of chromosome 7q11.2, which contains more than 20 genes including LIMK1. Although it is possible that the deletion of LIMK1 is a major component of Williams syndrome, particularly the behavioural and developmental defects in the central nervous system, additional genes in this region may contribute to the overall spectrum of symptoms, such as *CYLN2* which codes for the microtubule-binding protein CLIP-115 (Hoogenraad et al, 2002) and the elastin gene *ELN* which plays a key role in arterial development (Li et al, 1998a; Li et al, 1998b).

Mice deleted for *limk2* had reduced spermatogenic ability, likely due to diminished viability and differentiation of spermatogenic germ cells (Takahashi et al, 2002). The reported restriction of LIMK2 expression to elongated spermatids (Acevedo et al, 2006) does not seem consistent with an apparently critical role of LIMK2 in spermatogenesis (Takahashi et al, 2002). One possibility is that the requirement for LIMK2 function are fulfilled by alternative forms of LIMK2 protein, such as LIMK2t (Ikebe et al, 1998), which might be undetectable with the anti-PDZ domain monoclonal antibody that was used to determine tissue expression patterns (Acevedo et al, 2006). The double *limk1/limk2* null

mice were more profoundly affected for impaired synaptic function than either single knockout, suggesting that there may be some compensation between the proteins (Meng et al, 2004). The fact that the double *limk1/limk2* knockout was not embryonic lethal suggests that either these kinases have very tissue specific functions and are relatively unimportant in most tissues, or that there is significant redundancy with other proteins, such as TESK1 or TESK2, for essential functions.

### **1.6.2 Cancer cell metastasis**

As tumour cells become metastatic, the normal mechanisms that control the actin cytoskeleton, cell shape and motility may be subverted so as to promote invasiveness. Numerous lines of evidence indicate that the LIM kinases play central and critical roles in tumour cell invasion and metastasis. It has been proposed that the balance between phosphorylated and non-phosphorylated Cofilin determines the metastatic potential of tumour cells. Consistent with this proposal, LIMK1 has been found to be overexpressed in malignant melanoma cells (Okamoto et al, 2005), breast cancer tumours (Bagheri-Yarmand et al, 2006) and tumour cell lines (Yoshioka et al, 2003), and in prostate tumours (Davila et al, 2003) and tumour cell lines (Davila et al, 2003) (Yoshioka et al, 2003) where increased phosphorylated Cofilin was also observed (Davila et al, 2003). In addition, LIMK1 and Cofilin were co-ordinately up-regulated in invasive carcinoma cells, relative to non-invasive cells, within primary mammary tumours (Wang et al, 2004). Ectopic overexpression of LIMK1 increased motility (Yoshioka et al, 2003), invasiveness and metastatic ability of human breast cancer cells (Bagheri-Yarmand et al, 2006) as well as promoted the acquisition of an invasive phenotype by benign prostate epithelial cells (Davila et al, 2003). Conversely, over-expression of Cofilin inhibited the invasiveness of human lung cancer cells (Lee et al, 2005) and the motility of glioblastoma tumour cells (Yap et al, 2005). However, it has also been reported that over-expression of LIMK1 kinase domain (Zebda et al, 2000) or siRNA-mediated knockdown of Cofilin1 or destrin (Hotulainen et al, 2005) reduced cell motility. These results suggest that perturbing the balance between phospho-Cofilin and non-phospho Cofilin, for example by inhibiting LIMK activity, would result in reduced invasiveness and metastasis. In support of this conclusion, it has been reported that interfering

with LIMK function by anti-sense mediated inactivation of LIMK1 in metastatic prostate cancer cells (Davila et al, 2003), by overexpression of a dominant negative form of LIMK1 in metastatic breast cancer cells (Yoshioka et al, 2003) or by ribozyme-mediated knockdown of LIMK2 in metastatic fibrosarcoma cells (Suyama et al, 2004) inhibited motility, invasiveness and/or metastasis. These data are consistent with the hypothesis that LIMK inhibition would effectively reduce cancer metastasis.

## 1.7 Cancer Metastasis

In order to metastasise, cancer cells must break down cell:cell contacts to detach from the initial tumour mass and acquire migratory and invasive capabilities. These cells must be motile, able to reorganise sites of cell-matrix adhesion and secrete proteinases to degrade paths through the extracellular matrix (ECM). The generated paths made by degradation and force facilitate invasion through local tissue, cells travel along paths of chemo-attraction to reach circulation in either lymph or blood (Yilmaz & Christofori, 2009). This process is similar to one that occurs during embryonic development, the transdifferentiation of epithelial cells into mesenchymal cells, known as epithelial-mesenchymal transition (EMT). EMT facilitates the organised movement of cells during development and involves the loss of epithelial cell traits including; loss of E-cadherin, plakoglobin, cytokeratins and dismantling of adherens junctions. As cells become more mesenchymal they gain a more elongated fibroblast-like morphology and invasive features such as the expression of;  $\alpha$ -smooth-muscle actin, N-cadherin, fibronectin and metalloproteinases (Gavert & Ben-Ze'ev, 2008; Hay, 2005). Motile invasive carcinoma cells use a mesenchymal-like state to facilitate migration and invasion and have been found to share some of the key phenotypic and molecular characteristics of EMT (Gavert & Ben-Ze'ev, 2008) (Yilmaz & Christofori, 2009).

Initial stages of metastasis involving the breakdown of cell:cell junctions and detachment from the primary tumour are tightly associated with EMT, but once individual cells move away their motility is not solely limited to the mesenchymal form. Cells can also move in an amoeboid manner and change

between the two forms dependent on extracellular factors or intracellular signalling.

## 1.8 Individual cell invasion

Cells can invade using either amoeboid or mesenchymal modes of motility, interchanging between the two depending on the up or down regulation of specific molecular pathways governing the mode of motility. While EMT is quite a rigid process requiring extensive changes in gene transcription, switching between mesenchymal and amoeboid forms of motility (and vice versa) is more easily achieved and is probably used to facilitate movement at different stages of metastasis depending on the demands of the microenvironment (Pankova et al, 2009).

Mesenchymal cell migration is similar to fibroblast-like motility, cells are elongated and spindle like, and in 3D are polarised with leading pseudopods and a lagging cell body (Figure 1.9 part A). Mesenchymal cells move by the formation of actin rich filopodia and lamellipodia at the leading edge, driven by Rho GTPases Rac and Cdc42 (Daisuke et al, 2005). Cells attach to the ECM at both ends of the cell, clustering integrins which give rise to focal adhesions. Proteolytic enzymes such as matrix metalloproteases are then recruited to the focal adhesions (Brooks et al, 1996) and lead to ECM degradation and remodelling to generate a cell path.

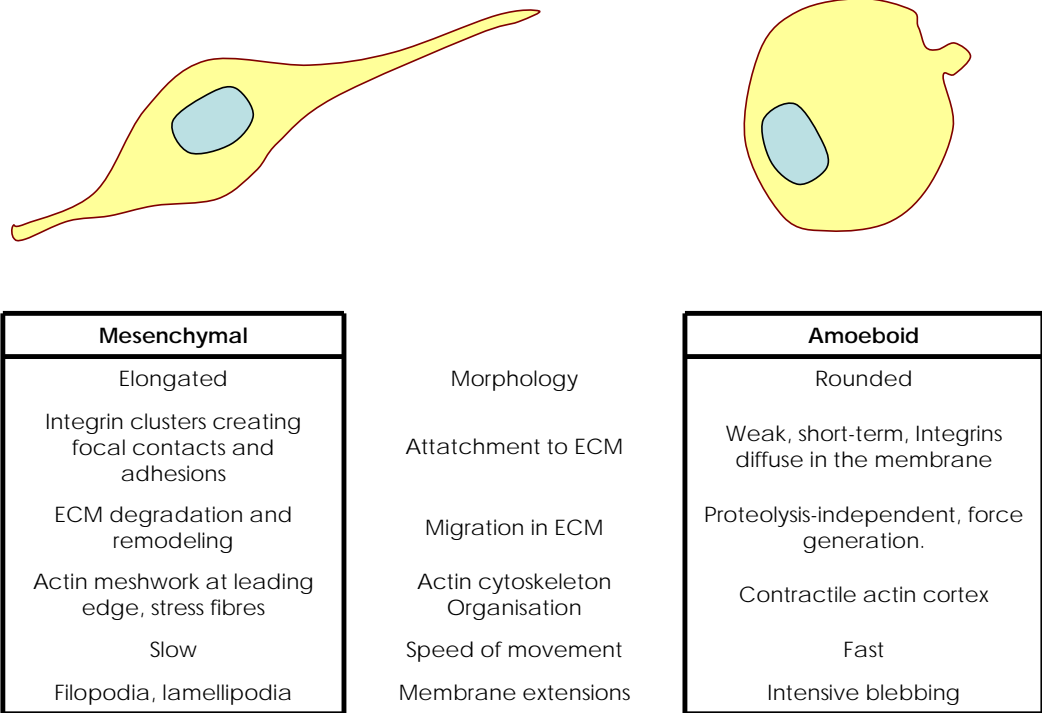
Amoeboid motility is characterised by cycles of expansion and contraction of the cell body, mediated by cortically localised actin and myosin (Pankova et al, 2009). Amoeboid motility is independent of ECM degradation, cells squeeze through existing gaps in the ECM without clustering integrins or concentrating proteinases to sites of adhesion (Wolf et al, 2003). This method of motility is promoted by Rho/ROCK signalling and the tension maintained by cortical actomyosin promotes membrane blebbing which contributes to cell motility (Keller & Egli, 1998). The low levels of attachments made by amoeboid migrating cells is believed to allow them to move at higher velocities through 3D environments than their mesenchymal counterparts (Pankova et al, 2009).

When mesenchymal HT1080 and MDAMB231 cells were subject to protease inhibitors in 3D they changed from an elongated morphology to a more rounded amoeboid morphology and mode of motility (Wolf et al, 2003). It has also recently been proposed that Rab5 may play a role in the process of amoeboid to mesenchymal transition of cancer cells (Palamidessi et al, 2008). These findings suggest that migrating cancer cells can compensate to environmental factors, changing from a mesenchymal 'path generating' form of motility to an amoeboid 'path finding' mode (Wolf et al, 2003).

## **1.9 Collective cell invasion**

The ability of tumor cells to move through tissues is the outcome of two processes: extracellular matrix (ECM) deformation/degradation to generate a path of reduced mechanical resistance, and cell motility to follow the path. Although considerable recent effort has been directed understanding how tumor cells invade three-dimensional environments as individual cells, epithelial cancer cells commonly invade collectively in strands, sheets and clusters, particularly in highly differentiated tumours that maintain epithelial characteristics (Friedl & Wolf, 2008). The cell collective may remain in contact with the primary mass, or may detach and spread away from the primary site. In this form of invasion, leading cells generate paths of low physical resistance by focalizing protease activity and/or generating force to remodel the extracellular matrix for the remainder of the collective to follow. Therefore, distinct cells in strands may have different roles; for example path generation which would require ECM remodelling activities such as those attributed to cells using a mesenchymal mode of motility, whereas path following cells which would only require more amoeboid features for cell motility (Friedl & Wolf, 2008; Wolf et al, 2003) see Figure 1.10.

A.



B.

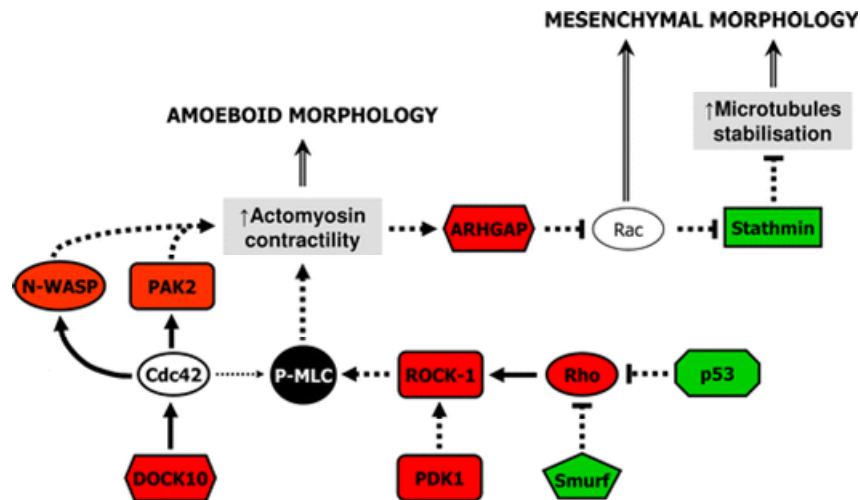
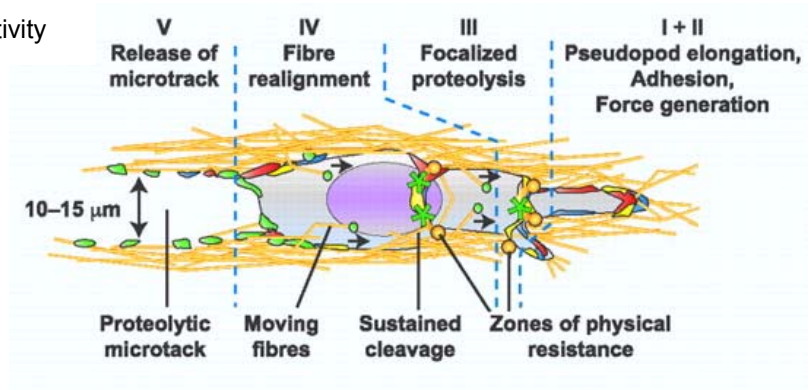


### Figure 1.9-Mesenchymal vs. Amoeboid invasion.

A. A comparison of the main phenotypic characteristics of the mesenchymal and amoeboid modes of invasion. Mesenchymal cells are elongated and polarised and degrade the ECM, amoeboid cells are rounded in morphology and move in a proteolysis independent manner. *Adapted from (Pankova et al, 2009)* B. Interactions among the components of signaling pathways documented to be involved in the MAT/AMT transitions of cells in a 3D environment. The inhibition of the activity of the proteins highlighted in red was shown to trigger amoeboid to mesenchymal transitions. Inactivation of the proteins depicted in green induces a conversion from the mesenchymal to the amoeboid mode of invasiveness. Solid lines direct connections, dashed lines indirect connections. *Figure taken from (Pankova et al, 2009).*

A

Zones of activity



B

Zones of activity

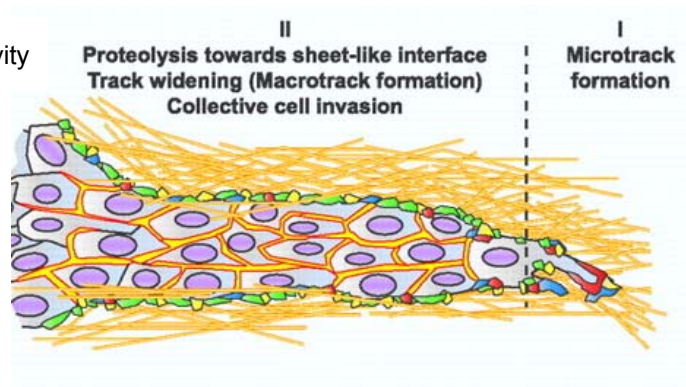


### Figure 1.10- Individual vs. Collective invasion

A. Individual invasion. Single-moving proteolytic cells cause ECM reorganisation. After protrusion of an anterior pseudopod (*step I*) and traction force generation (*step II*), focal cleavage of individual ECM fibers is executed slightly backward to leading adhesion sites (*step III*). Transport of loose fiber ends (*step IV*) results in a small microtrack detected upon forward gliding of the cell rear (*step V*). B. Collective invasion. ECM reorganisation is executed by multiple cells that collectively fill a small pre-existing tissue gap while remaining connected. By focalizing proteolytic activity toward the cell-ECM interface, a near-continuous ECM layer is generated and further cleaved. *Yellow*, proteases and MT1-MMP; *green*, degraded collagen; *blue*,  $\beta 1$  integrin; *red*, Filamentous-actin. *Figure taken and adapted from (Friedl & Wolf, 2008).*

## 1.10 Role of the actin cytoskeleton in invasion

Motility required for cancer cell metastasis is driven by remodelling of the actin cytoskeleton and cell:ECM contacts. RhoGTPases are regulators of both the actin cytoskeleton and cell adhesion (Sahai & Marshall, 2003). Activated Rac and Cdc42 induce cytoskeleton reorganisation at the leading edge of cells, from which localised actin polymerisation pushes the polarised cell membrane forward in filopodia or lamellipodia, propelling the cell forward (Nobes & Hall, 1995). Actin polymerisation from globular actin subunits (G-actin) into filamentous actin (F-actin) is then used by the cell to form either branched filaments, for sheet like protrusions, or bundled filaments for spike like membrane protrusions (Insall & Machesky, 2009). Branched filament networks are assembled by the Arp2/3 complex, an assembly of 7 subunits that include two actin related proteins Arp2 and Arp3 and five non-Arp components, p41/ARPC1, p34/ARPC2, p21/ARPC3, p20/ARPC4 and p16/ARPC5 (Machesky & Gould, 1999). Arp2/3 promotes the formation of new branches of F-actin at 70° from the original filament. Formins, on the other hand, are dimers that mediate the elongation of unbranched F-actin. Both formins and the Arp2/3 complex utilise profilin to recruit monomeric actin to the growing 'plus' ends of filaments (Figure 1.11). Wasp proteins, WASP, N-WASP, and WAVE1-3 disseminate extracellular signals to the actin reorganisation machinery. They regulate membrane protrusions by VCA binding of the Arp2/3 complex, a multi domain module of the WASP family consisting of a verprolin-homology domain (V), a Cofilin-like (C) and an acidic domain (A). This binding activates the Arp2/3 complex, catalysing Arp2/3 mediated actin polymerisation (Daisuke et al, 2005).

Growing filaments push the cell membrane forward, moving the cell. Contractile acto-myosin filaments, regulated by Rho through downstream effectors such as ROCK, pull in the tail of the cell and promote the translocation of the cell body (Daisuke et al, 2005). Coordinated protrusion of the leading edge and retraction of the tail of the cell results in forward movement of the cell.

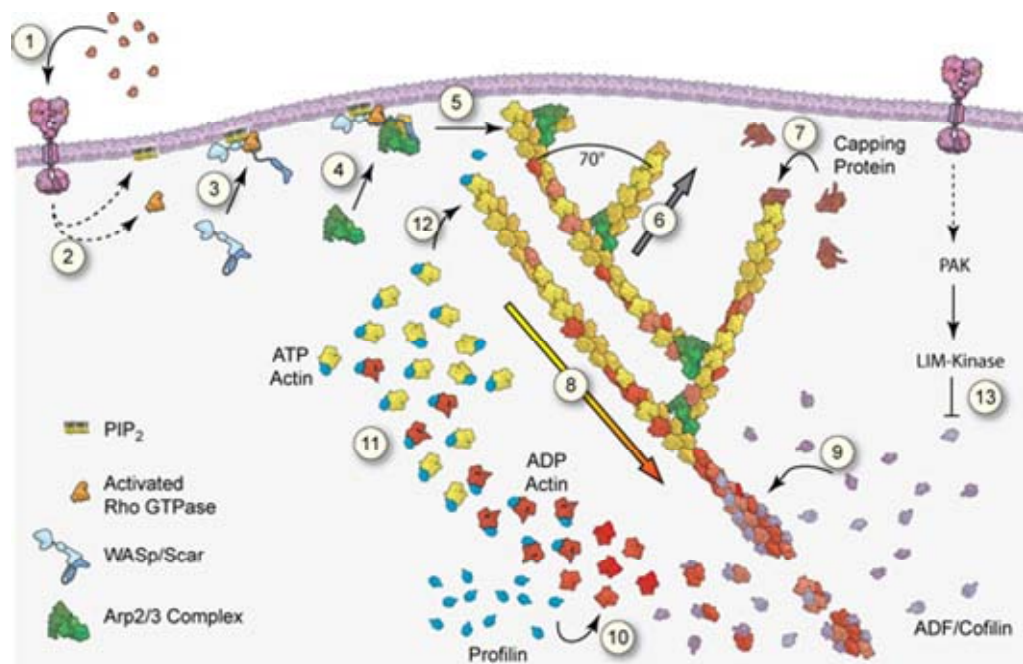


### Figure 1.11 Actin cycling at the leading edge

Cells move through the rapid rearrangement of the actin cytoskeleton. In the, (1) several signaling pathways (2) converge to (3) activate WASp/Scar proteins, which in turn (4) activate the Arp2/3 complex. (5) Active Arp2/3 complex binds to the side of an existing filament and nucleates (6) new filament growth towards the cell membrane. The combined force from many growing filaments pushes the cell membrane forward, moving the cell. Actin binding proteins, including (7) capping protein, (9) ADF/cofilin, (10) profilin, tropomyosin, formins, and Ena/VASP, modulate these events. Figure taken from the Website of J.Kuhn [www.biol.vt.edu/faculty/kuhn/research.html](http://www.biol.vt.edu/faculty/kuhn/research.html).

## 1.11 Invadopodia

Invadopodia and podosomes are both forms of actin rich protrusions that attach to and degrade the cellular substrate. Invadopodia and podosomes contain an actin core with proteins important for actin nucleation (WASP, N-WASP, WIP, Cortactin and the ARP 2/3 complex), this core is surrounded by integrins and associated proteins such as vinculin, talin and paxillin (Mueller et al, 1992; Desai et al, 2008; Albiges-Rizo et al, 2009). The integrins and integrin associated proteins form an 'adhesive ring' colocalising with part of the polymerised actin (the 'actin cloud') to cluster rings or chains of invadopodia or podosomes together (Albiges-Rizo et al, 2009). Figure 1.12, adapted from Albiges-Rizo et al, outlines the locations of these proteins and the manner in which invadopodia and podosomes are formed.

Invadopodia are more associated with carcinoma cells whilst podosomes are considered to be more common in monocytic cells such as macrophages and osteoclasts. Podosomes typically occur in cells such as osteoclasts as evenly spaced 'polka dots' or in rosette formations, whilst invadopodia are typically more condensed in small clusters in carcinoma cells (Linder et al, 2007). Podosomes are rapidly turned over, as fast as 2-4 minutes whereas invadopodia are thought to be longer lived, up to 30 minutes (Ochoa et al, 2000; Destaing et al, 2003; Badowski et al, 2003). There is some speculation that podosomes may be the precursors of invadopodia, and Src has been used to speed up the turnover of invadopodia to times similar to podosomes, but there is little evidence to show a mechanism by which to transform podosome structures into more aggressive invadopodia. Cofilin localises to invadopodia and is important for formation of free barbed ends in these cellular structures (Oser et al, 2009; Yamaguchi et al, 2005). Cofilin is believed to cycle between two compartments near invadopodia, the F-actin and cytosol compartments (Oser and Condeelis 2009). When bound to cortactin in the F-actin compartment Cofilin is inactive. Following Cortactin tyrosine phosphorylation Cofilin is no longer inhibited and is able to sever actin filaments, leading to the generation of barbed ends (as outlined in Figure 1.11) and actin polymerisation. Cofilin is then inactivated by phosphorylation by LIMK until Cofilin and Cortactin are dephosphorylated and the cycle begins again (Oser and Condeelis 2009).

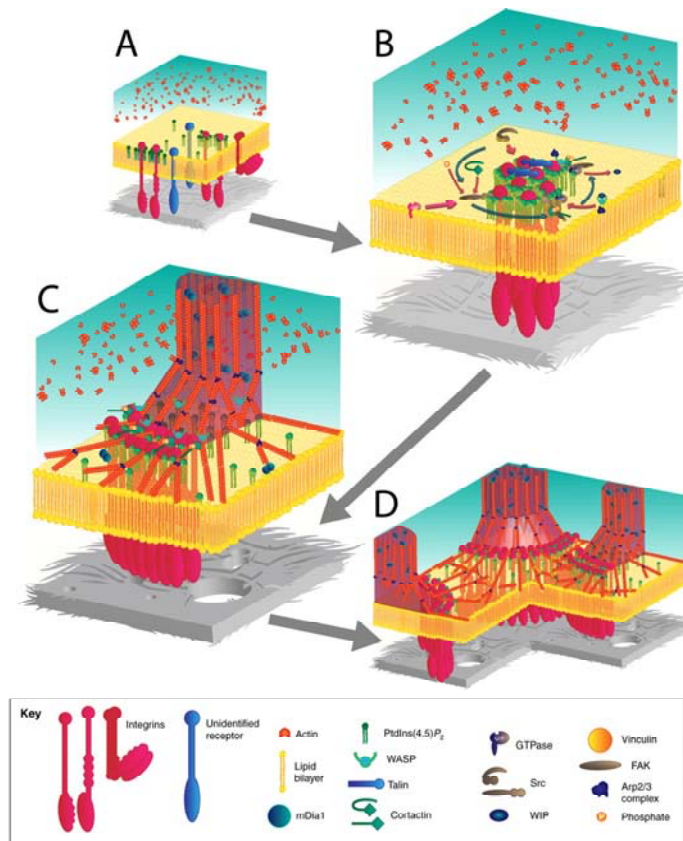


**Figure 1.12 Schematic view of signalling pathways that lead to actin organisation at invadopodia or podosomes.**

A. At the initial stage of adhesion formation, integrins or other unidentified receptors bind to components of the ECM (grey), leading to clustering of receptors into PtdIns(4,5)P<sub>2</sub>-enriched areas of plasma membrane. B. Recruitment of Src to adhesion sites leads to phosphorylation of several proteins such as cortactin, WASP, FAK and regulators of small GTPases. Continuous actin nucleation relies on the continuous and strong activation of the Arp2/3 complex at the membrane through the synergistic action of cortactin and WASP-family proteins. C. DRF/mDia1 elongates actin filaments into columnar structures from the branched actin network that was previously induced by N-WASP, the Arp2/3 complex and cortactin. D. Podosomes or invadopodia are mechanically connected through a network of radial actin filaments that lie parallel to the substratum.

## 2 Materials and Methods

### 2.1 Chemicals and Reagents

All Chemicals were purchased from Sigma-Aldrich or Fisher Scientific UK unless stated otherwise.

### 2.2 Bacterial techniques

#### 2.2.1 Reagents

Agarose gel DNA loading buffer (10X)	20 mM EDTA, 0.05% (w/v) bromophenol blue, 50% v/v glycerol	
Ampicillin		<i>Sigma-Aldrich</i>
Chloramphenicol		<i>Sigma-Aldrich</i>
DNA Ladder	100bp and 1kb	<i>Invitrogen</i>
LB Agar	1% w/v bacto tryptone, 86 mM NaCl, 0.5% w/v yeast extract, 1.5% w/v agar,	<i>Beatson Institute</i> <i>Central Services</i>
LB medium	1% w/v bacto tryptone, 85.5 mM NaCl, 0.5% w/v yeast extract	<i>Beatson Institute</i> <i>Central Services</i>
TBE	89 mM Tris Base, 89 mM boric Acid, 3.2 mM EDTA	

#### 2.2.2 Enzymes and kits

DNA polymerase and 10x reaction buffer	<i>Stratagene</i>
DNA Purification Kit	<i>QIAGEN</i>

Ethidium Bromide	<i>Invitrogen Ltd</i>
QIAGEN Plasmid Maxi Kit	<i>QIAGEN</i>
QIAprep Spin Mini-Prep Kit	<i>QIAGEN</i>
QIAquick Gel Extraction Kit	<i>QIAGEN</i>
QuikChange® Multi Site-Directed Mutagenesis Kit	<i>QIAGEN</i>
Rapid DNA Ligation Kit	<i>Roche</i>
Restriction enzymes and reaction buffers	<i>Invitrogen Ltd</i>
Restriction enzymes and reaction buffers	<i>New England Biolabs Ltd</i>
Shrimp Alkaline Phosphatase	<i>Promega</i>
SybrGreen (10000X stock)	<i>Invitrogen Ltd</i>

### **2.2.3 Bacterial strains**

All cloning was undertaken in *E. Coli* DH5 $\alpha$ . Recombinant protein synthesis was performed in *E. Coli* BL21 (P Lys). Both were supplied by the Beatson Institute Central Services.

### **2.2.4 Bacterial Transformation and culture**

*E. coli* DH5 $\alpha$  competent cells were thawed on ice and 50 $\mu$ l mixed with 2 $\mu$ l of plasmid DNA (various concentrations) or ligation reaction in a pre-chilled polypropylene tube. After incubation on ice for 45min, cells were subjected to heat-shock at 42°C for 45 seconds and then chilled on ice for a further 2 minutes before the addition of 180 $\mu$ l of SOC medium and incubation at 37°C whilst shaking. The transformation mixture was spread onto LB agar plates containing appropriate antibiotics and incubated overnight at 37°C.

Single bacterial colonies were picked from LB-agar plates and inoculated into 5ml of LB medium containing the appropriate antibiotics, this culture was then grown overnight at 37°C whilst shaking. For long-term storage, 500µl of this bacterial culture were mixed with 500µl of sterile glycerol in a cryo-tube for storage at -70°C.

### **2.2.5 Small-scale plasmid DNA preparation**

1.5ml of an overnight bacterial culture was pelleted by centrifugation at 3000rpm for 5min in a micro-centrifuge. The pellet was resuspended and processed using the QIAprep Spin Mini-Prep Kit according to the manufacturer's instructions. The eluted DNA was stored at -20°C.

### **2.2.6 Large-scale plasmid DNA preparation**

100ml of bacterial overnight culture was pelleted by centrifugation at 3500rpm for 20min at 4°C in a Beckman Coulter J6-M1 centrifuge (JS-4.2 series rotor). The pellet was resuspended and processed using the QIAGEN Plasmid Maxi Kit according to the manufacturer's instructions. The concentration and purity of the eluted DNA was determined using an Eppendorf biophotometer. The DNA was stored at -20°C.

### **2.2.7 Quantification of DNA**

Double stranded DNA was quantified using an Eppendorf biophotometer. Nucleic acid solutions were diluted in H<sub>2</sub>O before reading at an absorbance of 260nm.

### **2.2.8 Plasmids**

Plasmids used throughout this thesis are listed below in Table 1.

**Table 1 Plasmids**

Plasmid	Mutant used
pGEX-KG-hCofilin	WT, S3A, S3E, Tr (truncated)
mRFP-C3-6xG	
pBABE Puro hLIMK hER	WT, E, EE
pCMV6, pCMV6 -XL4 LIMK2a	
pCDNA 3.1, pCDNA 3.1 LIMK1	
pMAX GFP	

## **2.2.9 Cloning protocols**

### **2.2.9.1 Restriction enzyme digestion**

DNA restriction digests were performed using the appropriate restriction enzyme and the corresponding reaction buffer from Invitrogen or New England Biolabs Inc. Typically, 1µg plasmid DNA or 10 µl PCR amplified fragment was added to 1 unit (U) of restriction enzyme, 2µl appropriate 10X reaction buffer and the volume adjusted to 20µl with H<sub>2</sub>O. Digestion was carried out at the appropriate temperature recommended by the manufacturer, usually for around 2 hours.

### **2.2.9.2 Phosphatase Treatment**

Digested vector DNA in ligation reactions was treated with Shrimp Alkaline Phosphatase to remove 5' phosphate groups and prevent vector re-ligation. One unit of phosphatase was added per 20µl of restriction digest along with the appropriate volume of reaction buffer.

### **2.2.9.3 Agarose gel electrophoresis**

Gels for DNA electrophoresis were composed of 1% (w/v) ultra pure electrophoresis grade agarose in 1xTBE buffer and 2µg/ml ethidium bromide (except in cases where 1µl of a 1:400 dilution of SybrGreen was added to the sample, in which case no ethidium bromide was required in the gel). Once set the gels were placed in a horizontal gel apparatus from Stratagene containing 1xTBE running buffer. DNA samples were diluted in 1x DNA loading buffer and loaded alongside suitable DNA ladder markers in the outermost wells of the gel (for gels without ethidium bromide 1µl of 1:400 SybrGreen was added to each sample). Electrophoresis was performed at 80-100V and the DNA visualised using a UV trans-illuminator (UVB).

### **2.2.9.4 Acrylamide gel for DNA**

A non-denaturing acrylamide gel can be used to visualise annealed oligonucleotides. These gels were set up using 6.6ml 10% acrylamide (19:1 40% ratio), 13.28ml 1X TBE, 0.1 ml 0.05% APS and 0.02ml 0.1% TEMED up to 20 ml

final volume and the comb added directly to this as there is no separate stack. 1X TBE was used as running buffer and samples of forward, reverse and annealed oligonucleotides were prepared with DNA sample buffer and loaded next to an appropriate ladder. The gel was run at 100V until the bromophenol blue was two thirds of the way down the gel, then transferred to a tray with 10µl of 1mg/ml EtBr in 100mls of 1X TBE for 30 minutes for visualisation.

### **2.2.9.5 DNA Purification**

DNA from restriction digests or PCR reactions was purified using the QIAquick PCR purification Kit according to the manufacturer's instructions. In brief, the DNA fragment was cut from the agarose gel using a clean scalpel, placed in an eppendorf and weighed. Three volumes of QG buffer was added to one volume of gel and the mixture incubated on a heat block at 50°C for 10 minutes (or until the gel slice dissolved). One gel volume of isopropanol was then added to the sample and mixed, and the whole sample spun through a QIAquick column for 1 minute to bind DNA. Washes were performed with the appropriate buffers and the DNA eluted in EB buffer.

### **2.2.9.6 Phosphorylation and Ligation**

T4 kinase was used to phosphorylate annealed oligonucleotides in standard 30µl reactions. In brief, 20 U of T4 kinase (2µl), 1 µg annealed oligonucleotides (15ul), 3µl of ligation buffer (as ligation follows on from this reaction) and 10ul of nuclease free water were mixed and incubated at 37°C for 30 minutes, then 65°C for 20 minutes before ligation.

Ligation reactions were performed using T4 DNA ligase. In brief, 1 U of T4 DNA ligase with 1X T4 buffer and a 3-fold excess of phosphatased vector to insert DNA were incubated at 25°C for at least 2 hours.

### **2.2.10 *Generation of fragments by PCR***

Each standard 50µl reaction contained 20ng of plasmid DNA template, 25ng of each oligonucleotide primer, 2 U Vent DNA polymerase, 1X Thermopol buffer and 0.2mM dNTPs. PCR programme followed 96°C 30 seconds, 50°C 30 seconds, 72°C

1 minute for 25 cycles and the samples were then run on agarose gels for analysis.

### **2.2.11      *Annealing oligonucleotides***

Complementary oligonucleotides were mixed together at a 1:1 molar ratio in a micro-centrifuge tube and diluted to a final concentration of 1 pmol/ $\mu$ l with a Tris buffer containing salt; 10 mM Tris, 1 mM EDTA, 50 mM NaCl. A large glass beaker of water (400 ml) was brought to the boil and the small tube of oligonucleotides placed in the boiling water, then left to slowly cool to room temperature.

### **2.2.12      *Cloning***

DNA fragments for cloning amplified using oligonucleotide primers. Following PCR, samples were purified by agarose gel electrophoresis and spin columns before digestion and ligation as described. Constructs subject to cloning procedures were sequenced to identify desired clones; sometimes these were prescreened by 'wiggles'.

### **2.2.13      *PCR directly from Bacteria***

A PCR-based approach for screening antibiotic resistant bacterial colonies transformed from ligation reactions for positive clones. A single bacterial colony was picked with a sterile pipette tip and sequentially dipped in a standard PCR reaction and dropped into 15ml round bottomed tube containing 3ml of LB media. In general wiggle reactions used a 5' oligonucleotide specific to the vector backbone, and a 3' oligonucleotide specific to the insert to be sub-cloned in order to identify positive clones with the correct insert orientation. Following agarose gel electrophoresis to identify clones from which the correct size product was amplified, the corresponding bacterial cultures of these positive clones were amplified and plasmid DNA isolated as described.

### 2.2.14 *Mutagenesis*

Mutagenesis of both LIMK1 and Cofilin 1 was performed using the QuickChange site-directed mutagenesis kit from Stratagene, exactly as described in the manufacturers instructions. The oligonucleotides used were designed following the manufacturers guidelines and are described in the Table of oligonucleotides. Briefly, sample reactions contained 5µl 10X reaction buffer, 5µl (50ng) of template DNA, 1µl (125 ng) of forward primer, 1µl (125 ng) of reverse primer, and 1µl (10 nM) dNTP mix and made up to 50µl of dH<sub>2</sub>O before the addition of 2.5 U (1µl) *Pfu Turbo* DNA polymerase and thermal cycling was programmed on the PCR machine as follows;

Segment 1	1 cycle	95 °C	0.5 minutes
Segment 2	18 cycles	95 °C	0.5 minutes
		55 °C	1 minute
		66 °C	1 minute per kb of plasmid
			(e.g. 9minutes for LIMK:ER mutagenesis)
Segment 3	1 cycle	4 °C	Until recovered

Following generation of nicked circular strands that incorporate the mutant oligonucleotides, methylated parental DNA was digested with 10U *DpnI* restriction enzyme per sample at 37 °C for 1 hour. The remaining circular double stranded mutant DNA was then transformed into DH5α as described. Five to ten colonies were picked per mutant, the DNA purified and the insert sequenced to identify clones with the desired mutation. Usually around four out of five positive clones were identified using this technique.

To create a truncated Cofilin 1 initially a gradient block PCR reaction was performed to identify optimal PCR conditions. Each sample reaction contained 2.5µl 10X *Picomaxx* reaction buffer, 1µl of template DNA, 1µl (125 ng) of forward primer, 1µl (125 ng) of reverse primer, and 1µl (10 nM) dNTP mix and made up to

25µl of dH<sub>2</sub>O before the addition of 2.5µl *Picomaxx Taq* (hot start reader) DNA polymerase. Using the T<sub>m</sub> values of the oligonucleotides (designed to truncate the Cofilin1 insert) minus 4°C as top and bottom temperatures a gradient block PCR programme was set up to give a range of 6 different annealing temperatures as follows:

Segment 1	1 cycle	95 °C	5 minutes
Segment 2	34 cycles	94 °C	45 seconds
		50 °C - 62 °C	45 seconds
		72 °C	3 minutes
Segment 3	1 cycle	72 °C	7 minutes
Segment 4	1 cycle	4 °C	Until recovered

Products were then run on a 1% agarose gel to identify the optimal temperature for PCR. The remaining product from the optimal temperature was run on a 1% agarose gel, excised and purified as described and sequenced to confirm the correct truncations had been performed.

### **2.2.15 Sequencing**

Plasmid inserts were sequenced by Beatson Molecular Technology Services. Routine sequencing of plasmids or PCR products by this service was performed on an Applied Biosystems 3130xl (16 capillary) sequencer. The Applied Biosystems (BigDye 3.1) DNA sequencing protocol was used for the setup of sequencing reactions, precipitation of sequenced DNA and preparation for loading into the sequencer. The service analysed the sequencing data before releasing the sequencing data to help troubleshoot or solve any sequencing failures.

## 2.2.16 Primers

Oligonucleotides and Primers generated and used in this project are detailed below in Table 2.

**Table 2 Oligonucleotides and Primers**

	5' -3'
LK1 Bam For (LIMK1 sequencing)	GGG GGA TCC ATC GAC AGG TCT CCG
LK1 Eco Rev (LIMK1 sequencing)	GGG GAA TTC CGT CGG GGA CCT CAG GGT G
Cofilin Val7 for (sequencing)	GGG GCC ATG GTC TCT GAT GGT GTC
Cofilin Asp9 for (sequencing)	GGG GCC ATG GAT GGT GTC ATC AAG
TAT FLAG Forward (generation of TAT Cofilin protein)	AAT TTA TGC GCG TGC GGC GGC GCG TCA GGC GCG TGC GGG TGG TGA TTA TAA AGA TGA TGA TGA TAA AGC
TAT FLAG Reverse (generation of TAT Cofilin protein)	CAT GGC TTT ATC ATC ATC ATC TTT ATA ATC ACC ACC CGC ACG CGC CTG ACG CGC CGC CGC ACG CGC ATA
Cofilin S3E forward (SDM)	CTA GAC TCC ATG GCC GAA GGT GTG GCT GTCC TC
Cofilin S3E Reverse (SDM)	GAG ACA GCC ACA CCT TCG GCC ATG GAG TCT
PTD Cofilin S3E forward (SDM)	GAT AAA GCC ATG GCC GAG GGT GTG GCT GTC TC
PTD Cofilin S3E Reverse (SDM)	GAG ACA GCC ACA CCC TCG GCC ATG GCT TTA TC
Cofilin S3A forward (SDM)	CTA GAC TCC ATG GCC GCT GGT GTG GCT GTCC TC
PTD Cofilin S3E forward (SDM)	GAT AAA GCC ATG GCC GCT GGT GTG GCT GTC TC

## 2.2.17 Recombinant protein preparation

### 2.2.17.1 Buffers and reagents

PBS lysis buffer	PBS with 1mM PMSF
Protein production Buffer A	PBS with 50mM Tris pH7.5, 150mM NaCl, 3mM DTT
Thrombin cleavage buffer	PBS with 50mM Tris pH7.5, 150mM NaCl, 1 mM

	MgCl <sub>2</sub> , 1 mM CaCl <sub>2</sub> , 3 mM DTT	
p-aminobenzamidine beads	Washed in buffer A	<i>Sigma</i>
Protein A-Sepharose 4B	Washed in buffer A	<i>Sigma</i>
10ml columns	731-1550	<i>Bio-Rad</i>
Centrifugal Filter Devices	Ultracel YM-3, 3000 MWCO	<i>Microcon</i>

### 2.2.17.2 Protein preparation

For large scale protein production, single bacterial colonies of, for example, pGEX-KG COFILIN (WT) in BL21 (DE3) pLyss cells were cultured in six 50 ml batches of Terrific broth with 100 µg/ml ampicillin. Overnight cultures were each diluted 1:10 into one of six flasks containing 500 ml Terrific broth including 100 µg/ml ampicillin and grown to OD<sub>600</sub> 0.6 to 1.0 at 37°C before inducing with 100 µM IPTG for 3 hours at 37°C. Cells were pelleted by centrifugation in a Beckman Coulter J6-M1 centrifuge, resuspended in 5 ml of phosphate buffered saline (PBS) lysis buffer [PBS with 1 mM Phenylmethylsulphonylfluoride (PMSF)] and snap frozen in a dry ice/ethanol solution. At this point, samples could have been stored at -80 C indefinitely. After thawing in a 37°C water bath, samples were kept on ice while being disrupted by three 1 minute rounds of sonication at 20% intensity using a Branson Digital Sonifier, followed by removal of debris by centrifugation at 10,000 *g* for 20 minutes at 4°C (9092 rpm using a Beckman Avanti J-25 centrifuge with a JA 25.50 rotor). Clarified supernatants were incubated with 0.5 ml of protein production buffer A [PBS with 50mM Tris pH7.5, 150mM NaCl, 3mM DTT] washed glutathione-Sepharose (Sigma) bead slurry overnight at 4°C to bind GST fusion protein [this can be done in a 10ml capped column (Bio-Rad #731-1550), following overnight rotation the cap can be removed and washes performed through the column] . Beads were then washed six times with 50 ml of buffer A, followed by two washes with 50 ml of thrombin cleavage buffer [ 50mM Tris pH7.5, 150mM NaCl, 1 mM MgCl<sub>2</sub>, 1 mM CaCl<sub>2</sub>, 3 mM DTT in PBS]. The beads were resuspended in 0.5 ml of thrombin cleavage buffer and Cofilin released from the GST moiety by incubation with 25 units of bovine thrombin (Sigma) overnight at 4°C. The supernatant was removed, beads were

washed twice with 0.5 ml buffer A and the collected supernatants were incubated with 30  $\mu$ l of buffer A-washed p-aminobenzamidine beads (Sigma) for 1 hour at room temperature ( $\sim 20^{\circ}\text{C}$ ) to remove thrombin, before snap freezing aliquots and storing at  $-80^{\circ}\text{C}$ .

Protein concentration was determined using BCA protein assay kit (Sigma), and assessment of expression and purification of prepared was achieved with 1  $\mu$ g, 3  $\mu$ g and 10  $\mu$ g samples of protein with parallel samples of BSA at the same concentrations in 20  $\mu$ l [samples prepared with 6x sample buffer and PBS] and 10  $\mu$ l SDS-Page broad range standards (Bio-Rad) on 10% SDS-poly-acrylamide gels. Gels were stained with SimplyBlue Safe Stain and images acquired at 700nm with a Li-Cor Odyssey infrared imaging system.

## 2.3 Mammalian cell culture techniques

All cell culture work was performed using aseptic techniques inside a laminar flow hood.

### 2.3.1 Reagents

0.05% Trypsin EDTA	<i>GIBCO</i>
200mM L-Glutamine (100x)	<i>GIBCO</i>
6.5mm Transwells, 8.0um pore size	<i>ThermoScientific</i>
Calcein AM	<i>Invitrogen</i>
Cell line nucleofector kit V	<i>Amaxa</i>
Complete Matrigel	<i>BD Biosciences</i>
DMEM (Dulbecco's Modified Eagle's Medium)	<i>GIBCO</i>

ECL Western Blotting Detection Reagents	<i>GE Healthcare</i>
Foetal Bovine Serum	<i>Autogen Bioclear</i>
Growth Factor Reduced Matrigel	<i>BD Biosciences</i>
Lipofectamine 2000 Reagent	<i>Invitrogen</i>
Oligofectamine Reagent	<i>Invitrogen</i>
OptiMEM 1 (Reduced Serum Medium)	<i>Invitrogen</i>
Oris Cell Migration Assay	<i>Oris</i>
Penicillin Streptomycin	<i>GIBCO</i>
Poly-L-Lysine	<i>Sigma-Aldrich</i>
Puromycin	<i>Sigma-Aldrich</i>
RPMI	<i>GIBCO</i>
Sodium pyruvate 100mM	<i>GIBCO</i>
Sterile distilled water	<i>Beatson Institute Central Services</i>
Ascorbic acid	<i>Sigma</i>
2% Gelatine (G1393)	<i>Sigma</i>
10 ug/ml DNase I	<i>Roche</i>
CDM Extraction buffer	<i>20 mM NH<sub>4</sub>OH, 0.5% Triton X-100 in PBS</i>

Sterile PBS (Phosphate Buffered Saline) *Beatson Institute Central Services*

### **2.3.2 Growth conditions**

BE human colon carcinoma cells and breast cancer cell line MDAMB231 are both adherent and were grown at 37°C in 5% CO<sub>2</sub> in a humid incubator. The BE and MDAMB231 culture medium consists of DMEM supplemented with 10% FBS, 2mM L-glutamine plus 10Units/ml penicillin and 10µg/ml streptomycin. Both cell lines were passaged every 3-4 days by brief exposure to 0.05% trypsin-EDTA, aided by agitation, and then resuspended in serum containing medium to quench the trypsin, and diluted (1:10) into fresh medium.

BT549 breast cancer cells are adherent and were grown at 37°C in 5% CO<sub>2</sub> in a humid incubator. The BT549 culture medium consists of RPMI supplemented with 10% FBS, 2mM L-glutamine plus penn strep. BT549 cells were passaged every 3-4 days by brief exposure to 0.05% trypsin-EDTA, aided by agitation, and then resuspended in serum containing medium to quench the trypsin, and diluted (1:10) into fresh medium.

hTERT -HNCAF were cultured in DMEM supplemented with 10% FCS, 1% ITS, 2mM L-glutamine and penicillin streptomycin. These cells are very slow growing and thus were passaged every 7 days (media was changed after 3 days).

For long-term storage cells were frozen in 10% DMSO in FBS and stored in liquid nitrogen vapour phase tanks.

### **2.3.3 Transfection with siRNA**

All siRNA reagents were obtained from DHARMACON RNA Technologies.

**Table 3 siRNA duplex sequences**

Target	Sequence	Catalog #
LIMK1 (#1)	GAACGCAGACCCUGACUACUU 5'PGUAGUCAGGGUCUGCGUUCUU	D-007730-01
LIMK1 (#3)	UCAAGGAGGUGAAGGUCAUUU 5'PAUGACCUUCACCUCCUUGAUU	D-007730-03
LIMK2 (#6)	GAUCUGAACUCGCACAACUUU 5'PAGUUGUGCGAGUUCAGAUCUU	D-003311-06
LIMK2 (#7)	UGACUGAGGUGAAAGUGAUUU	D-003311-07

	5'PAUCACUUUCACCUCAGUCAUU	
ON-TARGETplus Non-targeting siRNA #1	Sequence not provided by manufacturer; negative control siRNA with at least 4 mismatches to any human, mouse or rat gene.	D-001810-01-05
ON-TARGETplus Non-targeting siRNA #2	Sequence not provided by manufacturer; negative control siRNA with at least 4 mismatches to any human, mouse or rat gene.	D-001810-02-05
Lamin A/C Control siRNA	Sequence not provided by manufacturer.	D-001050-01-20

Oligofectamine was used for transfection of siRNA on sub-confluent cells, for example MDAMB231 cells were seeded at  $2 \times 10^5$  per well of 6well dishes 24h prior to transfection and Oligofectamine reagents used according to the manufacturer's instructions. In brief, both siRNA (e.g. 50nM of siRNA pool, individual duplex or negative control) and Oligofectamine were diluted in OptiMEM, incubated at RT for 5min, then combined and incubated for a further 20 minutes. The cells were washed during this 20 minute incubation period with serum free media and covered with a set volume of OptimMEM before addition of the siRNA/Optimem/Oligofectamine mixture to the cells. Down regulation of protein levels was generally achieved after 24 hours in culture and confirmed by Western blotting.

#### **2.3.4 Transient transfection with plasmid DNA**

For transient transfection of plasmid DNA using Lipofectamine 2000, cells were set up at an appropriate density in culture dishes (e.g.  $1 \times 10^5$  per well of a 6well dish for MDAMB231). 16-24 hours later DNA was transfected according to the manufacturer's instructions. Both DNA (~5-10 $\mu$ g) and Lipofectamine 2000 were diluted in OptiMEM, incubated at RT for 5min, then combined and incubated for a further 20min before being added directly to the cells. Expression was then tested for after 24-48 hours.

The Amaxa nucleofactor kit V was also routinely used for the transient transfection of MDAMB231 cells.  $1 \times 10^6$  cells were pelleted, resuspended in 100 $\mu$ l of solution V and DNA, transferred to a nucleofection cuvette and placed in the Nucleofactor where Program X13 (optimised to this cell type) was used. Cells

were then re-plated on to 6-well culture dishes and allowed to recover for (Hennigan RF, 1994) between 24 hours, before being redistributed into the desired experiment (e.g. Inverse invasion assays).

### **2.3.5 Nucleofection**

Nucleofection provided an alternative method of DNA transfection, with high transfection efficiency rates. Cells were transfected using the appropriate nucleofection kit of the cell line according to the manufacturers instructions. In brief; MDAMB231 cells were passaged 2 days before nucleofection as cells should be nucleofected at 70-85% confluency. 5µg DNA was prepared for each sample. Nucleofector solution was allowed to warm to room temperature, 500µl of media per sample (complete with supplements) was warmed to 37°C. 6 well dishes were prepared with 1.5ml media per well and the desired cells harvested and counted.  $1 \times 10^6$  cells per nucleofection were centrifuged in individual tubes, the supernatant removed and the cell pellet resuspended in 100µl of Nucleofector solution for a final concentration of  $1 \times 10^6$  cells/100µl. The cell suspension was then mixed with 5µg DNA, transferred to an amaxa nucleofection cuvette and capped. The correct Nucleofector programme was selected for the cell and kit type, programme X13 for MDAMB231 cells using kit V, the cuvette inserted into the nucleofector and nucleofection carried out. The cuvette was then removed from the Nucleofector, 500µl media added and the whole suspension added to the prepared well of a 6 well plate. Cells were allowed to recover and settle for 12 hours before being used, such as for invasion assays.

### **2.3.6 Retrovirus Production**

BOSC (or Phoenix) cells were plated out at  $0.25 \times 10^6$  cells per well of a 6-well dish in 10% FBS/DMEM, 48 hours later cells were transfected using Effectene (Qiagen) according to the manufacturers instructions. 24 hours later cells were washed twice with FBS/DMEM (once in morning, once in evening) and add 1.5 ml of 10% FBS/DMEM per well. The virus was collected after 48 hours and centrifuged at 1600 rpm for 5 min to collect any cells and the supernatant removed to a clean tube and stored at -80°C.

### **2.3.7 Retrovirus Transduction**

NIH 3T3 (or desired cells already selected for ecotropic receptor expression) were plated out at  $1.5 \times 10^5$  cells per well of a 6 well dish and the next day cells were infected with 1ml of virus and 4 $\mu$ l polybrene (making a 1:250 final dilution) Following incubation for 5-6 hours 2 ml 10% FBS/DMEM was added to each well. The next day the media was replaced and when confluent, cells were trypsinised and selected for 2 passages before freezing down.

### **2.3.8 TAT (PTD) proteins**

PTD FLAG Cofilin1 was generated by the annealing of double stranded oligonucleotides coding for the PTD peptide (YARAAARQARA) and FLAG epitope, and subsequent ligation into pGEX KG Cofilin plasmid. The mutants were subsequently produced by site directed mutagenesis and the Cofilin proteins expressed in E.coli and purified as described.

TAT or PTD refers to the transactivator protein of HIV-1, a peptide that can be internalised by cells without transfection and is utilised for the delivery of TAT fused proteins into cells in tissue culture. The mechanism by which TAT proteins enter cells was previously poorly understood, it was thought that smaller fused proteins entered cells by an energy and receptor-independent process based on direct transport through the lipid bilayer but that larger proteins were actively imported in a clathryn dependent manner {Richard, 2005 #216}. It is thought that heparan sulfate (HS) proteoglycans may act as receptors for extracellular Tat uptake {Tyagi, 2001 #215}, however, the uptake of small TAT PTD peptides may be mediated by other pathways as internalization of TAT peptide is not ablated in cells without surface heparin {Richard, 2005 #216}. The uptake of TAT proteins is suggested to be endocytically regulated as it is both temperature and ATP dependent {Richard, 2005 #216}.

### **2.3.9 Wound healing**

For a classic wound healing assay or 'scratch' assay desired cells were seeded sub-confluently into 12 well dishes and left to settle and create a monolayer for 24-48 hours as desired. The monolayer was then disrupted by a p200 tip to

generate a wound across the well. The media in the well was gently changed to remove any floating cells from the wound interfering in imaging. The 12 well dish of 'wounds' was then transferred to a timelapse microscope and imaged at 15 minute intervals for 24 hours (or until the wound is closed).

### **2.3.9.1 Oris cell migration assay**

The Oris cell migration assay is a 96well format wound healing assay, on the same principles as explained for wound healing assays. Small rubber plugs are placed in each well of a 96well plate, occluding a central portion so that cells are seeded and settle around the plug. Once cells are settled the plugs are removed and each well has an identical central 'wound'. This assay makes each wound far more regular than is achievable by hand alone, and also does not lead to ragged edges on the wound. Following a suitable time for cell migration cells were imaged on an upright tissue culture microscope using 'QcapturePro' and a black 'mask' was fitted to the base of each plate. The mask used has holes corresponded to the area in each well that is kept free from cells during seeding. The mask was applied following fluorescent staining of the cells to quantify the level of migration into the centre of the well by a fluorescent plate reader. Calcein AM is a suitable live cell stain for this approach and was used routinely in the quantification of cell migration in this assay.

### **2.3.10 *Inverse Invasion assay***

This method is a modified version of that previously described (Hennigan RF, 1994). An aliquot of complete Matrigel was thawed slowly on ice. Once defrosted Matrigel was diluted 1:1 in ice cold PBS (along with any other additional treatments at 2x concentration in the PBS prior to dilution). 100  $\mu$ l of the diluted Matrigel was carefully pipetted into each Transwell (inserted into a well of a 24 well tissue culture plate) and left to incubate for about 30mins at 37° C to set. During this time cell suspensions of  $3 \times 10^5$  cells per ml from each pre-treated condition (e.g. siRNA) were prepared in their normal growth medium.

When the Matrigel was set the Transwells were inverted and 100  $\mu$ l of the cell suspension ( $3 \times 10^4$  cells) pipetted onto the underside of the filter (which was,

at that point, uppermost). The Transwells were then carefully covered with the base of the 24 well tissue culture plate, making contact with each droplet of cell suspension, and the plate then incubated in the inverted state for 4 hours to allow for cell attachment. Following this time the plates were turned right-side-up and each transwell washed by sequential dipping into 3 x 1 ml serum free medium. The Transwells were left in wash number 3 as the well in which the assay would be incubated, it therefore contained any additional drugs or treatments required. 100  $\mu$ l of 10% FBS DMEM plus EGF (25 ng/ml) was gently pipetted into the Transwell on top of the set Matrigel/PBS mixture, the lid replaced and the assay incubated for 5 days at 37°C with 5% CO<sub>2</sub>.

4 $\mu$ M Calcein AM (acetoxymethyl ester of calcein) was used to stain the assays as Calcein is a live cell dye that stains the whole cell green and requires no fixation. Transwells were placed in fresh 24 well dishes with 1ml of the stain solution pipetted on top of each Transwell as it spills over the sides and stains the matrigel plug from the top and bottom. After 1 hours incubation at 37°C with 5% CO<sub>2</sub> cells were fully stained and ready to be imaged by confocal microscopy. PI staining was adopted to visualise nuclei when the assays were fixed and before staining for f-actin.

### **2.3.11 Gelatin Degradation Assay**

#### **2.3.11.1 Preparation of gelatin coated coverslips**

The working area was coated with a strip of parafilm on which droplets of liquid were placed in order to coat coverslips. All stages, except the final step, were performed in a fume hood. Sterile, acid washed, 13 mm coverslips were placed on top of 100 $\mu$ l droplets of poly L lysine, coating one side, for 15 minutes at room temperature. Excess liquid was removed from the coverslip and the coated side placed on top of a 100 $\mu$ l drop of 0.5% glutaraldehyde (in PBS) for 10 minutes. During this time an aliquot of Molecular Probes Oregon Green 488 conjugated fluorescent gelatin (G-13186) was defrosted on a heat block at 37°C and the coverslips were then placed on a 60 $\mu$ l droplet of 488 fluorescent gelatin for 15 minutes in the dark. The coverslips were then transferred to a multiwell dish and washed gently 3 times with PBS. A 5mg/ml sodium borohydride solution

in PBS was then prepared (in the fume hood), and the coverslips incubated in this for 3 minutes. A further 6 washes with PBS were then performed before sterilizing the coverslips in 70% EtOH for 5 minutes. At this, the final step, the multiwell dishes containing coverslips were transferred to a tissue culture hood where the EtOH was aspirated and the coverslips quenched in 10% FBS DMEM for 1 hour at 37°C.

### **2.3.11.2 Gelatin Degradation**

Cells of interest were counted and made up into  $3 \times 10^5$  cell/ml suspensions, any desired pre-treatment had been performed by this point. Fluorescent gelatin coated 13mm coverslips were placed into 24well dishes containing 500ml of complete media with GM6001 MMP inhibitor at 10 $\mu$ M and 100 $\mu$ l of each cell suspension/condition added to a well, and the cells allowed to settle and adhere at 37°C overnight. The following morning the wells were washed 3 times with PBS to remove the MMP inhibitor before the addition of 500ml complete media. Where drug inhibition of LIMK was being examined, CRT 101106 was added to the well at this point. Cells were allowed between 4- 24 hours, 4 hours for MDAMB231, to degrade the gelatin. The coverslips were then washed 3 times with PBS before being fixed at room temperature with 4% Paraformaldehyde (PFA) for 15 minutes, washed 3 times with PBS, the cells permeabilised with 0.1% Triton X-100 in PBS for 15 minutes, washed again 3 times with PBS and blocked for 30 minutes in 5% BSA in PBS. The blocking solution was then replaced with a 1/1000 dilution of Texas Red phalloidin in BSA PBS for 3 hours to stain for filamentous actin. The coverslips were then mounted on glass slides using ProLong Gold antifade reagent and viewed on an upright fluorescent microscope.

### **2.3.12 Cell derived Matrix (CDM)**

#### **2.3.12.1 Generation of CDM**

Coverslips were first cleaned by boiling in MilliQ and autoclaved. Coverslips were then distributed into 24-well plates to grow matrix. Following a quick wash with sterile PBS the coverslips were incubated with 2ml 0.2% sterile gelatin for 1 hour at 37°C (2% gelatine stored at 4°C, diluted 1:10 in PBS). The gelatine was then

aspirated and the coverslips washed twice with PBS, then cross-linked with 2ml 1% sterile glutaraldehyde (25% stock 1:25) for 30 minutes at room temperature. Two washes with PBS were then performed and the cross-linker quenched with 2ml 1M sterile glycine in PBS (pH=7) for 20minutes at room temperature. The coverslips were then washed a further 2 times with PBS and then incubated with growth media (DMEM) for 30minutes at 37°C. The coverslips were then ready to be seeded with cells although could be stored at 4°C, if stored in PBS they were re-incubated with DMEM before seeding with HDF (human dermal fibroblast), grow in DMEM plus 10% serum and P/S.

Cells were plated onto the prepared coverslips at  $5 \times 10^4$  per well of a 24 well plate and cultured at 37°C in 5% CO<sub>2</sub> overnight before changing the media to complete media supplemented with 50 ug/ml Ascorbic acid. The ascorbic acid media was changed every second day until denudation as a fibronectin-rich matrix was desired. The ascorbic acid increases collagen production and stabilises the matrix, without it the matrix won't stick to the plate properly. Other protocols suggest changing the media everyday for the course of CDM production, 11-14 days.

The cells were then removed to reveal the matrix below. Firstly the medium was aspirated and the cells washed twice with PBS. 750µl pre-warmed extraction buffer was then gently added to each well (20 mM NH<sub>4</sub>OH, 0.5% Triton X-100 in PBS). Cell lysis is very quick so is carried out for around 2 minutes, or until no intact cells were visible by phase light microscopy. Matrix is delicate so extraction buffer was removed very gently and washed twice with PBS containing calcium and magnesium (Sigma). Residual DNA was digested with 10 ug/ml DNase I in PBS containing calcium and magnesium and incubated for 30 min at 37°C in 5% CO<sub>2</sub>. DNase was then gently aspirated and the matrix washed twice with PBS containing calcium and magnesium.

The matrix was then stored at 4°C in PBS containing calcium and magnesium with pen/strep and fungizone before use (up to 3 months). The matrix is visible by phase so was checked to be intact before use.

### 2.3.12.2 Cell motility on CDM

Cell derived matrix was generated as described, following storage at 4°C the wells were gently washed with PBS and incubated for one hour at 37°C with DMEM to prepare the wells for cell seeding. Cells were subject to pre-treatment as desired for the experiment and seeded sub-confluently into the 12 well dishes containing cell derived matrix. The plates were then transferred to a time-lapse microscope complete with a 37°C, 5% CO<sub>2</sub> incubation chamber for one hour to allow cells to settle and for the plasticware to equilibrate with the chambers conditions. Pictures were then taken using a 10x objective and bright field channels at 15 minute intervals over up to 24 hours. Analysis of experimental data was performed using ImageJ, or AndorIQ software.

## 2.4 Methods in Protein Extraction and Analysis

### 2.4.1 Reagents

Bicinchoninic acid		<i>Sigma</i>
Copper Sulphate		<i>Sigma</i>
Eelectrophoresis buffer	25 mM TrisCl, 192 mM glycine, 0.1% w/v SDS	
Kodak BoMax MR Film	(scientific imaging film)	<i>Kodak</i>
Laemmli buffer (6X)	125mM TrisCl pH 6.8, 6% w/v SDS, 30% glycerol, 225 mM DTT, 0.05% (w/v) bromophenol blue	
NuPAGE MOPS SDS running buffer	20x	<i>Invitrogen</i>
Protran Nitrocellulose Transfer membrane,	3mm filter paper	<i>Whatman International Ltd</i>

RIPA Lysis buffer	10mM Tris pH 7.5, 5mM EDTA, 150 mM NaCl, 300, 40 mM Nappi, 1mM Na <sub>3</sub> VO <sub>4</sub> , 50mM NaF, 1% NP40 0.5% Na Deoxycholate (NADE), 0.025% SDS, 1mM p-amino- ethybenzene sulphonyl fluoride (PMSF), 1X Complete protease inhibitor	
SimplyBlue safestain		<i>Invitrogen</i>
TBS	137 mM NaCl, 5 mM KCl, 25 mM TrisCl	
Transfer buffer	192 mM glycine, 25 mM TrisCl, 20% v/v methanol, 0.036% w/v SDS; pH 8.3	
Tris buffered saline (TBS) lysis buffer	TBS with 1 mM Dithiothreitol (DTT) and 1 mM Phenylmethylsulphonylfluoride (PMSF)	

### **2.4.2 Whole cell extracts**

Cells were pretreated as required per experiment and then harvested by scraping in RIPA lysis buffer on ice and consequent centrifugation at 14,000rpm at 4°C in a cooled micro-centrifuge. Supernatants were removed, analysed for protein concentration and stored at -80°C.

### **2.4.3 mRNA preparation**

MDAMB231 cells were seeded at  $1.5 \times 10^6$  per 15cm dish, following experimental manipulation media was removed from cells and RNA isolated using the Qiagen

Rneasy kit according to manufacturers instructions. In brief, cells were scraped into 600µl RLT lysis buffer containing 145 mM β-mercaptoethanol before homogenization through a Qia-shredder column. 600µl ethanol was added per sample before being added to a Rneasy column and removal of contaminants with sequential washes using the provided buffers. RNA was then eluted with 50µl Rnase free water and stored at -20°C.

#### **2.4.4 cDNA synthesis**

In order to analyze gene expression RNA must first be transcribed into cDNA, and Finnzymes' Dynamo SYBR Green 2-step qRT PCR kit has all the required reagents to do this and was used according to the manufacturers instructions. In brief, for each experimental condition RNA a cDNA synthesis premix was prepared by mixing 20µl RT buffer, 4µl M-MuLV RNase H<sup>+</sup> reverse transcriptase, 2µl Random hexamer (300ng/µl), 10µl PCR grade water, 4µl of template RNA (0.5µg/µl) for a 40µl reaction. The reactions were then placed in a thermal cycler for;

<i>Step 1</i>	Primer extension	25°C	10 minutes
<i>Step 2</i>	cDNA synthesis	37°C	30 minutes
<i>Step 3</i>	Reaction Termination	85°C	5 minutes
<i>Step 4</i>	Cooling of sample	4°C	Until recovered

Extra cDNA was generated for the Control conditions and when not being used immediately cDNA was stored at -20°C.

#### **2.4.5 qPCR**

Finnzymes' Dynamo SYBR Green 2-step qRT PCR kit was used to perform qPCR on a BioRAD DNA Engine thermal cycler, with a Chromo4 realtime PCR detector and Opticon Monitor 3. The qPCR reactions were performed as per the manufacturers instructions. In brief, the qPCR reaction contained 10µl 2x MasterMix, 2µl primer

mix, 6  $\mu$ l of PCR grade Water and 2 $\mu$ l of cDNA (diluted 1:6 in TE). The plate of reactions was placed in the thermal cycler on the appropriate optimized protocol.

#### **2.4.6 Protein quantification: BCA Assay**

Bovine serum albumin (BSA, Pierce's 2mg/ml BSA vials #23209) was used to prepare a dilution series of standard protein concentrations in lysis buffer ranging from 0mg/ml to 2mg/ml. 10 $\mu$ l of each BSA standard was added in series to a 96 well plate, 10 $\mu$ l of each sample was then added, in duplicate, to the following wells. 200 $\mu$ l of developing solution (50:1 of Bicinchoninic acid to Copper Sulphate) was added to each well, incubated for 30minutes at 37°C and the absorbance values used to generate a standard curve. The protein concentrations were determined for each sample from the standard curve.

#### **2.4.7 SDS-PAGE**

SDS-poly-acrylamide gels were used to run protein samples. Depending on the proteins of interest SDS percentage was varied as per Table 4. In general, 50 $\mu$ g of protein in SDS sample buffer (4 volumes of 5% SDS, 25% glycerol, 125mM Tris pH6.8, bromophenolblue and 1 volume of 1M DTT) were boiled for 5 min and then loaded into individual wells alongside a full-range molecular weight marker. Gels were run in a gel tank in SDS Running buffer (25mM Tris, 0.1% SDS, 0.19M glycine) at 20 to 200 V until the dye front migrated to the bottom of the gel tank. Gels were transferred onto nitrocellulose by Western blotting.

**Table 4** Acrylamide gel recipe

	8%	10%	15%	Stack
30% Acrylamide/Bis	5.3ml	6.6ml	9.9ml	2 ml
1M Tris pH6.8	-	-	-	1.9 ml
1M Tris pH8.8	7.5ml	7.5ml	7.5ml	-
10% SDS	200 $\mu$ l	200 $\mu$ l	200 $\mu$ l	150 $\mu$ l
Water	6.8ml	5.5ml	2.2ml	10.8 ml
10% APS	100 $\mu$ l	100 $\mu$ l	100 $\mu$ l	100 $\mu$ l
TEMED	100 $\mu$ l	100 $\mu$ l	100 $\mu$ l	100 $\mu$ l

### **2.4.8 Western blots**

Polyacrylamide gels were transferred onto a nitrocellulose filter using a Bio-rad electroblotter. The nitrocellulose and 4 pieces of 3mm paper were soaked in transfer buffer and assembled on the blotter, from anode to cathode, 2 pieces of 3mm paper, nitrocellulose, resolving polyacrylamide gel, and 2 pieces of 3mm paper. The transfer was performed at 110mA, overnight at 4°C for large gels. Or 200V at room temperature for 1 hour for small blots (small transfers rigs use ice-packs). The nitrocellulose filter blot was washed briefly in TBST (10mM Tris pH7.6, 100mM NaCl, 0.1% (v/v) Tween 20) and then blocked in 5% (w/v) Marvel in TBST for an hour. Appropriate dilutions of primary antibody were prepared in 5% Marvel/TBST or 5% (w/v) BSA in TBST depending on the antibody. The blot was incubated for at least one hour at room temperature or over night at 40C. Next, blots were washed 3x 5min in TBST before being incubated in 5% Marvel/TBST containing a 1/500 dilution of appropriate horseradish-peroxidase-conjugated secondary antibody for an hour. After washing once for 15min in 5% Marvel/TBST and a further 3x5 min in TBST, the blots were analysed with ECL detection reagent or Femto, exposed to film and developed with a Kodak processor.

### **2.4.9 Immunoprecipitation**

For each sample 2-5µg of antibodies were bound to 30 µl of 50% glutathione-Sepharose slurry at 4°C for 1 hour before removal of unbound antibody with wash buffer. For cells prepared with RIPA lysis buffer this is a modified RIPA buffer, RIPA minus sodium deoxycholate, plus 0.5% NP-40. Antibody bound beads were then added to whole cell lysates and incubated at 4°C for 1-8 hours. The beads were then centrifuged at 5000g for about 10 seconds (or at full speed on a bench-top mini centrifuge) and washed 3 times with wash buffer. At this point the IP's could be used in kinases assays, or the addition of 30µl of 6X Laemml buffer to the tubes used to precipitate the complexes. These could then be boiled and run out on an acrylamide gel for analysis

## 2.4.10 Antibodies

Antibodies were routinely used at 1:1000 for western blotting and 1:500 for immunofluorescence, unless stated otherwise. Antibodies used are listed below in Table 5.

**Table 5 Table of primary antibodies**

Antigen	Species	Company/Laboratory (Cat. No.)
Cofilin	Rabbit	Cell signalling (3312)
Cofilin	Rabbit	Cytoskeleton(ACFL02)
ERK2	Rabbit	Sourced from Chris Marshall
Lamin A/C (N-18)	Goat	Santa Cruz (sc6215)
LIMK1	Rabbit	Cell Signalling (3842)
LIMK2 (H78)	Rabbit	SantaCruz (Sc5577)
Tubulin	Rabbit	Lab generated
Flag	Mouse	Sigma F-3165
Phospho-Cofilin	Rabbit	Cell Signalling (3841)
MMP 14	Rabbit	Neomarkers RB 1544
MMP9	Mouse	Neomarkers MS 804
MMP2	Mouse	Neomarkers MS 816

## 2.5 Kinase activity

The activity of LIM Kinase against a selection of potential substrates was determined by a variety of different kinase assay techniques.

### 2.5.1 Buffers and reagents

Active LIM Kinase 1	(14-646)	<i>Upstate</i>
Gamma 32P ATP	500uCi (18.5MBq)	<i>Amersham</i>
Kinase Buffer	1.25% BSA, 62.5 mM TrisCl pH 7.5, 1mM BME (0.1%), EGTA 0.5mM, Brij35 0.01%	
NaCl-Tx	1% Triton X-100, 2M NaCl	

PBS-Tx	1% Triton X-100 in PBS	
Pepscan Kinase mastermix (2X)	125 mM TrisCl, 0.2M MgCl, 20% (v/v) Glycerol, 0.02mg/ml BSA, 0.02% (v/v) Brij-35	
P81 Chromatography paper (Cation exchanger)	(3698-915)	<i>Whatman International Ltd</i>
Phosphoric acid		<i>Fisher</i>
pre-stained SDS-PAGE broad range standards		<i>Bio-Rad</i>

### **2.5.2 In Vitro Kinase assay**

All work was carried out behind a perspex screen on a designated radioactivity work bench to isolate and protect myself from the radioactive isotope used.

A heated shaking block was set to 30°C and allowed to come to temperature whilst 2 cm<sup>2</sup> squares of p81 paper were prepared, numbered in pencil to denote the condition/time-point in the assay. A rinsing basket was filled with 0.5% phosphoric acid (1:200 dilution) and each assay condition made up, on ice, to contain 1.25% BSA, 62.5 mM TrisCl pH 7.5, 1mM BME (0.1%), EGTA 0.5mM, Brij35 0.01% (buffer A), 0.02µg LIMK plus 500µM peptide substrate or 0.2µg of Cofilin in a 50µl reaction, but was initially made up to 40µl as a further 10µl is added at the start point of the assay. In a separate screw top eppendorf a 0.1M MgCl and 1mM ATP solution (10µl per reaction/time point) was spiked with 3µl of fresh  $\gamma^{32}\text{P}$ . 10µl of this mix was added to each condition/time-point and the phosphorylation reaction started on the heat block with shaking at 1400 rpm. The clear perspex eppendorf holder from the heated shaking block was removed and placed in a tray of ice so that all eppendorfs could be given the ATP mix and transferred to the heat block simultaneously. To stop the reaction, at each time point 40µl of the 50µl reaction was pipetted with a filtered tip onto the corresponding (labelled) piece of p81 paper (held with forceps) and gently

dropped into the rinsing basket of phosphoric acid minimising the contact between the pieces of paper before they were fully submerged and 'fixed'.

Once the time course was complete or all the reactions complete the papers were rinsed for five to fifteen minutes in the phosphoric acid fix. The rinse was then carefully poured off down a radiation approved sink (with lots of water) and the papers rinsed with fresh phosphoric acid twice more for five to fifteen minutes. The last phosphoric acid rinse was removed, and the papers given a final five minute rinse in acetone to displace water. The acetone was removed (and saved to be used in the next kinase assay) and the rinsing basket filled with acetone soaked p81 papers transferred to a perspex box, with a cardboard grid covering the open basket. In a chemical fume hood, from behind perspex, the papers were dried with a hairdryer through the grid. This was done with caution, from a distance, to prevent the cardboard and acetone from catching alight. Once the papers were dry, they were folded and placed into eppendorfs corresponding to each papers pencilled label. Into two spare eppendorfs, 2 $\mu$ l of the  $\gamma^{32}\text{P}$  spiked ATP mix was aliquoted to be used as controls on the Cerenkov counter. The eppendorfs were then transferred to a scintillation counter and the incorporation of ATP calculated from the values generated by the Cerenkov count.

### **2.5.3 IP-Kinase Assay**

An immunoprecipitation (IP) was carried out, as described, until the final washes. At this point the beads were washed twice with RIPA lysis buffer and then twice with IPK (IP Kinase assay) wash buffer (10X IP Kinase buffer; 0.5M TRIS pH7.5, 0.1mM EGTA). On ice, 40 $\mu$ l of kinase buffer (plus 500 $\mu$ M peptide substrate or 0.2 $\mu$ g of Cofilin) was added to ~10 $\mu$ l bound beads for each condition/time point. In a separate screw top eppendorf a 0.1M MgCl and 1mM ATP solution (10 $\mu$ l per reaction/time point) was spiked with 3 $\mu$ l of fresh  $\gamma^{32}\text{P}$ . 10 $\mu$ l of this mix was added to each condition/time-point and the phosphorylation reaction started on the heat block with shaking at 1400 rpm and the reaction run at 30°C. The reaction was stopped after the desired amount of time (20 minutes for instance) by addition of 6X Laemmli buffer, boiled to remove the bound LIMK from the beads and the samples were then run on an SDS page gel. The gel was

dried onto Whatman paper using a gel drier and exposed to film and/or a phosphor-imager phosphor-storage screen for analysis. Where the assay was performed 'cold' western blotting was performed to determine the level of phosphorylated substrate using a phosphor specific antibody. Care to use appropriate safety methods and shielding during the handling of radioactive material was taken.

#### **2.5.4 Pep-Scan Peptide Array**

Pepchip kinase slides were used in attempts to identify novel substrates of LIMK1. On each slide is a glass mounted peptide array covering over 400 proteins and 1400 individual phosphorylation sites. Each array was performed in accordance with the manufacturers instructions. In brief, these slides fulfil the role of substrate and as such were submerged into  $\gamma^{32}\text{P}$  kinase reactions in order to identify which peptides were phosphorylated by LIMK1. Taking care to use appropriate safety methods and shielding, a 60 $\mu\text{l}$  reaction mixture was set up for each slide; pepscan kinase mastermix (filtered through 0.22 micron syringe filter), 500ng/ml kinase, 10 $\mu\text{M}$  ATP and 300 $\mu\text{Ci/ml}$   $\gamma^{32}\text{P}$ . 50 $\mu\text{l}$  of this reaction mixture was then pipetted into the centre of a coverslip and the slide and gently lowered onto it, spreading the mixture over the array by capillary action. The slide was then turned and incubated in a humidified chamber at 30 $^{\circ}\text{C}$  for 2 hours before having the coverslip washed off in PBS-Tx. The slide was then transferred to a NaCl-Tx wash for two 5 minute washes at room temperature (with shaking). Three 5 minute washes with  $\text{dH}_2\text{O}$  were performed before the slides were air dried. The dried slides were then transferred to exposure cassettes and exposed overnight to film or a phosphor-storage screen. The resulting films or screens were analysed by aligning the provided grid image for orientation of which positive result correlated with which peptide in Adobe Photoshop.

#### **2.6 F-actin severing assays**

F-actin severing assays were used to determine the activity of PTD FLAG WT Cofilin proteins *in vitro*. Pyrene fluorescence increases 10-20 fold when G-actin is incorporated into filaments and the converse of this was utilised to quantify f-

actin depolymerisation using steady state fluorescence (Ex = 339 nm; Em = 384nm).

### **2.6.1 Buffers**

G Buffer	2 mM Tris-Cl (pH 8.0), 0.2 mM ATP, 0.5 mM DTT and 0.2 mM CaCl <sub>2</sub>
F Buffer	2 mM Tris-Cl (pH 8.0), 0.2 mM ATP, 0.5 mM DTT and 0.2 mM CaCl <sub>2</sub> , 50 mM KCl, 2 mM MgCl <sub>2</sub> and 0.1 mM EGTA

### **2.6.2 F-actin preparation**

G-actin was purified from rabbit muscle as described previously (Spudich & Watt, 1971). G-actin was maintained in G-buffer: (2 mM Tris-Cl (pH 8.0), 0.2 mM ATP, 0.5 mM DTT and 0.2 mM CaCl<sub>2</sub>). Polymerisation of the actin was achieved by addition of 50 mM KCl, 2 mM MgCl<sub>2</sub> and 0.1 mM EGTA, the resulting buffer being F-buffer. Concentrations given for F-actin refer to the initial concentration of G-actin prior to polymerisation.

### **2.6.3 Pyrene labelling**

1mg/ml G-actin was labelled with pyrene (5mg/ml - approx. 15M excess) in DMF (dimethylformamide) for 15 hours and dialysed in G-buffer. The G-actin was then polymerised and ultracentrifuged to pellet the F-actin. The F-actin pellet resuspended in G-buffer and concentration determined.

### **2.6.4 F-actin Severing**

For the severing assay, G-actin (95% unlabelled: 5% pyrene labelled) was polymerised at 2.5µM (G-actin final concentration) over night. 50 µl of Labelled F-actin (at 2.5µM) was added to a PTI glass cuvette (with or without the addition of 10µM PTD FLAG WT Cofilin) and steady state fluorescence (Ex = 339 nm; Em =

384nm) measured on a spectrofluorimeter for 1000 seconds. Data was normalised to allow comparison between data sets, and reported as percentage fluorescence over time.

## 2.7 Zymography

Zymography was used to assess the levels of active matrix metalloproteases (MMPs) being excreted by MDAMB231 cells into the surrounding media, specifically MMP2 and MMP9 (gelatinases).

### 2.7.1 Buffers and Reagents

Zymogram precast gels and buffers were purchased from Invitrogen;

10% Zymogram Gelatin Gel	<i>Invitrogen</i>
Zymogram Renaturing Buffer	<i>Invitrogen</i>
Zymogram Developing Buffer	<i>Invitrogen</i>
Tris-Glycine SDS Running Buffer	<i>Invitrogen</i>
Tris-Glycine Non-reducing sample buffer	<i>Invitrogen</i>

### 2.7.2 Zymography – Gelatinase activity.

In brief, the enzyme sample was prepared in SDS buffer (non reducing conditions) and electrophoresed on a 10% Tris-Glycine gel with 0.1% gelatine incorporated as a substrate, without heating, using Tris-Glycine SDS running buffer at 125V for ~90 minutes. After the run was complete, the enzyme was re-natured by incubating the gel in Zymogram Renaturing Buffer (contains a non-ionic detergent). The gels were equilibrated in Zymogram Developing Buffer (to add the divalent metal cation required for enzymatic activity) and then the gel stained and destained using Invitrogen Safestain (coomassie blue). The protease bands should appear as clear bands against a dark background where the protease has digested the substrate within the gel.

## 2.8 Immunofluorescent microscopy

### 2.8.1 Reagents

Calcein AM, ProLong Gold antifade reagent (mount)	<i>Invitrogen</i>
Clear Nail Varnish	<i>MaxFactor</i>
Sterile PBS (Phosphate Buffered Saline)	<i>Beatson Institute Central Services</i>
Vectashield mounting medium, Vectashield with DAPI (4',6-diamidino-2-phenylindole)	<i>Vector Laboratories, Inc</i>

### 2.8.2 Fixing and staining cells on glass for microscopy

Cells were set up at appropriate concentration on glass cover slips in 12 or 24 well plates. After treatment, cells were washed 3x in PBS and fixed either in 4% paraformaldehyde for 15 minutes. Cover slips were then washed 3x in PBS, permeabilised for 15 minutes in 0.1% Triton X-100 in PBS, washed 3x PBS and blocked for 30 minutes in 1%-5% BSA in PBS. The blocking solution was then replaced with a 1/1000 dilution of primary antibody/antibodies in blocking buffer. After 1-24hours of incubation at room temperature (depending on the antibody) the cells were washed 3x 5 minutes in blocking buffer. Then the secondary antibody/antibodies added in a 1/500 dilution in blocking buffer (plus a suitable phalloidin at this stage if f-actin staining) for 1 hour and the whole dish being stained placed in a black box or wrapped in foil. Cover slips were then washed twice in blocking buffer and once in PBS before being mounted on a glass slide with Vectashield (clear or with Dapi) or ProLong Gold antifade reagent and sealed with clear nail varnish. The slides were then visualised using an appropriate microscope such as a Leica confocal microscope and windows based LCS software.

### ***2.8.3 Fixing and staining cells for 3D Confocal imaging***

Stained nuclei or whole cells were visualised by confocal microscope using a 20X objective. Optical sections (Z-sections) were scanned at 15  $\mu\text{m}$  intervals (Z-steps) moving up from the underside of the filter into the matrigel, producing a series of images. To quantify these “Image J” software was used. This programme gives each on-screen pixel an intensity value from 0 through to 255. The background pixel value is then operator-defined as the point (pixel value) on the 0-255 scale at which only cells from that individual section are visible with no bleed-through from bordering sections. Only pixels with an intensity value greater than background are then counted by “Image J”.

### ***2.8.4 Time-lapse microscopy***

Time-lapse microscopy was performed using an inverted Zeiss microscope system with temperature humidity 37°C and CO<sub>2</sub> control. Pictures were taken using a 10x objective and bright field channels at 15 minute intervals over up to 24 hours. Analysis of experimental data was performed using ImageJ, or AndorIQ software.

## **3 Requirement of LIMK in cancer cell motility and invasion**

### **3.1 Chapter Summary**

LIM Kinases act as convergence points for many upstream signals that influence the architecture of the actin cytoskeleton. Not only has LIMK1 been implicated in cancer (as it is found to be over expressed in melanoma cells(Okamoto et al, 2005), breast cancer tumours(Bagheri-Yarmand et al, 2006) and tumour cell lines(Yoshioka et al, 2003), prostate tumours and cell lines(Davila et al, 2003; Yoshioka et al, 2003), but perturbing the balance between active Cofilin (LIM Kinases primary substrate) and inactive Cofilin appears sufficient to affect cell motility(Hotulainen et al, 2005) .

LIMK1 has been shown recently to increase human breast cancer cell metastasis(Bagheri-Yarmand et al, 2006), but it was not known whether both LIM Kinase 1 and 2 were requirements of cancer cell motility and invasion when this project commenced, nor whether there were differing roles for the LIM Kinases in cancer cells. This chapter describes studies investigating the requirement for LIMK1 and LIMK2 by cancer cells during motility and invasion in both 2D and 3D environments.

### **3.2 Results**

#### ***3.2.1 LIMK knock down by siRNA in MDAMB231 cells***

In order to address the requirement of LIMK in cell motility or invasion an approach needed to be taken to reduce LIMK levels in cells. The principal technique used throughout this chapter to knockdown LIMK levels in cells was short interfering RNA.

Since its identification in plants (Hamilton & Baulcombe, 1999) short interfering RNA (siRNA) has become an invaluable tool for reducing expression of specific proteins in mammalian cell culture(Elbashir et al, 2001). It is not, however,

without its caveats, and genes with partially complimentary sequences may sometimes be inadvertently down regulated by an siRNA in an 'off-target' effect. Off target effects can lead to problems in data interpretation or even toxicity, but can be partly addressed by using multiple independent siRNAs side by side to confirm a genuine effect. Along with non-targeting negative controls, positive controls can be used using validated siRNAs that target an unrelated mRNA, for example Lamin A/C. These controls help to validate that transfections have worked and help with the identification of any potential off target effects.

To increase confidence in data gathered from reducing LIMK levels by siRNA, four different siRNAs for each kinase were tested. Twenty four hours following transfection, MDAMB231 were lysed with RIPA buffer and the lysates analysed by western blot, Figure 3.3.1 part A. LIMK1 was successfully knocked down by siRNAs numbered 1,3,4 and 5, without an effect on LIMK2 levels or Lamin A/C protein levels. LIMK2 was successfully knocked down by siRNAs 6,7,8 and 9 with no effect on LIMK1 or Lamin A/C protein levels. Lamin A/C positive control indicated that siRNA transfection worked and neither of the non-targeting siRNA controls reduced LIMK1, LIMK2 or LAMIN A/C levels.

To assess if the siRNA treatment had any toxic effect on cells, cell numbers were determined over time. Cells were pre-treated with two different siRNAs for each kinase (#1 and #3 for LIMK1 and #6 and #7 for LIMK2) and also in combination for both kinases (#1&#6, #3&#7) for 24 hours, counted and seeded in 12 well dishes and after 5 days trypsinised and counted again to determine any difference in cell numbers between conditions (Figure 3.3.1part B). No significant differences were observed between conditions, as determined by ANOVA.

Since LIMK is successfully knocked down by the above chosen siRNAs, and this process does not appear to affect cell viability, effects of LIMK siRNA on MDAMB231 cells could be confidently interpreted as specific to the loss of LIMK.

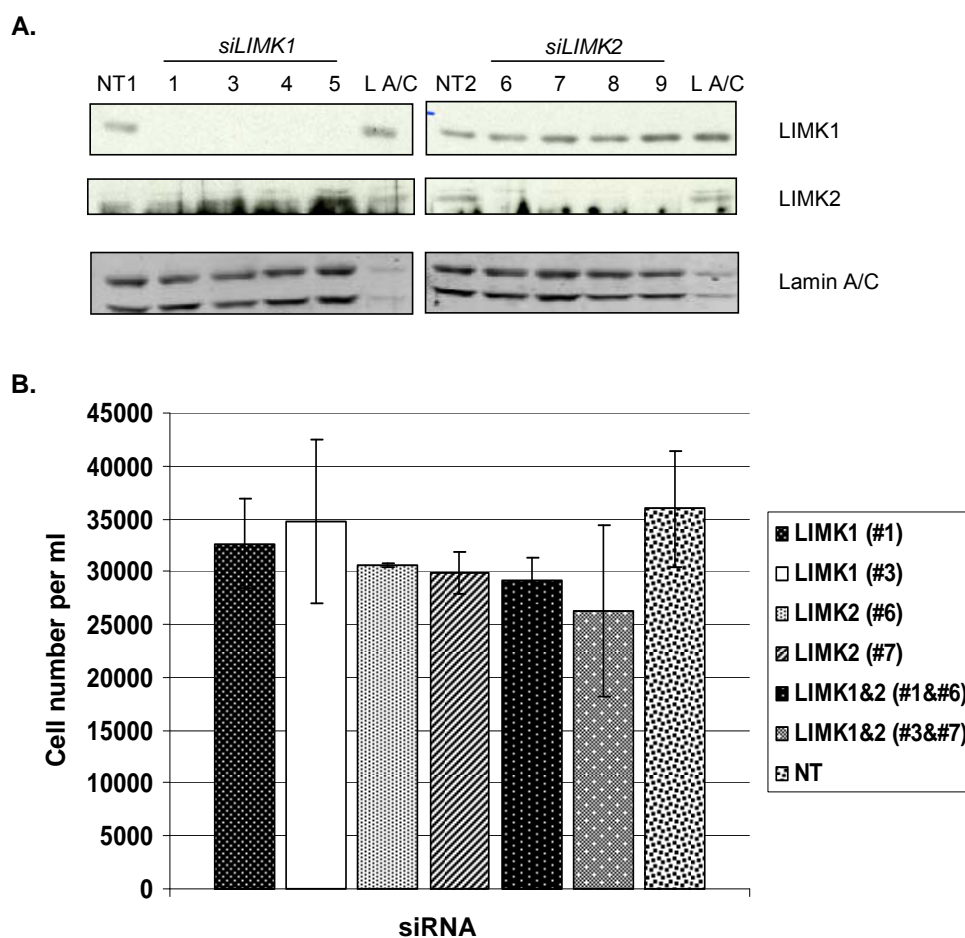


**Figure 3.3.1-siRNA of LIMK1 and LIMK2 in MDAMB231 and effect on proliferation.**

A. Western blot of MDAMB231 cell lysates following siRNA against LIMK1 (oligonucleotides numbered 1, 3, 4 and 5) and LIMK2 (oligonucleotides numbered 6,7,8 and 9) were tested for efficacy along with negative control non targeting siRNA (NT1 and NT2) and positive control Lamin A/C (L A/C). B. MDAMB231 cell number following treatment with siRNA; cells were counted 5 days after treatment, Error bars represent Standard Error, n=3. No significant differences were observed between conditions (Determined by ANOVA).

### **3.2.2 Knockdown of LIMK induces changes in the actin cytoskeleton**

LIM Kinases inactivate Cofilin by phosphorylating Serine 3, it would therefore be expected that reducing cellular LIMK levels would result in increased active Cofilin, and thus a decrease in F-actin cytoskeletal structures within cells.

In order to establish if this were the case, MDAMB231 cells were subject to transfection with LIMK siRNA, distributed onto coverslips, fixed and stained for F-actin and tubulin, and imaged using a Zeiss Axioplan 200 microscope to identify any changes to the cytoskeleton following knockdown of either LIM Kinase. Non-targeting siRNA treated cells showed cytoplasmic actin staining and strong peripheral staining with 'microspikes', seen in Figure 3.3.2. Whilst knockdown of LIMK1 caused a slight decrease in cytoplasmic F-actin staining and micro-spikes, these cells maintained some peripheral actin staining but with a slightly rounder, smoother cell shape in comparison to non-targeting (NT) siRNA treated control cells (first panel of Figure 3.3.2). Knockdown of LIMK2 caused a more dramatic loss of F-actin staining, both cytoplasmic and peripheral. Cells were rounded in comparison to controls, a morphology also seen in the double knockdown cells. Tubulin staining in the second panel shows little change following loss of LIMK; staining serves to outline the rounder, less spiky shape of the cells following treatment with siRNAs against the LIM Kinases. The third panel shows the loss of peripheral actin staining and microspikes by LIMK knockdowns in an overlay of F-actin (red) and tubulin (green) staining, the red edges of the cells were reduced following LIMK1 or LIMK2 knockdown and more so following double knockdown.

In a similar experiment BT549 cells were subject to siRNAs against LIM Kinases, and fixed and stained as described above. Knockdown of both LIM Kinases in these cells reduced peripheral actin staining as was seen in MDAMB231. This is particularly clear in the merged images where F-actin staining (red) is seen at the periphery of only the control cells (Figure 3.3.3).

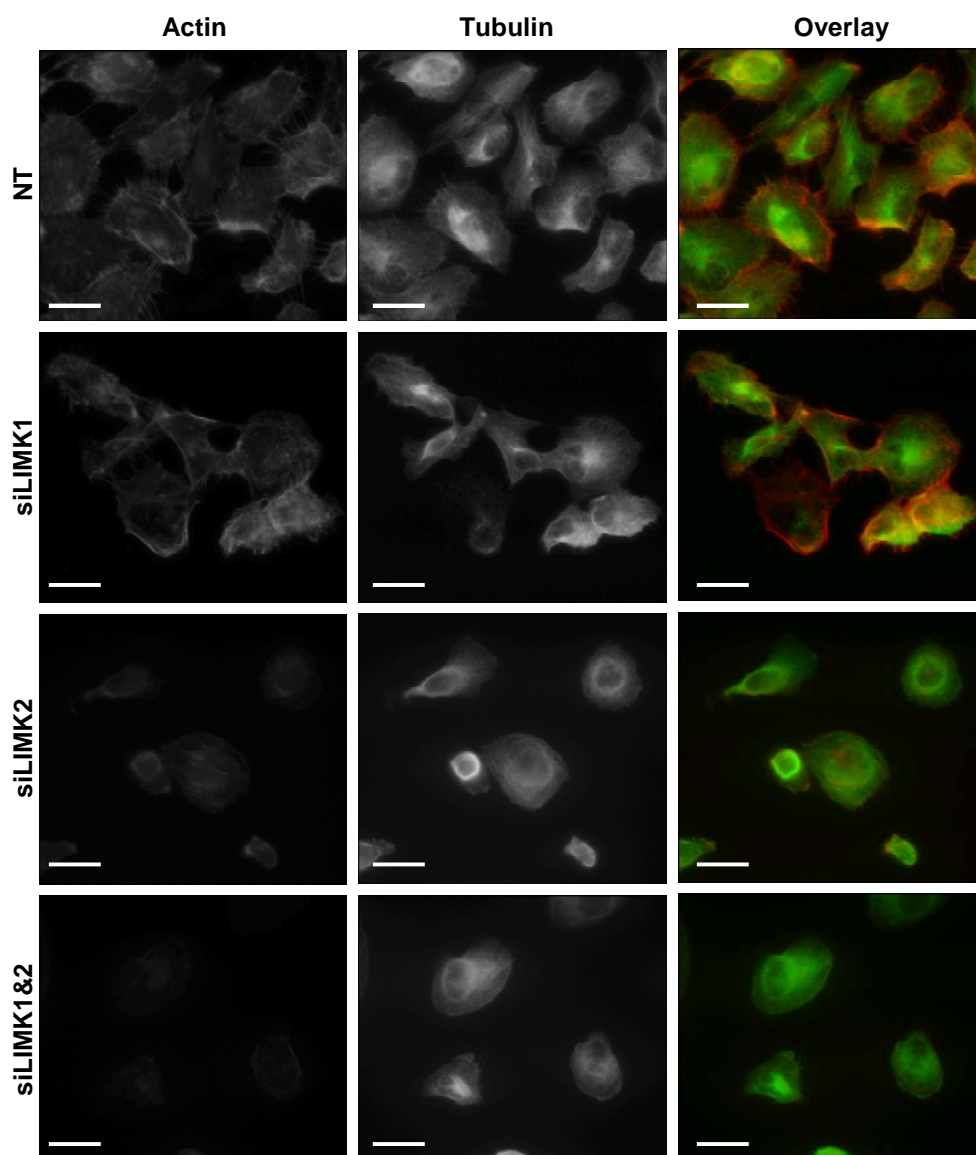


**Figure 3.3.2-MDAMB231 morphology on glass.**

Following siRNA treatment against LIMK1, LIMK2, both in combination or with a non-targeting oligonucleotide; The first column shows staining of the actin cytoskeleton for F-actin using Texas Red phalloidin, column number two shows staining of the microtubule network with an anti-alpha tubulin antibody and FITC secondary antibody, the third column shows an overlay of the two; where red corresponds to F-actin staining and green to microtubules. Images captured on the Zeiss Axioplan 200 at x40 using Imaging Associates Isis software. Scale bar equals 20µm.

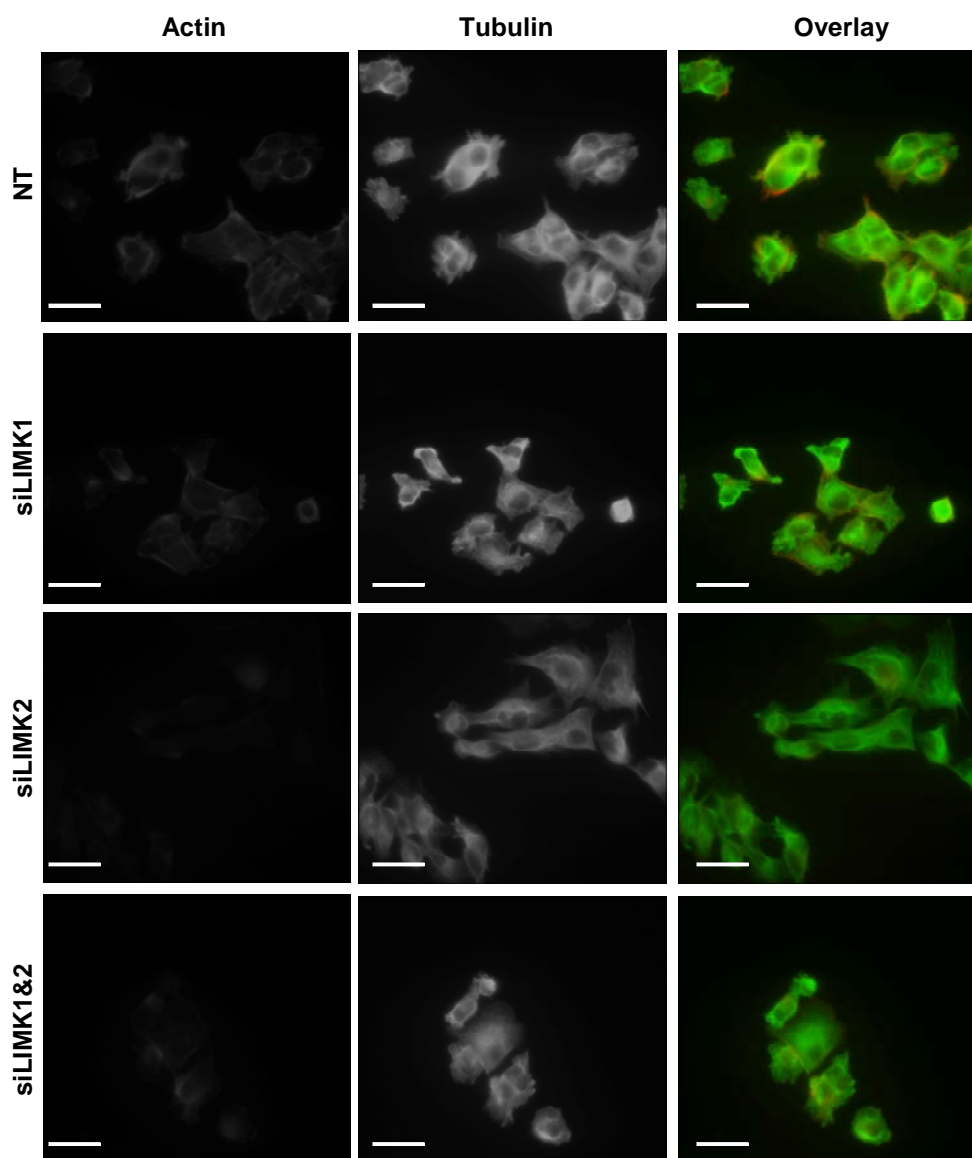


**Figure 3.3.3-BT549 morphology on glass.**

Following siRNA treatment against LIMK1, LIMK2, both in combination or with a non-targeting oligonucleotide; The first Column shows weak staining of the actin cytoskeleton for F-actin using Texas Red phalloidin, the second shows staining of the microtubule network with an anti-alpha tubulin antibody and FITC secondary antibody, and the third column an overlay of the two. Images captured on the Zeiss Axioplan 200 at x40 using Imaging Associates Isis software. Scale bar equals 20 $\mu$ m.

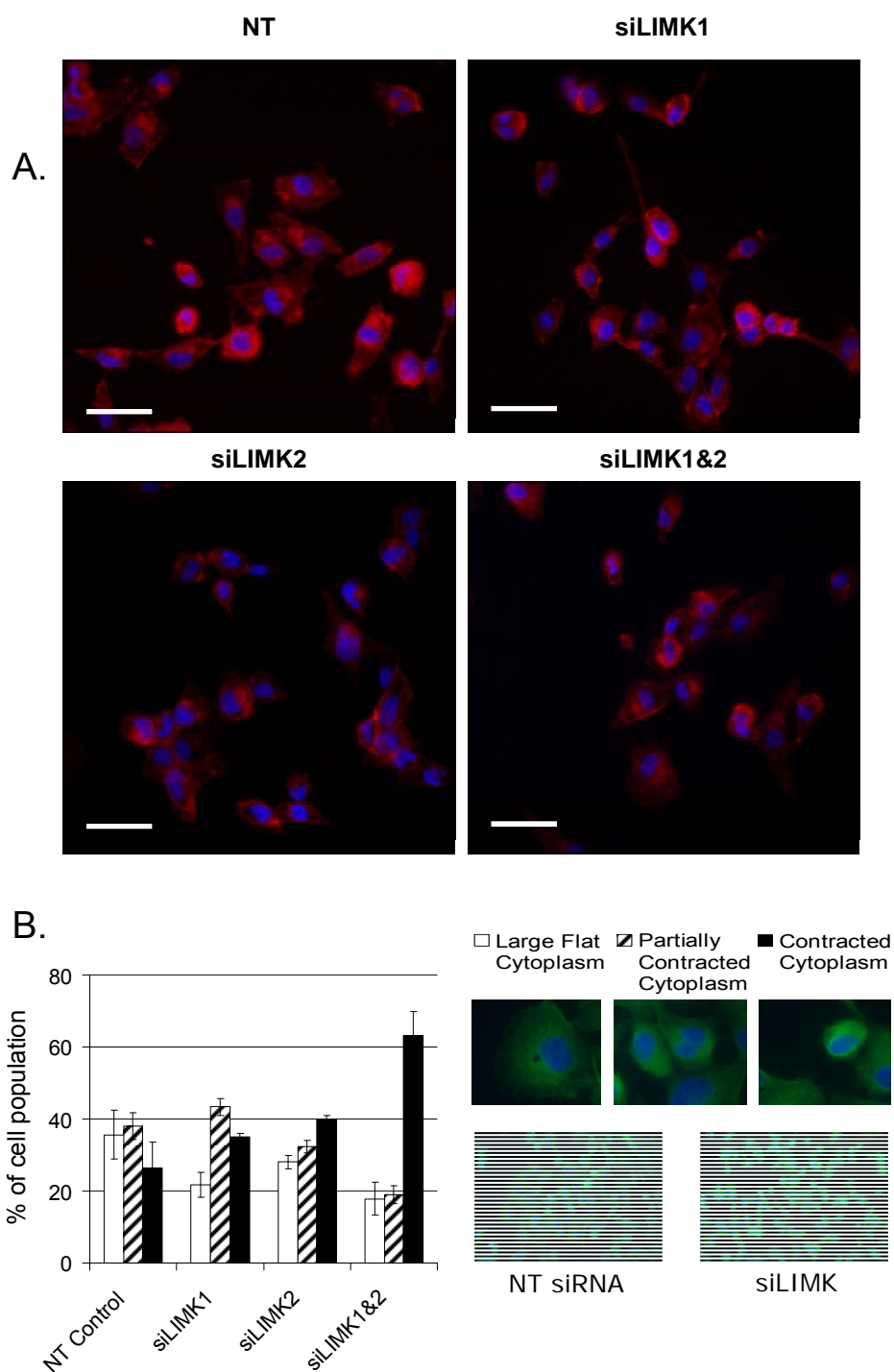


**Figure 3.3.4-BE morphology on glass.**

A. Following siRNA treatment against LIMK1, LIMK2, both in combination or with a non-targeting oligonucleotide; Staining of the actin cytoskeleton for F-actin using Texas Red phalloidin is shown in red, staining of the nucleus with DAPI in blue shown as an overlay of the two. Images captured on the Zeiss Axioplan 200 at x20 using Imaging Associates Isis software. Scale bar equals 40 $\mu$ m.

B. Quantification of the shift in cell morphology from mixed (in this case described as with a large flat cytoplasm, a partially contracted cytoplasm or a contracted cytoplasm, illustrated by examples under the graphs legend) to more contracted following knockdown of both LIM Kinases by siRNA. Examples of wider fields of cells following transfection with non-targeting control siRNAs or LIMK1& siRNAs are shown below the legend. All images captured on the taken Zeiss Axioplan 200 at x20.

Knockdown of LIMK caused a decrease in F-actin staining in MDAMB231, BT549 and BE cells, and a loss of peripheral micro-spikes in MDAMB231. This fits in with our current understanding of LIMK function as a regulator of Cofilin activity. Loss of LIMK by knockdown leads to a reduction in Cofilin phosphorylation which equates with more active Cofilin being present within the cell, in turn leading to a decrease in polymerised actin. Loss of F-actin staining in the three cell lines examined following knockdown of LIMK additionally validated that the LIMK siRNA oligonucleotides have direct and targeted effects.

BE cells respond in a similar manner to knockdown of LIM Kinases (Figure 3.3.4 part A), displaying a reduction in F-actin staining following loss of either LIMK or both LIMK1 and LIMK2 in combination. When stained for alpha tubulin to visualise the whole cell it became apparent that the morphology of BE cells as a population was changing. In culture they can be described as split into roughly 3 morphologies; A) a large, flat, spread cytoplasm, B) a partially contracted cytoplasm, and C) a contracted cytoplasm. Following transfection with siRNA against LIMK1, 2 or both in combination there was a shift from equal distributions of these morphologies to an increase in the contracted population of cells (Figure 3.3.4 part B).

### ***3.2.3 Initial observations suggest LIM Kinases are important in cell motility.***

Most published LIMK literature describes effects of either LIMK1 or LIMK2, but a systematic comparison of the roles both kinases could be playing in cell motility or invasion had not been undertaken. Wound healing assays are a simple method used to measure cell migration *in vitro* and are based upon the observation that cells on the edge of an artificially created scratch or 'wound' will move toward the opening in the monolayer until new cell-cell contacts are made (Liang et al, 2007). This method aims to mimic the migration of cells *in vivo*, similar to the effect seen in rat studies where endothelial cells migrate into wounded areas of blood vessels to close up deliberately damaged areas (Haudenschild CC, 1979). With the aid of time-lapse microscopy and imaging software it is possible not just to image wound size at the start and end of an experiment, but also the migratory paths of individual cells. These tracks can then be compared between

experimental conditions and controls to determine the role of a protein (in this case LIMK1 or LIMK2) in directional cell migration.

In order to address whether LIMK1, LIMK2 or both LIMK1 and LIMK2 were required for cell migration, wound healing assays (also referred to in some literature as scratch assays) were performed. MDAMB231 cells were subject to siRNA against either LIMK1 (siRNA #1), LIMK2 (siRNA#2) or both kinases in combination in 6well dishes. 48hrs after siRNA transfection, a scratch was made across the confluent monolayer using a micro pipette tip and the media gently changed to reduce the likelihood of free floating cells moving into the field of view during imaging. The wounds were then imaged using a Zeiss time-lapse microscope for 24 hours at 15minute intervals, creating image timelines for each wound. Images of each wound at T=0 and T=24 hours are compared in Figure 3.3.5 part A. After 24 hours, control cells transfected with non-targeting siRNA (NT) closed the wound, as did cells subjected to siRNA against LIMK1 (siLIMK1). Cells with reduced levels of LIMK2 (siLIMK2) did not close the breach in the monolayer, and cells siRNA treated for both LIMK1 and 2 (siLIMK1&2) managed to cross the wound but did not close it fully. Individual cells along the leading edge of the 'wounds' were tracked using imaging software (ImageJ) to visualise the directionality of cells under each knockdown condition, as illustrated in Figure 3.3.5 part B. The tracks mapped for control cells and those with knocked down LIMK1 appear longer and smoother than the twisting tracks taken by cells with knocked down LIMK2 or those with LIMK1 and 2 knocked down. The distance over which these tracks spread was also reduced in the LIMK2 and LIMK1&2 knock downs, cells rarely travelled further than the 200 unit point, compared to siLIMK1 where some reach 250 or the NT control cells that travelled up to around the 300 limit. In the cells with reduced LIMK fewer cells were seen to move up and down the leading edge of the wound in comparison to NT control, the tracks were predominantly directional, closing the wound.

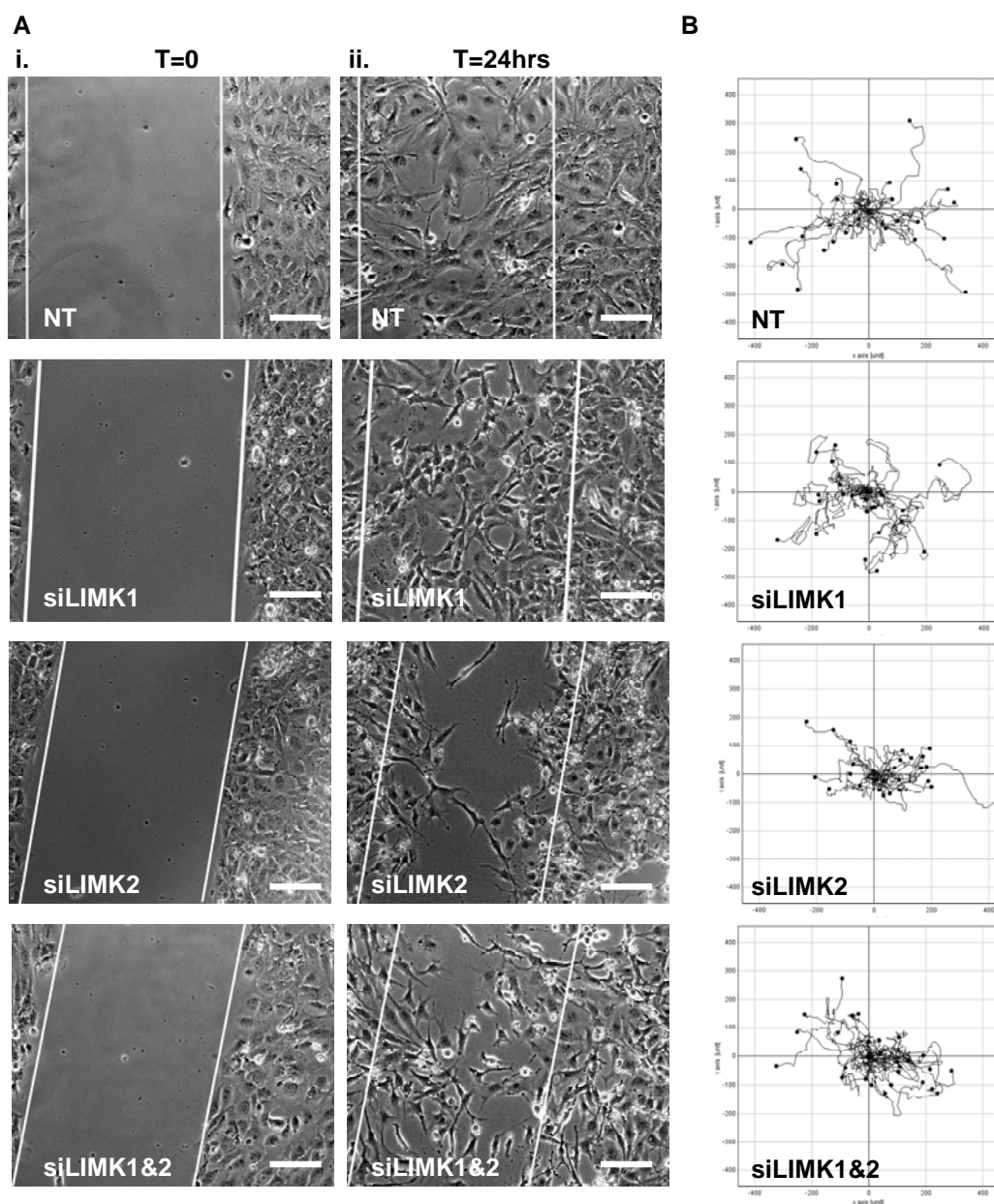


**Figure 3.3.5-MDAMB231 wound healing assay.**

Following siRNA treatment LIMK1 (#1&#3), LIMK2 (#6&#7) or both LIMK1 and LIMK2 (#1&#6 or #3&#7) in combination or with a non-targeting oligonucleotide; A.i. Time equals zero, confluent MDAMB231 were denuded to create a 'wound'. A.ii. Time equals 24 hours. Cells subject to knockdown of LIMK1 appear to have unaffected wound healing, knockdown of LIMK2 or both in combination show slightly reduced capacity for wound healing. Scale bar for A equals 100 $\mu$ m B. Tracks of individual cells during wound healing. Cells with reduced LIMK have shorter, more compact tracks than control cells. Images captured on a Zeiss Timelapse Microscope at x20 using Andor IQ software. Cells were followed manually using ImageJ software to visualise cell tracks during wound healing, arbitrary units displayed.

These early observations indicated that loss of LIMK1 had little effect on directional motility but that reducing LIMK2 reduced wound healing capability, and that loss of both kinases had an intermediate effect. The intermediate effect seen when both LIMK1 and LIMK2 were knocked down could have been due to the design of the experiment. siRNA treatment against both LIMK1 and LIMK2 used the same total concentration of RNA as the knockdowns targeting LIMK1 or LIMK2, but this was achieved by using half the amount used against each individual LIMK to make a mixture targeting both. This could have made the LIMK2 knockdown less efficient and cause an intermediate reduction in motility.

### ***3.2.4 Knockdown of LIMK has little effect on cell motility in 2D on plastic.***

Having confirmed that LIMK levels can be successfully knocked down by siRNA in MDAMB231, cell motility assays were used to examine if a reduction in LIMK affected cell motility. Initial observations were obtained from a traditional wound healing assay, a scratch made across a monolayer of cells using a micro pipette tip, and suggested that reducing LIMK2 levels had a greater effect (Figure 3.3.5). The wounds in these assays can vary between conditions, as can the force generated to denude the area of the dish. In order to perform a more reproducible and quantifiable motility assay, one that generates a regular wound size between all conditions, the Oris cell migration assay was employed.

Oris migration assays were performed in a 96well dish format. Rubber plugs are placed within each well of the dish and cells seeded around the plug, after a suitable time for cells to settle has passed the plugs are removed and the centre of each well is clear of cells, leaving a regular and repeatable 'wound'. This technique was used to compare the motility of cells over plastic following knockdown of LIMK1, LIMK2 or both in comparison to those treated with non targeting control oligonucleotides. Twenty four hours following siRNA knockdown MDAMB231, BT549 and BE cells were seeded into individual Oris migration plates in quadruplicate for each condition, with one row of 4 wells retaining their plugs to act as a control (i.e. 'no motility'). All other wells were given 24 hours to move into the wound following removal of the plug. Subsequent staining with the live cell dye Calcein AM was performed and the plates were then imaged on

an upright fluorescent microscope. A 'mask' was added to the bottom of each plate to allow visualisation of only the 'wound' and then the plate was either read on a Tecan Safire plate reader to quantify the fluorescence (cells) in the wound, or the images taken used to quantify the area of cells in the wound by ImageJ Software. Despite confirmation of LIMK knockdown by western blot there did not appear to be any difference in motility between cells that had lost LIMK1, LIMK2 or both by siRNA in comparison with control MDAMB231 cells (Figure 3.3.6). There was a reduction in pCofilin (phospho-Cofilin) levels following LIMK knockdown, further confirming a reduction in LIMK activity. This would have predicted a change in cell motility as Cofilin has been found to determine the migration behaviour of metastatic cancer cells (Sidani et al, 2007). In contrast to the results observed in MDAMB231 cells, there was a significant reduction in motility of BT549 cells following knockdown of LIMK1, LIMK2 or both in comparison with control cells (Figure 3.3.7), and a similar trend was seen in BE cells. Knockdown of LIMK2 in BE cells caused a consistently significant reduction of motility (Figure 3.3.8). The trend for BE cells suggest a loss of motility following LIMK1 knockdown or when both LIMK1 and LIMK2 are knocked down, but only one of each set of oligonucleotides per condition could be considered statistically significant. Results from Oris migration assays suggest that LIM Kinases are important for the motility of some cells across plastic, but not all. MDAMB231 cells are known to be a motile cell line, capable of interacting with their environment to facilitate invasion. There appeared to be no requirement for LIMK in MDAMB231 motility on plastic following wound healing experiments, despite initial indications from traditional 'scratch' assays. The original scratch assays were somewhat flawed. Cells were plated, siRNA treated and then the monolayer disrupted, without counting cells before the wounds were generated. The later experiments using Oris migration assays counted cells before generating a wound, so any subtle change in cell number could be accounted for and not suggest a false effect on cell migration via proliferation. Although there was not a statistical difference between cells with knockdown LIMK compared to controls, there was a subtle change in number. A malleable substrate more reflective of physiological conditions could present changes in motility following knockdown of LIMK compared to the rigid plastic substrate.

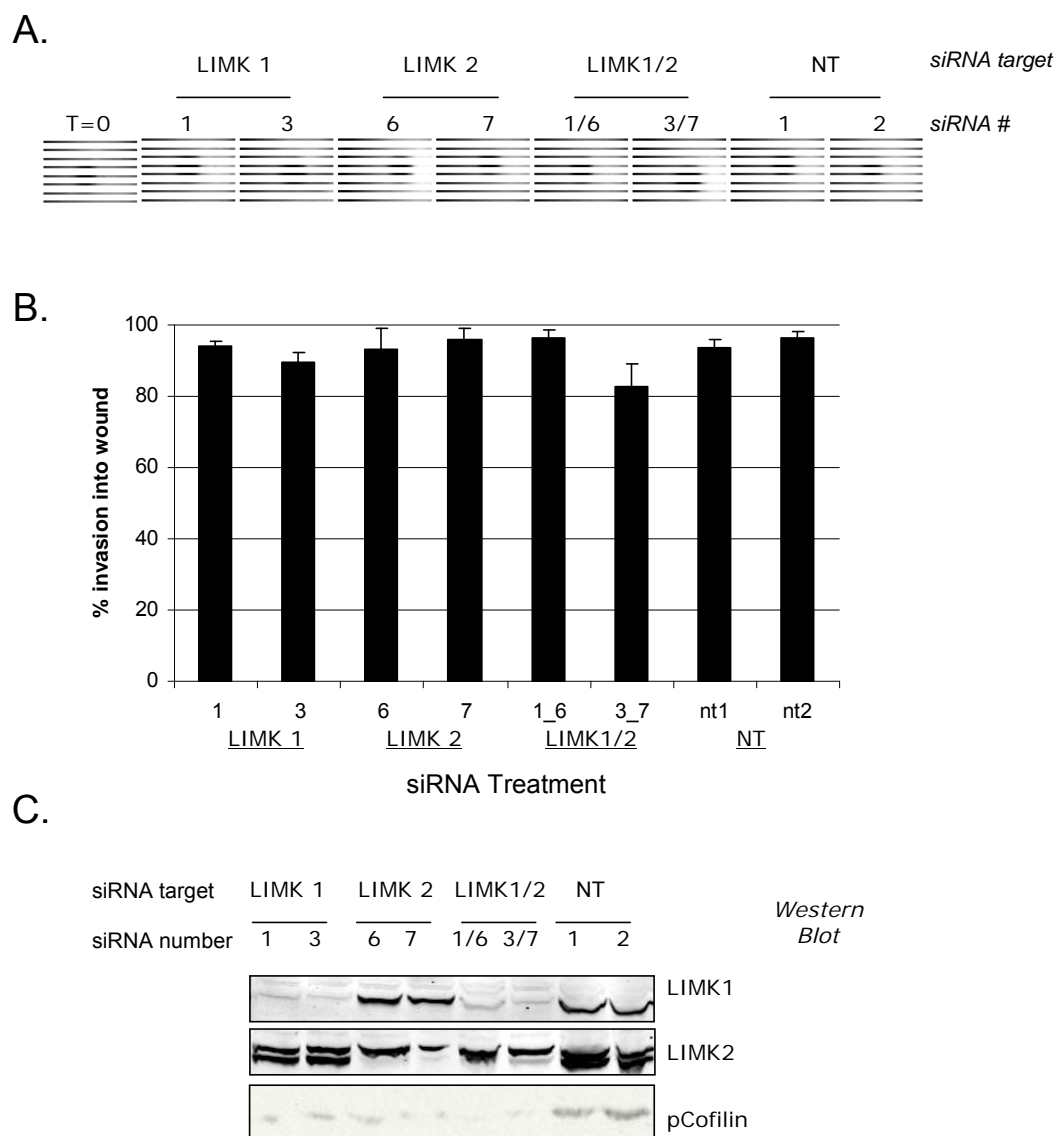


### Figure 3.3.6-Motility of MDAMB231 using the Oris cell migration assay

MDAMB231 cells subject to loss of LIMK1, LIMK2 or both LIMK1 and LIMK2 in combination by siRNA oligonucleotides closed the 'wound' in a comparable way to cells subject to non-targeting control oligonucleotides. A. Brightfield images of wounds after 24hours, imaged on an Olympus tissue culture microscope at x2.5. B. Quantification of cells in centre of wound using Imaging software (ImageJ), no significant differences were observed between conditions (as determined by ANOVA). C. Western blot confirmation of LIMK knockdown, and reduction in phospho-Cofilin levels.

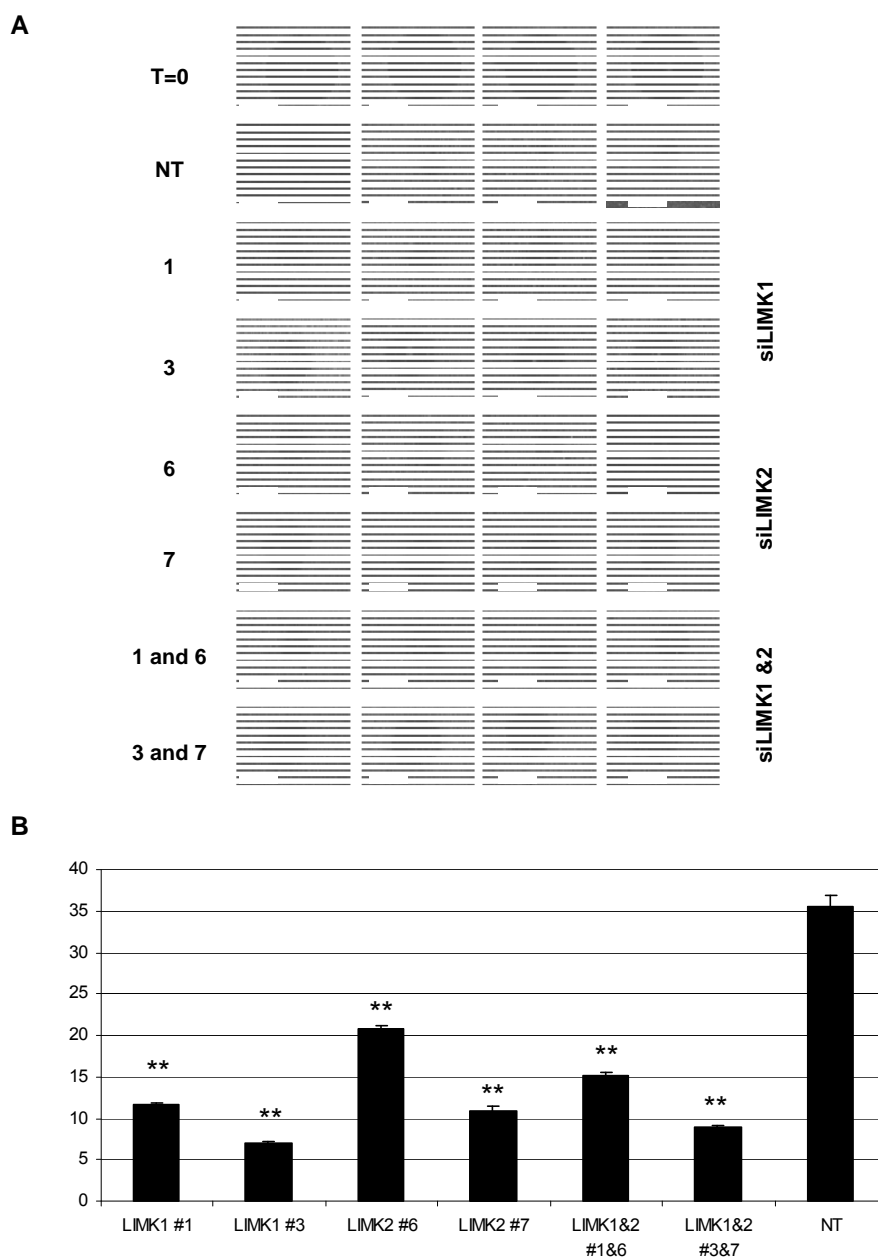


**Figure 3.3.7-Motility of BT549 using the Oris cell migration assay**

Following siRNA treatment against LIMK1, LIMK2, both in combination or with a non-targeting oligonucleotide; A shows images of wounds after 24hours, cells stained in all conditions using Calcein AM. B. Quantification of cells in centre of wound using Tecan Safire plate reader. Double asterisk indicates  $P < 0.01$  as determined by a Student T test. Images captured on Olympus Fluorescent Tissue Culture Microscope at x2.5 Scale bar equal to 750 $\mu$ m.

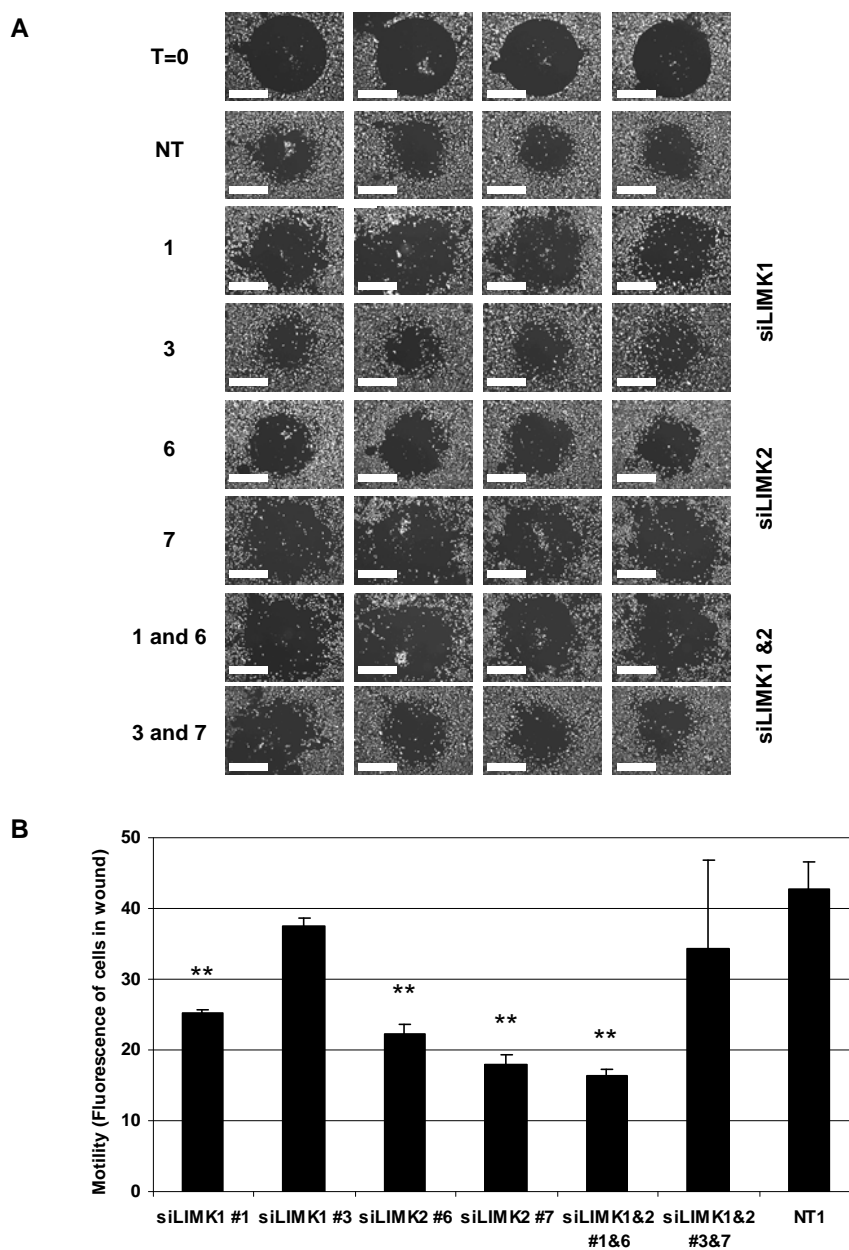


**Figure 3.3.8- BE wound healing and motility on plastic.**

Following siRNA treatment against LIMK1, LIMK2, both in combination or with a non-targeting oligonucleotide; A shows images of wounds after 24hours, cells stained in all conditions using Calcein AM. B. Quantification of cells in centre of wound using Tecan Safire plate reader. Double asterisk indicates  $P < 0.01$  as determined by a Student T test. Images captured on Olympus Fluorescent Tissue Culture Microscope at x2.5 Scale bar equal to 750 $\mu$ m.

### **3.2.5 Knockdown of LIMK has no effect on cell motility on CDM.**

Cell derived matrix (CDM) in the following experiments refers to the oriented 3D fibrillar extracellular matrix generated by primary cultured human dermal fibroblasts (Cukierman et al, 2001) and secreted into their environment, in this case onto tissue culture plastic-ware. After the removal of the transformed fibroblast cells, the remaining structured matrix can be used to study motility of chosen cell types. The CDM provides a substrate that moving cells can adhere to, distort and degrade but it does not require the generation of low-resistance paths by ECM remodeling. Cell movement is guided by the meshwork of long fibronectin fibrils secreted by the fibroblasts which promotes polarity and results in efficient directional protrusion, making this model ideal for measuring the persistence of cells (ratio between vectorial and accumulated distance travelled).

Following knockdown for LIMK1, LIMK2, LIMK1&2 or non targeting siRNA, MDAMB231 cells were plated sub-confluently onto CDM and imaged every 15 minutes for 12 hours using phase contrast microscopy on a time-lapse microscope. Individual cells were then tracked using ImageJ software. MDAMB231 placed on CDM predominantly moved along the 'tracks' left by the removed TIF cells (telomerase-immortalised human fibroblasts), occasionally moving between these 'tracks' that outline the previous cell positions (Figure 3.3.9). Quantification of accumulated distance (total distance travelled by cells), vectorial distance (direct distance between start point and end point of cell track) saw no difference between the knockdown conditions (Figure 3.3.10) and the level of persistence shown by cells (the most persistent being considered '1', with no difference between vectorial and accumulative distances) was also statistically insignificant between conditions. There was, however a visible difference in cell morphology between control cells and those subjected to LIMK1&2 knockdown, as can be seen in Figure 3.3.11, knockdown cells were more refractile and maintained a more 'raised' morphology as they moved (like snails with larger shells but a similar sized footprint to their control counterparts). The morphological differences between control cells and those with reduced LIMK did not translate into a difference in motility by invasive MDAMB231 cells in the conditions used, but all of these experiments were

essentially performed in 2D. Where CDM, a more interactive substrate than tissue culture plastic, was used to examine the effects of blocking LIMK activity on cell motility a morphological change was observed using phase contrast microscopy.

### ***3.2.6 LIMK is a requirement of cell invasion into 3D matrix***

Over expression of LIMK1 can increase motility and invasiveness of human breast cancer cells(Yoshioka et al, 2003) and can promote the acquisition of an invasive phenotype in benign prostate epithelial cells(Davila et al, 2003), it was therefore concluded that loss of LIMK1 or loss of LIMK2 could reduce the capability of invasive cancer cells to invade. In 2D motility there is no requirement for degradation or the use of force in path generation, cells are free to move in any direction across a 2D field. In 3D cells require both the ability to move but also the ability to generate a path along which to move, this may be achieved by proteolytic activity or in combination with the cells ability to physically deform its environment. In order to understand the potential role LIM Kinases play in cancer cell invasion, a physiologically relevant assay was employed; one in which the cells could both interact with their substrate but also have the opportunity to move in a 3-dimensional manner, allowing for degradation and deformation. Inverse invasion assays(Hennigan RF, 1994) provide a 3D environment through which cells can invade and interact and the assay is outlined in Figure 3.3.12. The matrix used as a 3D interactive substrate is produced by BD Biosciences and mimics the complex extracellular matrix secreted by cells in tissue. It is extracted from Engelbreth-Holm-Swarm (EHS) mouse sarcoma, and although its exact composition has not been determined it is known to contain, (along with other growth factors from the EHS tumour), laminin, collagen IV, TGF- $\beta$ , EGF, insulin-like growth factor and FGF(BD Biosciences <http://www.bdbiosciences.com/nvCategory.jsp?modeCategory=FULL>).

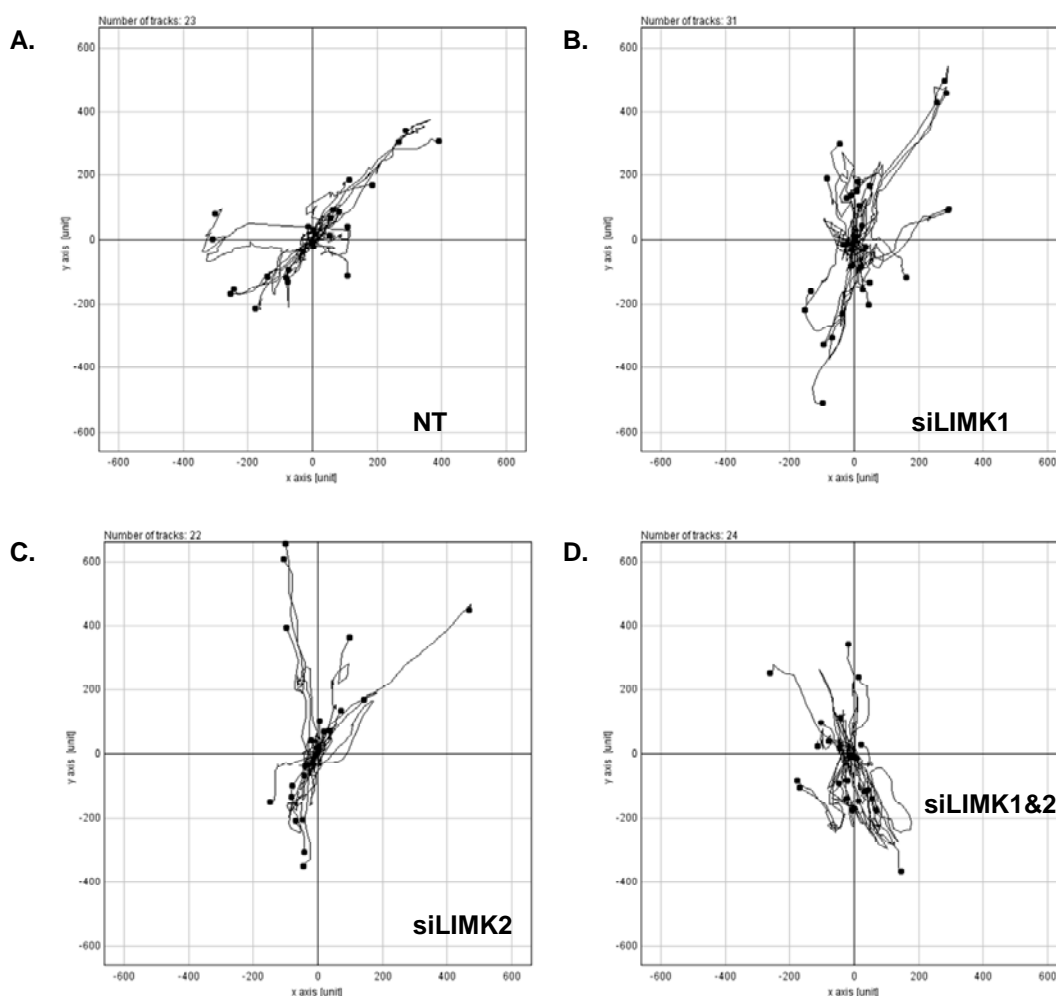


### Figure 3.3.9-MDAMB231 Motility on Cell Derived Matrix mapped.

Representative data from tracks of cells moving on cell derived matrix following knockdown of LIMK1, 2 or both in combination by siRNA. A. shows the tracks of MDAMB231 cells following transfection with a non-targeting control siRNA. The direction of growth of Tiffs used to generate the CDM is reflected in the routes taken by the MDAMB231. B. Tracks of MDAMB231 following siRNA against LIMK1, 2 (C.) or both in combination (D.) no significant differences were observed between conditions (determined by ANOVA on the quantitative data used to plot these graphs).

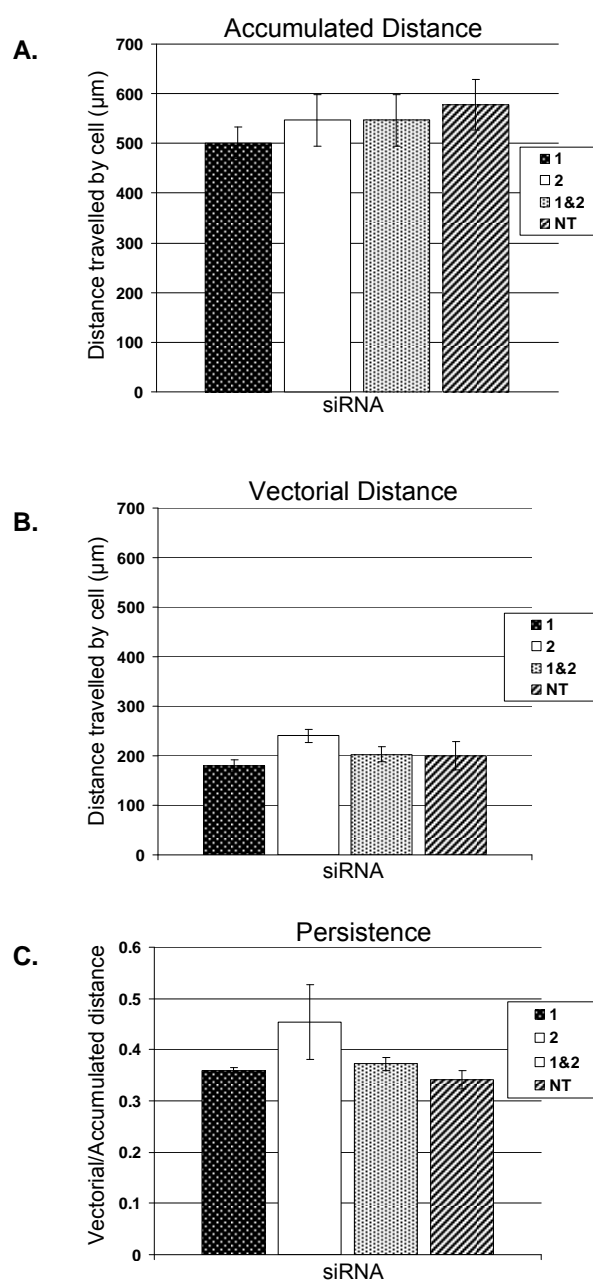


**Figure 3.3.10-MDAMB231 Motility on Cell Derived Matrix quantified.**

A. Mean accumulated distance travelled by cells following siRNA treatment against LIMK1, LIMK2, both in combination or with a non-targeting siRNA. B. Mean Vectorial distance travelled by cells following siRNA treatment. C. Persistence of cells travelling over CDM following siRNA treatment. Error bars refer to Standard Error, n=3 throughout, no significant differences were observed between conditions (determined by ANOVA).

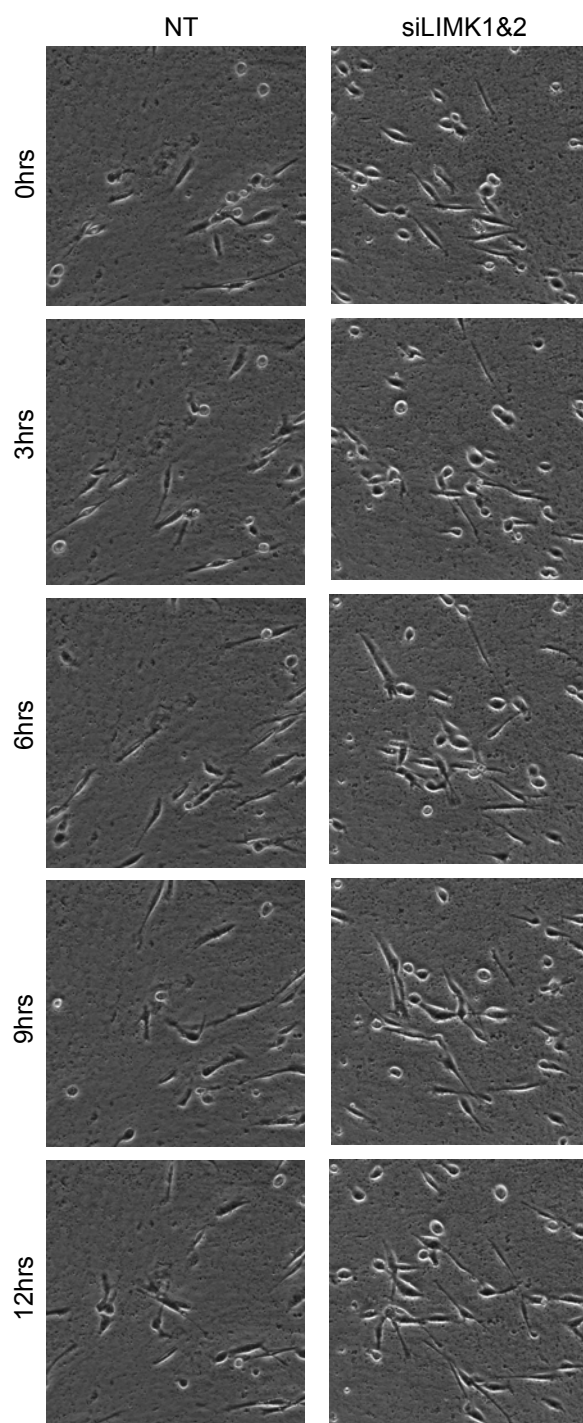


**Figure 3.3.11-Timeline of MDAMB231 motility on CDM, LIMK knockdown cells refract more than controls.**

MDAMB231 cells moving across Cell Derived Matrix (CDM). Following knockdown of both LIMK1 and LIMK2 by siRNA cells refract more in comparison with control cells subject to non-targeting siRNA, appearing to maintain a more 'raised' morphology as they move across the substrate. Images captured on a Zeiss Timelapse Microscope at x20 using Andor IQ software.

To assess the role LIM Kinases play in 3D invasion MDAMB231 cells, which have previously been shown to be an invasive cell line (Munoz-Najar et al, 2005; Nizamutdinova et al, 2008), were subject to knockdown of LIMK1, LIMK2 LIMK1&2 or non targeting (NT) siRNA and placed into inverse invasion assays (as described in Figure 3.3.12). Following a 5 day period to allow for cell invasion, cells were stained with Calcein AM and Z-stacks imaged of each matrigel invasion 'plug' using a Leica Confocal microscope at x10 magnification; examples of which can be seen for MDAMB231 cells in part A of Figure 3.3.13. Before quantification, a clear reduction in invasion by MDAMB231 following knockdown of both LIMK1&2 can be seen. Image stacks such as these were then quantified using ImageJ software. The cumulative invasion of MDAMB231 is illustrated in part A of Figure 3.3.14. Although many cells in all conditions crossed the initial filter barrier at the bottom of the transwell invasion assay, NT control cells achieved a greater overall level of invasion. This can be seen by the initially steeper curves of the lines representing control cells in this cumulative graph, and the larger values 135 $\mu$ m into the matrigel (total invasion). One way to standardise the quantification of invasion is to score cells that have moved over 45 $\mu$ m into the matrigel (Spence et al, 2006). This method of quantification similarly illustrates the importance of both LIMK1 and LIMK2 in the invasiveness of MDAMB231 (Figure 3.3.14). Loss of either kinase reduced invasion beyond 45 $\mu$ m, loss of both LIMK1 and LIMK2 caused an equally large reduction in invasiveness. This contrasts with the lack of requirement for LIMK for MDAMB231 2D motility. The cells that required LIMK for 2D motility (BT549 and BE) showed no clear requirement for LIMK in invasion (Figure 3.3.15 and Figure 3.3.16). However, this data cannot be interpreted fully as even in control conditions these cells failed to invade the matrigel fully, most not reaching the 45 $\mu$ m cut off often referenced in publications investigating invasion. Considering this, further investigations into 3D invasion were then conducted using the invasive cell line MDAMB231.

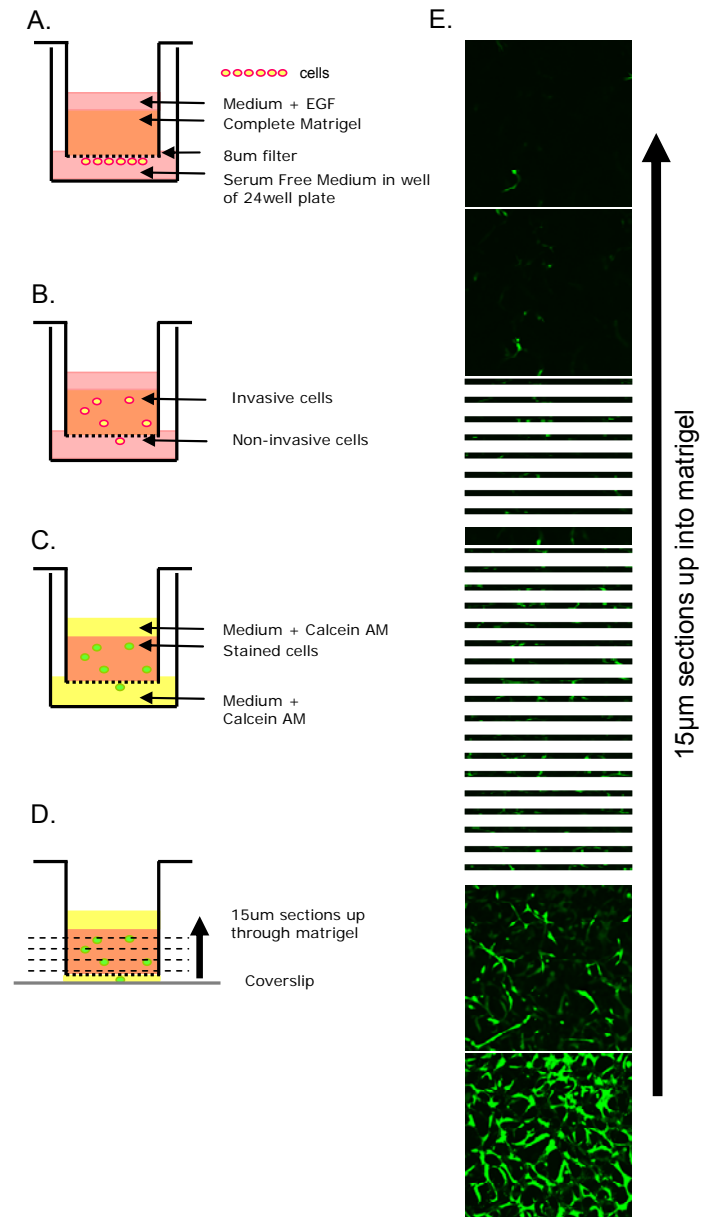
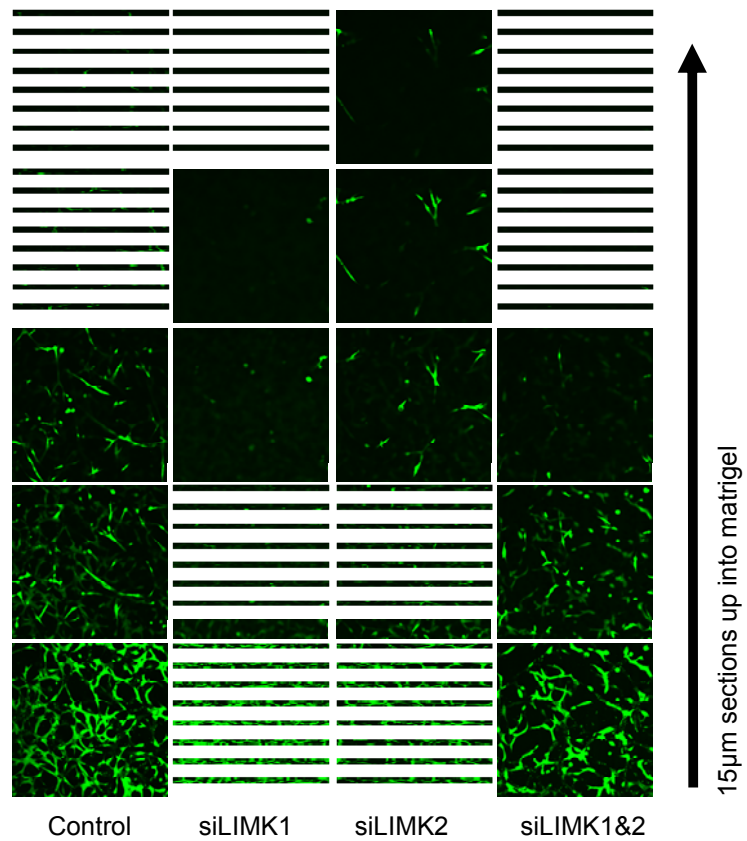


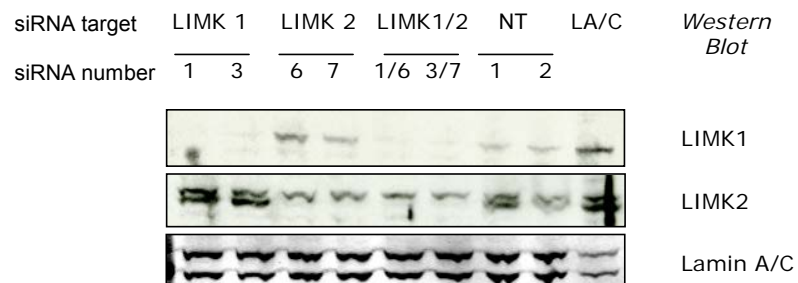
**Figure 3.3.12-Inverse invasion assay.**

The inverse invasion technique uses 8  $\mu$ m filter transwells filled with matrigel to provide a 3D environment for cells to invade into (A. and B.). Cells are stained in the matrigel plug with Calcein (C) and imaged by confocal microscopy in 15  $\mu$ m sections (D. and E.). E. shows the invasion of MDAMB231 cells into matrigel in 15  $\mu$ m sections.

A.

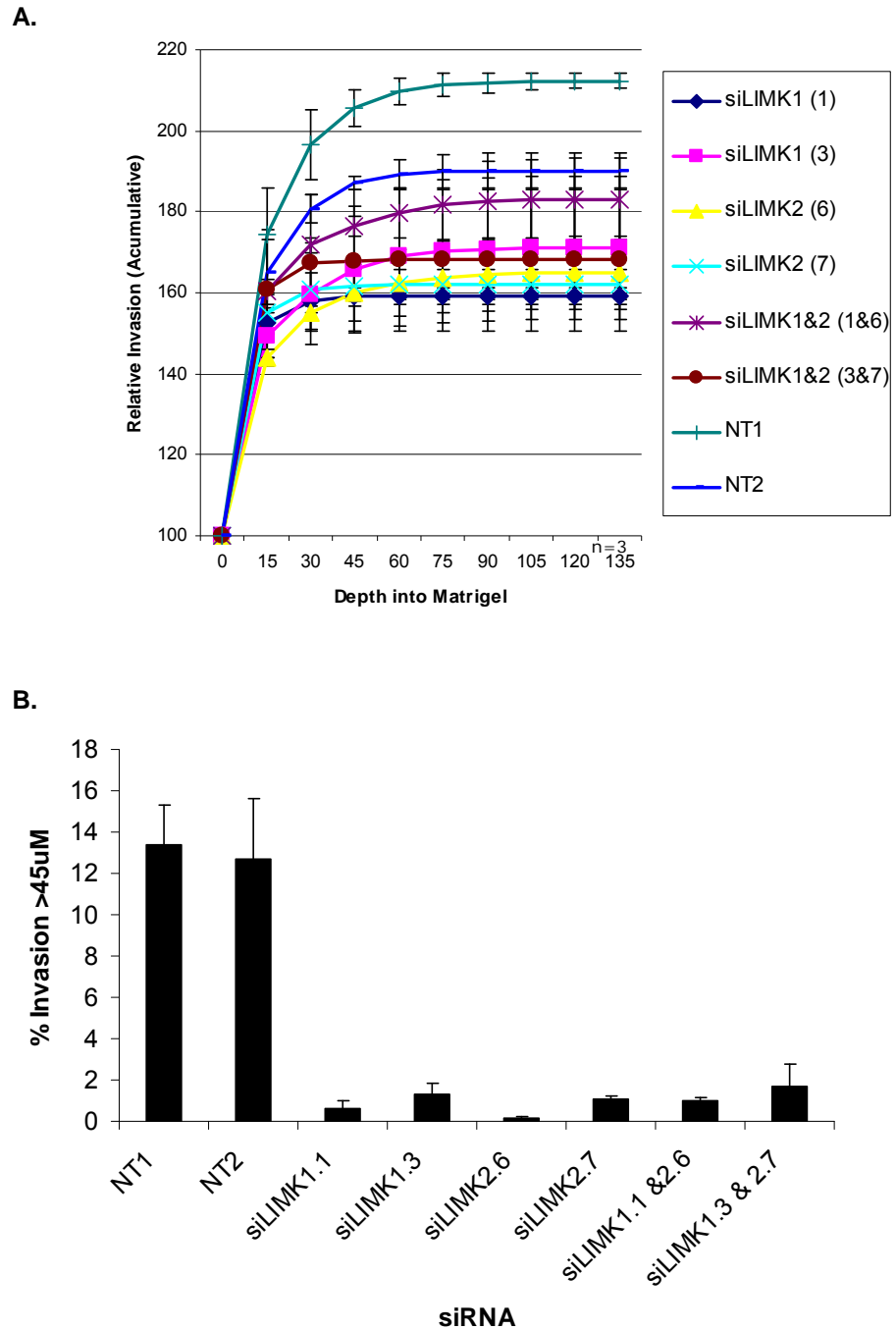


B.



### Figure 3.3.13-Loss of LIMK reduces MDAMB231 3D Invasion

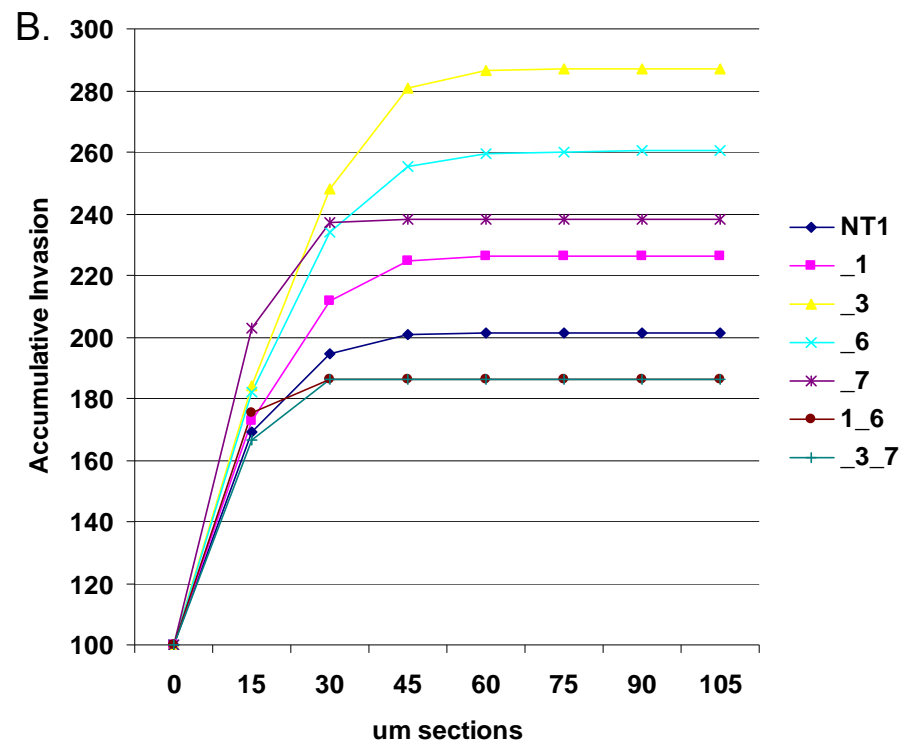
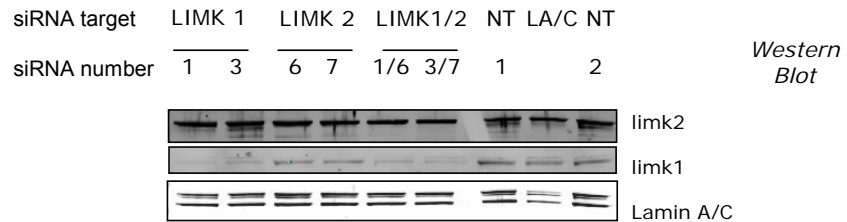
A. 15µm Z sections of MDAMB231 cells invading through matrigel following knockdown of LIMK1, LIMK2 or both in comparison with control cells transfected with a non-targeting siRNA. Images obtained using a Leica Confocal microscope at x10. B. Western Blot of LIMK levels following siRNA treatment for siLIMK1, siLIMK2, a combination of both siLIMK1 & siLIMK2 and non-targeting siRNA controls. Lamin A/C siRNA functions as a loading control, as well as a positive control for siRNA activity.



**Figure 3.3.14-Quantification of MDAMB231 loss of Invasion following knockdown of LIM Kinases**

A. Cumulative invasiveness of MDAMB231 cells invading into Matrigel; Cells that have been siRNA treated against LIMK1, LIMK2 or LIMK1 and LIMK2 invade less into the Matrigel, and those that have invaded following loss of LIMK do not go as far into the matrigel in comparison with controls. B. Percentage invasion of MDAMB231 cells over 45 $\mu$ m following LIMK1, 2 or both knock-down by siRNA in comparison with cells treated with non targeting control siRNA.

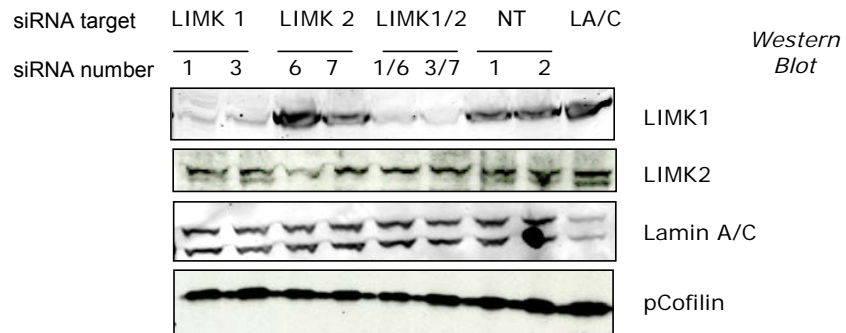
A.

*BT549*

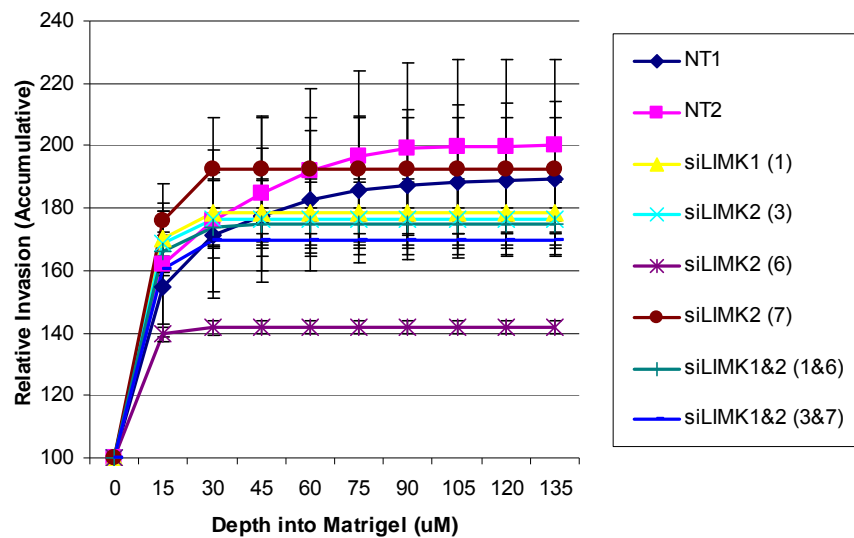
**Figure 3.3.15-Quantification of BT549 loss of Invasion following knockdown of LIM Kinases**

A. Western Blot of LIMK levels following siRNA treatment for siLIMK1, siLIMK2, a combination of both siLIMK1 & siLIMK2 and non-targeting siRNA controls. Lamin A/C siRNA functions as a loading control, as well as a positive control for siRNA activity. A. Cumulative invasiveness of BT549 cells invading into Matrigel; There is no clear pattern of effect on invasion into the matrigel by cells that have been siRNA treated against LIMK1, LIMK2 or LIMK1 and LIMK2 in comparison with controls.

A.

*BE Colon Carcinoma*

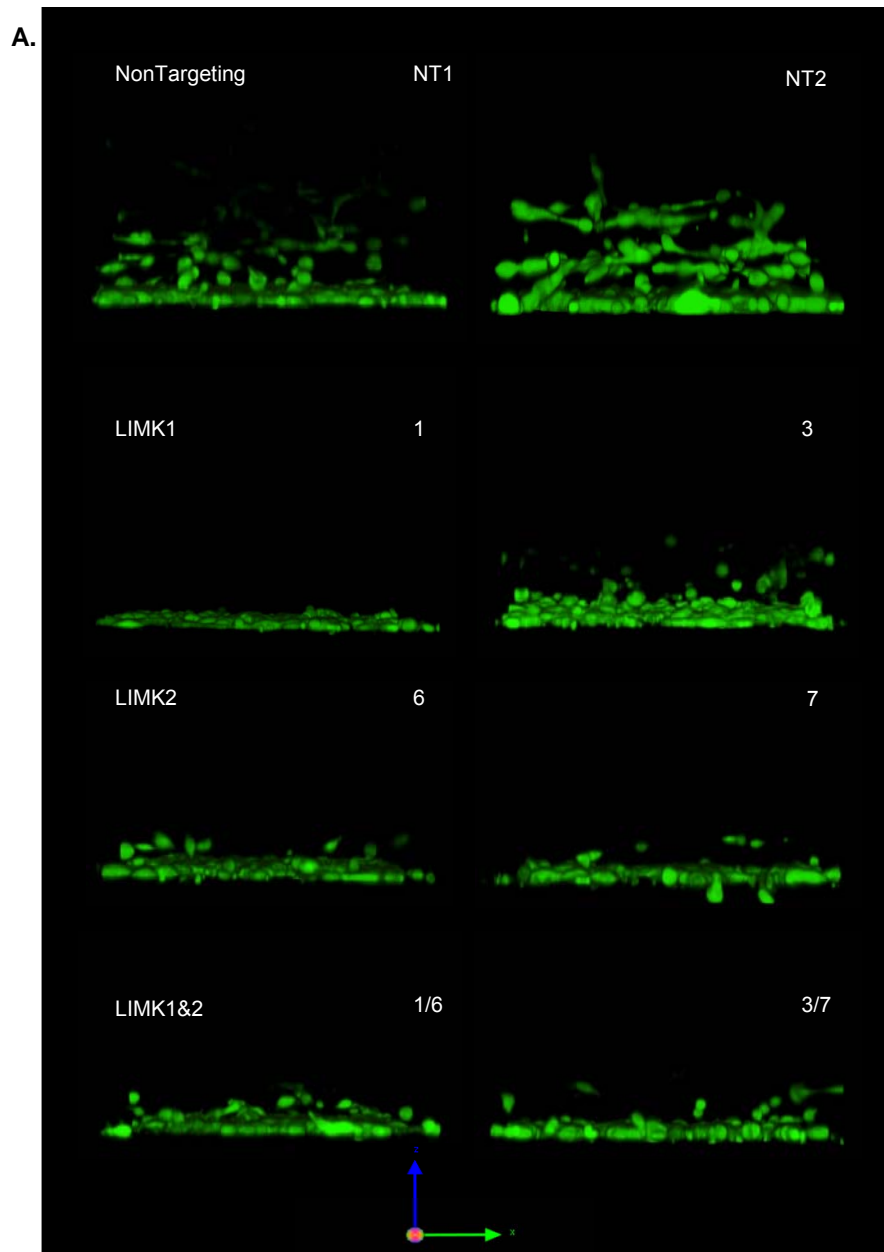
B.

**Figure 3.3.16 Quantification of BE loss of Invasion following knockdown of LIM Kinases**

A. Western Blot of LIMK levels following siRNA treatment for siLIMK1, siLIMK2, a combination of both siLIMK1 & siLIMK2 and non-targeting siRNA controls. Lamin A/C siRNA functions as a loading control, as well as a positive control for siRNA activity. A. Cumulative invasiveness of BE cells invading into Matrigel; There is no clear pattern of effect on invasion into the matrigel by cells that have been siRNA treated against LIMK1, LIMK2 or LIMK1 and LIMK2 in comparison with controls.

### **3.2.7 Cell morphology in 3D following loss of LIMK**

MDAMB231 cells showed subtle morphological changes following knockdown of LIMK when cultured on cell derived matrix, an interactive 2D substrate. Previous work has shown environmental cues can also alter the morphology of cells in culture (Kenny et al, 2007). Whether this was the case in 3D, and correlated with loss of invasion following knockdown of LIMK, was then investigated. MDAMB231 cells were pre-treated with siRNA against LIMK1, LIMK2, LIMK1&2 or a non targeting oligonucleotide and transferred to the inverse invasion assay to provide a 3D substrate for invasion. The cells in the matrigel plug were then fixed and stained with a whole cell dye (in this case Calcein AM) for visualisation on a FV100 Olympus confocal microscope. Using a water lens, 2µm sections were taken up through the matrigel 'plug' until the point where no cells were detected. These image stacks were then processed using Volocity 6.0 imaging software to construct a 3D model of the MDAMB231 cell invasion (Figure 3.3.17 A and B - movie on supplementary CD). As expected from the images in Figure 3.3.13 cells with knockdown of LIMK1, LIMK2 or both LIMK1&2 invaded less than control cells transfected with non targeting siRNAs. In all conditions cells moved through the 8µm filter and were sitting on top of the filter, just beneath the matrigel. From this 'base' layer of cells on the filter, control cells were seen as elongated globular chains; suggesting that cells may have tracked after each other into the matrix as well as invading the matrix individually. Of the cells with reduced levels of LIMK1, the small number of cells that managed to invade a short distance into the matrix did so in a singular manner, there were no visible 'tracks' of cells. This was also the case for cells subject to LIMK2 knockdown, in the image for oligonucleotide number '7' against LIMK2, it is interesting to see some cells that were captured moving up through the filter to sit beneath the matrigel. Knockdown of both LIMK1 and LIMK2 appeared to reduce cell size/shape in 3D, the few cells that invaded were smaller and more rounded in appearance than control cells. In all the knockdown conditions tested, cells were still able to cross the 8µm filter and position themselves beneath the matrigel.



B.



**Figure 3.3.17-3D morphology of MDAMB231 cells invading into matrigel.**

3D reconstruction of MDAMB231 invasion into matrigel and staining with Calcein AM. Following siRNA treatment against LIMK1 (oligonucleotides 1 and 3), LIMK2 (oligonucleotides 6 and 7), both in combination (oligonucleotides 1 and 6 or 3 and 7), or with a non-targeting oligonucleotide (NT1 or NT2). Control cells invade into matrigel, tracking after each other, loss of LIMK1, 2 or both respectively causes a loss of invasion and tracking phenotype. B. Movie of 3D reconstructed invasion following knockdown of LIMK in MDAMB231. Invasion was imaged on an FV1000 Olympus Confocal at x40 (water lens) using FV10-ASW.1.7b software and reconstructed using Velocity 6.0. Invasion sections are approximately 140µm wide.

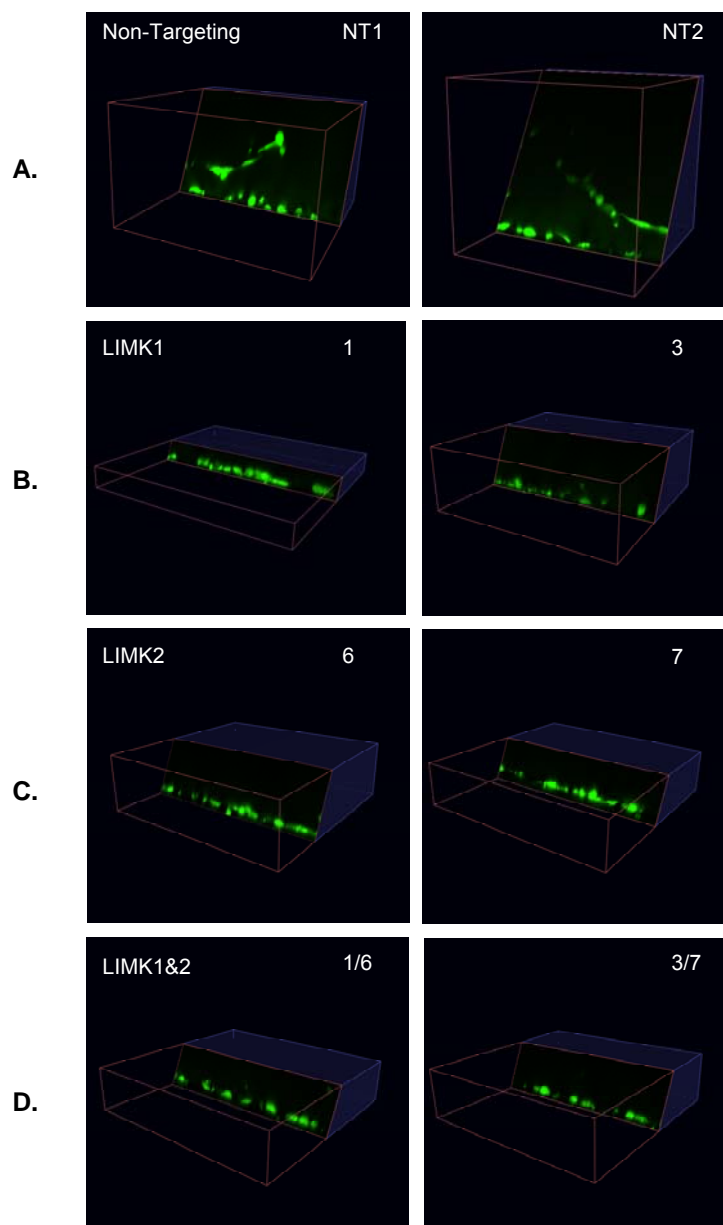


**Figure 3.3.18-MDAMB231 cells lose the ability to invade in tracks following LIMK knockdown.**

Optical slices of 3D reconstructions of MDAMB231 invasion into matrigel (staining with Calcein AM). Following siRNA treatment against LIMK1, LIMK2, both in combination or with a non-targeting oligonucleotide A. Control cells invade into matrigel, tracking after each other. B, C and D. show loss of LIMK1, 2 or both respectively causes a loss of invasion and tracking phenotype. Invasion was imaged on an FV1000 Olympus Confocal at x40 (water lens) using FV10-ASW.1.7b software and reconstructed using Volocity 6.0. Invasion sections are approximately 140µm wide.

### **3.2.7.1 MDAMB231 cells invade into Matrigel in tracks**

MDAMB231 cells appeared to invade into matrigel collectively, following each other up through the matrix in a strand (previously described by (Wolf et al, 2007)), and knockdown of either LIMK both reduced invasion and this morphology in 3D. In order to further assess whether this was the case optical slices were made through reconstructed invasion plugs, such as those seen in Figure 3.3.17. These slices more clearly show cells following each other up into the matrigel, but not in the event of LIMK knockdown (Figure 3.3.18). These are not long cells stretched out through the matrix, they are individual cells as was confirmed by PI staining of nuclear DNA. This can be seen in parts A and B of Figure 3.3.19 where a 3D reconstruction of MDAMB231 invading into matrigel (stained with Phalloidin (green) to visualise F-actin, and PI (red) for nuclei) demonstrates that multiple cells track together through the matrix. part A. shows a Z-section of the 3D reconstruction of MDAMB231 3D invasion in part B, illustrating how MDAMB231 cross the filter of the transwell but only a proportion of the population of cells then invades in tracks into the matrigel.

### **3.2.7.2 Loss of F-actin structures in 3D corresponds with loss of invasiveness following reduction in LIMK levels**

In 2D cells were seen to lose F-actin staining following knockdown of LIMK, knockdown of both kinases was achieved using two different combinations of oligonucleotides. In the later stages of these investigations a potent LIMK inhibitor became available to use within our lab, the structure of which is presented in Figure 3.3.19 part C (Ross-Macdonald et al, 2008). This inhibitor was used to investigate whether changes observed in 2D F-actin structures were also seen in 3D, in turn to determine whether this did in fact correlate with loss of invasion. Cells treated with 3 $\mu$ M inhibitor have reduced F-actin staining (and invasion) in comparison with control cells treated only with an equivalent volume of DMSO vehicle. 10 $\mu$ M LIMKi further reduced cell invasion and F-actin staining in 3D as can be seen in Figure 3.3.19 where invasion plugs are viewed from the side and have been stained with Phalloidin (green) to visualise F-actin, and PI (red) for nuclei. This was also the case for cells that had LIMK knocked down and was thus a specific effect (Figure 3.3.20), Z slices visualise the cells

just above the filter in the inverse invasion assay set up. Reduction of LIMK by either drug or siRNA dramatically reduced F-actin staining in 3D, correlating with a loss of invasiveness (Figure 3.3.20). In all of these assays, under all conditions (including controls) there was also a non invasive and non motile (did not cross the filter) population of cells. These too lost F-actin structures following reduction of LIMK levels by siRNA or Drug (Figure 3.3.21).

LIM Kinases have been shown here to be a requirement of 3D cancer cell invasion, but not necessarily a requirement of 2D cell motility. As a requirement of invasion it could be hypothesised that increasing cellular levels of LIMK in these cells would increase invasiveness, as previous work with benign epithelial cells suggests (Davila et al, 2003).

### ***3.2.8 Is LIMK a driver of cell motility or invasion?***

LIMK has thus far been shown to be a requirement for 3D invasion by cells by the data presented in this chapter, but it is not known whether LIMK is also a driver of invasion. It has previously been reported that LIMK1 is elevated in cancer cell lines (Davila et al, 2003; Okamoto et al, 2005; Yoshioka et al, 2003) and tumours (Bagheri-Yarmand et al, 2006; Davila et al, 2003), and following commencement of this project, that LIMK1 over expression increases the invasiveness of human breast cancer cells (Bagheri-Yarmand et al, 2006). In order to address if LIMK is a driver of invasion, a conditionally activated LIMK fusion protein was generated.

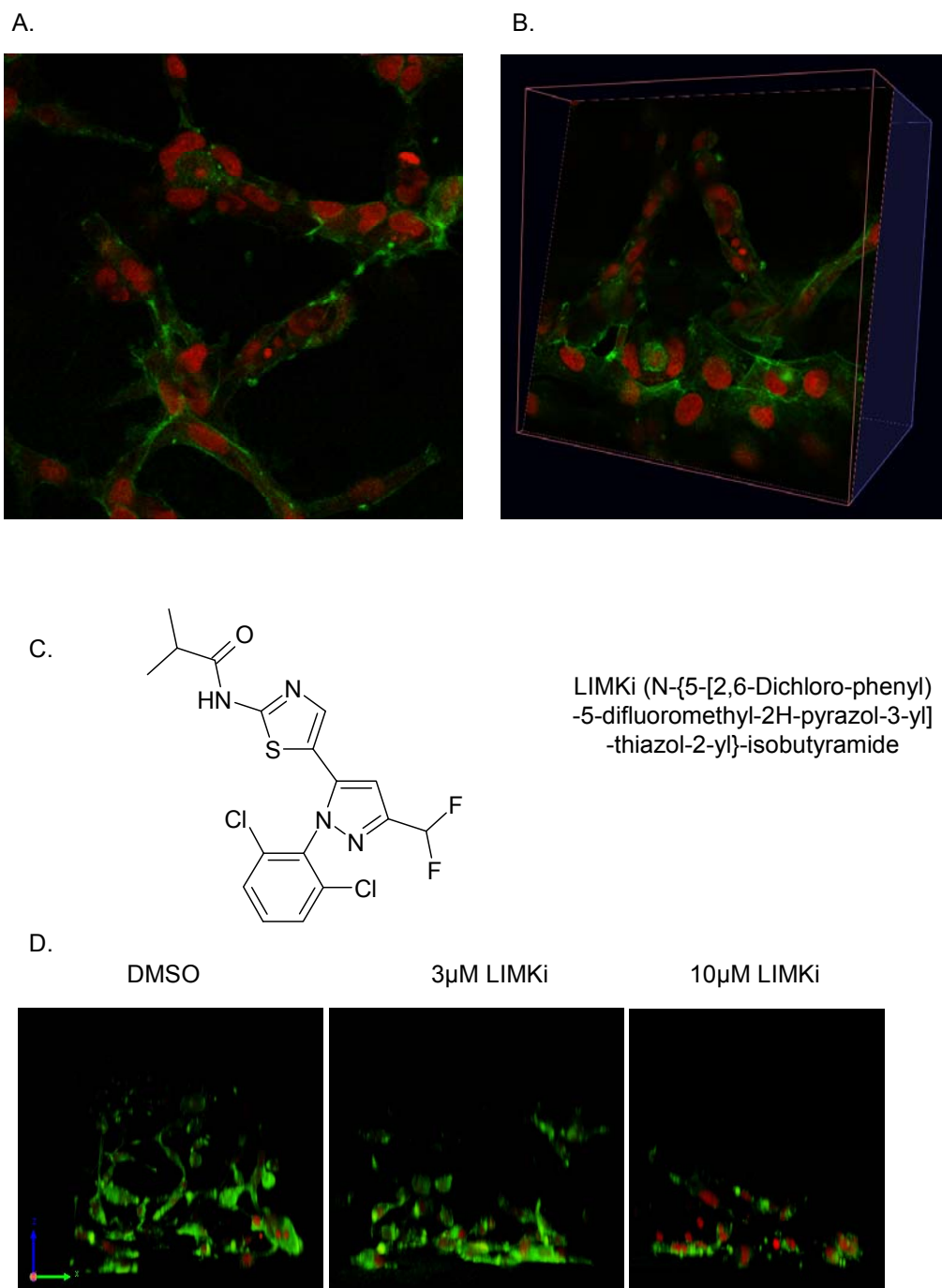


**Figure 3.3.19-3D F-actin staining and invasion of MDAMB231 is reduced by LIMK inhibitor.**  
 A. Z section of 'B.', MDAMB231 cells invading matrigel in columns, cells 'following' each other. B. 3D reconstruction of MDAMB231 invasion into matrigel and staining with Phalloidin (green) to visualise F-actin, and PI to visualise nuclei demonstrating that multiple cells track together. C. LIMK inhibitor. D. Cells treated with LIMK inhibitor at 3 $\mu$ M and 10 $\mu$ M show both a reduction in F-actin staining and invasion in comparison with control cells treated with DMSO. Invasion was imaged on an FV1000 Olympus Confocal at x40 (water lens) using FV10-ASW.1.7b software and reconstructed using Volocity 6.0. Invasion sections are 100 $\mu$ m wide.

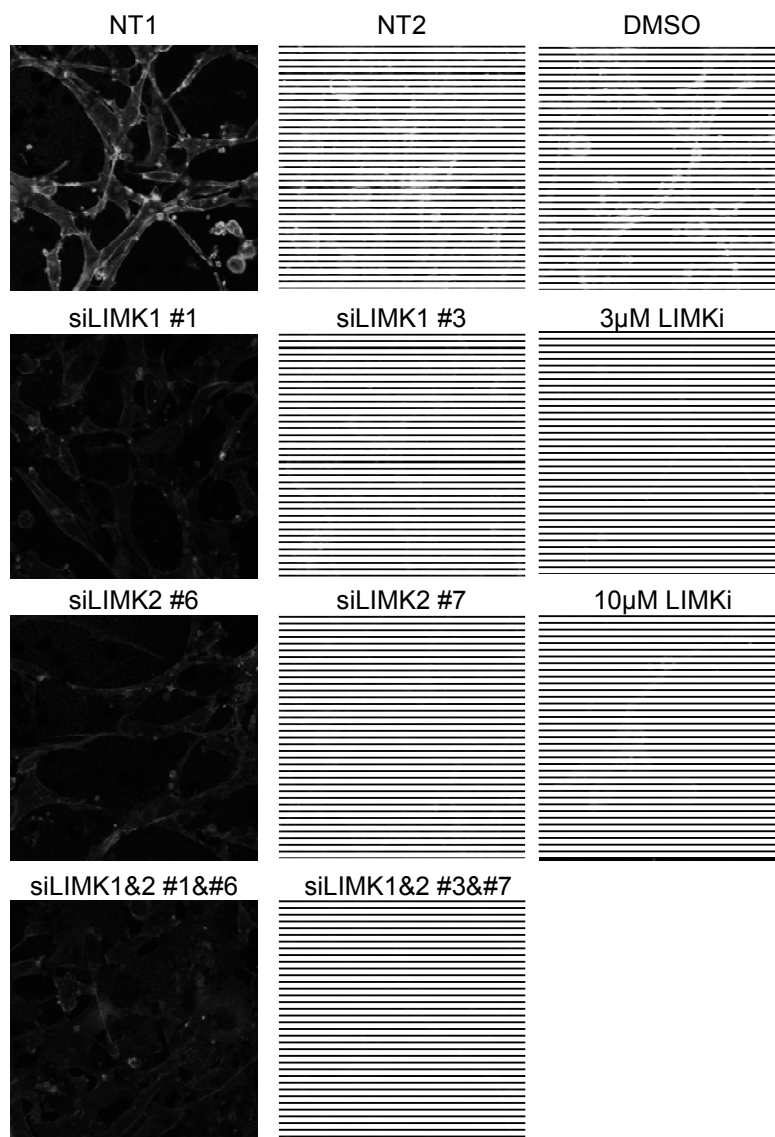


**Figure 3.3.20- F-actin staining of MDAMB231 in 3D is reduced by siRNA knockdown of LIM Kinases in the invasive population of cells.**

Cells on top of the filter at the end of a 5 day invasion assay display a loss of F-actin staining following knockdown of LIMK1, 2 or both in combination by siRNA or inhibition by LIMK inhibitor. F-actin was stained with Texas Red phalloidin and imaged on an FV1000 Olympus Confocal at x40 (water lens) using FV10-ASW.

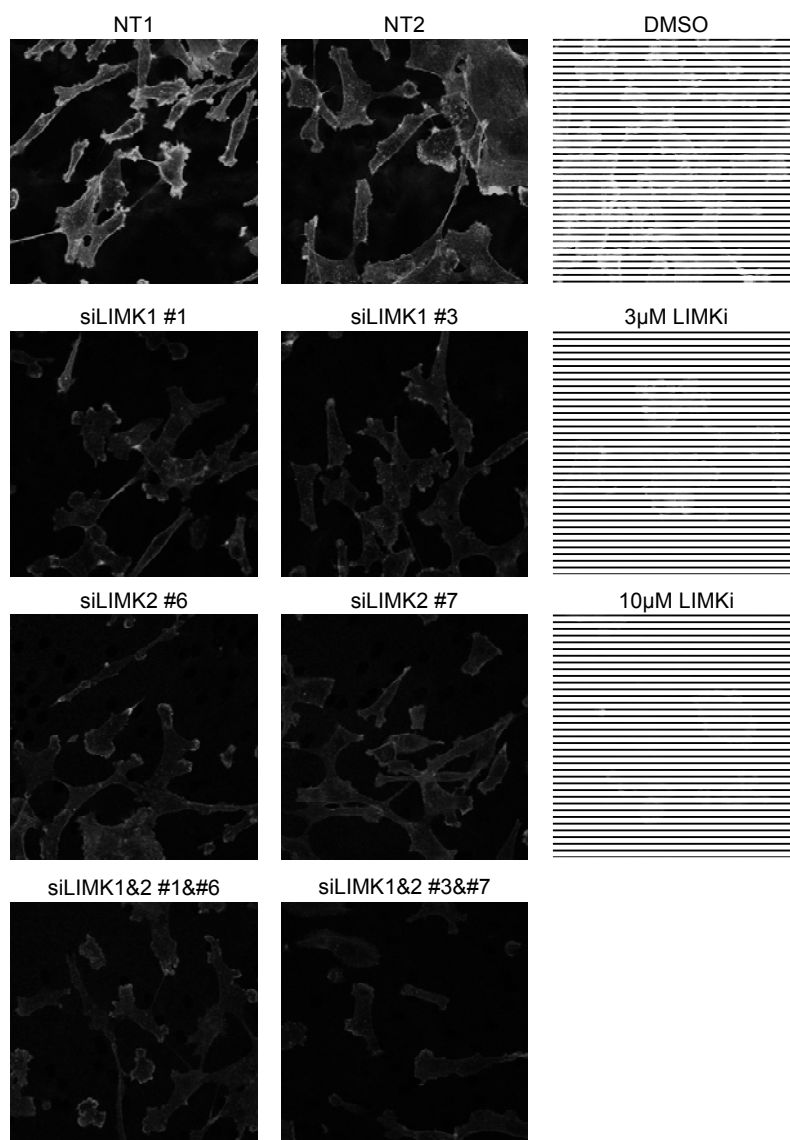


**Figure 3.3.21-F-actin staining in 3D is reduced by siRNA knockdown of LIM Kinases in the non invasive population of cells.**

Cells under the filter at the end of a 5 day invasion assay (the non invasive population of cells) also display a loss of F-actin staining following knockdown of LIMK1, 2 or both in combination by siRNA or inhibition by LIMK inhibitor. F-actin was stained with Texas Red phalloidin and imaged on an FV1000 Olympus Confocal at x40 (water lens) using FV10-ASW.

### 3.2.8.1 Generation of LIMK:ER inducible cell lines

To produce a conditionally regulated system to study the consequences of LIMK activation, a conditionally activated form of LIMK1 was created, made conditionally activate by fusion with the hormone binding region of estrogen receptor (ER). Activated only in cells only in the presence of estrogen analogs, the structure of the LIMK:ER fusion protein is illustrated in Figure 3.3.22 part A. This kind of fusion protein has been used extensively with a variety of proteins such as transcription factors and kinases, and within our lab a fusion protein to ROCK has been used to analyse its role in regulation of the actin cytoskeleton (Croft et al, 2006; Croft et al, 2004).

Retroviral vectors encoding LIMK:ER were subject to site directed mutagenesis to generate two 'active' phospho-mimetic mutants; Thr508Glu referred to as LIMK:ER (E), and Thr508GluGlu referred to as LIMK:ER (EE) (illustrated as a red band in the kinase domain in Figure 3.3.22 part A), and the estrogen receptor hormone-binding domain expressed at the C terminus. The LIMK:ER, LIMK:ER (E) and LIMK:ER (EE) retroviral vectors were each packaged as ecotropic virus and then introduced into mouse (NIH3T3) cells or stably transfected ecotropic receptor expressing cells (SAOS). The estrogen receptor hormone-binding domain was stimulated with estrogen analogs tamoxifen or 4-HT, but this did not lead to a 4HT dependent increase in pCofilin as hoped, illustrated for NIH3T3 cells in Figure 3.3.22 part B. The addition of 4-HT led to a slight increase in LIMK:ER (WT), LIMK:ER (E) and LIMK:ER (EE) levels; potentially an indicator of the stability of the protein following 4-HT activation. GFP and LIMK antibodies were overlaid using different species and wavelength LiCor secondary antibodies to identify the fusion protein. Although there was not an increase in pofilin levels following 4-HT activation, it was hoped that there may still have been a phenotypic effect on the actin cytoskeleton of the cells.

Effects of an increase in active LIMK:ER on the actin cytoskeleton was difficult to discern. The selection process for generating stable LIMK:ER expressing cell lines appears to have selected for a different phenotype to the parental cells, as can be seen in the first panel of Figure 3.3.23. LIMK:ER expressing cells are less ruffled at the edges and have slightly stronger cortical F-actin staining and more

stress fibres. Sixteen hours following 4-HT addition in the absence of serum the control cells show no difference in morphology, LIMK:ER (E) expressing cells look more like Control NIH3T3 cells, slightly more ruffled, and LIMK:ER (EE) cells also have slightly more ruffled edges and appear flatter, more spread out (Figure 3.3.23). The subtle changes in morphology in this cell line following 4-HT induction led to the generation of SAOS LIMK:ER cells, in the attempt to make a cell line with more easily identifiable LIMK dependent morphological changes. SAOS cells were retrovirally transduced with LIMK:ER constructs and drug selected before being subject to induction with 4-HT as the NIH3T3 before them, Figure 3.3.24. As with the NIH3T3 LIMK:ER cells, the construct expressed at low levels without induction and drug selection led to the un-stimulated cells having a markedly different morphology to the parental Control cells as can be seen in the first panel of images in Figure 3.3.24. LIMK:ER (E) expressing cells had a smaller, more compacted and less polarised morphology in comparison with control cells when un-stimulated. Following 4-HT stimulation the LIMK:ER (E) SAOS cells displayed reduced F-actin staining in comparison with un-stimulated cells (Figure 3.3.23, middle row). LIMK:ER (WT) cells were considerable larger than the parental Control cells when unstimulated, less polarised and with stronger cortical F-actin staining and stress fibres. However, following 4-HT stimulation, they were smaller than control cells and had greatly reduced F-actin staining, more resembling LIMK:ER (E) un-stimulated cells (Figure 3.3.24). Stimulation in the presence of serum had no discernable effect upon the morphology of LIMK:ER WT cells, and under these unstressed conditions there was only a subtle difference in cell size between the un-stimulated control cells and un-stimulated LIMK:ER WT cells (Figure 3.3.25).

LIMK:ER activation in cells resulted in very subtle phenotypic changes in the actin cytoskeleton, raising doubt over the activity of LIMK:ER. In order to determine the activity of LIMK:ER in cells immunoprecipitation (IP) kinase assays were performed.

A.



pBABE:EGFP:hLIMK1:ER

- CGCTACGAAGAA GTGGTG, Thr508GluGlu (EE mutant)
- CGCTACGAAGTGGTG, Thr508Glu (E mutant)
- CGCTACACCGTGGTG, (WT construct)

B.

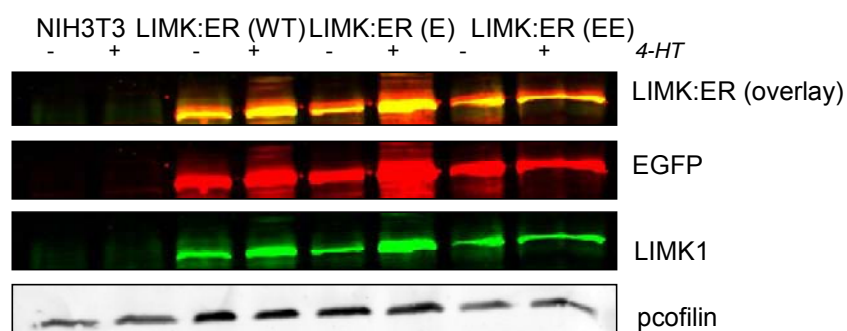


### Figure 3.3.22-Conditional activation of LIMK:ER by 4-Hydroxytamoxifen

A. Illustration of LIMK:ER structure and component domains. Red band indicates point of point mutation for E and insertion for EE mutants. B. Western blot illustrating the conditional activation of LIMK:ER, LIMK:ER (E) and LIMK:ER (EE) following addition of 4-HT. Blots were imaged using LiCor software to allow visualisation of the colocalisation of EGFP and LIMK, confirming LIMK:ER construct expression.

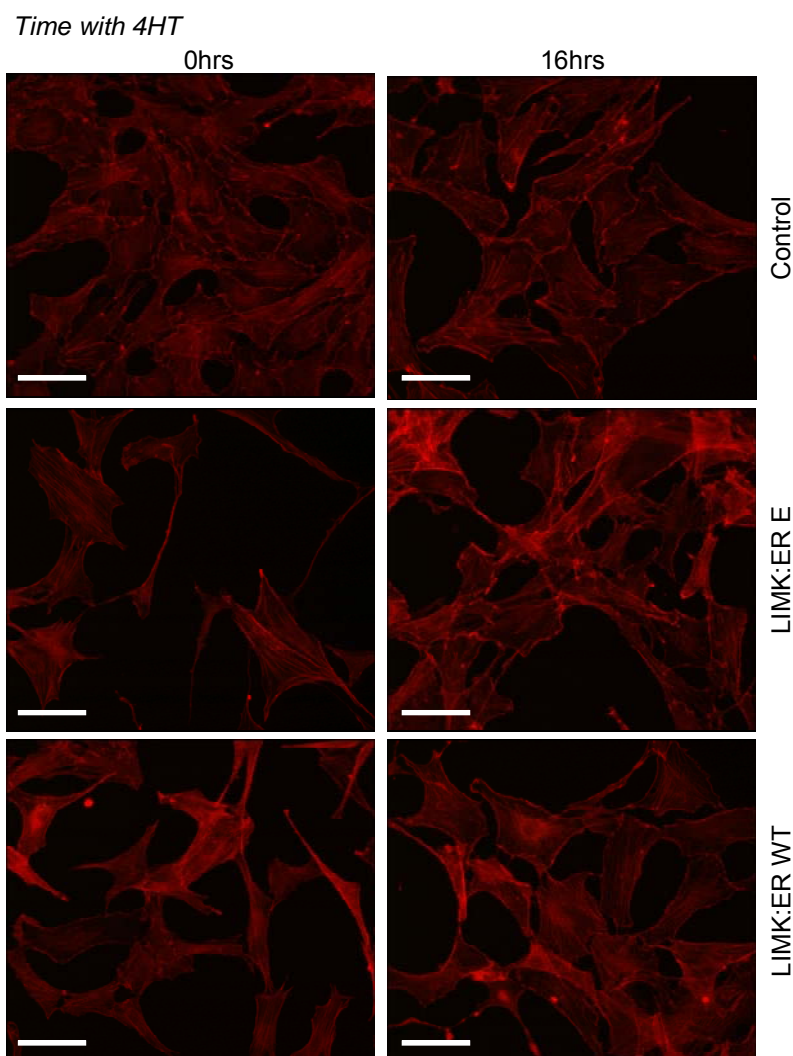


**Figure 3.3.23-NIH3T3 Express LIMK:ER, exhibiting a very subtle phenotype following induction with 4HT.**

NIH3T3 expressing LIMK:ER constructs and stained to visualise F-actin. Un-stimulated cells across conditions do not show the same cell shape or actin staining, selection for stable LIMK:ER expression has led to selection of a cell line which is phenotypically different from the parental cell line used (Control). Following stimulation with 4-HT LIMK:ER expressing cells display a subtle change in F-actin staining; both LIMK:ER (WT) and LIMK:ER (E) become slightly more spread out than un-stimulated cells, and have a slightly more ruffled cell edge. Cells stained with Texas Red Phalloidin to visualise F-actin and treated with 4-HT in the absence of serum for 16 hours. Images captured on the Zeiss Axioplan 200 at x20 using Imaging Associates Isis software. Scale bar equals 40 $\mu$ m.

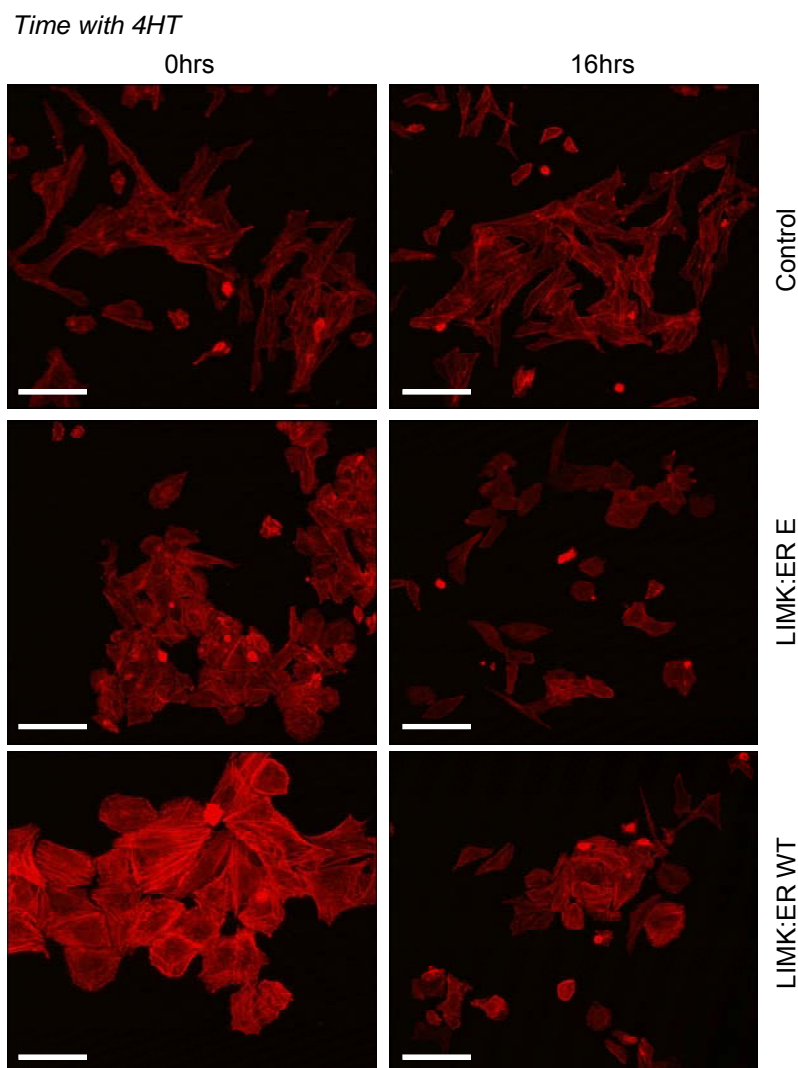


**Figure 3.3.24-SAOS express LIMK:ER but do not exhibit a consistent phenotype following induction with 4HT.**

SAOS expressing LIMK:ER constructs and stained to visualise F-actin. Un-stimulated cells across conditions do not show the same cell shape or actin staining, selection for stable LIMK:ER expression has led to selection of a cell line which is phenotypically different from the parental cell line used (Control). Following stimulation with 4-HT LIMK:ER expressing cells display a subtle change in F-actin staining; LIMK:ER (WT) cells become smaller, with less F-actin staining and stress fibres following 4-HT stimulation, LIMK:ER (E) show less F-actin staining, with a reduction in stress fibres and cortical actin. Cells were stained with Texas Red Phalloidin to visualise F-actin and treated with 4-HT in the absence of serum for 16 hours. Images captured on the Zeiss Axioplan 200 at x20 using Imaging Associates Isis software. Scale bar equals 40µm.

B.

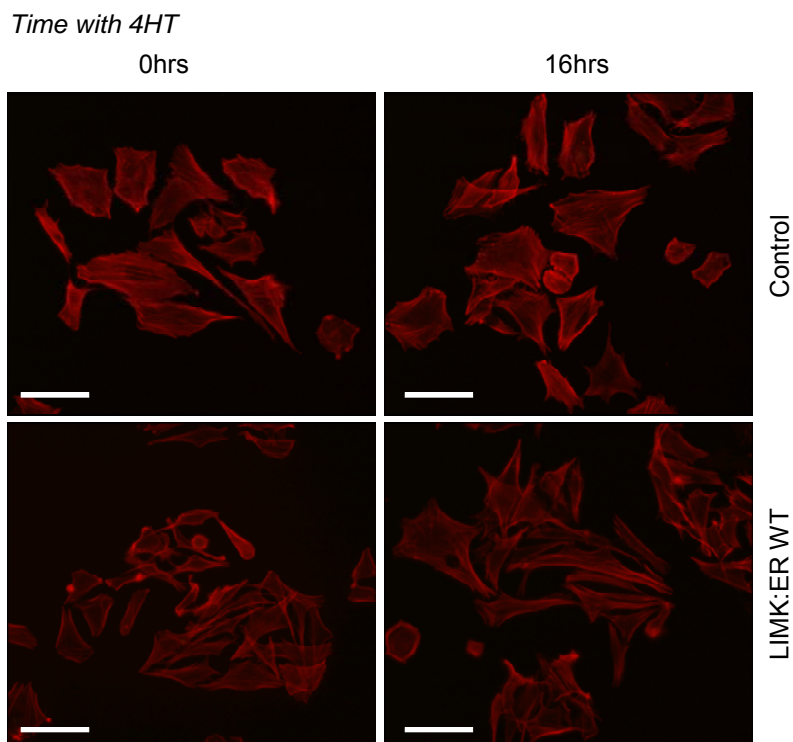


**Figure 3.3.25-SAOS express LIMK:ER but do not exhibit a consistent phenotype following induction with 4HT.**

SAOS expressing LIMK:ER constructs and stained to visualise F-actin. Un-stimulated cells across conditions do not show the same cell shape or actin staining, selection for stable LIMK:ER expression has led to selection of a cell line which is phenotypically different from the parental cell line used (Control). Following stimulation with 4-HT LIMK:ER expressing cells displayed a subtle change in morphology; LIMK:ER (WT) cells appear slightly more spread than un-stimulated, there was no obvious difference in the actin cytoskeleton following 4-HT stimulation. Cells were stained with Texas Red Phalloidin to visualise F-actin and treated with 4-HT in the presence of serum for 16 hours. Images captured on the Zeiss Axioplan 200 at x20 using Imaging Associates Isis software. Scale bar equals 40 $\mu$ m.

### 3.2.8.2 LIMK:ER Activity

Immunoprecipitation (IP) Kinase assays give a direct measurement *in vivo* kinase activity and can be used to assess fusion protein activity (Croft et al, 2004). Using Cofilin as a substrate, pCofilin levels would indicate *in vitro* activity and therefore reflect the activity status of LIMK:ER in cells.

The kinase assay conditions were optimised to increase the chance of seeing LIMK:ER activity, as can be seen in Figure 3.3.26. The optimised kinase assay conditions were then employed in the following experiments. The dose of 4-HT and treatment time was also optimised.

LIMK:ER is up-regulated in a 4-HT dose dependent manner in both NIH3T3 and SAOS, part A and B of Figure 3.3.27 respectively. The slight increase in pCofilin levels seen in NIH3T3 whole cell lysates suggested that the fusion protein was active, but Cofilin phosphorylation did not increase with dose, it had reached its maximum level. Although LIMK:ER was expressed in cells, the protein levels do not give a gauge of its activity and so using the optimal kinase assay conditions determined in Figure 3.3.26 the activity of LIMK:ER was re-examined, with further optimisation of 4-HT dose and timing. The optimal dose of 4-HT for LIMK:ER induction was confirmed as 100nM from the experiments in part B of Figure 3.3.27, and the optimal time for induction was then ascertained by a time course experiment as reported in part C of Figure 3.3.27.

Under the assay conditions tested, immunoprecipitated LIMK:ER exhibits no *in vitro* activity. This may be an insight into the requirements of full length LIMK activity *in vivo*, perhaps the added domains inhibit the activation of LIMK. The LIMK:ER may also have been activated but could then have been unable to phosphorylate Cofilin due to the additional EGFP and ER structures, interfering with substrate interaction. Since the activity of LIMK:ER could not be confirmed *in vitro*, and the 'phenotypes' of stably transfected cells were so subtle, the use of LIMK:ER to address the role of LIMK as a driver of cell invasion was abandoned.

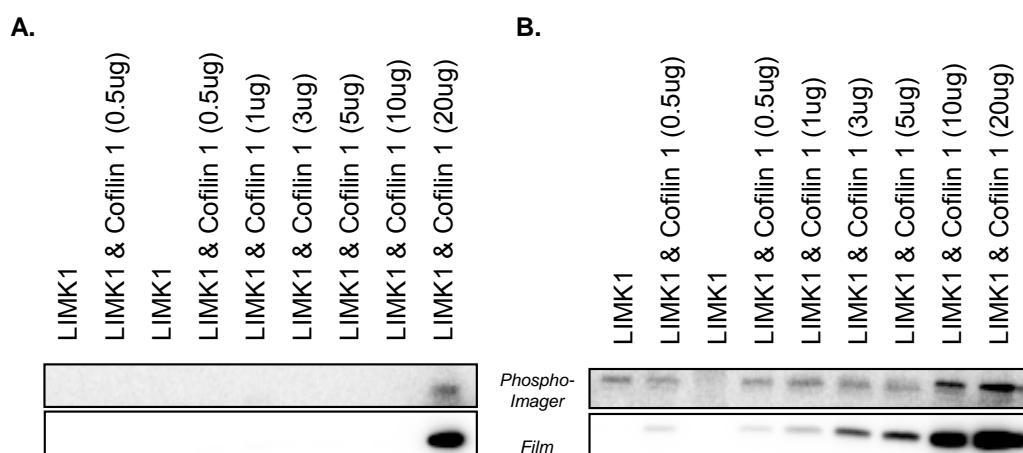


**Figure 3.3.26-LIMK:ER activity in vitro, optimisation of kinase assays**

Kinase assay buffer optimisation (as described in the methods); Phospho-imager imaged gels showing kinase assays performed to assess the ability of recombinant LIM Kinase to phosphorylated Cofilin *in vitro* using kinase buffer A. or the superior kinase buffer B which was optimised for kinase assays. Black bands indicate Cofilin phosphorylation, increased at lower concentrations of Cofilin following optimisation.

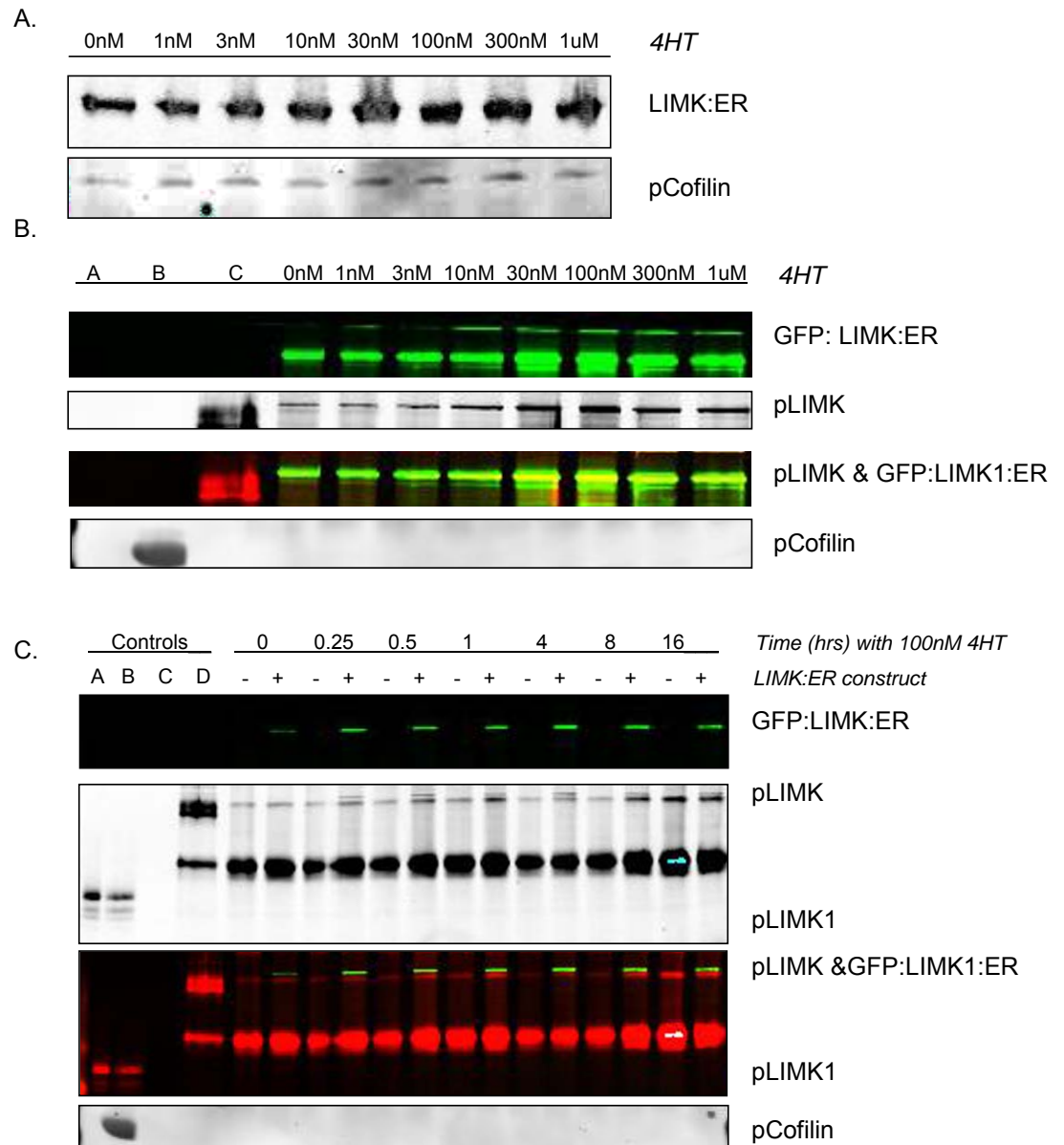


**Figure 3.3.27- Identification of optimal dose and timeframe in which to assess LIMK:ER activity in cells.**

A. Western Blot of dose response to 4HT after 16hrs. 30nM 4HT appears to be sufficient to increase pCofilin levels from background levels. B. IP Kinase assay corresponding to A. None of the doses tested increased LIMK:ER activity in the described IP kinase assay conditions. Lanes 1, 2 and 3 correspond to kinase assay controls *A*: LIMK1, *B*: LIMK1 +Cofilin1, *C*: Reaction mix (containing cofilin1). C. IP kinase assay at 100nM 4HT following different exposures to 4HT. None of the lysates from the time-points tested at 100nM yielded a LIMK:ER capable of phosphorylating cofilin1 under these conditions. Controls in lanes 1-3 as with B., control *D* contains antibody and beads. N denotes lysates from cells containing no construct, L denotes LIMK:ER expressing cells.

### **3.2.8.3 Increased levels of cellular LIMK reduces cell invasion**

The generation of a LIMK:ER cell line was initially undertaken to address whether LIMK could also be a driver of invasion, but failed to yield a useful tool. Instead, LIMK was transiently transfected into cells to deduce whether either LIMK1 or LIMK2 (or both kinases) were drivers of invasion, and the inverse invasion (Figure 3.3.12) was used to provide a 3D environment for cell invasion.

Cells were co-transfected by nucleofection with GFP and a combination of empty vectors (control nucleofection), LIMK1 & empty vector, LIMK2 & empty vector, or both LIMK1 & LIMK2 cDNA. Transfection efficiency was deemed high by fluorescent microscopy of cells (>90% of cells were GFP positive) and the cells transferred to invasion assays. In comparison with control cells there was a decrease in invasion following up regulation of LIMK, LIMK2 or both kinases as seen when graphed in an accumulative manner in Figure 3.28 part A. This was consistent with a decrease in the percentage of cells invading over 45 $\mu$ m with increased LIMK1, LIMK2 or both LIMK1 and LIMK2 (Figure 3.28 part B). Cells were also more rounded in morphology following the increase in cellular LIMK1 or LIMK2 (Figure 3.28) which was similar to the morphology of cells following reduction of LIMK (Figure 3.3.17).

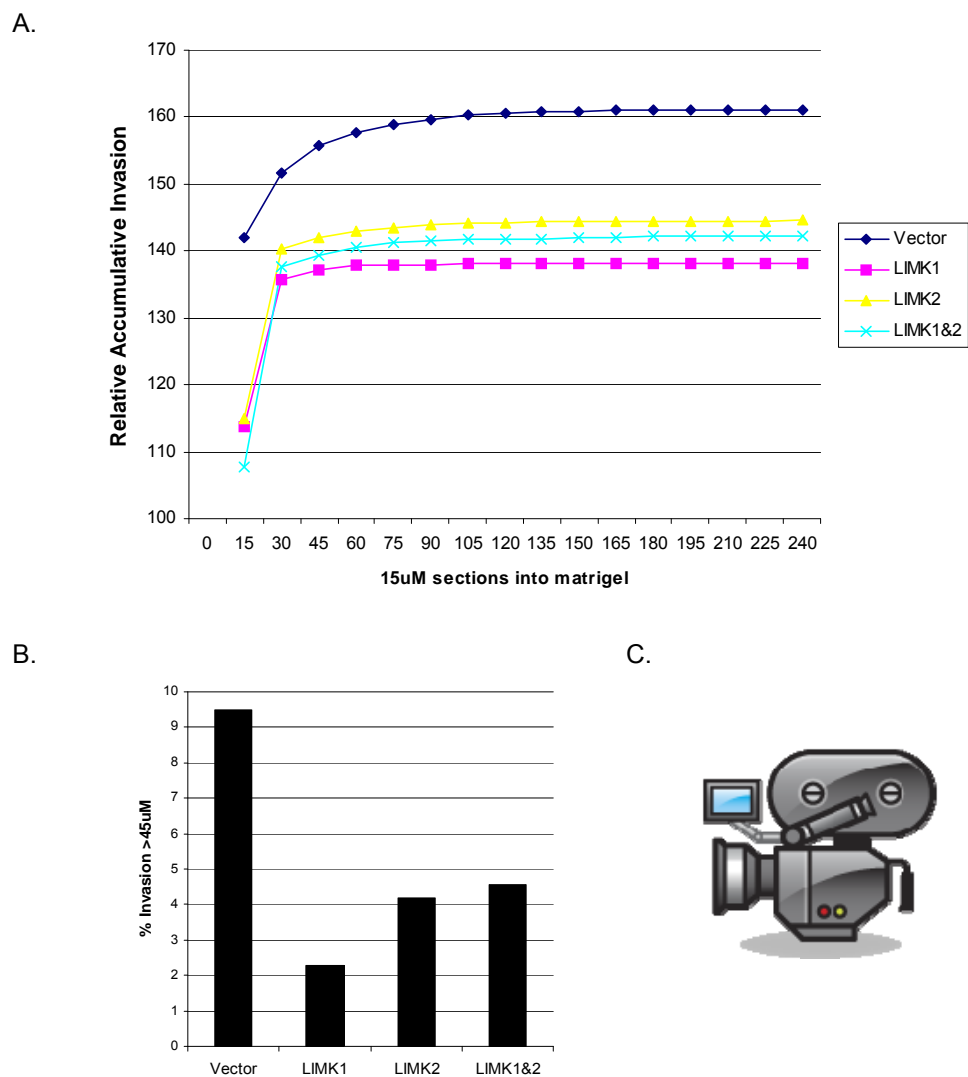


**Figure 3.28-Increased levels of LIMK reduces 3D invasion of MDAMB231 cells.**

A. Cells Transfected with LIMK1, LIMK2 or both LIMK1&2 all displayed reduced invasion in comparison with cells transfected with a vector control. All plasmids were co-transfected with GFP as a transfection efficiency control by the method of 'nucleofection'. B. % Invasion of cells over 45um following nucleofection of LIMK is reduced by LIMK1 and LIMK2, as well as both in combination. C. Movie Showing 3D reconstruction of invading MDAMB231 cells following nucleofection.

### 3.3 Conclusions

Both LIMK1 and LIMK2 have been shown in this chapter to be required for BE and BT549 cell motility in 2D. Neither LIMK1 nor LIMK2 was found to be required for 2D motility of MDAMB231 cells. It could not be concluded from the assays used whether LIMK1 or LIMK2 is required for the 3D invasion in BE or BT549 cell lines as they did not successfully invade in the conditions tested. MDAMB231 cells, which invaded well into the trans-well inverse invasion assays, both LIMK1 and LIMK2 were shown to be requirements of invasion. This effect was not found to be additive upon the reduction of both kinases protein levels by siRNA, but this may be because the effectiveness of the LIMK double knockdown by siRNA is at its maximum, perhaps only complete inhibition of LIMK activity by LIMK inhibitors would show a greater effect. It could also be that the double knockdown has reached the threshold of the effect of reducing LIMK levels, and that this is the maximal effect that will be seen by interfering with LIMK protein levels or activity.

Reduction of either LIMK1 or LIMK2 levels lowered F-actin staining in BE, BT549 and MDAMB231 in 2D, loss of both kinases caused a greater reduction of F-actin staining in all cell lines examined. In a 3D setting, the inhibition of LIMK by LIMKi reduced F-actin staining in a dose dependent manner. Reduced F-actin levels correlated with reduced invasive capacity in 3D for MDAMB231 which had lost peripheral spike-like actin structures in initial 2D formats, structures that may play a role in 3D invasion but, it would seem, not 2D motility. One possible explanation for the lack of effect of LIMK inhibition in 2D was that the two dimensional migration across a rigid substrate is principally propelled by actin polymerization and forward protrusion (DesMarais et al, 2002). Since Cofilin activation could result in F-actin severing and an increased number of barbed ends available to provide sites for monomer addition and filament extension, it is possible to hypothesise how this form of 2D motility could be insensitive to LIMK knockdown as the potential for leading edge protrusion would not be impaired.

In the 3D invasion assays the majority of cells, control and knockdown, were able to move through the filter to the bottom of the matrigel through the

predefined 'tracks' (pores). The pores may have allowed MDAMB231 movement as the form of motility did not require proteolytic activity or force generation (Vignjevic & Montagnac, 2008). In contrast invasion, which requires both deformation and degradation of a substrate, was reduced by LIMK knockdown (the level of invasion from the filter up was dependent on LIMK status). Cells subject to LIMK knockdown lost 'invasiveness' but also lost the ability to make tracks through matrigel. Those cells that did manage to migrate a short distance into the matrix following LIMK knockdown displayed a more amoeboid morphology than the usual MDAMB231 mesenchymal invasive form.

Given that LIMK is a requirement of invasion, it was hypothesised to be a driver of invasion. However, increasing levels of LIMK in MDAMB231 cells by transient transfection reduced invasion of cell into a 3D matrix. The work in this chapter suggests that perturbing the balance between active Cofilin (LIM Kinases primary substrate) and inactive Cofilin by increasing or decreasing LIMK levels is sufficient to interfere with cell motility. This compliments previous work describing motility defects upon Cofilin knockdown (Hotulainen et al, 2005; Sidani et al, 2007) and observations where over expression of Cofilin inhibited the invasion of human lung cancer cells (Lee et al, 2005) and the motility of glioblastoma cell lines (Yap et al, 2005).

In conclusion, the data presented in this chapter suggests that LIMK is not necessarily a requirement for cell motility, but that it is a requirement for successful 3D cell invasion.

## 4 LIM Kinase regulation of invasion

### 4.1 Chapter summary

LIM kinases have previously been shown to be important in cancer cell motility and invasion (Yoshioka et al, 2003) and are implicated in increasing the invasive phenotype of cells (Bagheri-Yarmand et al, 2006; Davila et al, 2003). Results from Chapter 2 suggest that both LIM Kinase 1 and LIM Kinase 2 are important for invasion, and this correlates with a loss of F-actin staining following LIMK inhibition. The actin cytoskeleton is a crucial element in maintaining the invasive capability of cancer cells (Daisuke et al, 2005), and structures such as invadopodia have emerged as potential facilitators of invasion (Liu et al, 2009). This chapter describes studies investigating the mechanism by which LIM Kinases influence 3D invasion via; invadopodia formation, extracellular matrix degradation and regulating the invasiveness of leading cells in collective forms of invasion.

### 4.2 Results

#### ***4.2.1 Knock down of LIM Kinase reduces functional invadopodia formation and gelatin degrading activity in MDAMB231 cells***

It was observed in Chapter 2 that the invasive cancer cell line MDAMB231 exhibited a more rounded morphology in 2D following LIM Kinase knockdown, and similarly that BT549 cells showed a reduction in peripheral F-actin staining. Knocking down either LIM Kinase 1 or LIM Kinase 2 by siRNA also reduced F-actin staining in 3D invading cells, and this effect was enhanced by lowering activity of both kinases (either by siRNA or CRT101106 LIMK inhibitor). Invadopodia are actin rich peripheral structures associated with localised proteolytic activity that contribute to invasiveness *in vitro* (Coopman et al, 1998). To invade and metastasise through tissue, cancer cells must produce and secrete proteolytic enzymes to degrade extracellular matrix. The studies in this section try to address whether the cytoskeletal changes observed following LIM Kinase

knockdown during 3D invasion in the previous chapter affect the formation of invasive structures such as invadopodia, or reduction in proteolytic activity.

To ascertain whether LIM Kinases play a role in invadopodia formation, gelatin degradation assays were performed. FITC-labelled gelatin was gluteraldehyde cross-linked on glass cover-slips to provide a malleable substrate for MDAMB231 cells. Following a four hour time period to allow degradation, the cells were fixed and F-actin stained with Texas Red phalloidin to visualise F-actin. The assay measures the formation of invadopodia by visualising focalised degradation of matrix; confirmation that actin structures are involved can be seen in Figure 4.4.1. In these two examples of MDAMB231 cells making invadopodia, red F-actin staining can be seen to protrude into the layer of green gelatin, both when viewed from below in the XY plane, or from the side in the XZ or YZ panels that cut through the cells. The outlines of the cells are seen as yellow when viewed from below due to the co-localisation of FITC gelatin and F-actin staining with Texas Red phalloidin. The invadopodia are visible in red where localised degradation of the gelatin matrix has occurred and there is, therefore, no co-localisation with FITC gelatin. Not all cells plated had degraded matrix by the four hour end-point, only a proportion of the population appears to be making invadopodia at any given time (Figure 4.4.4). The previously observed effects that reducing LIM Kinase levels had on the actin cytoskeleton could have affected the ability of MDAMB231 to settle on to the gelatin substrate. Taking this into consideration, MDAMB231 cells were transfected with siRNA (against LIMK1, LIMK2, both LIMK1 and LIMK2 or non-targeting controls) 24 hours before being seeded on to gelatin cover-slips in the presence of GM6001 (matrix metalloproteinase inhibitor). The MMP inhibitor allowed the cells to settle onto the gelatin overnight so that when it was washed out of the media, matrix degradation was a reflection of invadopodia activity, not the cells ability to settle following loss of LIMK. The cells were left for four hours after GM6001 washout before being fixed, stained for F-actin, and imaged using OpenLab software. Examples are shown in Figure 4.4.2; less degradation of the gelatin substrate appears to have taken place under cells subjected to either LIMK1 or LIMK2 siRNA in comparison with those treated with non-targeting siRNA. Knocking down both LIMK1 and LIMK2 by siRNA reduced the level of gelatin degradation but this did not appear to have an additive effect. Reducing levels

of either LIMK1 or LIMK2 was sufficient to reduce gelatin degradation by MDAMB231 cells. Similarly, when CRT101106 was used to inhibit LIMK activity in MDAMB231, reduced gelatin degradation was observed at all doses (3  $\mu$ M, 10  $\mu$ M and 20  $\mu$ M). 3 $\mu$ M was sufficient to reduce invadopodia formation and gelatin degradation, increasing the dose of inhibitor did not seem to increase the inhibitory effect (Figure 4.4.3). The observed effects of knocking down or inhibiting LIM Kinases were quantified using images of gelatin degradation such as the examples in Figure 4.4.2 and Figure 4.4.3. Images were analysed using ImageJ software to calculate the area of degradation per cell. The program firstly uploads F-actin images of cells, to determine each cells area, and then the corresponding images of gelatin degradation to work out the area of degradation under each cell (Figure 4.4.5). Knockdown of LIMK1, LIMK2 or both LIMK1&2 by siRNA reduced the area degraded per cell in comparison with cells transfected with non-targeting control siRNA (Figure 4.4.6 A), as does inhibition of LIMK by CRT101106 (LIMKi) at 3 $\mu$ M, 10 $\mu$ M or 20 $\mu$ M in comparison with DMSO control treated cells (Figure 4.4.6 B.).

These results suggest that the changes in F-actin staining observed following LIM Kinase knockdown in the previous chapter led to a corresponding loss of F-actin rich invadopodia structures, which are important for invasion and proteolysis of extracellular matrix during invasion. The matrix metalloproteinases responsible for gelatin (denatured collagen) degradation are the collagenases MMP2, MMP9 and membrane bound MT1-MMP (Stylli et al, 2008). It was hypothesised that the loss of gelatin degradation observed in this chapter following a reduction in LIM Kinase protein levels could relate to either a reduction in MMP2, MMP9 or MT1-MMP activation and/or MMP2 and MMP9 secretion by cells.

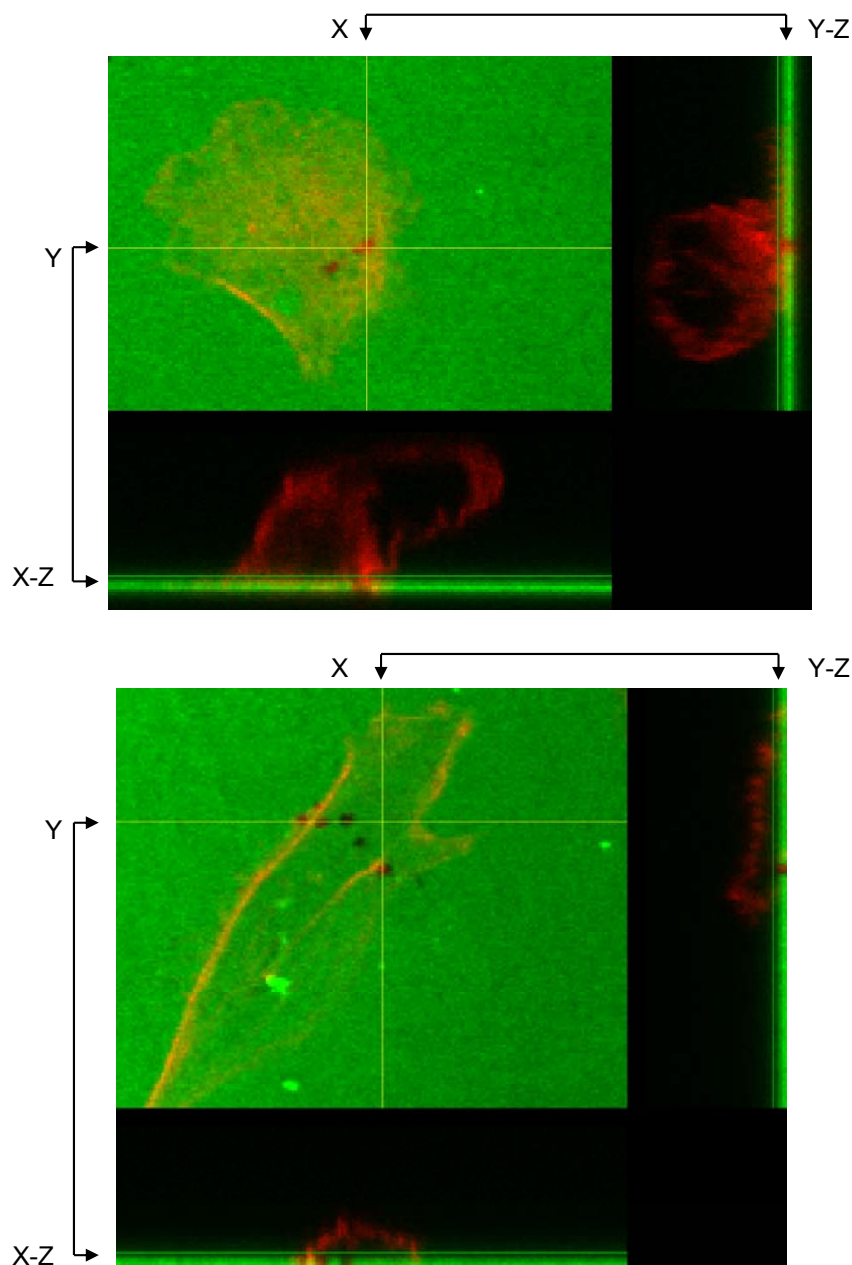


**Figure 4.4.1-F-actin rich invadopodia of MDAMB231 degrade FITC labelled gelatin matrices.** MDAMB231 cells stained with Texas Red Phalloidin for F-actin degrading FITC gelatin matrices. MDAMB231 cells form F-actin rich invadopodia (stained with Texas red phalloidin) that protrude into the fluorescent gelatin (FITC) substrate (dissected here by the yellow gridlines). A dark cavity of degraded gelatin surrounds each F-actin rich invadopodia, (visualised by a lack of yellow co-localisation) in the red regions protruding into the FITC gelatin. Images taken in  $2\mu\text{m}$  Z sections on an Olympus FV1000 confocal microscope using a x60 oil objective and reconstructed in 3D using Volocity imaging software.

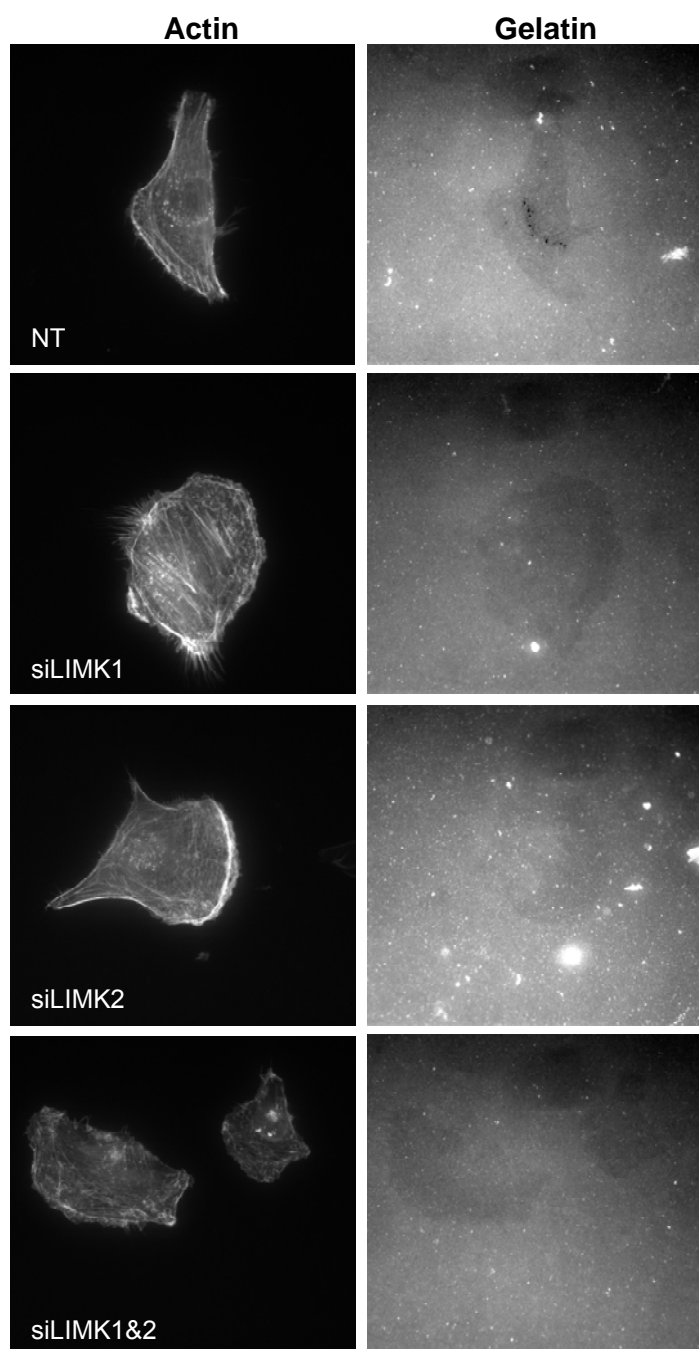


**Figure 4.4.2-Knock-down of LIM Kinase 1 and 2 by siRNA reduces invadopodia formation.** Gelatin degradation assay showing MDAMB231 degradation of FITC gelatin following knockdown of LIMK1, LIMK2 or both LIMK1 & LIMK2 in combination by siRNA. Left panel shows Texas-Red phalloidin staining of F-actin in each condition, punctate F-actin staining in control cells (treated with Non-Targeting control siRNA (NT)) correlates with gelatin degradation, imaged here as dark cavities in the gelatin surface. Actin staining after siLIMK1 or siLIMK2 still shows punctate staining but does not correspond with gelatin degradation (right panel). F-actin staining following siLIMK1&2 is weaker and less defined than control cells and corresponds with a lack of gelatin degradation. Images were taken using OpenLab software on a Zeiss Axioskop2 microscope fitted with a Hamamatsu black and white camera.

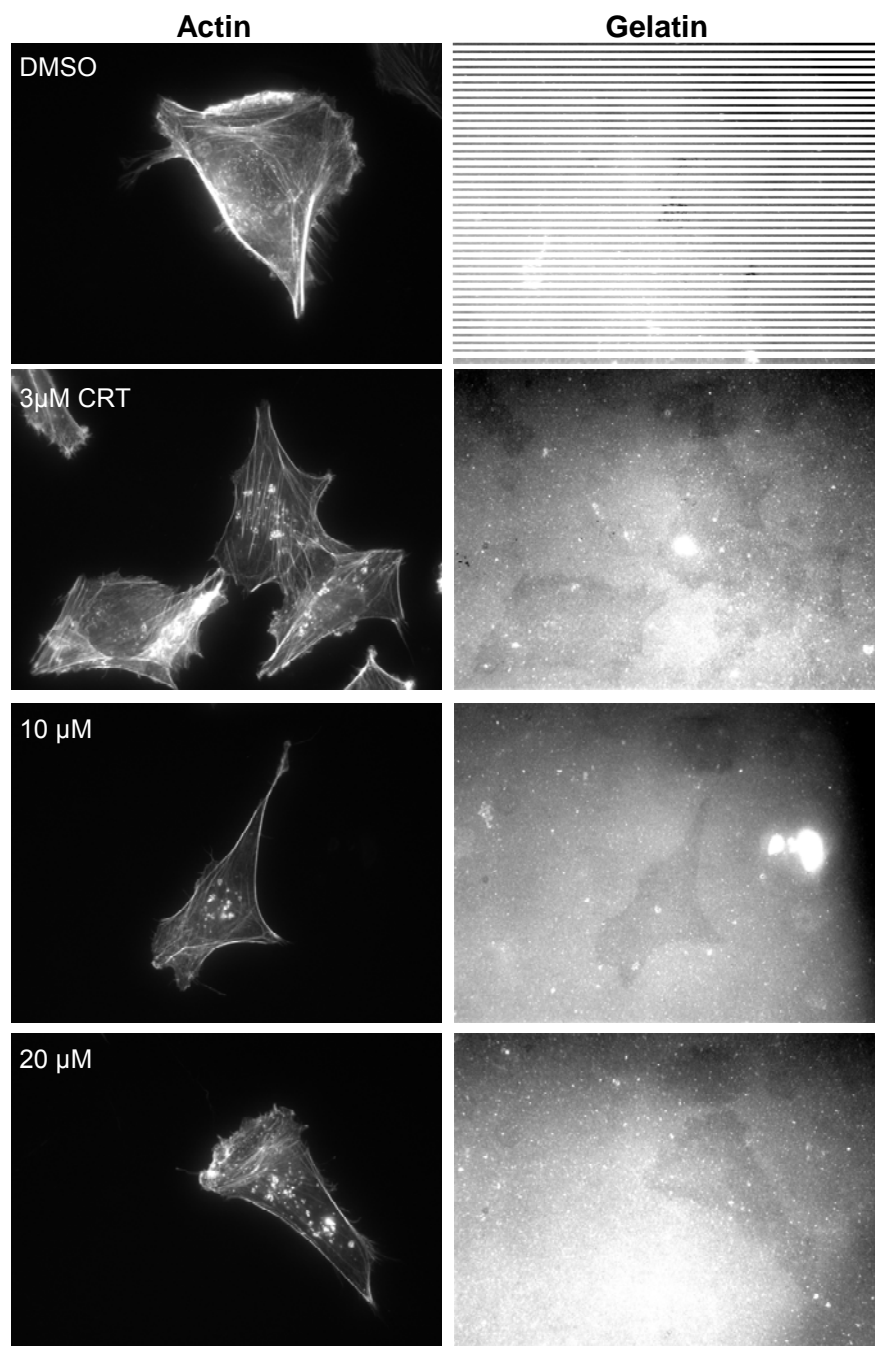


**Figure 4.4.3-Inhibition of LIMK1 and 2 by CRT101106 reduces invadopodia formation.**

Gelatin degradation assay showing MDAMB231 degradation of FITC gelatin following inhibition of LIM Kinases by CRT101106 at 3µM and 10µM. Invadopodia formation is reduced in cells exposed to all doses of CRT101106 but not in control cells exposed only to DMSO. The cells exposed to CRT101106 have reduced overall F-actin staining and fine punctate staining associated with invadopodia, but an increase in larger punctate structures. Images were taken using OpenLab software on a Zeiss Axioskop2 microscope fitted with a Hamamatsu black and white camera.

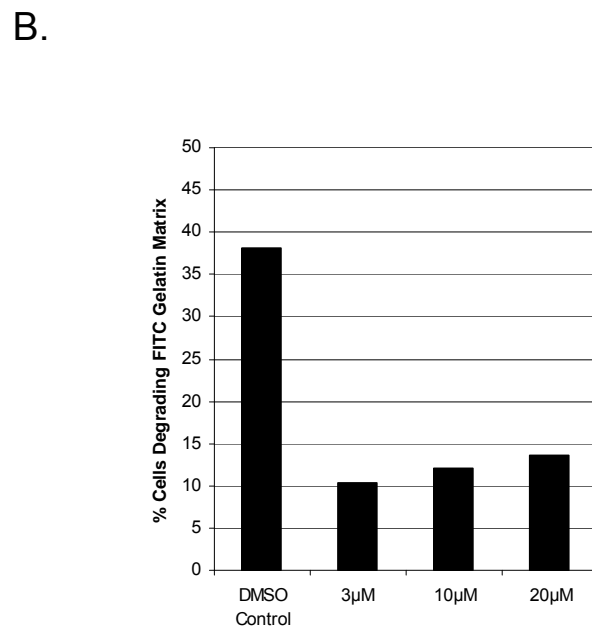
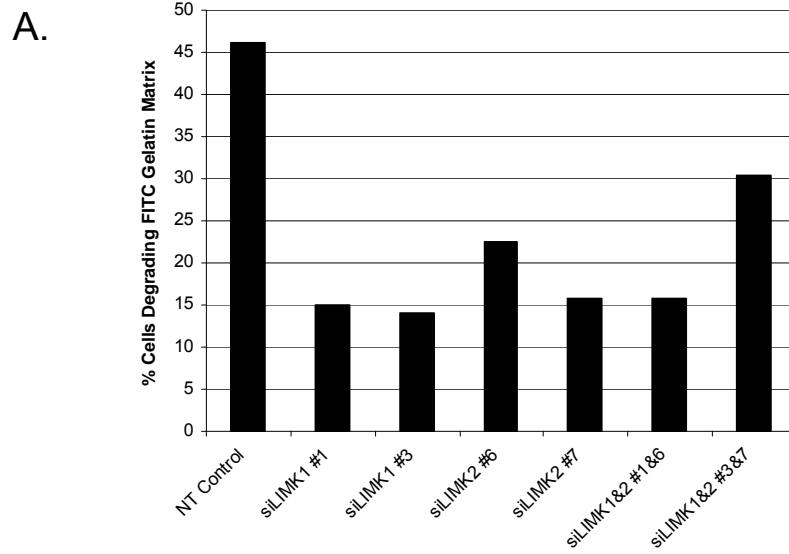


**Figure 4.4.4-Inhibition of LIMK reduces the percentage of cells making invadopodia.**

A. Graph of the percentage of cells degrading FITC gelatin in degradation assays following knockdown of LIMK1, LIMK2 or both LIM Kinases. Knockdown reduces the proportion of cells making invadopodia in a 4 hour time frame. B. Graph of the percentage of cells degrading FITC gelatin in degradation assays following CRT101106 LIMK inhibition at 3µM, 10 µM and 20µM. Inhibition of LIMK reduces the proportion of cells making invadopodia in a 4 hour time frame at all doses, and to a greater degree than siRNA against LIMK.

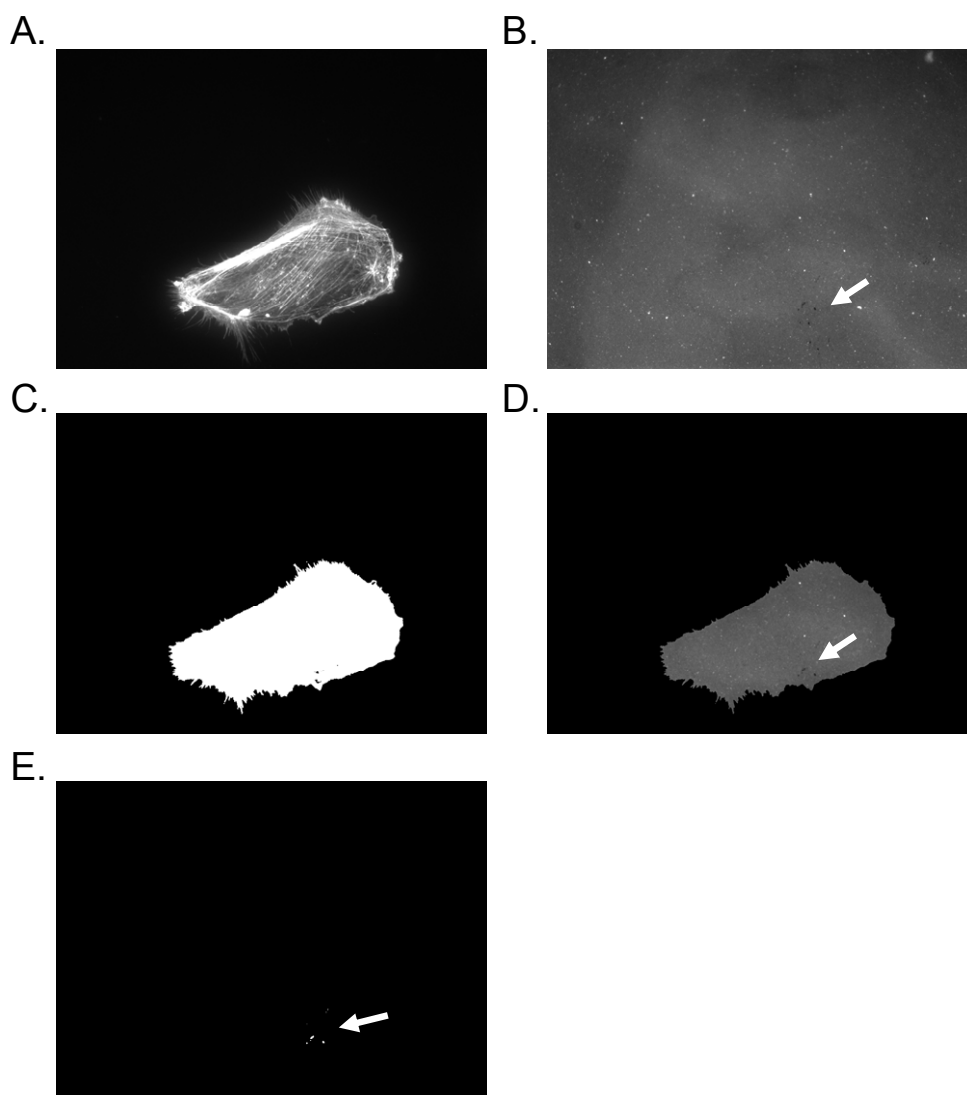


**Figure 4.4.5-ImageJ method for analysis of invadopodia.**

F-actin Images of cells plated on FITC Gelatin (A.) and the corresponding images of FITC Gelatin (B.) where the arrow indicates the area of degradation. The area of each cell is calculated using the peripheral F-actin staining (C.) and this area overlaid with the gelatin image (D.) to determine the area in which to convert the image to binary and quantify pixels corresponding to gelatin degradation (E.). Images were taken using OpenLab software on a Zeiss Axioskop2 microscope fitted with a Hamamatsu black and white camera. The area degraded under this example MDAMB231 cell was 151 pixels, as calculated using ImageJ software and a software 'plug in' kindly provided by L.Machesky.

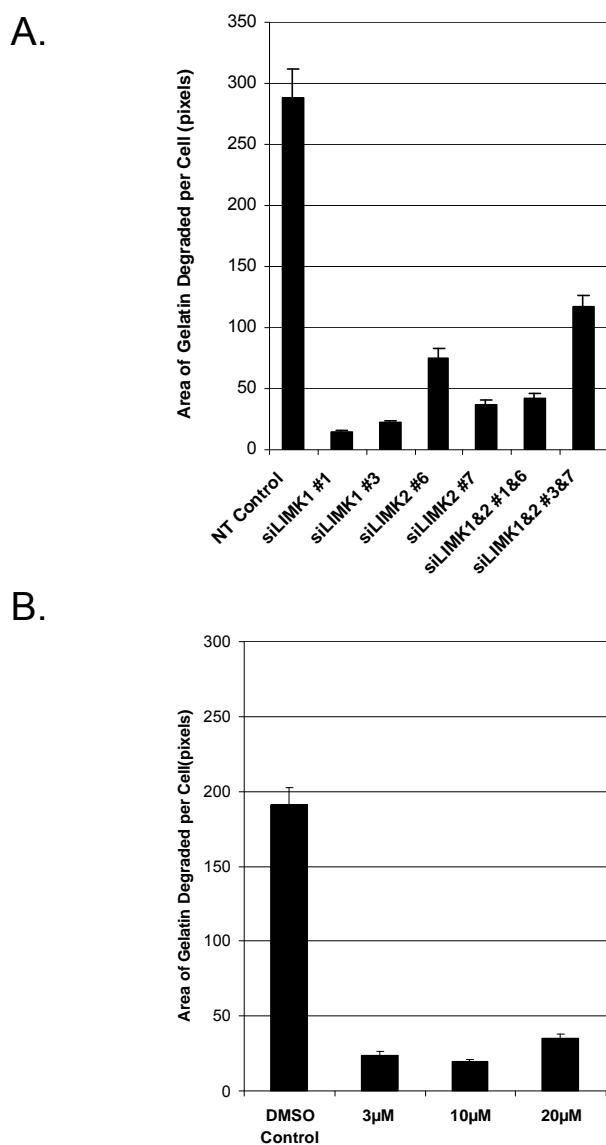


**Figure 4.4.6-Quantification of gelatin degradation following LIM Kinase inhibition by CRT101106 or knockdown by siRNA.**

A. Graph of the area of gelatin degraded per cell following FITC gelatin degradation assays is reduced by knockdown of LIMK1, LIMK2 or both LIM Kinases. B. The area of gelatin degraded per cell following FITC gelatin degradation assays is reduced by CRT101106 LIMK inhibition at 3µM, 10 µM and 20µM.

#### **4.2.2 Knockdown of LIMK reduces levels of secreted active MMP9**

Invadopodia are organised actin rich membrane protrusions with localised proteolytic enzyme activity, the formation of which have recently shown to be regulated by Cortactin (Amanda Gatesman & Scott, 2008). Cortactin has been shown to regulate invadopodia assembly by binding and inhibiting Cofilin actin severing. Phosphorylation of Cortactin releases Cofilin from this inhibition and this cycle of Cofilin inhibition and release is proposed to regulate invadopodia formation by exerting control over rates of actin severing (Oser et al, 2009). LIMK is also a negative regulator of Cofilin, and as such could play a similar role in the development of invadopodia by influencing the level of barbed ends available for polymerisation. Recent work using live cell imaging has identified 4 phases of invadopodia formation: (i) localisation of cortactin to ventral puncta, (ii) recruitment of membrane bound MMPs to these sites (such as MT1-MMP), (iii) the appearance of degraded foci in matrix, and (iv) the dissociation of cortactin from the site of degradation (Artym et al, 2006; Stylli et al, 2008). Cortactin binds Cofilin and stops it from severing F-actin, stabilising invadopodia. Therefore, if LIMK regulates invadopodia formation in the same manner, by regulating Cofilin activity, LIMK inhibition would destabilise invadopodia and prevent the recruitment of MMPs. Studies have shown that MT1-MMP is the key metalloprotease for matrix degradation in MDAMB231 (Kelly et al, 1998) and that the ability of MDAMB31 cells to invade matrigel was impaired by MMP inhibitor Ilomastat (Canning et al, 2001). Gelatin degradation assays give an indication of the activity of the collagenases MMP2, MMP9 and the membrane bound MT1-MMP, but perhaps the loss of punctate gelatin degradation observed following LIMK inhibition is due to a reduction in cortical actin structures required to deliver membrane bound MMPs such as MT1-MMP to the site of invadopodia formation. MMP activity across the whole cell may not be reduced following LIMK siRNA, perhaps it reduced the focalisation of proteolytic activity.

To ascertain if the loss of invadopodia activity seen in MDAMB231 cells following LIMK inhibition related to a loss of total MMP2 or MMP9 activity, a zymography approach was taken. Zymogram gels were used to analyse MMP activity in concentrated conditioned media following LIMK knockdown or inhibition. 24 hours following transfection of MDAMB231 with siRNA against the LIM Kinases,

fresh media (DMEM 10% FCS) was added to each well of cells and 'conditioned' for 24 hours (allowing cells to secrete MMPs into the media). The media was then collected, concentrated by centrifugation and denatured in SDS buffer using a non-reducing buffer. Samples were electrophoresed on gelatin zymogram gels (10% Tris-Glycine gel with 0.1% gelatin incorporated as a substrate), the gels re-natured in a zymogram renaturing buffer (containing a non-ionic detergent) and equilibrated in a developing buffer (to add  $Zn^{2+}$  required for enzymatic activity). Zymogram gels were stained (as described) to reveal protease activity as clear bands against a dark blue background. Knock-down of LIMK1 or LIMK2 reduced extracellular MMP9 activity and thus the intensity of the corresponding white bands seen in Figure 4.4.7. Knock-down of both Lim Kinases in combination enhanced this effect on MMP9 activity in an additive manner. No detectable MMP2 activity was observed in the conditioned media of MDAMB231, nor were there any discernable pro-MMP bands visible on the zymogram. Previous work using MDAMB231 cells to look at metalloprotease activity have found that MMP2 activity was higher than MMP9 (Kim et al, 2008), however other earlier work with this cell line was unable to detect MMP2 activity in comparison with MMP9 (Antonietta et al, 1998). This suggests that MMP2 levels vary between clones, and could explain the absence of MMP2 activity on these zymograms.

#### **4.2.3 Knockdown of LIMK has no effect on MMP9 transcription**

QPCR was performed to determine the whether knockdown of LIMK was causing a reduction in MMP activity by reducing transcription. Cellular levels of RNA following knockdown of LIMK1, LIMK2 or both in combination were compared to control transfections in MDAMB231, (using the housekeeping gene 18S as a reference). LIMK1 RNA levels were reduced following knockdown of LIMK1 or in combination with LIMK2 as a double knockdown (Figure 4.4.8part A.). LIMK2 RNA levels were reduced following knockdown of LIMK2 or in combination with LIMK1 in a double knockdown (Figure 4.4.8part B.). There was a slight trend towards a reduction in MMP14 RNA levels following LIMK1, LIMK2 or LIMK1&2 knockdown (Figure 4.4.8 part C.) but there was no discernible effect on MMP9 RNA levels (Figure 4.4.8 part D.).

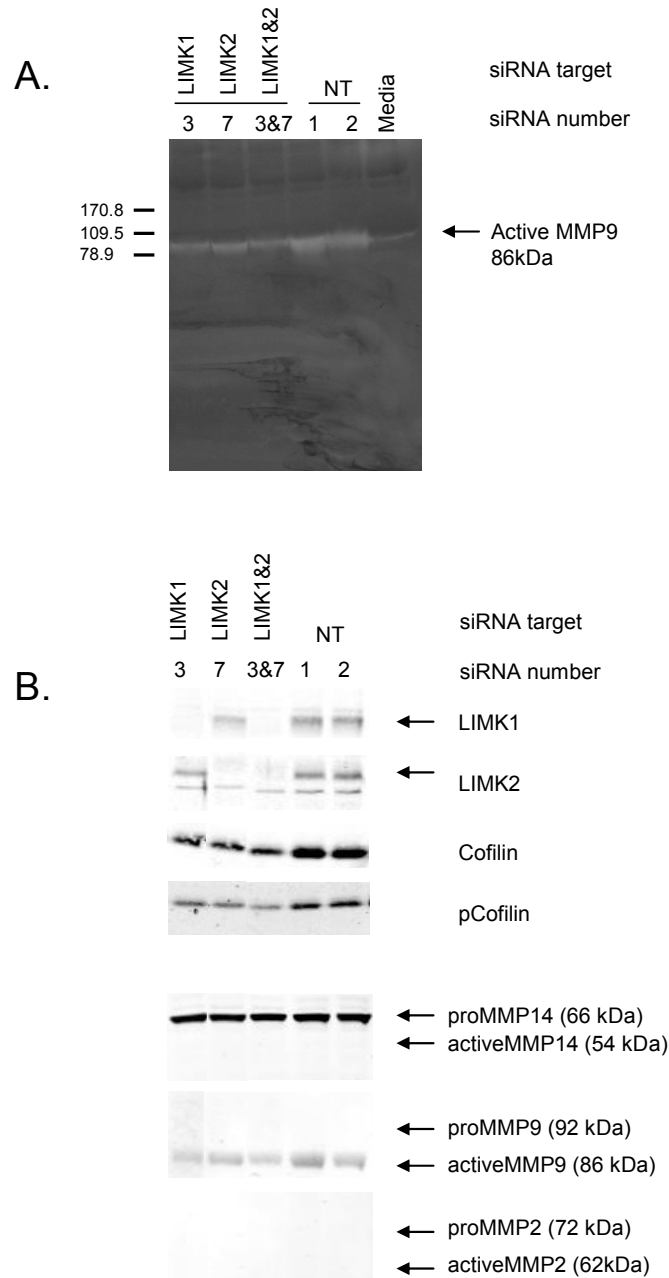


#### Figure 4.4.7-Knockdown of LIM Kinases reduces MMP9 activity in MDAMB231

A. Gelatin Zymogram gel, white bands indicate areas of matrix metalloproteinase activity. Control cells (treated with Non-targeting siRNA) degrade the gelatin laced gel in a band the correct size to indicate MMP9 activity. LIMK1 or 2 knock-down by siRNA results in reduced MMP9 activity, further reduced by knockdown of both LIMK1 and LIMK2 in combination. Media alone (DMEM 10% FCS) has very low levels of MMP9 activity, this activity can be accounted for by the serum supplementing the media. Gel was imaged using a Syngene imaging system. B. Western Blot of whole cell lysates confirming knockdown of LIMK1, LIMK2 and both LIMK1&2. Knockdown of LIMK1 or LIMK2 reduces both total cofilin and pcofilin levels but has no effect on MMP14 or MMP9 protein levels. Knockdown of both LIMK1 and LIMK2 further reduces pcofilin levels, does not effect MMP14 levels but may have a slight effect on total MMP9 levels. Irrelevant bands have been excised for illustrative purposes.

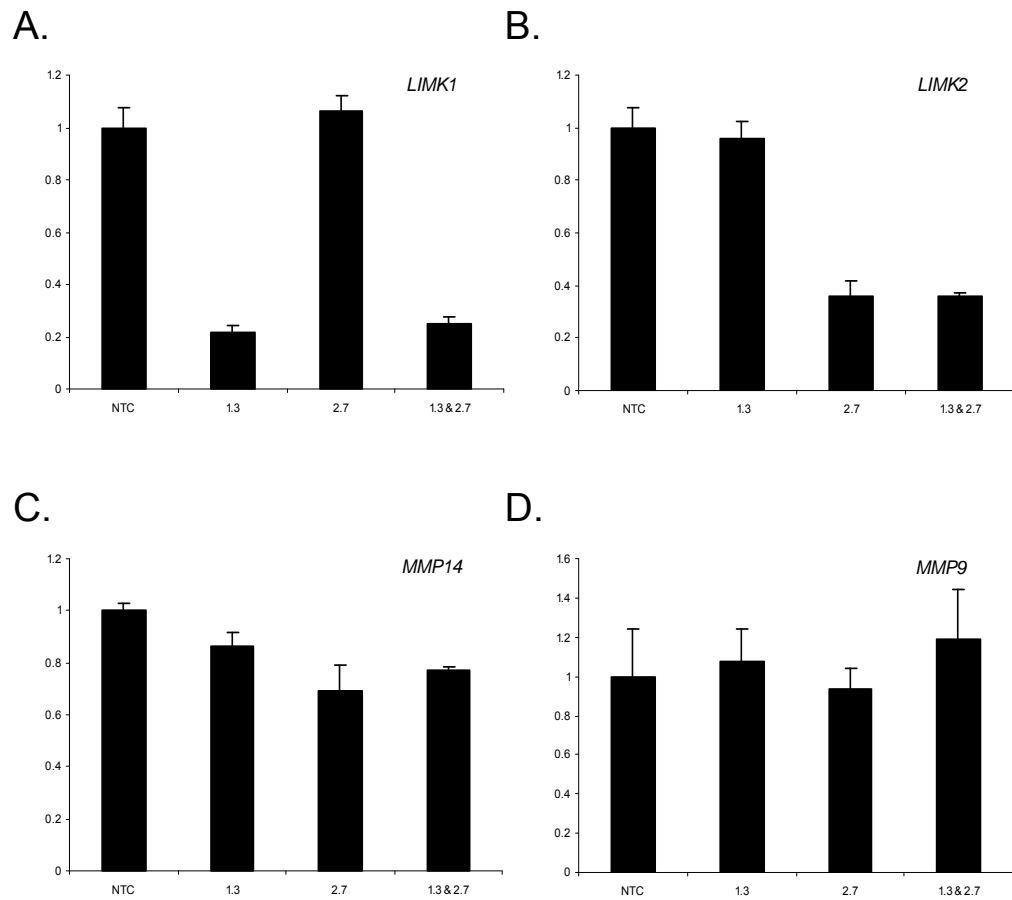


#### Figure 4.4.8-Effects of LIM Kinase Knockdown on MMP RNA levels

QPCR to determine cellular levels of RNA following knockdown of LIMK1, LIMK2 or both in combination compared to control transfections in MDAMB231, (referencing gene 18S). A. LIMK1 RNA levels are reduced following knockdown with siLIMK1 number 3 (1.3) or when siLIMK1 number 3 (1.3) is used in combination with siLIMK2 number 7 (1.3&3.7). B. LIMK2 RNA levels are reduced following knockdown with siLIMK2 number 7 (2.7) or when siLIMK2 number 7 (2.7) is used in combination with siLIMK1 number 3 (1.3&3.7). C. There is a slight trend towards a reduction in MMP14 RNA levels following LIMK1, LIMK2 or LIMK1&2 knockdown. D. Knockdown of LIMK1, LIMK2 or both in combination has no discernible effect on MMP9 RNA levels.

#### **4.2.4 LIMK is required for optimal collagenase activity in 3D**

Having seen a reduction of MMP9 activity in the conditioned media of cells with reduced LIMK levels cultured in 2D, the next step was to identify if this 2D effect was also relevant to 3D invasion. To visualise collagenase activity in 3D, matrigel plugs (set up in invasion assay trans-wells as previously described) were spiked with DQ collagen. DQ collagen fluoresces upon degradation, and can be used to qualitatively identify areas of activity or degradation by cells. Supplied by Invitrogen, it is described as ‘analogs of the natural substrate that have an excessive number of fluorescent dyes attached’. Their close proximity on the intact substrate causes the signal to be quenched and fluorescence to be reduced to almost nothing, hydrolysis by MMPs causes separation of the dye molecules and thus an increase in fluorescence

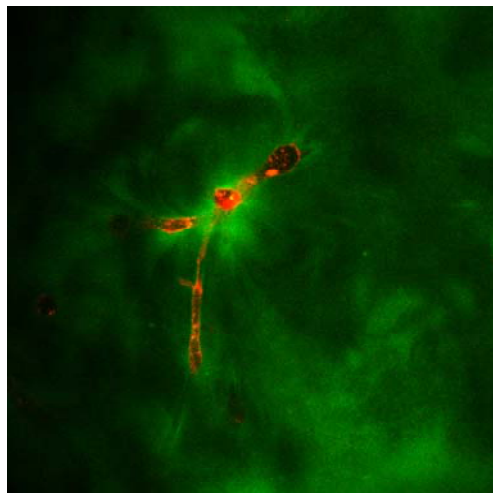
(<http://products.invitrogen.com/ivgn/en/US/adirect/invitrogen?cmd=catProductDetail&entryPoint=adirect&productID=D12060&messageType=catProductDetail>).

By adding it to the matrigel matrix, MMP activity can be visualised in 3D.

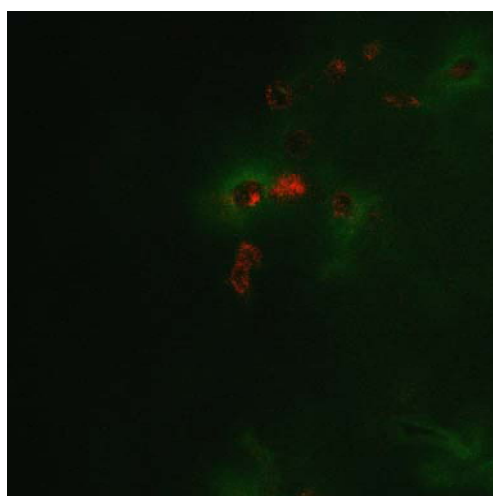
Following LIMK1&2 knockdown or transfection with non targeting controls, MDAMB231 RFP cells (stably transfected with membrane bound RFP) were allowed to invade DQ collagen spiked matrigel for 5 days (Figure 4.4.9) Control cells invaded into the matrix, tracking after each other and displaying ‘halos’ of green fluorescence, reflecting collagenase activity (Figure 4.4.9 part A.). Cells that invaded following knockdown of both LIMK1&2 were more rounded in morphology, as described in the previous chapter, and displayed reduced collagenases activity (Figure 4.4.9 B.). MMP activity was not completely ablated, consistent with the low level invasion that was observed following LIMK knockdown and the reduced levels of MMP9 activity observed by zymography.

This data is consistent with previous studies on MMP activity and invasion. It has previously been shown that siRNA treatment of MDAMB231 for MT1-MMP reduces hypoxia induced invasion (Munoz-Najar et al, 2005), and MT1-MMP (also known as MMP14) has been shown to be important in cell invasion through matrix (Sabeh et al, 2004) and the pathway leading to activation of MMP9 in chondrocytes (Dreier et al, 2004). A link could be hypothesised between LIMK activity and MMP14 activation of MMP9.

A.



B.

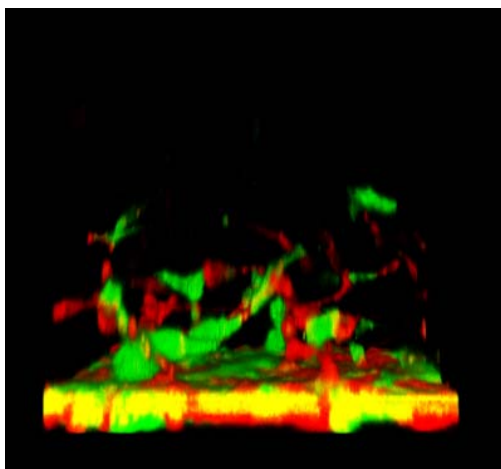
**Figure 4.4.9-Knockdown of LIMK reduces Collagenase activity in 3D**

MDAMB231 cells invading into a matrigel and collagen matrix, DQ collagen fluoresces (green) upon degradation. A. MDAMB231 cells stably transfected with membrane bound RFP invading into a DQ collagen/matrigel matrix following transfection with a non targeting siRNA. The green halo around each red cell indicates collagenase activity (MMP2 or MMP9). B. MDAMB231 cells stably transfected with membrane bound RFP invading into a DQ collagen/matrigel matrix following knockdown of LIMK1&2 by siRNA. The faint green halo around each red cell indicates less collagenase activity than control cells in B.

#### **4.2.5 LIMK is important in cells 'leading' invasion**

MMP activity has been reported to be important in the collective invasion of cells (Friedl & Wolf, 2008; Wolf et al, 2007) and the invasion of MDA MB 231 cells into 3-D matrigel appeared to be via collective tube-like strands, as could be seen in the previous chapter and as reported by Wolf et al (Wolf et al, 2007). Since MDAMB231 cells are capable of providing the path generating activity required in leading cells during collective invasion, MDAMB231 cell lines stably expressing either membrane bound either green or red fluorescent proteins (GFP or RFP) were generated by drug selection, and further mechanically sorted for the greatest RFP and GFP expression. While GFP expressing cells were untreated, RFP expressing cells were transfected either with NT or LIMK1&2 siRNA. Consistent with earlier results presented in this thesis, NT siRNA did not affect matrigel invasion and RFP and GFP cells invaded in strands together (Figure 4.4.10 part A and Figure 4.4.11 part A) and the occurrence of RFP-expressing cells leading the collective strands was approximately 50% (Figure 4.4.11 part C). As could be predicted from the previous chapter LIMK1&2 siRNA treatment of only the RFP expressing cells slightly reduced over all invasion (Figure 4.4.10 part B), and there were fewer RFP cells invading into the matrigel, and the RFP-expressing cells observed were largely restricted to following GFP-positive cells (Figure 4.4.11 part B). The occurrence of RFP-expressers as leading cells of invasion dropped significantly to 18%. These results indicate that LIMK activity is required for path generation by the leading cells in collective invasion.

A.



B.

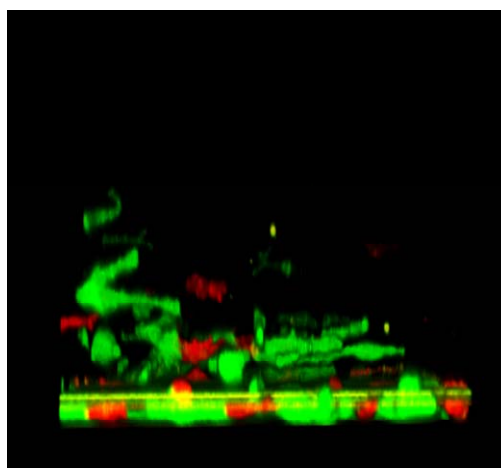


**Figure 4.4.10-Cells leading collective invasion require LIMK**

**A.**MDAMB231 cells stably expressing either RFP or GFP when mixed together in a 1:1 ratio invade matrigel collectively. Both red and green cells lead this invasion. **B.** RFP cells following siRNA against LIMK1 and 2 do not invade as successfully as controls, and appear to 'lead' invasion less. Images were acquired on an Olympus FV1000 using a x40 water lens, z-stacks were used to reconstruct 3D invasion on Volocity imaging software.

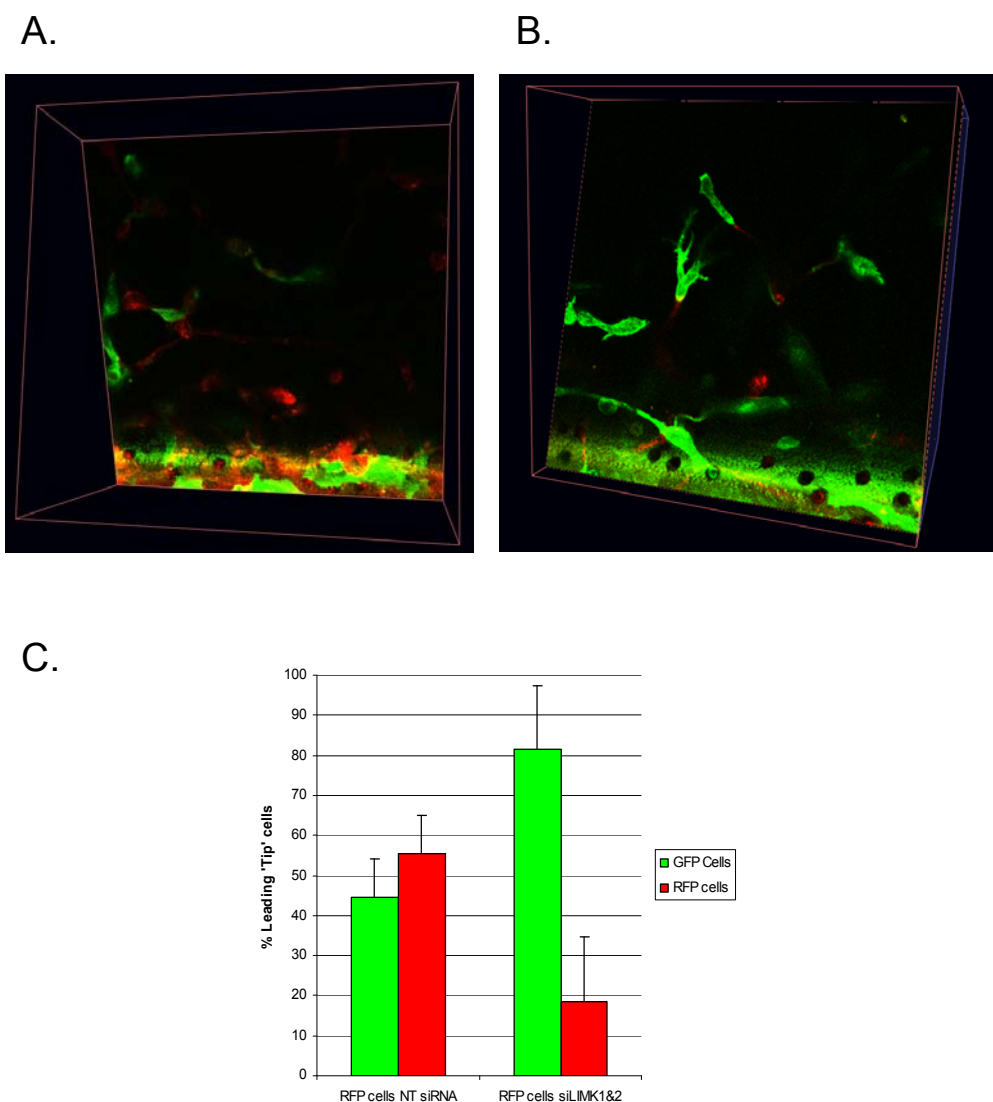


**Figure 4.4.11-Loss of leading ‘tip’ position during invasion by cells following LIMK knockdown.**

Optical slices through z stacks show MDAMB231 cells stably expressing either RFP or GFP mixed together in a 1:1 ratio invading matrigel collectively. A. Both red and green cells lead this invasion when red cells are transfected with non targeting siRNA oligonucleotides. B. RFP cells following siRNA against LIMK1 and 2 shows although some red cells still invade following knockdown of LIMK1 and 2 they tend to ‘follow’ more invasive green cells. C. Quantification of the proportion of RFP MDAMB231 cells to GFP MDAMB231 cells leading invasion as a ‘tip’ cell following invasion into matrigel (cells were mixed 1:1). Following knockdown of LIMK in RFP MDAMB231 the proportion of GFP MDAMB231 leading ‘tip’ cells increases. Images were acquired on an Olympus FV1000 using a x40 water lens, z-stacks were used to reconstruct 3D invasion on Volocity imaging software.

## 4.3 Conclusion

Both LIMK1 and LIMK2 have been shown to play a role in the formation of functional invadopodia in gelatin degradation assays. Loss of LIMK by siRNA was shown in Chapter 2 to reduce F-actin staining, correlating with a loss of invadopodia in this chapter and a reduction of MMP activity. Gelatin zymography confirmed that reducing LIMK levels reduced levels of active MMP9 being secreted by cells, which could in turn play a role in the loss of 3D invasion observed in Chapter 2. Collagenase activity in 3D invasion was reduced following knockdown of both LIM Kinases and this could be important in the role LIMK plays in cells leading invasion. The proportion of RFP MDAMB231 cells to GFP MDAMB231 cells leading invasion as a 'tip' cell is relatively equal when mixed 1:1 and allowed to invade into matrigel. Following knockdown of both LIM Kinase 1 and LIM Kinase 2 in RFP MDAMB231 cells this changes and the majority of leading 'tip' cells are GFP MDAMB231. However, the RFP cells that have been subject to knockdown of both LIMK1&2 still follow GFP cells into the matrigel, the cells that have full proteolytic activity. The 'following' cells are still motile, and could have adapted to a more amoeboid form of motility to follow the leading cells that degrade the substrate to facilitate motility (Friedl & Wolf, 2003; Wyckoff et al, 2006). This is somewhat similar to previous observations in the preceding chapter where MDAMB231 invasion into matrigel was reduced by siRNA knockdown of LIMK, but that the cells could still move through the filter with its preformed holes.

In conclusion, the data presented in this chapter suggests a role for LIMK regulated matrix degradation in cells leading collective forms of invasion, but that LIMK does not play a role in the capability of cells to follow 'leading' cells with a more invasive phenotype.

## 5 Cofilin phosphorylation and invasion

### 5.1 Chapter Summary

Cofilin is the most well documented and characterised LIMK substrate. Its activity is believed to relate inversely to that of LIMK as it is the primary substrate and downstream effector of LIM Kinase; Cofilin is rendered inactive by LIMK phosphorylation on Serine 3. It can bind to both F-actin filaments and G-actin monomers, severing F-actin filaments as part of a cycle of polymerisation and depolymerisation (Hawkins et al, 1993). Previous work has implicated Cofilin as an important regulator of migratory behaviour in metastatic cancer cells (Sidani et al, 2007), and work presented in previous chapters of this thesis has outlined the link between a loss of filamentous actin levels and a loss of invasiveness in cancer cells. As these previous observations were made to identify the role LIMK plays in invasion, the work completed in this chapter aimed to elucidate if the phosphorylation status of the LIM Kinase substrate was enough to affect cell invasion.

An optimised protein transduction domain (PTD) derived from HIV TAT (transactivator of transcription) protein amino acids 47-57 was used in the generation of a membrane permeable PTD Cofilin, a phosphomimetic mutant Cofilin and a non-phosphorylatable Cofilin mutant. These were then used to examine the effects of cofilin phosphorylation on cancer cell motility and invasion.

#### 5.1.1 PTD Flag Cofilin1

TAT fusion proteins have been used previously to give quick high efficiency transduction of proteins and peptides into cells without need for transfection (Ho et al, 2001; Sahai et al, 2006). An optimized protein transduction domain based on the HIV TAT protein (Ho et al, 2001) was fused to Cofilin1 to promote cellular uptake. The version of optimised TAT protein used was PTD4 (YARAAARQARA, optimised Protein Transduction Domain 4, as described in reference (Ho et al, 2001)), found to be 33 times more effective at cell transduction than wild type TAT due to additional strengthening of the putative

$\alpha$ -helix with Alanine residues and limiting the Arginine content to three residues down one face of the helix (Figure 5.5.1 part A and B.). The fusion constructs made included a PTD wild type Cofilin, a phospho-mimetic mutant (constitutively inactive S3E mutant), and a non phosphorylatable mutant (constitutively active S3A mutant) as well as PTD GST as a control for protein transduction (Figure 5.5.1 part C.).

### **5.1.1.1 Generation of PTD Flag Cofilin**

PTD FLAG Cofilin1 was generated by the annealing of double stranded oligonucleotides coding for the PTD peptide (YARAAARQARA) and FLAG epitope, and subsequent ligation into pGEX KG Cofilin plasmid. The mutants were subsequently produced by site directed mutagenesis. The Cofilin proteins were expressed in *E. coli* and purified as described, cleaving fused GST in all but the control protein for final products as outlined in Figure 5.5.1 part C. The PTD cofilin proteins routinely expressed and purified well, as can be seen by an example gel run during protein production in Figure 5.5.2 part A. At high concentrations PTD Cofilin had fewer contaminants than commercially sourced BSA. The PTD proteins were added directly to media on cells and entered cells in a dose dependent manner; as can be seen in the example western blot of Figure 5.5.2 part B. showing PTD Cofilin1 WT entering NIH3T3 cells at doses ranging from 0-800 $\mu$ g per ml media. Endogenous cofilin levels were unchanged by the addition of PTD Cofilin. The PTD proteins enable direct entry of Cofilin into the cell, without the need for transfection or the constraints of expressing an already abundant protein.

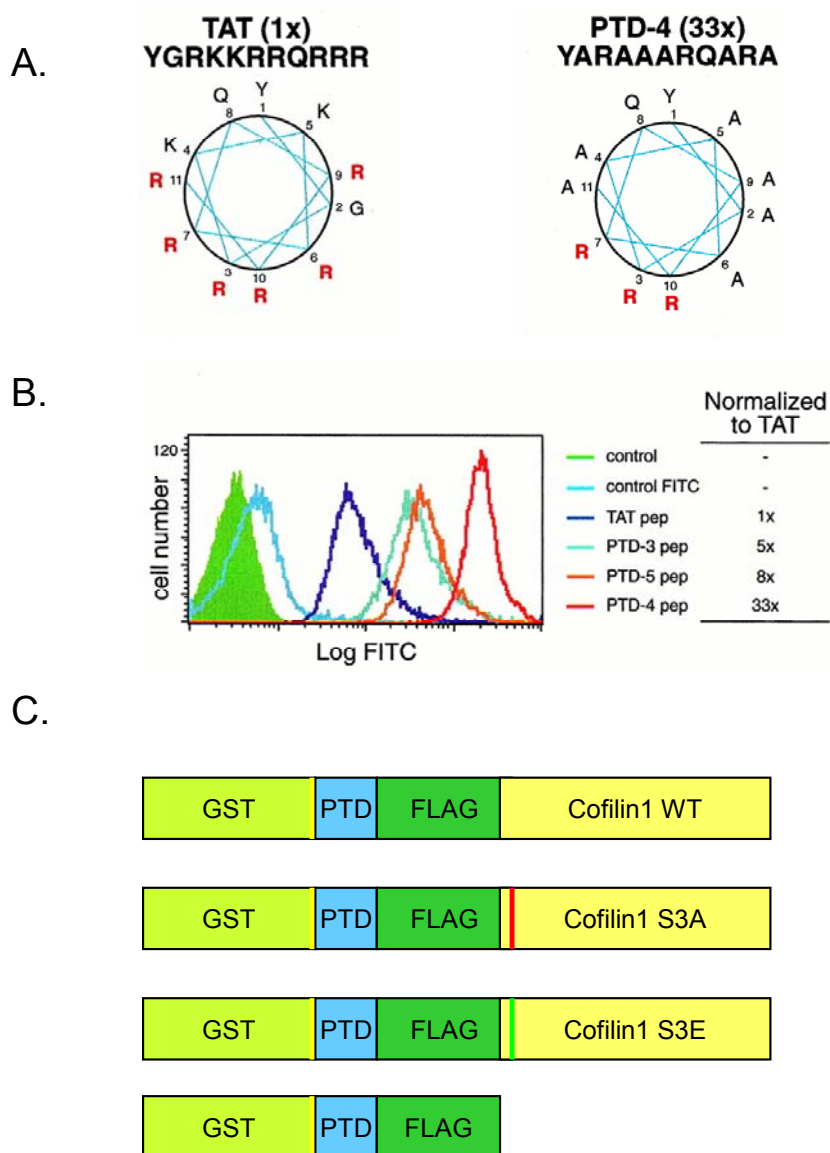


**Figure 5.5.1-PTD, an optimised TAT protein.**

A. Predicted  $\alpha$ -helical wheels of TAT and the optimised PTD number 4 (single-letter amino acid code) (Ho et al, 2001). Note the reduction of Arginine residues in PTD4, the optimised TAT protein. Numbering refers to sequential amino acid position; the values in parentheses refer to the fold change of FITC emission normalized to TAT peptide (1x) (as expanded in part B.). B. Characterization of PTD-FITC peptides in vitro (Ho et al, 2001). Flow cytometry comparison of untreated and treated Jurkat T cells with equal molar amounts of control FITC and TAT, and PTD-3, PTD-4, and PTD-5 peptides. Normalized fluorescent values are to that of TAT peptide (1x; right). C. Diagrammatic illustration of the PTD fused proteins generated. From top to bottom; PTD FLAG Cofilin1 WT, PTD FLAG Cofilin1 S3A (non-phosphorylatable), PTD FLAG Cofilin1 S3E phosphomimetic and GST construct control. A. and B. Adapted from Ho, A. et al. *Cancer Res* 2001;61:474-477, Copyright ©2001 American Association for Cancer Research.

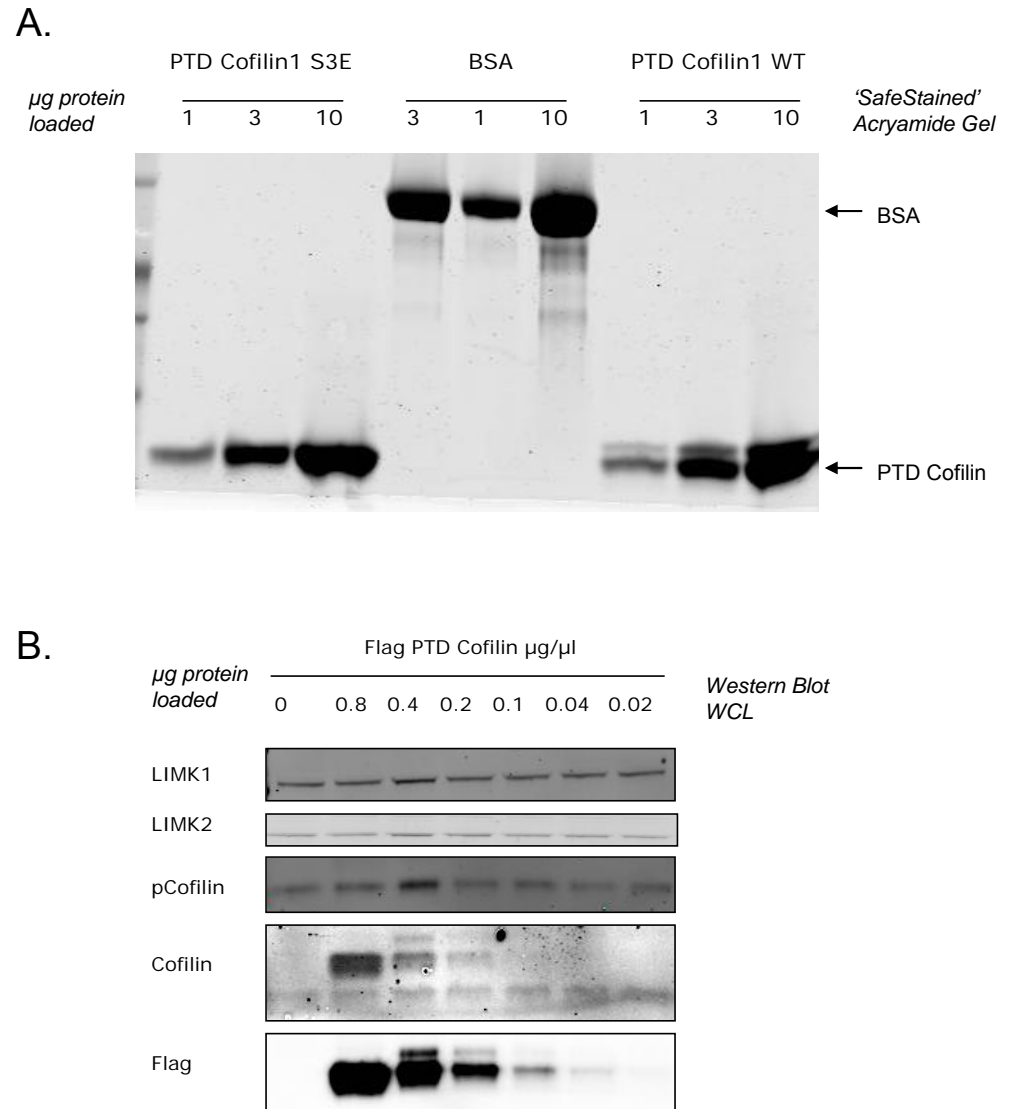


**Figure 5.5.2-PTD Cofilin purification and cell permeability.**

PTD proteins were expressed in bacteria and purified before being added to cells in media. A. An example of a SafeStain stained acryamide gel showing high purity during the production of PTD Cofilin proteins. Left hand lanes show BSA protein and right hand lanes show PTD Cofilin1 at comparable concentrations. B. Western Blot of whole cell lysates following 24 hour treatment with PTD Cofilin1 WT. PTD Cofilin1 WT entered NIH3T3 cells in a dose dependent manner, with no discernable effect on endogenous Cofilin levels.

### 5.1.1.2 2D localisation of PTD cofilin in cells

Loading cells with PTD FLAG Cofilin should counteract the effect of LIM Kinase by shifting the Cofilin:pCofilin balance with the active non phosphorylated form of Cofilin. By flooding cells with WT Cofilin1 we would expect to see a reduction in F-actin staining for structures such as stress fibres. MDAMB231 cells were seeded onto coverslips and cultured in media containing PTD Cofilin proteins at 800µg per ml. 24 hours later the MDAMB231 cells were fixed and stained for F-actin; to establish if any cytoskeletal changes had occurred following an excess of unphosphorylated cellular Cofilin, and FLAG antibody; to identify cells successfully transduced with PTD FLAG Cofilin protein or PTD FLAG GST control (Figure 5.5.3). All PTD Cofilin proteins and GST control were successfully delivered into cells, and were distributed in a diffuse manner as determined by immunofluorescence using a FLAG antibody. PTD FLAG Cofilin also showed some localisation with cortical F-actin staining. Cells exposed to the S3E Cofilin mutant appeared slightly more spread than control cells, S3A Cofilin and WT Cofilin treated cells appeared fractionally more rounded or ruffled than controls. To validate if the subtle morphological changes observed in cell shape were due to the activity of these PTD Cofilin fusion proteins an *in vitro* line of investigation was used.

### 5.1.2 In Vitro activity of PTD Cofilins

Pyrene fluorescence increases 10-20 fold when G-actin is incorporated into filaments and the converse of this can be utilised to quantify F-actin depolymerisation by steady state fluorescence (Cooper JA, 1983). The F-actin severing activities (Hawkins et al, 1993) of PTD Cofilin WT, S3E, S3A and PTD GST were validated *in vitro* using this pyrene labelled F-actin severing assay. Pyrene labelled F-actin was added to a cuvette (with or without the PTD FLAG WT Cofilin) and steady state fluorescence measured on a spectrofluorimeter as described in the methods chapter. Data gathered was normalised and reported as a percentage of fluorescence over time (Figure 5.5.4). F-actin depolymerisation, described here as the reduction in Pyrene fluorescence was reduced by less than 10% after 900 seconds for polymerised Pyrene F-actin

alone and after the addition of PTD GST control, PTD FLAG S3E Cofilin or PTD FLAG S3A Cofilin. PTD WT Cofilin (WT) depolymerised Pyrene F-actin by almost 75% over the 900 second time-course. Despite the subtle morphological changes seen, although the PTD FLAG Cofilin WT had actin severing activity and the controls reassuringly had no activity, PTD FLAG Cofilin S3A also did not have actin severing activity. This makes it difficult to interpret whether the phosphomimetic mutant, PTD FLAG Cofilin S3E, which was not expected to show activity *in vitro* (the glutamate (E) negative charge mimics the negative charge of phosphate to render the protein inactive) did not have activity because the mutation makes the protein misfold rather than altering the serine 3 phosphorylation site. With this in mind, knowing that only the activity of the WT protein can be validated *in vitro*, the influence of Cofilin levels on motility in 2D was assessed simply using the WT protein.

### **5.1.3 Increased levels of Wild Type Cofilin do not affect cell motility in 2D**

In order to assess if perturbing the ratio of phosphorylated to non-phosphorylated Cofilin had an effect on cell motility MDAMB231 cells were plated onto CDM (generated as previously described) and dosed with either PTD GST control protein, or equivalent levels of PTD FLAG Cofilin WT. Since PTD FLAG Cofilin S3E could not be validated it was not used in investigations into motility. Cells were then imaged every 15 minutes by timelapse microscopy for a period of 12 hours, and the images analysed using ImageJ software to trace individual cell tracks. Following the introduction of equivalent amounts of PTD GST or PTD FLAG Cofilin to MDAMB231 initial observations suggested a subtle difference in cell motility between conditions (Figure 5.5.5); cells appeared to turn less frequently following an increase of cellular Cofilin, but the 3% increase in persistence from 0.18 to 0.21 was not statistically significant.

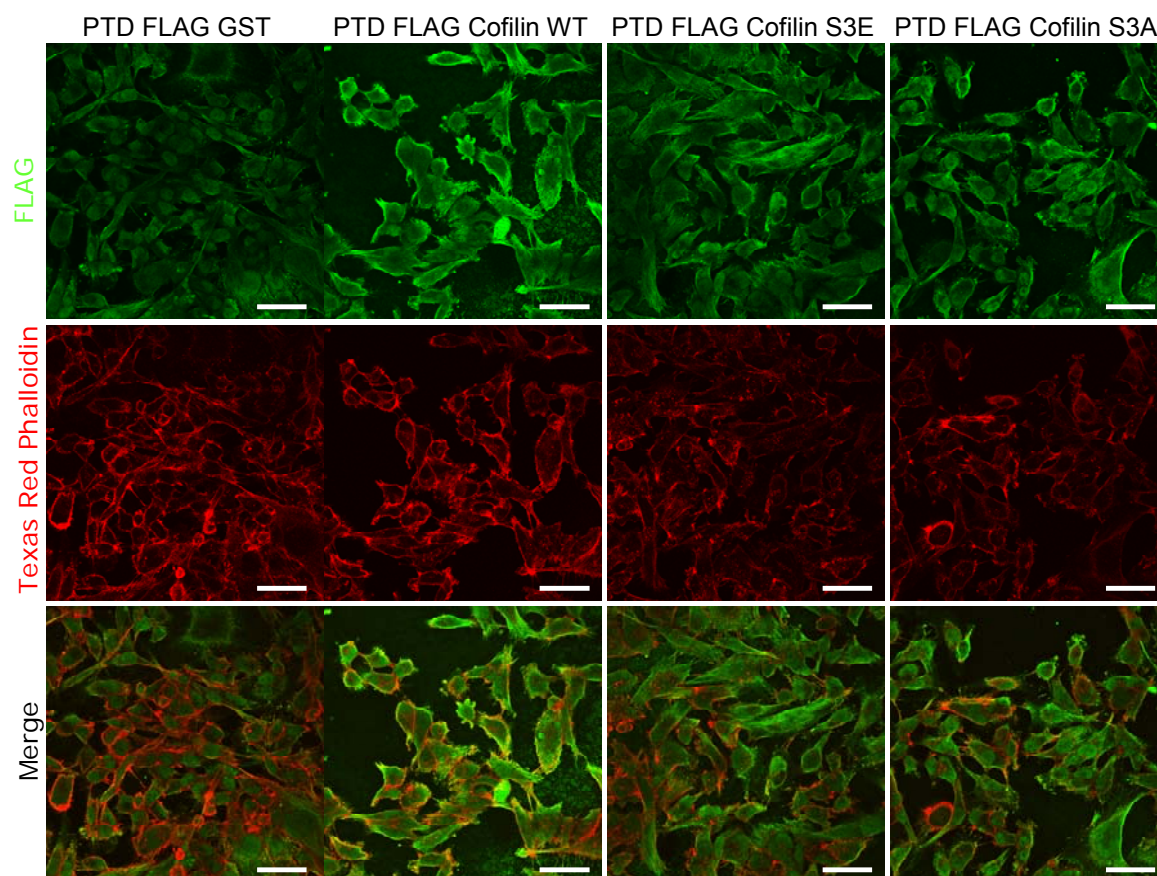


**Figure 5.5.3-Localisation of PTD FLAG Cofilin in MDAMB231 cells.**

All PTD FLAG Cofilin proteins and control PTD FLAG GST successfully entered MDAMB231 cells, with 100% efficiency. The localisation of the PTD proteins was determined using an anti-FLAG antibody, and the cells stained with Texas Red phalloidin to visualise F-actin. All PTD proteins were distributed diffusely through out the cells, except PTD FLAG Cofilin WT which also had strong peripheral staining, colocalising with cortical actin. Images were captured. Images captured on the Zeiss Axioplan 200 at x40 using Imaging Associates Isis software. Scale bar equals 40 $\mu$ m.

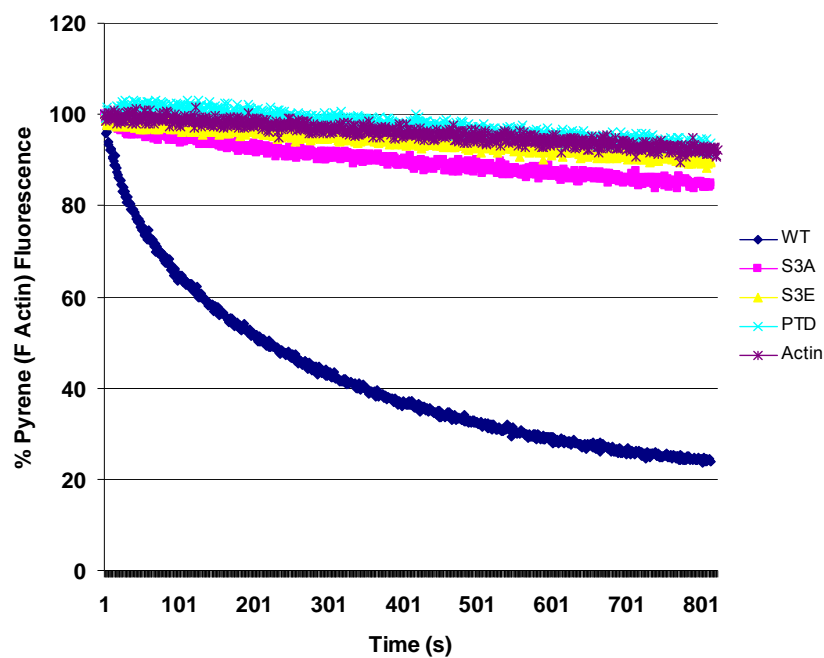
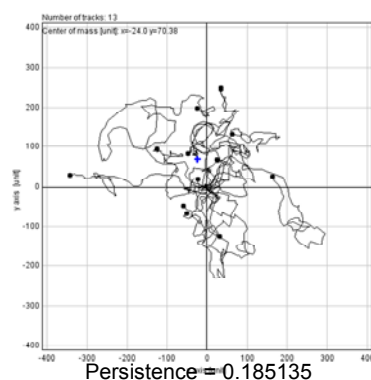


#### Figure 5.5.4-In Vitro F-actin severing activity of PTD Cofilin

The F-actin severing activity of PTD Cofilin was validated in vitro. F-actin severing is quantified as percentage reduction in Pyrene Fluorescence over time. F-actin depolymerisation (fluorescence reduction) was <10% after 900 seconds for control PTD GST (PTD), PTD S3E Cofilin (S3E), PTD S3A Cofilin (S3A) and Polymerised Pyrene Actin alone (Actin) conditions. PTD WT Cofilin (WT) depolymerised Pyrene F-actin by up to 75% over time. Data shown from a representative experiment.

A. CONTROL



B. PTD FLAG Cofilin WT

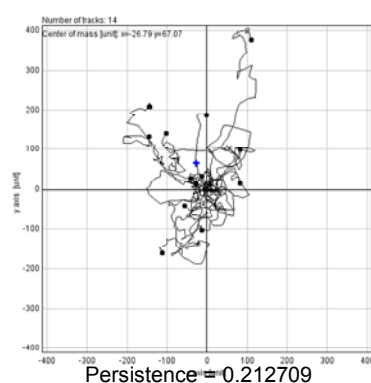


**Figure 5.5.5-Motility in 2D following an increase in cellular levels of Cofilin.**

Following the introduction of equivalent amounts of PTD GST or PTD FLAG Cofilin to MDAMB231 individual tracks were traced. A. Individual cell tracks of cells moving across CDM following exposure to PTD GST. B. Individual cell tracks of cells moving across CDM following exposure to PTD FLAG Cofilin WT. A subtle increase in persistence was noted between the two conditions, this trend may reflect a reduction in turning frequency by cells. Example tracks shown are representative of replicate experiments and were analysed using ImageJ imaging software.

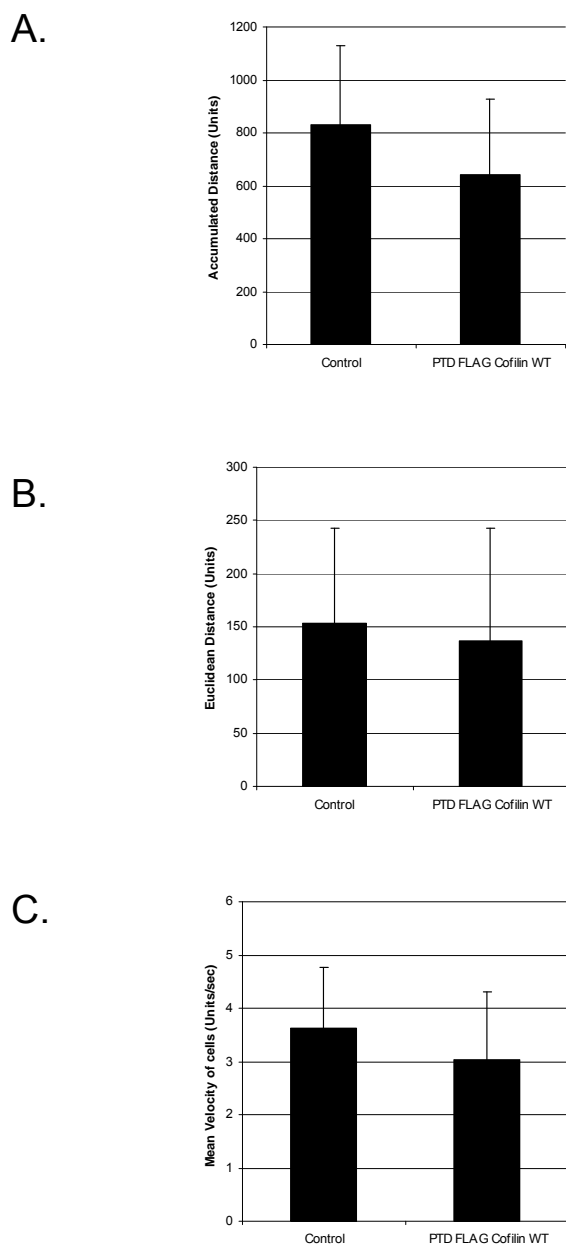


**Figure 5.5.6- Quantification of motility in 2D following an increase in cellular levels of Cofilin**

Following the introduction of equivalent amounts of PTD GST or PTD FLAG Cofilin to MDAMB231 the effects on cell motility across CDM was quantified. A. The Accumulative distance (Vectorial distance) travelled by cells was slightly reduced following an increase in cellular Cofilin, but this was not deemed statistically significant (as determined by ANOVA). B. The Euclidean distance travelled by cells following a cellular increase in Cofilin levels was not altered in a statistically significant manner (as determined by ANOVA). C. The mean velocity of cells was reduced slightly following exposure to high levels of cellular Cofilin, but this was also deemed statistically insignificant by ANOVA.

#### ***5.1.4 3D Invasiveness is altered by disruption of the Cofilin phosphorylation balance***

In Chapter 3 it was shown that LIMK knockdown reduced the relative proportion of phosphorylated to unphosphorylated Cofilin and reduced cell invasion. To determine if introducing an excess of unphosphorylated Cofilin into cells would affect invasion, a return was made to 3D inverse invasion assays.

Following the introduction of equivalent amounts of PTD GST or PTD FLAG Cofilin WT, a statistically significant effect of PTD FLAG Cofilin WT on inhibiting matrigel invasion was observed. There was a significant reduction of invasion in cells treated with wild type PTD Cofilin compared to the PTD GST control treated cells (Figure 5.5.4).

These results demonstrate that disruption of the active to inactive balance of Cofilin is enough to perturb actin regulation, and thus invasion.

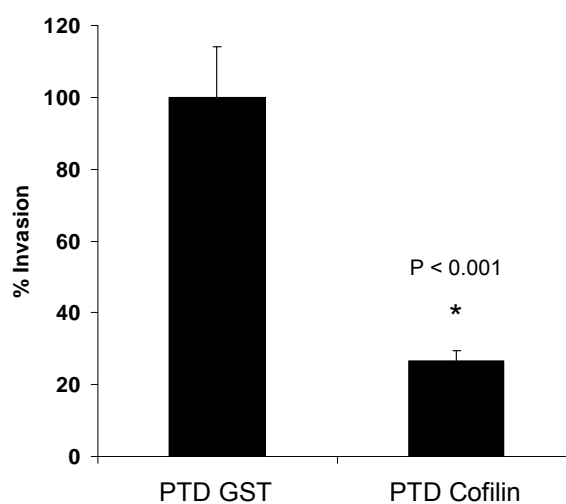


**Figure 5.5.7-Disruption of the Cofilin balance reduces cell invasion.**

Following the introduction of equivalent amounts of PTD GST or PTD FLAG WT Cofilin, to MDAMB231 cells and the corresponding matrigel invasion plugs, cells were given 5 days for invasion, then fixed and stained for imaging, (part A). B. Quantification of invasion images is graphed showing a significant reduction in invasion of cells subject to increased levels of PTD FLAG Cofilin WT compared to PTD GST control treated cells. Invasion was imaged on an FV1000 Olympus Confocal at x40 water lens using FV10-ASW.1.7b software.  $P < 0.001$  as determined by Students t-test.

## 5.2 Conclusions

Data from the previous chapters suggested that the phosphorylation status of Cofilin was important in invasion as inhibiting LIMK reduced MDAMB231 invasion of matrigel. This inhibition also led to a reduction in phospho-Cofilin levels, as demonstrated previously by western blot following knockdown of LIMK by siRNA. It was also found in those chapters that knockdown of LIM Kinases did not have a significant effect on 2D cell motility. This chapter aimed to determine if these effects were mediated by Cofilin, and if Cofilin phosphorylation status was important for cell motility or invasion. 2D motility was not significantly affected by increasing levels of unphosphorylated (active) Cofilin into cells; 3D invasion was, however, significantly reduced by increasing the levels of unphosphorylated cellular Cofilin. Data from WT PTD Cofilin indicates that Cofilin phosphorylation status is important in invasion, but no conclusions could be drawn from the generated mutants. Although specific amino acid substitution should allow correct protein folding, and provide the desired change to mimic or prevent phosphorylation, it is not a foolproof system. The mutant Cofilin proteins may have been misfolded and therefore not had the expected activity.

Although the transduction method of PTD proteins is advantageous as it reduces the time taken to 'transfect' cells, allowing rapid analysis of the effect of increasing Cofilin levels the system still relies upon a tagged protein. Tagged proteins are 'carrying' extra protein and are not the same as endogenous, potentially interfering with the activity of the tagged protein. In many studies PTD-based delivery of fusion proteins results in nuclear targeting but the use of PTD4 in my studies results in cytoplasmic localisation {Chauhan, 2007 #217}. It would be good to do this work with an untagged protein to compare the cellular effects of Cofilin on F-actin structures aswell as the *in vitro* F-actin severing activity incase the tags also influenced the activity of the mutants.

Perturbing the ratio of phosphorylated to non-phosphorylated Cofilin had similar consequences to LIMK inhibition. Increasing the levels of active to inactive Cofilin resulted in inhibition of three dimensional collective invasion, inferring that the requirement of LIMK in cell invasion is mediated by the phosphorylation status of its primary substrate, Cofilin.

Invasion requires cell motility and remodelling of the extracellular matrix, through proteolysis and force-mediated deformation. 2D cell motility was unaffected by increased Cofilin levels, but in 3D cells became less invasive. The two aspects of invasion, cell motility and ECM remodelling, can be tested in the inverse invasion assay. Cells that are motile can move through the filter, and if they are also able to remodel ECM they can also invade the matrigel. Following reduction in LIMK activity or an increase in unphosphorylated Cofilin levels cells were able to cross the filter at the bottom of the transwell, but were unable to invade the matrigel. This, in conjunction with the results showing both LIMK and Cofilin levels having no effect on 2D motility, suggests that through Cofilin LIMK is influencing ECM remodelling, not cell motility.

## 6 Identification of Novel LIMK1 substrates

### 6.1 Chapter Summary

As described in the previous chapter, Cofilin is the most well characterised LIMK substrate. LIMK inactivates Cofilin by phosphorylation on serine 3 and is a useful readout of LIMK activity. In addition to Cofilin proteins, recent research has identified the nuclear transcription factors CREB and Nurr1 (Sacchetti et al, 2006; Yang et al, 2004a) as putative LIMK substrates in neurons, and the microtubule assembly protein p25/TPPP was shown to be inactivated by LIMK phosphorylation (Acevedo et al, 2007).

These recent discoveries suggest that there may be other undiscovered substrates of LIMK within cells. This chapter outlines attempts made to identify and validate putative substrates of LIMK using glass mounted peptide arrays and the Kestrel approach to substrate identification.

### 6.2 LIMK1 phosphorylates Cofilin1 on Serine 3 and potentially Serine 8

Wild type Cofilin1 is known to be phosphorylated on residue Serine 3 (Nebl et al, 1996). To confirm this as the only site of phosphorylation by LIMK1, Cofilin1 was mutated by site directed mutagenesis (SDM) on residue 3 from serine to alanine (S3A) to make a non-phosphorylatable mutant protein. This S3A Cofilin was then subjected to *in vitro* phosphorylation by recombinant LIMK1 in parallel with WT Cofilin in a  $\gamma$ 32p kinase assay, stopped and fixed on Whatman P81 phosphocellulose cation exchanger paper, as detailed in the methods section. Mutation of Serine 3 almost completely ablates phosphorylation by LIMK1 *in vitro* (Figure 6.6.1 part A), indicating that Serine 3 is the primary site of phosphorylation by LIMK1. However, the first 10 amino acids of Cofilin1 are 'MASGVAVSDG'; it contains a further Serine (S8) potentially accessible for phosphorylation as the initial 'arm' of Cofilin is not buried within the protein structure (Agnew et al, 1995; Pope et al, 2004). To identify whether residual phosphorylation of the S3A Cofilin is due to S8 phosphorylation a truncated

Cofilin was generated, phosphorylated in an *in vitro*  $\gamma$ 32p kinase assay and run out on SDS PAGE gel in parallel with both WT and S3A Cofilin (Figure 6.6.1 part B). LIMK strongly phosphorylates WT Cofilin, weakly phosphorylates S3A Cofilin but does not phosphorylate truncated Cofilin. This would suggest that LIMK can also weakly phosphorylate Serine 8 of Cofilin1. This second Serine is not conserved in the other Cofilin family members ADF or Cofilin 2, it is specific to Cofilin1.

### 6.3 Peptide Array

Having confirmed the *in vitro* activity of recombinant LIMK1 in Figure 6.6.1 a Pepscan glass mounted peptide array was employed to identify potential novel substrates of LIMK1.

The Pepscan peptide array produced 148 possible substrates for LIMK1, some of these were overlapping peptide sequences from the same protein, many of those with serine repeats. Twenty two spots were considered to have greater phosphate incorporation than the rest, and were also repeated well on both peptide arrays on either side of the slide. Once ranked the 'hottest' spots corresponded to:

- Kros (p08941) *Proto-oncogene tyrosine kinase c- ROS*
- FIBA (p02671) *Fibrinogen alpha chain*
- Lyc (p00698) *Lysozyme C*
- Glr2 (p19491) *Glutamate Receptor 2*

Peptides corresponding to the overlapping sequences for each of the proteins above were generated to be tested in *in vitro* kinase assays to confirm if they were substrates of LIMK1.

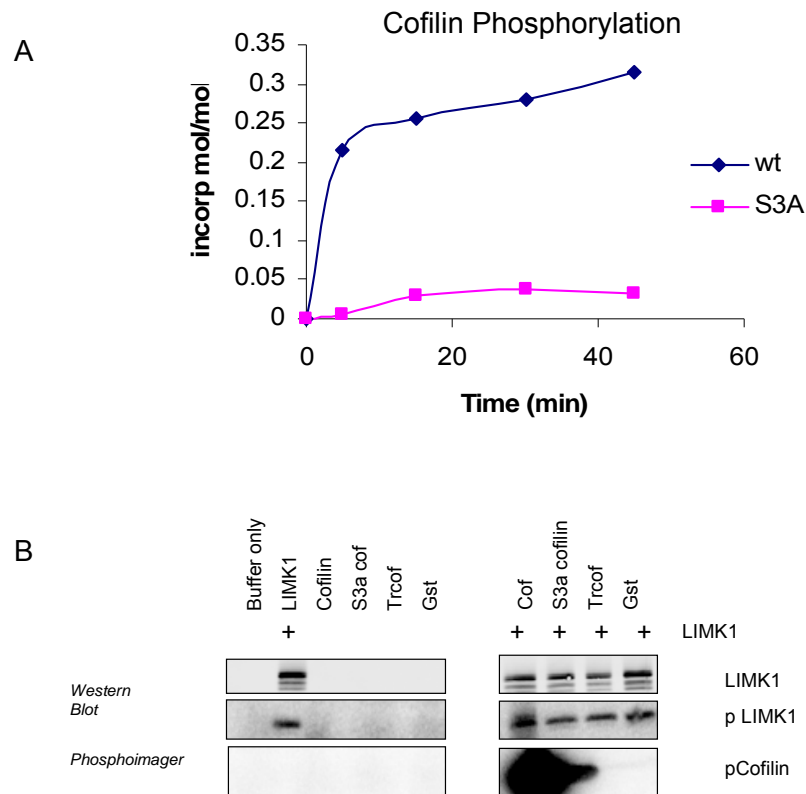


**Figure 6.6.1- LIMK1 phosphorylates Cofilin 1 predominantly on Serine 3.**

A. Incorporation of phosphate over time following an *in vitro* kinase assay in the presence of  $^{32}\text{p}$  to test LIMK phosphorylation of WT Cofilin and S3A Cofilin in parallel. Mutation of this Serine 3 to Alanine almost completely ablates phosphorylation of Cofilin by LIMK1. B. Western blot and phosphoimaging of *In vitro*  $^{32}\text{p}$  kinase assay following SDS page demonstrating that truncation of Cofilin completely ablates phosphorylation by LIMK1. S3A mutant Cofilin is phosphorylated at a low level in comparison with WT Cofilin.

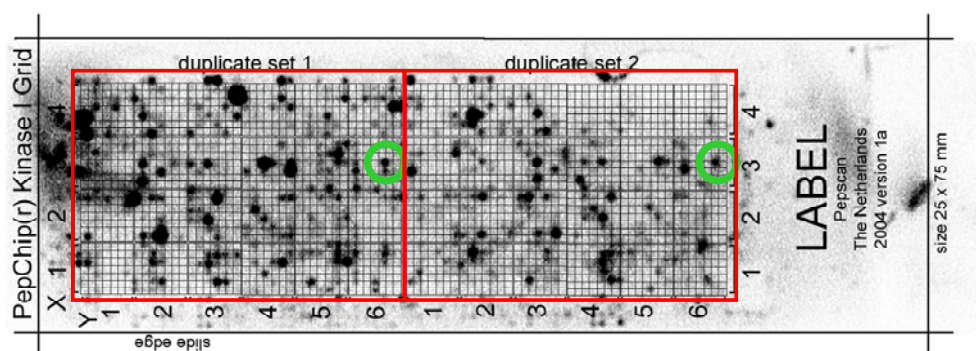


**Figure 6.6.2- Pepscan Peptide Array.**

Merged image of peptide orientation grid and the phosphoimage of array following an *in vitro*  $\gamma^{32}\text{P}$  kinase assay. The replicate arrays are outlined in red, and an example of a phosphorylated peptide that is repeated in both arrays is outlined in green. The peptide array produced 148 possible substrates for LIMK1, some of these were overlapping sequences from the same peptide and many of these contained serine repeats. 22 were 'hotter' than the rest and well repeated on both sides of the slide. The hottest spots included; Kros (p08941), FIBA (p02671), Lyc (p00698), Glr2 (p19491).

### **6.3.1 Proto-oncogene tyrosine kinase c-ROS (Kros)**

Proto-oncogene tyrosine-protein kinase c-ROS (KROS) is one of the last orphan receptors, as of yet its ligand has not been identified. As a potential substrate of LIMK it is interesting, LIMK has been shown to be upregulated in a variety of cancers and c-ROS has been found ectopically expressed in malignant gliomas, suggesting that over expression of c-ROS may be tumorigenic (Jun et al, 2009). Chromosomal rearrangements that result in c-ROS fusion kinases have also been identified in sarcomas, glioblastoma multiforme (GBM), and non-small cell lung cancers (Acquaviva et al, 2009).

An *in vitro* kinase assay was performed to establish whether LIMK1 could phosphorylate a peptide corresponding to the region of c-ROS identified as a putative site of phosphorylation by LIMK1. The generated c-ROS peptide was not found to be phosphorylated by LIMK1 *in vitro*, despite being a target when mounted on glass, and was therefore eliminated as a potential new substrate of LIMK1 (Figure 6.6.3).

### **6.3.2 Fibrinogen alpha chain (FIBA)**

Fibrinogen alpha chain is a blood-borne glycoprotein composed of three pairs of non identical polypeptide chains. Fibrinogen is cleaved by thrombin to form fibrin which is the most abundant component of blood clots (Farrell et al, 1992). The various cleavage products of fibrinogen and fibrin are also believed to regulate cell adhesion and spreading, display vasoconstrictor and chemotactic activities, and are mitogens for several cell types (Entrez Gene <http://www.ncbi.nlm.nih.gov/sites/entrez?Db=gene&Cmd=ShowDetailView&TermToSearch=2243>).

An *in vitro* kinase assay was performed to establish whether LIMK1 could phosphorylate a peptide corresponding to the region of Fibrinogen identified as a putative site of phosphorylation by LIMK1. The generated Fibrinogen peptide was not found to be phosphorylated by LIMK1 *in vitro*, despite being a target when mounted on glass, and so was also eliminated as a potential new substrate of LIMK1 (Figure 6.6.4).

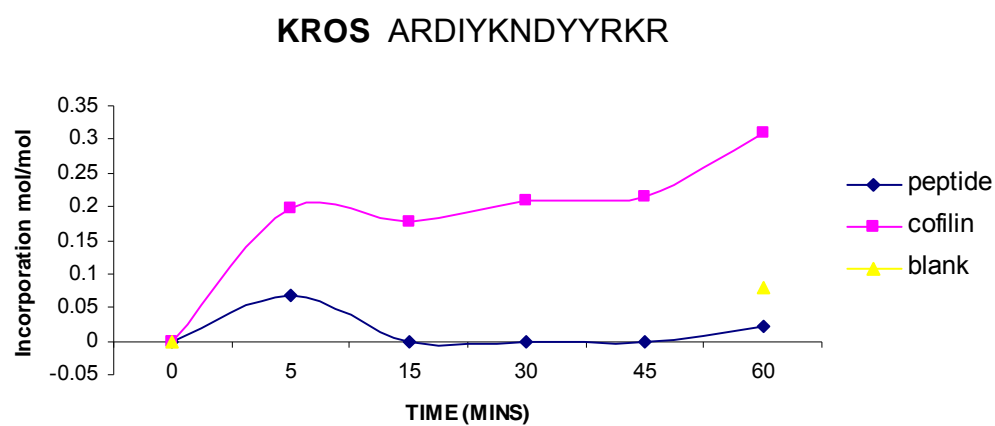


**Figure 6.6.3- c-ROS peptide is not phosphorylated by LIMK1 *in vitro*.**

Under these *in vitro* kinase conditions c-ROS peptide ARDIYKNDYYRKR is not a substrate of LIMK1.

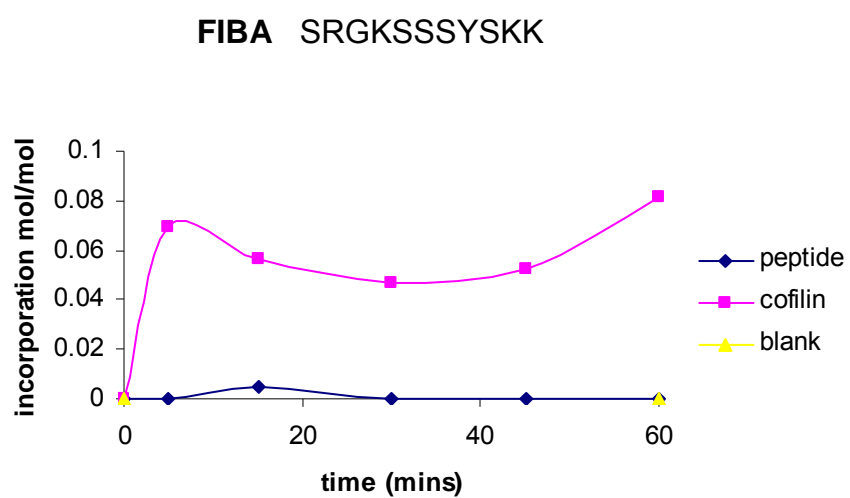


**Figure 6.6.4- Fibrinogen alpha chain peptide is not phosphorylated by LIMK1 *in vitro*.**  
Under these conditions FIBA peptide SRGKSSSYSKK is not a substrate of LIMK1.

### **6.3.3 Lysozyme C**

Lysozymes have a bacteriolytic function in the body and Lysozyme C is capable of both hydrolysis and transglycosylation (Masschalck & Michiels, 2003). It is found in tissues and body fluids, such as in ocular secretions, and is associated with the monocyte-macrophage system and enhancement of the activity of immunoagents in the body (Uniprot <http://www.uniprot.org/uniprot/P00698>).

An *in vitro* kinase assay was performed to establish whether LIMK1 could phosphorylate a peptide corresponding to the region of Lysozyme C identified as a putative site of phosphorylation by LIMK1. The generated Lysozyme C peptide was not found to be phosphorylated by LIMK1 *in vitro*, despite being a target when mounted on glass, and was therefore eliminated as a potential new substrate of LIMK1 Figure 6.6.5.

### **6.3.4 Glutamate Receptor 2 (GLR2)**

Glutamate receptors are transmembrane receptors located on the membranes of neuronal cells, these receptors bind the neurotransmitter glutamate, the most prominent neurotransmitter in the body. GLR2 is a metabotropic glutamate receptor, part of a family of G protein-coupled receptors Entrez Gene <http://www.ncbi.nlm.nih.gov/sites/entrez?Db=gene&Cmd=ShowDetailView&TermToSearch=2912>).

An *in vitro* kinase assay was performed to establish whether LIMK1 could phosphorylate a peptide corresponding to the region of Glutamate receptor 2 identified as a putative site of phosphorylation by LIMK1. The generated GLR2 peptide was not found to be phosphorylated by LIMK1 *in vitro*, despite being a target when mounted on glass, and was therefore eliminated as a potential new substrate of LIMK1 (Figure 6.6.).

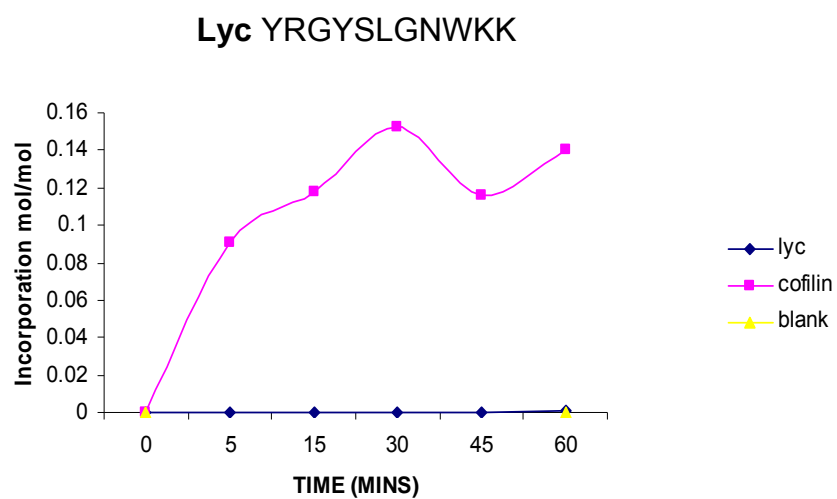


**Figure 6.6.5- LYC does not appear to be phosphorylated by LIMK1.**  
Under these conditions LYC peptide YRGYSLGNWKK is not a substrate of LIMK1.

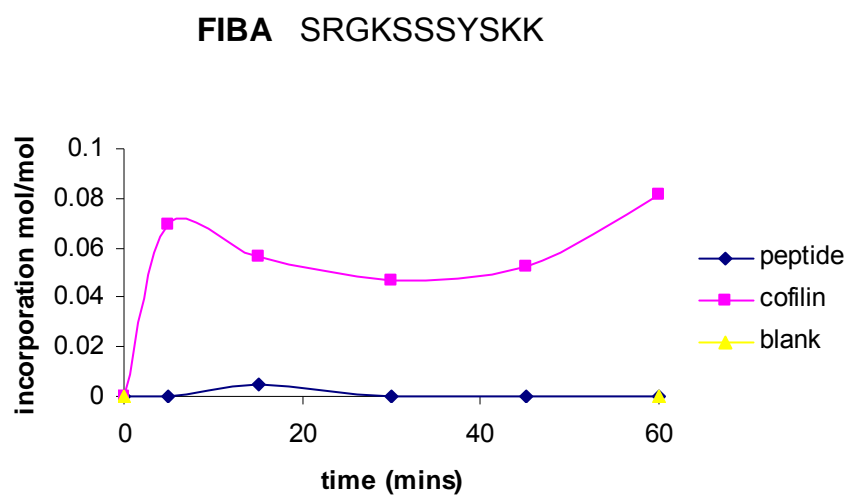


**Figure 6.6.6- GLR2 does not appear to be phosphorylated by LIMK1.**  
Under these conditions GLR2 SRGKSSYSKK is not a substrate of LIMK1.

### **6.3.5 LIMK1 does not phosphorylate peptides *in vitro***

LIMK does not appear to phosphorylate any of the previously identified peptide substrates in *in vitro* kinase assays. To establish whether the technique of identifying novel LIMK substrates using peptides was a valid approach experiments to phosphorylate peptides *in vitro* from the known LIMK1 substrate were performed, peptides were also phosphorylated in the presence of truncated Cofilin. It was hypothesised that peptides were unable to interact with LIMK1 sufficiently to facilitate phosphorylation, the proposed mechanism by which truncated Cofilin might enable peptides to be phosphorylated by LIMK is outlined in Figure 6.6.7 and the results of these experiment combined in Figure 6.6.8. Cofilin peptide containing the known site of phosphorylation by LIMK1 was not phosphorylated *in vitro* by LIMK (lanes 11 and 16 of Figure 6.6.8). Cofilin peptide was not phosphorylated in the presence of truncated Cofilin either, thus disproving the hypothesis outlined in Figure 6.6.7.

LIMK did not phosphorylate peptides *in vitro* in the conditions used, and thus this was not a suitable approach for the identification of novel substrates. The glass mounted peptide arrays may have returned many false positive results due to the orientation or charge of the peptides on glass, and it has now been suggested that cellulose mounted peptide arrays are more suitable.

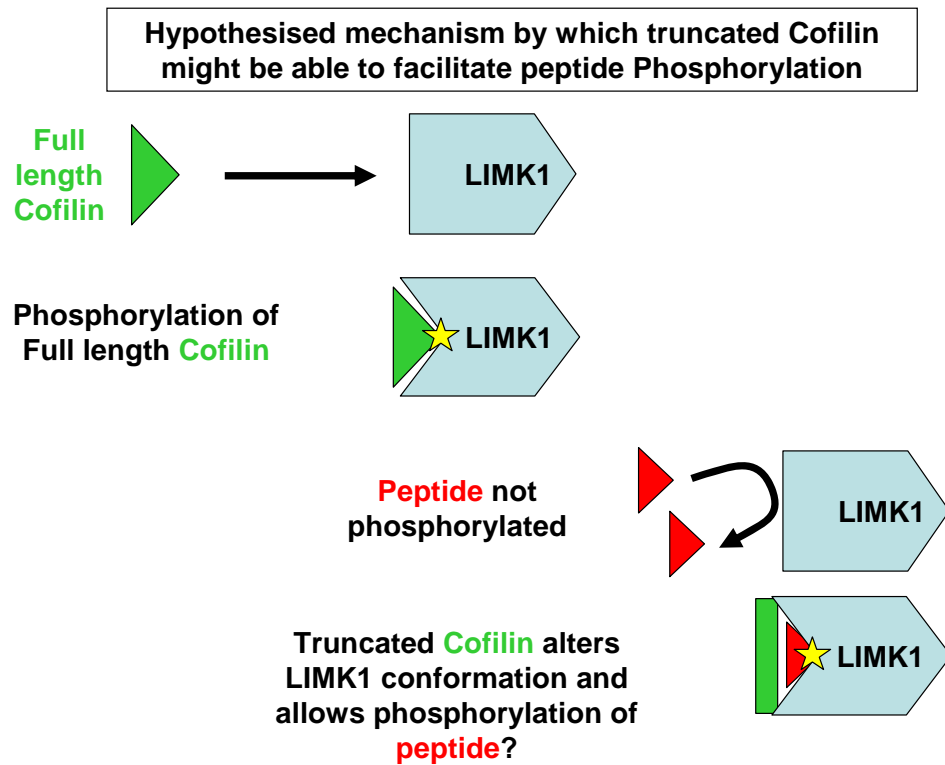


**Figure 6.6.7- Hypothesised mechanism by which peptides may be phosphorylated by LIMK1.**

Truncated Cofilin could facilitate phosphorylation of peptide substrates, if the peptides are unable to interact appropriately with LIMK1 to facilitate phosphorylation.



## 6.4 Kestrel approach to novel substrate identification.

In order to identify novel substrates of LIMK a collaboration with Axel Knebel was formed to perform a Kestrel screen (Kinase substrate tracking and elucidation) with the aim of validating any potential substrates *in vitro* at the Beatson. Kestrel screening takes large quantities of active purified kinase (in this case LIM Kinase1) and incubates them with cell extracts in the presence of ATP of a high specificity. This approach is different to previous ones as the extracts are first been depleted of ATP and other nucleotides by gel filtration, and subject to ion-exchange chromatography to separate endogenous substrates from their kinases before the reaction takes place (Cohen & Knebel, 2006).

For this collaboration with Kinasource, rat brain and skeletal muscle extracts were prepared, desalted and chromatographed on heparin sepharose. 30 column fractions were diluted in kinase buffer with LIMK and the fractions run out on gels, an example gel showing the potential LIMK substrates is shown in Figure 6.6.9. EF1a2, Creatine kinase M chain, GAPDH, Phosphoglycerate mutase 2 (PGM2) and Cofilin were all identified in this screen.

Work to validate these novel substrates was limited to Ef1a2.

### 6.4.1 Ef1a2

EF1 $\alpha$  proteins bind guanine nucleotides and in the GTP-liganded form can interact with amino acyl-tRNA to direct its association with mRNA codons and ribosomes (Gareth & Christopher, 2002). Elongation Factor 1a2 is the second of two isoforms of the eukaryotic elongation factor 1 alpha protein (eEF1 $\alpha$ ). The two isoforms share greater than 90% identity but although Ef1a1 is ubiquitously expressed, Ef1a2 is only expressed in the heart, brain and skeletal muscle (Sanne et al, 1993).

An *in vitro* kinase assay was performed to establish whether LIMK1 could phosphorylate recombinant Ef1a2, identified as a putative substrate of LIMK1 by Kestrel analysis performed by Axel Knebel. The  $\gamma$ 32p kinase assay was performed as described in the Methods section, BSA added to a duplicate set of reactions to

reduce the likelihood of Ef1 $\alpha$ 2 sticking to the reaction tubes, and all reactions stopped with 6x loading buffer. The reactions were run out by SDS PAGE and the gel stained for protein with 'Safestain'. The gel was exposed and imaged using a phosphoimager. Control reactions were successfully phosphorylated but Ef1 $\alpha$ 2 was not found to be phosphorylated by LIMK1 *in vitro* under these conditions, and so Ef1 $\alpha$ 2 could not be confirmed as a new substrate of LIMK1 (Figure 6.6.10).

## 6.5 Conclusions and Discussion

Identification of novel substrates of LIMK by peptide array proved fruitless as LIMK did not phosphorylate peptides *in vitro*, not even peptides of validated substrates and phosphorylation sites.

Kestrel screening for potential novel substrates of LIMK identified EF1 $\alpha$ 2, Creatine kinase M chain, GAPDH, and Phosphoglycerate mutase 2 (PGM2), although only EF1 $\alpha$ 2 was subject to further investigation. Although it was not phosphorylated as a recombinant protein *in vitro*, EF1 $\alpha$ 2 appeared to be phosphorylated by LIMK in cell extracts, perhaps the recombinant protein was incorrectly folded and did not provide the appropriate site for phosphorylation. It is also a possibility that the bands extracted from gels to identify EF1 $\alpha$ 2 as a substrate of LIMK harboured a less abundant protein substrate that was masked by the more abundant Ef1 $\alpha$  2. However, EF1 $\alpha$ 2 is a good potential candidate as a LIMK substrate as Ef1 $\alpha$  has been found to co-localise with F-actin, and its cellular localisation has been found to correlate with changes in the actin cytoskeleton during chemotaxis. Ef1 $\alpha$ 1 and Ef1 $\alpha$ 2 have both been implicated in cell transformation (Tatsuka M, 1992 ) and linked to ovarian cancer (Lee, 2003), and it is also over-expressed at the mRNA level in metastatic rat mammary adenocarcinoma (Edmonds et al, 1996). Before Ef1 $\alpha$ 2 can be confirmed to be a substrate of LIMK further work to confirm phosphorylation in cells needs to be performed. Since in the conditions tested LIMK did not phosphorylate *in vitro* perhaps there were cofactors missing for the facilitation of phosphorylation. If Ef1 $\alpha$ 2 could be immunoprecipitated from cells, perhaps it would co-IP other proteins it is complexed with in the cell, potentially leading to successful *in vitro* phosphorylation of the protein and identification of a novel substrate.

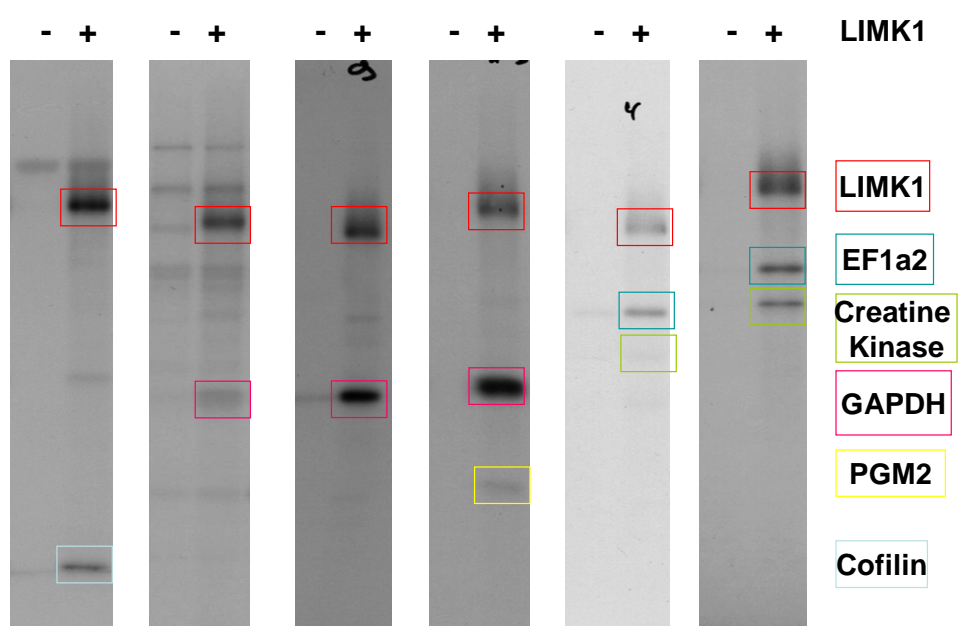


**Figure 6.6.9- Kestrel screening for novel substrates.**

Four possible new LIMK1 substrates were identified through kestrel screening, outlined in colour are; EF1a2, Creatine kinase M chain, GAPDH, and Phosphoglycerate mutase 2 (PGM2). Cofilin, the only confirmed substrate of LIMK, was also identified during the screening process.

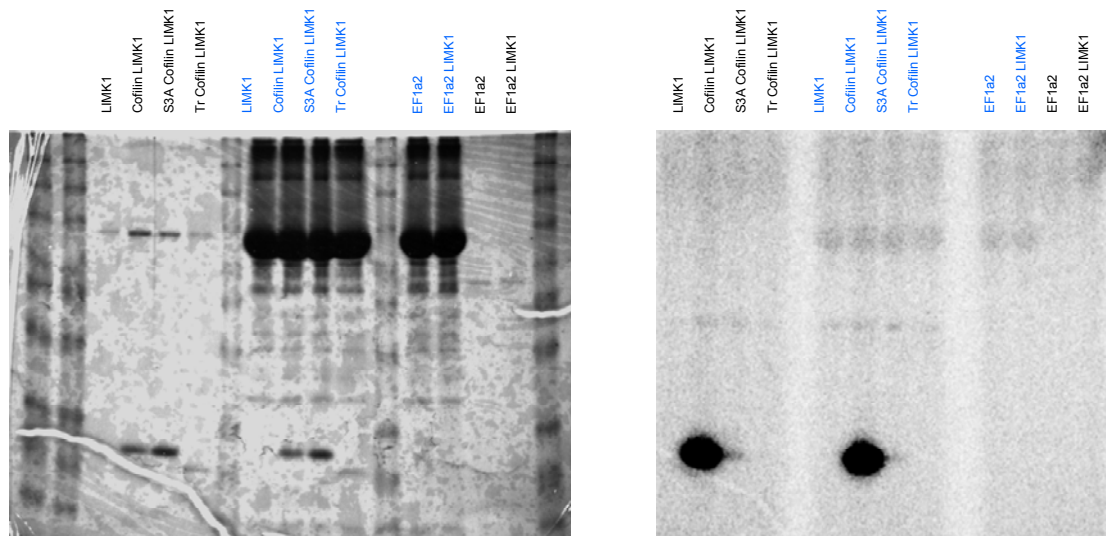


**Figure 6.6.10-Ef1a2 kinase assay.**

A. Safestained gel of kinase assay. Control lanes contain kinase reaction mix and LIMK alone, Cofilin, S3A Cofilin and trCofilin, with or without BSA. Lanes 8-11,13 and 14 have added BSA. B. Phosphoimager analysis of gel shown in part A. Ef1a2 was not phosphorylated by LIMK1 under these conditions, with or without BSA. Control reactions using Cofilin as a substrate were successfully phosphorylated.

## 7 Discussion

### 7.1 Chapter Summary

This thesis details experiments undertaken with the aim of understanding the role LIM Kinases play in cell motility and invasion. In Chapter 3 I provide evidence that LIMK1 and LIMK2 are requirements for cancer cell invasion, and that altering the actin cytoskeleton by up or down regulation of LIMK is sufficient to reduce invasion. The results in Chapter 4 describe a role for LIMK in invadopodia formation and matrix degradation, and a novel role for LIMK in the leading cells of collective invasion. Chapter 5 outlines the role of Cofilin in disseminating LIMK signalling in invasion and the results in Chapter 6 outline attempts made to identify novel substrates of LIMK. The data presented in this thesis and their relevance to previous literature and future work are discussed in this chapter.

### 7.2 Requirement for LIMK in cell motility and Invasion

Individual cell invasion has been classified into two forms, either mesenchymal or amoeboid. Mesenchymal invasion is characterised by the proteolytic degradation of ECM by morphologically elongated cells, followed by force generation by actin polymerisation to push the cell through the remodelled matrix (Croft & Olson, 2008). During amoeboid invasion, cells adopt a rounded morphology and use the force of actin-myosin contraction to physically deform the ECM and push through the 3D environment (Croft & Olson, 2008). The mode of motility used by a cell probably depends on environmental factors, cells may respond to cues from the micro-environment in order to use the most appropriate mode of motility suitable for the environment challenges they are subjected to. Both of these forms of motility have been observed *in vivo* in invading tumour cells (Wyckoff et al, 2006), and tumour cells can switch between rounded and elongated modes of movement (Sidani et al, 2007), indicating that they retain all the activities necessary for either mode of invasion (Croft & Olson, 2008). However, how the activity of LIMK1 or LIMK2 regulates the mechanisms that contribute to cell invasion had not been previously characterized prior to this investigation.

### 7.3 Role for LIMK in motility and invasion

As investigations into LIMK in cancer cell motility and invasion commenced it was not known whether both LIM Kinase 1 and 2 were requirements of cancer cell motility, or whether there were any compensation between the two kinases. As detailed in the introduction, LIMK1 has been found to be overexpressed in malignant melanoma cells (Okamoto et al, 2005), breast cancer tumours and tumour cell lines (Bagheri-Yarmand et al, 2006) (Yoshioka et al, 2003), in prostate tumours and tumour cell lines (Davila et al, 2003; Yoshioka et al, 2003) and up-regulated in invasive carcinoma cells in comparison with non-invasive cells within primary mammary tumours (Wang et al, 2004). Data presented in Chapter 3 shows that both LIMK1 and LIMK2 were necessary for 2D cell motility in wound healing assays for BE and BT549 cell lines, but not for the invasive cell line MDAMB231. The lack of effect seen on 2D motility following LIMK knockdown could have been because this form of migration relies on actin polymerization and leading edge protrusions to propel the cell forward (DesMarais et al, 2002). Reducing cellular levels of LIMK would have led to more active Cofilin, resulting in F-actin severing and an increase in the number of barbed ends available for filament extension and leading edge propulsion, which would not negatively affect motility that was the result of actin polymerisation.

When active, LIM kinases phosphorylate and inactivate Cofilin proteins, thereby reducing filamentous-actin (F-actin) severing leading to F-actin stabilization. Although a reduction in cytoskeletal F-actin was observed in both 2D and 3D following LIMK inhibition, cell morphology in 2D was more affected by LIMK1&2 knockdown when cells were plated on the fibroblast-derived matrix than they had been on plastic. Cells were more rounded and refractile in appearance in general with shortening of polarized extensions, however tracks of individual cell movement did not appear to greatly differ from non-targeting siRNA transfected cells. Analysis of multiple experiments revealed that the vectorial and accumulated distances were no different between NT or LIMK1&2 siRNA transfected cells. Persistence of movement, which is a directional ratio of vectorial over accumulated distances, also did not differ between treatments. These results indicate that the directionality and velocity of cell motility was driven by intrinsic properties of the cell that were as unaffected on fibroblast-

derived oriented matrices (CDM) by LIMK inhibition as the wound-healing induced MDAMB231 motility on plastic.

LIMK1 and LIMK2 were both found to be requirements for MDAMB231 invasion in 3D. Consistent with these findings, interfering with LIMK function by anti-sense mediated knockdown of LIMK1 in metastatic prostate cancer cells (Davila et al, 2003) or metastatic mammary carcinoma cells (Mouneimne et al, 2006), by overexpression of a dominant negative form of LIMK1 in metastatic breast cancer cells (Yoshioka et al, 2003) or by ribozyme-mediated knockdown of LIMK2 in metastatic fibrosarcoma cells (Suyama et al, 2004) inhibited chemotaxis and invasiveness/metastasis. Reduction of both LIMK1 and LIMK2 by siRNA did not have an additive effect on the reduction of MDAMB231 cell invasion in the data presented in Chapter 3, as might have been expected. This may have been because the effectiveness of the double knockdown by siRNA was reduced compared to the individual knockdowns because there was half the siRNA used against each individual LIMK in the double knockdown compared to individual conditions to retain consistent levels of siRNA between conditions. The data presented show that both LIMK1 and 2 are important for invasion, and are consistent with the hypothesis that LIMK inhibition would effectively reduce cancer metastasis and support LIMK as a potential anti-metastatic drug target.

### ***7.3.1 LIMK levels important for invasion***

It was hypothesised that LIMK could be a driver of cell motility and invasion. Results presented in chapter 3 reveal LIMK as a requirement of cell invasion, and it has been found over expressed in a variety of cancer cell lines and tumours detailed above (Bagheri-Yarmand et al, 2006; Davila et al, 2003; Okamoto et al, 2005; Yoshioka et al, 2003). Over expression of LIMK1, LIMK2 or both LIMK was expected to increase invasion of MDAMB231 cells in 3D in line with observations in metastatic models (Bagheri-Yarmand et al, 2006). However, increased levels of either or both kinases reduced invasion to a similar degree as observed upon knockdown of LIMK. This is consistent with a report that over expression of LIMK1 kinase domain reduced cell motility (Zebda et al, 2000), and suggests that the “correct” level of LIMK activity is required for cells to move and invade

effectively. This likely reflects the activity status of the principle substrate of LIMK, Cofilin.

### **7.3.2 Cofilin regulation**

Spatially and temporally-regulated cycles of Cofilin inactivation and activation, regulated principally by phosphorylation mediated by LIMK and dephosphorylation mediated by phosphatases such as SSH1-3 and cofilin, initiate dynamic alterations to the actin cytoskeleton (Van Troys et al, 2008). Cofilin activity is related inversely to LIMK activity, Cofilin is phosphorylated by LIMK and rendered inactive. LIMK inhibition lead to a reduction in F-actin structures and a corresponding reduction in invasion in chapters 3 and 4, and disruption of the Cofilin:phosphoCofilin balance was shown in chapter 5 to be sufficient to affect cell invasion. Increasing the levels of active to inactive Cofilin inhibited three dimensional collective invasion, suggesting that the role of LIMK in cell invasion is mediated by Cofilin phosphorylation status. This fits in well with the current understanding of the role Cofilin plays in invasion, that LIMK-mediated increases and decreases in Cofilin activity relate directly to invasiveness (Sidani et al, 2007; Wang et al, 2006). Although LIMK plays an important role in regulating Cofilin activity, additional factors have been found to influence Cofilin activity such as; pH (Frantz et al, 2008), PIP2 release (Leyman et al, 2009; van Rheenen et al, 2007) and oxidation (Klemke et al, 2008). Therefore, although LIMK is the primary regulator of Cofilin activity, these additional factors may modulate the effects on invasion.

### **7.3.3 LIMK inhibition impairs matrix degradation**

Since LIMK inhibition significantly reduced invasion into a three-dimensional matrix without affecting cell motility in chapter 3, one possible explanation was that the processes required for 3D path generation were affected. Collective invasion requires proteolytic remodelling of ECM for leading cells to initiate path generation. In Chapter 4, 3D invasion assays of RFP-labelled MDA MB 231 cells through DQ collagen cells were used to visualise proteolytic activity in 3D. Cells transfected with non-targeting siRNA were associated with fluorescence (collagenase activity) both directly adjacent and further afield from the cells,

possibly activity left by motile cells or cells outside of the focal plane. In contrast, cells transfected with both LIMK1&2 siRNA had lower levels of fluorescence, both distal and proximal to the cells, indicating reduced proteolytic activity. Similarly, in the quantifiable 2D gelatin degradation system, and consistent with previous reports (Lizarraga et al, 2009), MDA MB 231 cells had large numbers of actin-rich projections into the gelatin matrix. These were identified as discrete dark foci, and are dependent on the membrane-associated MT1-MMP (Stylli et al, 2008). Knockdown of LIMK1&2 resulted in significantly reduced area of gelatin degradation per cell, similarly, LIMKi treatment at 3 or 10  $\mu$ M significantly lowered the area of gelatin degradation. The requirement for MT1-MMP in invadopodia (Artym et al, 2006; Poincloux et al, 2009) likely reflects direct proteolytic actions on the ECM, but also the secretion and/or activation of soluble proteases such as MMP 9 (Dreier et al, 2004; Itoh & Seiki, 2004). Knockdown of LIMK1&2 decreased cofilin phosphorylation without affecting MT1-MMP expression. However, LIMK1&2 knockdown reduced the secreted gelatin-degradation activity almost to the background levels observed in concentrated cell-free serum-containing media. The molecular weight of the gelatin-degrading activity was 86 kDa, consistent with the mobility of activated MMP 9 (Curran & Murray, 2000; Lindenmeyer et al, 1997). Despite the lower activity of this MMP 9-like protein, RT-PCR analysis revealed that LIMK1&2 knockdown did not significantly reduce MMP 9 expression.

MT1-MMP was shown to be the membrane bound protease necessary for invasion through matrix (Sabeh et al, 2004) and actin skeleton integrity has been found to be important for MMP2 and MT1-MMP activity in fibroblasts (Tomasek et al, 1997). Actin skeleton disruption has been shown to reduce MMP activity in trabecular meshwork (TM) cells (Sanka et al, 2007) and microtubules play a role in MMP2/MMP9 secretion during human melanoma cell invasion (Schnaeker et al, 2004), highlighting the relationship between MMP activity and the cytoskeleton. The results of Chapter 4 reveal that LIMK inhibition significantly affected ECM degradation in 3-D and 2-D contexts, this could be by inhibiting the formation of stable F-actin structures required to focalize MT1-MMP activity to areas of matrix degradation and MMP secretion. The link between MMP secretion and both actin cytoskeletal and tubulin structures could be mediated through LIMK, as LIMK is also now known to regulate p25/TPPP tubulin polymerisation

activity (Acevedo et al, 2007). LIMK activity could be important in regulation of the cytoskeleton during the processes to recruit MT1-MMP to sites of degradation, and future work could be performed to examine the role LIMK plays in the dynamic actin structures at points of matrix degradation (Baldassarre et al, 2006).

It has been recently suggested that LIMK1 increases expression levels of the serine protease urokinase type plasminogen activator (uPA) and its receptor, thought to be involved in metastasis (Bagheri-Yarmand et al, 2006). LIMK1 overexpression was found to increase tumor growth in female athymic nude mice, tumor angiogenesis and metastasis to livers and lungs, and this was associated with increasing uPA expression in the tumors (Bagheri-Yarmand et al, 2006). MMPs are also thought to interact with the urokinase-type plasminogen activator (uPA)-plasmin system, MT1-MMP is proteolytically activated by plasmin by means of cleavage between its pro- and catalytic domains, the region associated with pro-MMP-2 activation (Curran & Murray, 2000; Okumura et al, 1997). These findings suggest a regulatory connection between LIMK1 and the uPA system and MMP activity during invasion, a second line of potential future investigation.

## **7.4 LIMK is required in leading path-generating cells for collective invasion**

The inability of cells to remodel ECM by proteolysis, without affecting 2-D motility, following LIMK inhibition suggests that down regulation of LIMK affects path generation in collective invasion to a greater extent than path following. The invasion of MDA MB 231 cells into 3-D matrigel appeared to be via collective strands in chapter 3 and 4, as previously reported (Wolf et al, 2007). Since MDA MB 231 cells are capable of providing the path generating activity required in leading cells during collective invasion, in chapter 4 cells were labeled with either green or red fluorescent proteins and one colour pool subject to knockdown of LIMK1&2 or treatment with NT siRNA. Knockdown of LIMK in red cells reduced the number of cells leading invasion from roughly 50% to < 20%, but these cells were still able to follow green invasive cells into the matrix. LIMK inhibition was shown in Chapter 4 to reduce extracellular MMP activity, an

important cellular function for cells leading collective invasion (Friedl & Wolf, 2008; Wolf et al, 2007). These results indicate that LIMK activity is required for path generation by leading cells in collective invasion, but not for ‘following’. This would agree with previous work presented in this thesis suggesting LIMK was not required for 2D cell motility, or motility through a preformed path such as the holes in a transwell filter used in invasion assays.

## 7.5 Investigations into novel substrates of LIMK

Recent investigations have identified novel substrates of LIMK in the form of nuclear transcription factors CREB (Yang et al, 2004a) and Nurr1 (Sacchetti et al, 2006) and the microtubule bundling protein p25/TPPP (Acevedo et al, 2007). Peptide arrays mounted on glass in a microarray format were used in chapter 6 when trying to identify further novel substrates of LIMK. It was found that LIMK did not phosphorylate peptides *in vitro*, from which it could be concluded that the potential substrates identified in such screens were false positives. Shortly after this line of investigation was underway a Nature Protocols paper cast doubt over the use of glass mounted peptide arrays in the identification of novel substrates of kinases known to have few dedicated substrates (Turk et al, 2006). The technique required LIM kinase to be very efficient in substrate phosphorylation, and assumed that it did not require interaction with parts of the protein outside of the active site to facilitate phosphorylation. Data presented in chapter 6 would suggest that LIMK requires interaction with other parts of its substrates to facilitate phosphorylation (as is the case for eIF-2 $\alpha$  kinases and MAP kinase kinases (Turk et al, 2006)), and since *in vitro* phosphorylation of full length Cofilin, but not a peptide of the Cofilin phosphorylation site, was possible.

Kestrel (Kinase substrate tracking and elucidation) screening for novel LIMK substrates did not rely on the use of peptides, this technique screened for LIMK phosphorylation of endogenous proteins in cell extract fractions. Only one substrate from this screen was investigated further, and there is still the possibility that within the potential substrates identified in chapter 6 there are genuine cellular substrates. Although Ef1 $\alpha$ 2 was not confirmed as a substrate by further *in vitro* testing, it could still be a substrate but the conditions for

phosphorylation were not optimal for that particular protein. Identifying novel substrates of LIMK using full length proteins extracted from cells could yield success in the future if further investigation of the putative substrates identified by Kestrel is carried out. It is also possible that low abundance substrates were masked by similarly sized high abundance proteins in the gel. Potential solutions to which could be the use of 2-D gels to separate out similarly sized proteins, or further purification or fractionation before phosphorylation.

## 7.6 Final conclusions

When this project was first undertaken it had been suggested that LIMK was important in cancer invasion and thought that either LIMK1 or LIMK2 might make a suitable anti-metastatic drug target (Davila 2008, Suyama 2004, Davila 2003, Yoshioka 2003). However, that either LIMK1 or LIMK2 played a role in invasion had not been studied in a comparative manner to elucidate how LIMK regulates invasion, nor whether pharmacological inhibition of LIMK was a valid anti-metastatic approach. This thesis presents data to suggest that targeting either LIM kinase, or both in combination, would be a suitable anti-invasive therapy. Previous work considered invasion as one activity, but in this body of work cell invasion was considered as two separate functions, cell motility or proteolysis and deformation, and investigated as separate cell activities and leading to the elucidation of how LIMK regulates invasion. LIMK is not required in 2D cell motility but is a requirement for both proteolysis and deformation, leading to a novel understanding of the role LIMK plays in collective invasion. LIMK is required in leading, path generating cells of collective invasion, and not cells 'following' in collective invasion (see Figure 7.1). The path generating cells need not necessarily be cancer cells and as such we now understand that LIMK inhibitors would not be targeting the cancer cells in a tumour but would be anti-invasive by targeting cells leading invasion, whether they be tumour or stromal.

There is currently debate over the usefulness of developing anti-metastatic therapeutics, some would argue that using such drugs would often be like "shutting the door after the horse has bolted". This attitude has left industry reluctant to invest in such areas of drug development. However, there are obvious avenues for anti-metastatic drug use. Cancers that are well screened

and often caught at early stages, such as cervical or prostate cancers, could benefit from the use of adjuvant anti-metastatic drug use alongside current treatments. In instances where cancers are caught early following metastatic events, anti-metastatic drugs could be used to limit cell invasion and motility at sites of micro-metastasis, preventing cancer cells from spreading out with the immediate metastatic microenvironment. Anti-metastatics are also no doubt of great interest to those researching glioma, the prognosis for which is currently very poor and is characterised by localised invasion which does significant damage to the brain, also often breaking down the blood brain barrier. The potential benefits of anti-metastatic therapies should not be dismissed at this early stage in understanding the mechanisms of metastasis.

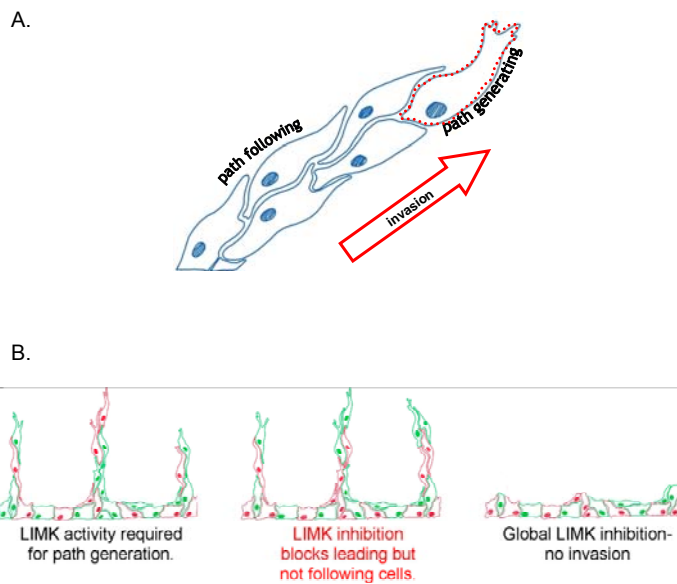


### Figure 7.1 Novel understanding of LIMK Role in cell invasion

A. Cell invasion requires 2 activities, Cell motility – LIMK not required, and matrix remodelling – LIMK required for both proteolysis and deformation. B. LIMK is required for path generation by leading cells in collective invasion (illustrated in the model above as the cell outlined in red), the red cell requires LIMK to degrade and deform its environment in order to lead collective invasion of the other cells (green).

## 8 References

- Acevedo K, Li R, Soo P, Suryadinata R, Sarcevic B, Valova VA, Graham ME, Robinson PJ, Bernard O (2007) The phosphorylation of p25/TPPP by LIM kinase 1 inhibits its ability to assemble microtubules. *Experimental Cell Research* 313(20): 4091-4106
- Acevedo K, Moussi N, Li R, Soo P, Bernard O (2006) LIM Kinase 2 Is Widely Expressed in All Tissues. *J Histochem Cytochem* 54(5): 487-501
- Acquaviva J, Wong R, Charest A (2009) The multifaceted roles of the receptor tyrosine kinase ROS in development and cancer. *Biochimica et Biophysica Acta (BBA) - Reviews on Cancer* 1795(1): 37-52
- Agnew BJ, Minamide LS, Bamburg JR (1995) Reactivation of phosphorylated actin depolymerizing factor and identification of the regulatory site. *J Biol Chem* 270(29): 17582-17587
- Aizawa H, Wakatsuki S, Ishii A, Moriyama K, Sasaki Y, Ohashi K, Sekine-Aizawa Y, Sehara-Fujisawa A, Mizuno K, Goshima Y, Yahara I (2001) Phosphorylation of cofilin by LIM-kinase is necessary for semaphorin 3A- induced growth cone collapse. *Nat Neurosci* 4(4): 367-373.
- Akagawa H, Tajima A, Sakamoto Y, Krischek B, Yoneyama T, Kasuya H, Onda H, Hori T, Kubota M, Machida T, Saeki N, Hata A, Hashiguchi K, Kimura E, Kim CJ, Yang TK, Lee JY, Kimm K, Inoue I (2006) A haplotype spanning two genes, ELN and LIMK1, decreases their transcripts and confers susceptibility to intracranial aneurysms. *Hum Mol Genet* 15(10): 1722-1734
- Amanda Gatesman A, Scott AW (2008) Cortactin branches out: Roles in regulating protrusive actin dynamics. *Cell Motility and the Cytoskeleton* 65(9): 687-707
- Amano T, Kaji N, Ohashi K, Mizuno K (2002) Mitosis-specific activation of LIM motif-containing protein kinase and roles of cofilin phosphorylation and dephosphorylation in mitosis. *J Biol Chem* 277(24): 22093-22102
- Amano T, Tanabe K, Eto T, Narumiya S, Mizuno K (2001) LIM-kinase 2 induces formation of stress fibres, focal adhesions and membrane blebs, dependent on its activation by Rho-associated kinase- catalysed phosphorylation at threonine-505. *Biochem J* 354(Pt 1): 149-159.
- Antonietta RF, Anna C, Antonella T, Antonella T, Alessandra T, Gulia C, Alberto G, Andrew RM (1998) Transforming growth factor- $\beta$ 1 enhances the invasiveness of human MDA-MB-231 breast cancer cells by up-regulating urokinase activity. *International Journal of Cancer* 75(5): 721-730
- Arber S, Barbayannis FA, Hanser H, Schneider C, Stanyon CA, Bernard O, Caroni P (1998) Regulation of actin dynamics through phosphorylation of cofilin by LIM-kinase. *Nature* 393(6687): 805-809.

- Artym VV, Zhang Y, Seillier-Moiseiwitsch F, Yamada KM, Mueller SC (2006) Dynamic Interactions of Cortactin and Membrane Type 1 Matrix Metalloproteinase at Invadopodia: Defining the Stages of Invadopodia Formation and Function. *Cancer Res* 66(6): 3034-3043
- Bagheri-Yarmand R, Mazumdar A, Sahin AA, Kumar R (2006) LIM kinase 1 increases tumor metastasis of human breast cancer cells via regulation of the urokinase-type plasminogen activator system. *Int J Cancer* 118(11): 2703-2710
- Baldassarre M, Ayala I, Beznoussenko G, Giacchetti G, Machesky LM, Luini A, Buccione R (2006) Actin dynamics at sites of extracellular matrix degradation. *European Journal of Cell Biology* 85(12): 1217-1231
- Bamburg JR (1999) Proteins of the ADF/cofilin family: essential regulators of actin dynamics. *Annu Rev Cell Dev Biol* 15: 185-230
- Bernard O, Ganiatsas S, Kannourakis G, Dringen R (1994) Kiz-1, a protein with LIM zinc finger and kinase domains, is expressed mainly in neurons. *Cell Growth Differ* 5(11): 1159-1171
- Besson A, Assoian RK, Roberts JM (2004) Regulation of the cytoskeleton: an oncogenic function for CDK inhibitors? *Nat Rev Cancer* 4(12): 948-955
- Brooks PC, Stromblad S, Sanders LC, von Schalscha TL, Aimes RT, Stetler-Stevenson WG, Quigley JP, Cheresch DA (1996) Localization of matrix metalloproteinase MMP-2 to the surface of invasive cells by interaction with integrin alpha v beta 3. *Cell* 85(5): 683-693
- Canning MT, Postovit LM, Clarke SH, Graham CH (2001) Oxygen-Mediated Regulation of Gelatinase and Tissue Inhibitor of Metalloproteinases-1 Expression by Invasive Cells. *Experimental Cell Research* 267: 88-94
- Chen X, Macara IG (2005) Par-3 controls tight junction assembly through the Rac exchange factor Tiam1. *Nat Cell Biol* 7(3): 262-269
- Chen X, Macara IG (2006) Par-3 mediates the inhibition of LIM kinase 2 to regulate cofilin phosphorylation and tight junction assembly. *J Cell Biol* 172(5): 671-678
- Cheng AK, Robertson EJ (1995) The murine LIM-kinase gene (limk) encodes a novel serine threonine kinase expressed predominantly in trophoblast giant cells and the developing nervous system. *Mech Dev* 52(2-3): 187-197
- Cohen P, Knebel A (2006) KESTREL: a powerful method for identifying the physiological substrates of protein kinases. *Biochem J* 393(1): 1-6
- Coleman ML, Sahai EA, Yeo M, Bosch M, Dewar A, Olson MF (2001) Membrane blebbing during apoptosis results from caspase-mediated activation of ROCK I. *Nat Cell Biol* 3(4): 339-345.
- Cooper JA WS, Pollard TD. (1983) Pyrene actin: documentation of the validity of a sensitive assay for actin polymerization. *J Muscle Res Cell Motil* 4(2): 253-262

- Coopman PJ, Do MT, Thompson EW, Mueller SC (1998) Phagocytosis of cross-linked gelatin matrix by human breast carcinoma cells correlates with their invasive capacity. *Clin Cancer Res* 4(2): 507-515
- Corpet F (1988) Multiple sequence alignment with hierarchical clustering. *Nucleic Acids Res* 16(22): 10881-10890.
- Croft DR, Coleman ML, Li S, Robertson D, Sullivan T, Stewart CL, Olson MF (2005) Actin-myosin-based contraction is responsible for apoptotic nuclear disintegration. *J Cell Biol* 168(2): 245-255
- Croft DR, Olson MF (2006) The Rho GTPase effector ROCK regulates cyclin A, cyclin D1 and p27Kip1 levels by distinct mechanisms. *Mol Biol Cell* 26(12)
- Croft DR, Olson MF (2008) Regulating the conversion between rounded and elongated modes of cancer cell movement. *Cancer Cell* 14(5): 349-351
- Croft DR, Olson MF (2006) Conditional Regulation of a ROCK Estrogen Receptor Fusion Protein. In *Methods in Enzymology* Vol. Volume 406, pp 541-553. Academic Press
- Croft DR, Sahai E, Mavria G, Li S, Tsai J, Lee WMF, Marshall CJ, Olson MF (2004) Conditional ROCK Activation In vivo Induces Tumor Cell Dissemination and Angiogenesis. *Cancer Res* 64(24): 8994-9001
- Cukierman E, Pankov R, Stevens DR, Yamada KM (2001) Taking Cell-Matrix Adhesions to the Third Dimension. *Science* 294(5547): 1708-1712
- Curran S, Murray GI (2000) Matrix metalloproteinases: molecular aspects of their roles in tumour invasion and metastasis. *European Journal of Cancer* 36(13): 1621-1630
- Daisuke Y, Shusaku K, Tadaomi T (2005) Regulation of cancer cell motility through actin reorganization. *Cancer Science* 96(7): 379-386
- Dan C, Kelly A, Bernard O, Minden A (2001) Cytoskeletal changes regulated by the PAK4 serine/threonine kinase are mediated by LIM kinase 1 and cofilin. *J Biol Chem* 276(34): 32115-32121.
- Davila M, Frost AR, Grizzle WE, Chakrabarti R (2003) LIM Kinase 1 Is Essential for the Invasive Growth of Prostate Epithelial Cells: IMPLICATIONS IN PROSTATE CANCER. *J Biol Chem* 278(38): 36868-36875
- DesMarais V, Ichetovkin I, Condeelis J, Hitchcock-DeGregori SE (2002) Spatial regulation of actin dynamics: a tropomyosin-free, actin-rich compartment at the leading edge. *J Cell Sci* 115(23): 4649-4660
- Dreier R, Grassel S, Fuchs S, Schaumburger J, Bruckner P (2004) Pro-MMP-9 is a specific macrophage product and is activated by osteoarthritic chondrocytes via MMP-3 or a MT1-MMP/MMP-13 cascade. *Experimental Cell Research* 297(2): 303-312

- Edmonds BT, Wyckoff J, Yeung YG, Wang Y, Stanley ER, Jones J, Segall J, Condeelis J (1996) Elongation factor-1 alpha is an overexpressed actin binding protein in metastatic rat mammary adenocarcinoma. *J Cell Sci* 109(11): 2705-2714
- Edwards DC, Gill GN (1999) Structural features of LIM kinase that control effects on the actin cytoskeleton. *J Biol Chem* 274(16): 11352-11361.
- Edwards DC, Sanders LC, Bokoch GM, Gill GN (1999) Activation of LIM-kinase by Pak1 couples Rac/Cdc42 GTPase signalling to actin cytoskeletal dynamics. *Nat Cell Biol* 1(5): 253-259.
- Elbashir SM, Harborth J, Lendeckel W, Yalcin A, Weber K, Tuschl T (2001) Duplexes of 21-nucleotide RNAs mediate RNA interference in cultured mammalian cells. *Nature* 411(6836): 494-498
- Endo M, Ohashi K, Sasaki Y, Goshima Y, Niwa R, Uemura T, Mizuno K (2003) Control of growth cone motility and morphology by LIM kinase and Slingshot via phosphorylation and dephosphorylation of cofilin. *J Neurosci* 23(7): 2527-2537
- Farrell DH, Thiagarajan P, Chung DW, Davie EW (1992) Role of fibrinogen alpha and gamma chain sites in platelet aggregation. *Proc Natl Acad Sci U S A* 89(22): 10729-10732
- Foletta VC, Lim MA, Soosairajah J, Kelly AP, Stanley EG, Shannon M, He W, Das S, Massague J, Bernard O (2003) Direct signaling by the BMP type II receptor via the cytoskeletal regulator LIMK1. *J Cell Biol* 162(6): 1089-1098
- Foletta VC, Moussi N, Sarmiere PD, Bamburg JR, Bernard O (2004) LIM kinase 1, a key regulator of actin dynamics, is widely expressed in embryonic and adult tissues. *Experimental Cell Research* 294(2): 392-405
- Frantz C, Barreiro G, Dominguez L, Chen X, Eddy R, Condeelis J, Kelly MJ, Jacobson MP, Barber DL (2008) Cofilin is a pH sensor for actin free barbed end formation: role of phosphoinositide binding. *J Cell Biol* 183(5): 865-879
- Friedl P, Wolf K (2003) Tumour-cell invasion and migration: diversity and escape mechanisms. *Nat Rev Cancer* 3(5): 362-374
- Friedl P, Wolf K (2008) Tube Travel: The Role of Proteases in Individual and Collective Cancer Cell Invasion. *Cancer Res* 68(18): 7247-7249
- Gareth JB, Christopher GP (2002) Regulation of peptide-chain elongation in mammalian cells. *European Journal of Biochemistry* 269(22): 5360-5368
- Gavert N, Ben-Ze'ev A (2008) Epithelial-mesenchymal transition and the invasive potential of tumors. *Trends in Molecular Medicine* 14(5): 199-209
- Geneste O, Copeland JW, Treisman R (2002) LIM kinase and Diaphanous cooperate to regulate serum response factor and actin dynamics. *The Journal Of Cell Biology* 157(5): 831-838

- Ghosh M, Song X, Mouneimne G, Sidani M, Lawrence DS, Condeelis JS (2004) Cofilin Promotes Actin Polymerization and Defines the Direction of Cell Motility. *Science* 304(5671): 743-746
- Goyal P, Pandey D, Siess W (2006) Phosphorylation-dependent regulation of unique nuclear and nucleolar localization signals of lim-kinase 2 in endothelial cells. *J Biol Chem*: M603399200
- Hall A (2005) Rho GTPases and the control of cell behaviour. *Biochem Soc Trans* 33(Pt 5): 891-895
- Hamilton AJ, Baulcombe DC (1999) A Species of Small Antisense RNA in Posttranscriptional Gene Silencing in Plants. *Science* 286(5441): 950-952
- Hanahan D, Weinberg RA (2000) The Hallmarks of Cancer. *Cell* 100(1): 57-70
- Hanks SK, Quinn AM, Hunter T (1988) The protein kinase family: conserved features and deduced phylogeny of the catalytic domains. *Science* 241(4861): 42-52
- Haudenschild CC SS (1979) Endothelial regeneration. II. Restitution of endothelial continuity. *Lab Invest* 41(5): 407-418
- Hawkins M, Pope B, Maciver SK, Weeds AG (1993) Human actin depolymerizing factor mediates a pH-sensitive destruction of actin filaments. *Biochemistry* 32(38): 9985-9993
- Hay ED (2005) The mesenchymal cell, its role in the embryo, and the remarkable signaling mechanisms that create it. *Developmental Dynamics* 233(3): 706-720
- Hennigan RF HK, Ozanne BW (1994) Fos-transformation activates genes associated with invasion. *Oncogene* 9(12): 3591-3600
- Heredia L, Helguera P, de Olmos S, Kedikian G, Sola Vigo F, LaFerla F, Staufenbiel M, de Olmos J, Busciglio J, Caceres A, Lorenzo A (2006) Phosphorylation of actin-depolymerizing factor/cofilin by LIM-kinase mediates amyloid beta-induced degeneration: a potential mechanism of neuronal dystrophy in Alzheimer's disease. *J Neurosci* 26(24): 6533-6542
- Hiraoka J, Okano I, Higuchi O, Yang N, Mizuno K (1996) Self-association of LIM-kinase 1 mediated by the interaction between an N-terminal LIM domain and a C-terminal kinase domain. *FEBS Letters* 399(1-2): 117-121
- Hisaoka M, Tanaka A, Hashimoto H (2002) Molecular alterations of h-warts/LATS1 tumor suppressor in human soft tissue sarcoma. *Lab Invest* 82(10): 1427-1435
- Ho A, Schwarze SR, Mermelstein SJ, Waksman G, Dowdy SF (2001) Synthetic protein transduction domains: enhanced transduction potential in vitro and in vivo. *Cancer Res* 61(2): 474-477
- Hoogenraad CC, Akhmanova A, Galjart N, De Zeeuw CI (2004) LIMK1 and CLIP-115: linking cytoskeletal defects to Williams syndrome. *Bioessays* 26(2): 141-150

- Hoogenraad CC, Koekkoek B, Akhmanova A, Krugers H, Dortland B, Miedema M, van Alphen A, Kistler WM, Jaegle M, Koutsourakis M, Van Camp N, Verhoye M, van der Linden A, Kaverina I, Grosveld F, De Zeeuw CI, Galjart N (2002) Targeted mutation of *Cyln2* in the Williams syndrome critical region links CLIP-115 haploinsufficiency to neurodevelopmental abnormalities in mice. *Nat Genet* 32(1): 116-127
- Hotulainen P, Paunola E, Vartiainen MK, Lappalainen P (2005) Actin-depolymerizing Factor and Cofilin-1 Play Overlapping Roles in Promoting Rapid F-Actin Depolymerization in Mammalian Nonmuscle Cells. *Mol Biol Cell* 16(2): 649-664
- Hurd TW, Gao L, Roh MH, Macara IG, Margolis B (2003) Direct interaction of two polarity complexes implicated in epithelial tight junction assembly. *Nat Cell Biol* 5(2): 137-142
- Ikebe C, Ohashi K, Mizuno K (1998) Identification of Testis-Specific (*Limk2t*) and Brain-Specific (*Limk2c*) Isoforms of Mouse LIM-Kinase 2 Gene Transcripts. *Biochemical and Biophysical Research Communications* 246(2): 307-312
- Insall RH, Machesky LM (2009) Actin Dynamics at the Leading Edge: From Simple Machinery to Complex Networks. *Developmental Cell* 17(3): 310-322
- Itoh Y, Seiki M (2004) MT1-MMP: an enzyme with multidimensional regulation. *Trends in Biochemical Sciences* 29(6): 285-289
- Joseph B, Wallen-Mackenzie A, Benoit G, Murata T, Joodmardi E, Okret S, Perlmann T (2003) p57(Kip2) cooperates with Nurr1 in developing dopamine cells. *Proc Natl Acad Sci U S A* 100(26): 15619-15624
- Jun HJ, Woolfenden S, Coven S, Lane K, Bronson R, Housman D, Charest A (2009) Epigenetic Regulation of c-ROS Receptor Tyrosine Kinase Expression in Malignant Gliomas. *Cancer Res* 69(6): 2180-2184
- Kaji N, Ohashi K, Shuin M, Niwa R, Uemura T, Mizuno K (2003) Cell Cycle-associated Changes in Slingshot Phosphatase Activity and Roles in Cytokinesis in Animal Cells. *J Biol Chem* 278(35): 33450-33455
- Keller H, Egli P (1998) Protrusive activity, cytoplasmic compartmentalization, and restriction rings in locomoting blebbing Walker carcinosarcoma cells are related to detachment of cortical actin from the plasma membrane. *Cell Motil Cytoskeleton* 41(2): 181-193
- Kelly T, Yan Y, Osborne RL, Athota AB, Rozypal TL, Colclasure JC, Chu WS (1998) Proteolysis of extracellular matrix by invadopodia facilitates human breast cancer cell invasion and is mediated by matrix metalloproteinases. *Clin Exp Metastasis* 16(6): 501-512
- Kenny PA, Lee GY, Myers CA, Neve RM, Semeiks JR, Spellman PT, Lorenz K, Lee EH, Barcellos-Hoff MH, Petersen OW, Gray JW, Bissell MJ (2007) The morphologies of breast cancer cell lines in three-dimensional assays correlate with their profiles of gene expression. *Molecular Oncology* 1(1): 84-96

- Kim SO, Lee IJ, Kim M-K, Choe WK, Choi YH (2008) Genistein reduced invasive activity of human MCF-7 and MDA-MB 231 breast carcinoma cells through decreased tight junction permeability and regulation of related tight junction proteins. *FASEB J* 22(1\_MeetingAbstracts): 1062.1062-
- Klemke M, Wabnitz GH, Funke F, Funk B, Kirchgessner H, Samstag Y (2008) Oxidation of Cofilin Mediates T Cell Hyporesponsiveness under Oxidative Stress Conditions. *J Biol Chem* 283(3): 404-413
- Kobayashi M, Nishita M, Mishima T, Ohashi K, Mizuno K (2006) MAPKAPK-2-mediated LIM-kinase activation is critical for VEGF-induced actin remodeling and cell migration. *Embo J* 25(4): 713-726
- Koshimizu U, Takahashi H, Yoshida MC, Nakamura T (1997) cDNA cloning, genomic organization, and chromosomal localization of the mouse LIM motif-containing kinase gene, *Limk2*. *Biochem Biophys Res Commun* 241(2): 243-250
- Lee-Hoeflich ST, Causing CG, Podkowa M, Zhao X, Wrana JL, Attisano L (2004) Activation of LIMK1 by binding to the BMP receptor, BMPRII, regulates BMP-dependent dendritogenesis. *Embo J* 23(24): 4792-4801
- Lee J (2003) The role of protein elongation factor eEF1A2 in ovarian cancer. *Reproductive Biology and Endocrinology* 1(1): 69
- Lee S, Helfman DM (2004) Cytoplasmic p21Cip1 is involved in Ras-induced inhibition of the ROCK/LIMK/cofilin pathway. *J Biol Chem* 279(3): 1885-1891
- Lee YJ, Mazzatti DJ, Yun Z, Keng PC (2005) Inhibition of invasiveness of human lung cancer cell line H1299 by over-expression of cofilin. *Cell Biol Int* 29(11): 877-883
- Leyman S, Sidani M, Ritsma L, Waterschoot D, Eddy R, Dewitte D, Debeir O, Decaestecker C, Vandekerckhove J, van Rheenen J, Ampe C, Condeelis J, Van Troys M (2009) Unbalancing the PI(4,5)P2-Cofilin Interaction Impairs Cell Steering. *Mol Biol Cell*: E09-02-0121
- Li DY, Brooke B, Davis EC, Mecham RP, Sorensen LK, Boak BB, Eichwald E, Keating MT (1998a) Elastin is an essential determinant of arterial morphogenesis. *Nature* 393(6682): 276-280
- Li DY, Faury G, Taylor DG, Davis EC, Boyle WA, Mecham RP, Stenzel P, Boak B, Keating MT (1998b) Novel arterial pathology in mice and humans hemizygous for elastin. *J Clin Invest* 102(10): 1783-1787
- Li R, Soosairajah J, Harari D, Citri A, Price J, Ng HL, Morton CJ, Parker MW, Yarden Y, Bernard O (2006) Hsp90 increases LIM kinase activity by promoting its homo-dimerization. *FASEB J*: fj.05-5258fje
- Liang C-C, Park AY, Guan J-L (2007) In vitro scratch assay: a convenient and inexpensive method for analysis of cell migration in vitro. *Nat Protocols* 2(2): 329-333

Lindenmeyer F, Legrand Y, Menashi S (1997) Upregulation of MMP-9 expression in MDA-MB231 tumor cells by platelet granular membrane. *FEBS Letters* 418(1-2): 19-22

Liu J, Yue P, Artym VV, Mueller SC, Guo W (2009) The Role of the Exocyst in MMP Secretion and Actin Dynamics during Tumor Cell Invadopodia Formation. *Mol Biol Cell*: E08-09-0967

Lizarraga F, Poincloux R, Romao M, Montagnac G, Le Dez G, Bonne I, Rigall G, Raposo G, Chavrier P (2009) Diaphanous-Related Formins Are Required for Invadopodia Formation and Invasion of Breast Tumor Cells. *Cancer Res* 69(7): 2792-2800

Lorenz M, DesMarais V, Macaluso F, Singer RH, Condeelis J (2004) Measurement of barbed ends, actin polymerization, and motility in live carcinoma cells after growth factor stimulation. *Cell Motility and the Cytoskeleton* 57(4): 207-217

Machesky LM, Gould KL (1999) The Arp2/3 complex: a multifunctional actin organizer. *Curr Opin Cell Biol* 11(1): 117-121

Maekawa M, Ishizaki T, Boku S, Watanabe N, Fujita A, Iwamatsu A, Obinata T, Ohashi K, Mizuno K, Narumiya S (1999) Signaling from Rho to the actin cytoskeleton through protein kinases ROCK and LIM-kinase. *Science* 285(5429): 895-898.

Masschalck B, Michiels CW (2003) Antimicrobial properties of lysozyme in relation to foodborne vegetative bacteria. *Crit Rev Microbiol* 29(3): 191-214

Meng Y, Takahashi H, Meng J, Zhang Y, Lu G, Asrar S, Nakamura T, Jia Z (2004) Regulation of ADF/cofilin phosphorylation and synaptic function by LIM-kinase. *Neuropharmacology* 47(5): 746-754

Meng Y, Zhang Y, Tregoubov V, Janus C, Cruz L, Jackson M, Lu WY, MacDonald JF, Wang JY, Falls DL, Jia Z (2002) Abnormal spine morphology and enhanced LTP in LIMK-1 knockout mice. *Neuron* 35(1): 121-133

Meyer-Lindenberg A, Mervis CB, Faith Berman K (2006) Neural mechanisms in Williams syndrome: a unique window to genetic influences on cognition and behaviour. *Nat Rev Neurosci* 7(5): 380-393

Miralles F, Posern G, Zaromytidou A-I, Treisman R (2003) Actin Dynamics Control SRF Activity by Regulation of Its Coactivator MAL. *Cell* 113(3): 329-342

Misra UK, Deedwania R, Pizzo SV (2005) Binding of activated alpha2-macroglobulin to its cell surface receptor GRP78 in 1-LN prostate cancer cells regulates PAK-2-dependent activation of LIMK. *J Biol Chem* 280(28): 26278-26286

Mizuno K, Okano I, Ohashi K, Nunoue K, Kuma K, Miyata T, Nakamura T (1994) Identification of a human cDNA encoding a novel protein kinase with two repeats of the LIM/double zinc finger motif. *Oncogene* 9(6): 1605-1612

Mori T, Okano I, Mizuno K, Tohyama M, Wanaka A (1997) Comparison of tissue distribution of two novel serine/threonine kinase genes containing the LIM motif

(LIMK-1 and LIMK-2) in the developing rat. *Molecular Brain Research* 45(2): 247-254

Morinaga N, Shitara Y, Yanagita Y, Koida T, Kimura M, Asao T, Kimijima I, Takenoshita S, Hirota T, Saya H, Kuwano H (2000) Molecular analysis of the h-warts/LATS1 gene in human breast cancer. *Int J Oncol* 17(6): 1125-1129

Mouneimne G, DesMarais V, Sidani M, Scemes E, Wang W, Song X, Eddy R, Condeelis J (2006) Spatial and temporal control of cofilin activity is required for directional sensing during chemotaxis. *Curr Biol* 16(22): 2193-2205

Munoz-Najar UM, Neurath KM, Vumbaca F, Claffey KP (2005) Hypoxia stimulates breast carcinoma cell invasion through MT1-MMP and MMP-2 activation. *Oncogene* 25(16): 2379-2392

Nagata-Ohashi K, Ohta Y, Goto K, Chiba S, Mori R, Nishita M, Ohashi K, Kousaka K, Iwamatsu A, Niwa R, Uemura T, Mizuno K (2004) A pathway of neuregulin-induced activation of cofilin-phosphatase Slingshot and cofilin in lamellipodia. *J Cell Biol* 165(4): 465-471

Nagata K, Ohashi K, Yang N, Mizuno K (1999) The N-terminal LIM domain negatively regulates the kinase activity of LIM-kinase 1. *Biochem J* 343 Pt 1: 99-105

Nakano K, Kanai-Azuma M, Kanai Y, Moriyama K, Yazaki K, Hayashi Y, Kitamura N (2003) Cofilin phosphorylation and actin polymerization by NRK/NESK, a member of the germinal center kinase family. *Experimental Cell Research* 287(2): 219-227

Nebl G, Meuer SC, Samstag Y (1996) Dephosphorylation of serine 3 regulates nuclear translocation of cofilin. *J Biol Chem* 271(42): 26276-26280

Nishimura Y, Yoshioka K, Bernard O, Bereczky B, Itoh K (2006) A role of LIM kinase 1/cofilin pathway in regulating endocytic trafficking of EGF receptor in human breast cancer cells. *Histochem Cell Biol* 126(5): 627-638

Nishimura Y, Yoshioka K, Bernard O, Himeno M, Itoh K (2004) LIM kinase 1: evidence for a role in the regulation of intracellular vesicle trafficking of lysosomes and endosomes in human breast cancer cells. *Eur J Cell Biol* 83(7): 369-380

Nishiya N, Sabe H, Nose K, Shibamura M (1998) The LIM domains of hic-5 protein recognize specific DNA fragments in a zinc-dependent manner in vitro. *Nucleic Acids Res* 26(18): 4267-4273

Niwa R, Nagata-Ohashi K, Takeichi M, Mizuno K, Uemura T (2002) Control of actin reorganization by Slingshot, a family of phosphatases that dephosphorylate ADF/cofilin. *Cell* 108(2): 233-246

Nizamutdinova IT, Lee GW, Lee JS, Cho MK, Son KH, Jeon SJ, Kang SS, Kim YS, Lee JH, Seo HG, Chang KC, Kim HJ (2008) Tanshinone I suppresses growth and invasion of human breast cancer cells, MDA-MB-231, through regulation of adhesion molecules. *Carcinogenesis* 29(10): 1885-1892

Nobes CD, Hall A (1995) Rho, rac, and cdc42 GTPases regulate the assembly of multimolecular focal complexes associated with actin stress fibers, lamellipodia, and filopodia. *Cell* 81(1): 53-62

Nomoto S, Tatematsu Y, Takahashi T, Osada H (1999) Cloning and characterization of the alternative promoter regions of the human LIMK2 gene responsible for alternative transcripts with tissue-specific expression. *Gene* 236(2): 259-271

Nunoue K, Ohashi K, Okano I, Mizuno K (1995) LIMK-1 and LIMK-2, two members of a LIM motif-containing protein kinase family. *Oncogene* 11(4): 701-710

Ohashi K, Hosoya T, Takahashi K, Hing H, Mizuno K (2000a) A Drosophila Homolog of LIM-Kinase Phosphorylates Cofilin and Induces Actin Cytoskeletal Reorganization. *Biochemical and Biophysical Research Communications* 276(3): 1178-1185

Ohashi K, Nagata K, Maekawa M, Ishizaki T, Narumiya S, Mizuno K (2000b) Rho-associated kinase ROCK activates LIM-kinase 1 by phosphorylation at threonine 508 within the activation loop. *J Biol Chem* 275(5): 3577-3582.

Okamoto I, Pirker C, Bilban M, Berger W, Losert D, Marosi C, Haas OA, Wolff K, Pehamberger H (2005) Seven novel and stable translocations associated with oncogenic gene expression in malignant melanoma. *Neoplasia* 7(4): 303-311

Okano I, Hiraoka J, Otera H, Nunoue K, Ohashi K, Iwashita S, Hirai M, Mizuno K (1995) Identification and Characterization of a Novel Family of Serine/Threonine Kinases Containing Two N-terminal LIM Motifs. *J Biol Chem* 270(52): 31321-31330

Okumura Y, Sato H, Seiki M, Kido H (1997) Proteolytic activation of the precursor of membrane type 1 matrix metalloproteinase by human plasmin: A possible cell surface activator. *FEBS Letters* 402(2-3): 181-184

Olson MF, Sahai E (2008) The actin cytoskeleton in cancer cell motility. *Clin Exp Metastasis*

Oser M, Yamaguchi H, Mader CC, Bravo-Cordero JJ, Arias M, Chen X, DesMarais V, van Rheenen J, Koleske AJ, Condeelis J (2009) Cortactin regulates cofilin and N-WASp activities to control the stages of invadopodium assembly and maturation. *J Cell Biol* 186(4): 571-587

Palamidessi A, Frittoli E, Garré M, Faretta M, Mione M, Testa I, Diaspro A, Lanzetti L, Scita G, Di Fiore PP (2008) Endocytic Trafficking of Rac Is Required for the Spatial Restriction of Signaling in Cell Migration. *Cell* 134(1): 135-147

Pankova K, Rosel D, Novotny M, Brabek J (2009) The molecular mechanisms of transition between mesenchymal and amoeboid invasiveness in tumor cells. *Cell Mol Life Sci*

Poincloux R, Lizarraga F, Chavrier P (2009) Matrix invasion by tumour cells: a focus on MT1-MMP trafficking to invadopodia. *J Cell Sci* 122(17): 3015-3024

Pope BJ, Zierler-Gould KM, Kuhne R, Weeds AG, Ball LJ (2004) Solution structure of human cofilin: actin binding, pH sensitivity, and relationship to actin-depolymerizing factor. *J Biol Chem* 279(6): 4840-4848

Proschel C, Blouin MJ, Gutowski NJ, Ludwig R, Noble M (1995) Limk1 is predominantly expressed in neural tissues and phosphorylates serine, threonine and tyrosine residues in vitro. *Oncogene* 11(7): 1271-1281

Roovers K, Klein EA, Castagnino P, Assoian RK (2003) Nuclear Translocation of LIM Kinase Mediates Rho-Rho Kinase Regulation of Cyclin D1 Expression. *Dev Cell* 5(2): 273-284

Ross-Macdonald P, de Silva H, Guo Q, Xiao H, Hung CY, Penhallow B, Markwalder J, He L, Attar RM, Lin TA, Seitz S, Tilford C, Wardwell-Swanson J, Jackson D (2008) Identification of a nonkinase target mediating cytotoxicity of novel kinase inhibitors. *Mol Cancer Ther* 7(11): 3490-3498

Rosso S, Bollati F, Bisbal M, Peretti D, Sumi T, Nakamura T, Quiroga S, Ferreira A, Caceres A (2004) LIMK1 Regulates Golgi Dynamics, Traffic of Golgi-derived Vesicles, and Process Extension in Primary Cultured Neurons  
10.1091/mbc.E03-05-0328. *Mol Biol Cell* 15(7): 3433-3449

Sabeh F, Ota I, Holmbeck K, Birkedal-Hansen H, Soloway P, Balbin M, Lopez-Otin C, Shapiro S, Inada M, Krane S, Allen E, Chung D, Weiss SJ (2004) Tumor cell traffic through the extracellular matrix is controlled by the membrane-anchored collagenase MT1-MMP. *J Cell Biol* 167(4): 769-781

Sacchetti P, Carpentier R, Segard P, Olive-Cren C, Lefebvre P (2006) Multiple signaling pathways regulate the transcriptional activity of the orphan nuclear receptor NURR1. *Nucleic Acids Res*

Sahai E, Marshall CJ (2003) Differing modes of tumour cell invasion have distinct requirements for Rho/ROCK signalling and extracellular proteolysis. *Nat Cell Biol* 5(8): 711-719

Sahai E, Olson MF, William E, Balch CJD, Alan H (2006) Purification of TAT[hyphen (true graphic)]C3 Exoenzyme. In *Methods in Enzymology* Vol. Volume 406, pp 128-140. Academic Press

Sanka K, Maddala R, Epstein DL, Rao PV (2007) Influence of Actin Cytoskeletal Integrity on Matrix Metalloproteinase-2 Activation in Cultured Human Trabecular Meshwork Cells. *Invest Ophthalmol Vis Sci* 48(5): 2105-2114

Sanne MK, Jane F, Brian FCC, Henrik L (1993) Tissue-dependent variation in the expression of elongation factor-1 $\beta$ ; isoforms: Isolation and characterisation of a cDNA encoding a novel variant of human elongation-factor 1 $\beta$ . *European Journal of Biochemistry* 215(3): 549-554

Schnaeker E-M, Ossig R, Ludwig T, Dreier R, Oberleithner H, Wilhelmi M, Schneider SW (2004) Microtubule-Dependent Matrix Metalloproteinase-2/Matrix Metalloproteinase-9 Exocytosis: Prerequisite in Human Melanoma Cell Invasion. *Cancer Res* 64(24): 8924-8931

Schratt GM, Tuebing F, Nigh EA, Kane CG, Sabatini ME, Kiebler M, Greenberg ME (2006) A brain-specific microRNA regulates dendritic spine development. *Nature* 439(7074): 283-289

Scott RW, Olson MF (2007) LIM kinases: function, regulation and association with human disease. *J Mol Med* 85(6): 555-568

Sebbagh M, Renvoize C, Hamelin J, Riche N, Bertoglio J, Breard J (2001) Caspase-3-mediated cleavage of ROCK I induces MLC phosphorylation and apoptotic membrane blebbing. *Nat Cell Biol* 3(4): 346-352.

Sidani M, Wessels D, Mouneimne G, Ghosh M, Goswami S, Sarmiento C, Wang W, Kuhl S, El-Sibai M, Backer JM, Eddy R, Soll D, Condeelis J (2007) Cofilin determines the migration behavior and turning frequency of metastatic cancer cells. *J Cell Biol* 179(4): 777-791

Soosairajah J, Maiti S, Wiggan O, Sarmiere P, Moussi N, Sarcevic B, Sampath R, Bamburg JR, Bernard O (2005) Interplay between components of a novel LIM kinase-slingshot phosphatase complex regulates cofilin. *Embo J* 24(3): 473-486

Sotiropoulos A, Gineitis D, Copeland J, Treisman R (1999) Signal-regulated activation of serum response factor is mediated by changes in actin dynamics. *Cell* 98(2): 159-169.

Spence HJ, McGarry L, Chew CS, Carragher NO, Scott-Carragher LA, Yuan Z, Croft DR, Olson MF, Frame M, Ozanne BW (2006) AP-1 Differentially Expressed Proteins Krp1 and Fibronectin Cooperatively Enhance Rho-ROCK-Independent Mesenchymal Invasion by Altering the Function, Localization, and Activity of Nondifferentially Expressed Proteins. *Mol Cell Biol* 26(4): 1480-1495

Spudich JA, Watt S (1971) The Regulation of Rabbit Skeletal Muscle Contraction. I. BIOCHEMICAL STUDIES OF THE INTERACTION OF THE TROPOMYOSIN-TROPONIN COMPLEX WITH ACTIN AND THE PROTEOLYTIC FRAGMENTS OF MYOSIN. *J Biol Chem* 246(15): 4866-4871

St John MA, Tao W, Fei X, Fukumoto R, Carcangiu ML, Brownstein DG, Parlow AF, McGrath J, Xu T (1999) Mice deficient of Lats1 develop soft-tissue sarcomas, ovarian tumours and pituitary dysfunction. *Nat Genet* 21(2): 182-186

Stylli SS, Kaye AH, Lock P (2008) Invadopodia: At the cutting edge of tumour invasion. *Journal of Clinical Neuroscience* 15(7): 725-737

Sumi T, Hashigasako A, Matsumoto K, Nakamura T (2006) Different activity regulation and subcellular localization of LIMK1 and LIMK2 during cell cycle transition. *Exp Cell Res* 312(7): 1021-1030

Sumi T, Matsumoto K, Nakamura T (2001a) Specific activation of LIM kinase 2 via phosphorylation of threonine 505 by ROCK, a Rho-dependent protein kinase. *J Biol Chem* 276(1): 670-676.

Sumi T, Matsumoto K, Nakamura T (2002) Mitosis-dependent phosphorylation and activation of LIM-kinase 1. *Biochem Biophys Res Commun* 290(4): 1315-1320

Sumi T, Matsumoto K, Shibuya A, Nakamura T (2001b) Activation of LIM Kinases by Myotonic Dystrophy Kinase-related Cdc42-binding Kinase alpha. *J Biol Chem* 276(25): 23092-23096

Sumi T, Matsumoto K, Takai Y, Nakamura T (1999) Cofilin phosphorylation and actin cytoskeletal dynamics regulated by rho- and Cdc42-activated LIM-kinase 2. *J Cell Biol* 147(7): 1519-1532

Suyama E, Wadhwa R, Kawasaki H, Yaguchi T, Kaul SC, Nakajima M, Taira K (2004) LIM kinase-2 targeting as a possible anti-metastasis therapy. *J Gene Med* 6(3): 357-363

Takahashi H, Koshimizu U, Miyazaki J, Nakamura T (2002) Impaired spermatogenic ability of testicular germ cells in mice deficient in the LIM-kinase 2 gene. *Dev Biol* 241(2): 259-272

Takahashi T, Aoki S, Nakamura T, Koshimizu U, Matsumoto K, Nakamura T (1997) Xenopus LIM motif-containing protein kinase, Xlimk1, is expressed in the developing head structure of the embryo. *Dev Dyn* 209(2): 196-205

Takahashi T, Koshimizu U, Abe H, Obinata T, Nakamura T (2001) Functional involvement of Xenopus LIM kinases in progression of oocyte maturation. *Dev Biol* 229(2): 554-567

Tanaka H, Yamashita T, Asada M, Mizutani S, Yoshikawa H, Tohyama M (2002) Cytoplasmic p21(Cip1/WAF1) regulates neurite remodeling by inhibiting Rho-kinase activity. *J Cell Biol* 158(2): 321-329

Tatsuka M MH, Wada M, Nagata A, Nojima H, Okayama H. (1992 ) Elongation factor-1 alpha gene determines susceptibility to transformation. *Nature* 359(6393): 333-336

Tomasek JJ, Halliday NL, Updike DL, Ahern-Moore JS, Vu T-KH, Liu RW, Howard EW (1997) Gelatinase A Activation Is Regulated by the Organization of the Polymerized Actin Cytoskeleton. *Journal of Biological Chemistry* 272(11): 7482-7487

Tomiyoshi G, Horita Y, Nishita M, Ohashi K, Mizuno K (2004) Caspase-mediated cleavage and activation of LIM-kinase 1 and its role in apoptotic membrane blebbing. *Genes to Cells* 9(6): 591-600

Toshima J, Toshima JY, Amano T, Yang N, Narumiya S, Mizuno K (2001a) Cofilin Phosphorylation by Protein Kinase Testicular Protein Kinase 1 and Its Role in Integrin-mediated Actin Reorganization and Focal Adhesion Formation. *Mol Biol Cell* 12(4): 1131-1145

Toshima J, Toshima JY, Takeuchi K, Mori R, Mizuno K (2001b) Cofilin Phosphorylation and Actin Reorganization Activities of Testicular Protein Kinase 2 and Its Predominant Expression in Testicular Sertoli Cells. *J Biol Chem* 276(33): 31449-31458

- Turk BE, Huttu JE, Cantley LC (2006) Determining protein kinase substrate specificity by parallel solution-phase assay of large numbers of peptide substrates. *Nat Protocols* 1(1): 375-379
- Tursun B, Schluter A, Peters MA, Viehweger B, Ostendorff HP, Soosairajah J, Drung A, Bossenz M, Johnsen SA, Schweizer M, Bernard O, Bach I (2005) The ubiquitin ligase Rnf6 regulates local LIM kinase 1 levels in axonal growth cones 10.1101/gad.1340605. *Genes Dev* 19(19): 2307-2319
- van Rheenen J, Song X, van Roosmalen W, Cammer M, Chen X, DesMarais V, Yip S-C, Backer JM, Eddy RJ, Condeelis JS (2007) EGF-induced PIP2 hydrolysis releases and activates cofilin locally in carcinoma cells. *J Cell Biol* 179(6): 1247-1259
- Van Troys M, Huyck L, Leyman S, Dhaese S, Vandekerkhove J, Ampe C (2008) Ins and outs of ADF/cofilin activity and regulation. *Eur J Cell Biol* 87(8-9): 649-667
- Vartiainen MK, Mustonen T, Mattila PK, Ojala PJ, Thesleff I, Partanen J, Lappalainen P (2002) The three mouse actin-depolymerizing factor/cofilins evolved to fulfill cell-type-specific requirements for actin dynamics. *Mol Biol Cell* 13(1): 183-194
- Vignjevic D, Montagnac G (2008) Reorganisation of the dendritic actin network during cancer cell migration and invasion. *Seminars in Cancer Biology* 18(1): 12-22
- Wang W, Goswami S, Lapidus K, Wells AL, Wyckoff JB, Sahai E, Singer RH, Segall JE, Condeelis JS (2004) Identification and testing of a gene expression signature of invasive carcinoma cells within primary mammary tumors. *Cancer Res* 64(23): 8585-8594
- Wang W, Mouneimne G, Sidani M, Wyckoff J, Chen X, Makris A, Goswami S, Bresnick AR, Condeelis JS (2006) The activity status of cofilin is directly related to invasion, intravasation, and metastasis of mammary tumors. *J Cell Biol* 173(3): 395-404
- Wolf K, Mazo I, Leung H, Engelke K, von Andrian UH, Deryugina EI, Strongin AY, Bocker EB, Friedl P (2003) Compensation mechanism in tumor cell migration: mesenchymal-amoeboid transition after blocking of pericellular proteolysis. *J Cell Biol* 160(2): 267-277
- Wolf K, Wu YI, Liu Y, Geiger J, Tam E, Overall C, Stack MS, Friedl P (2007) Multi-step pericellular proteolysis controls the transition from individual to collective cancer cell invasion. *Nat Cell Biol* 9(8): 893-904
- Wu H, Zheng Y, Wang ZX (2003) Evaluation of the catalytic mechanism of the p21-activated protein kinase PAK2. *Biochemistry* 42(4): 1129-1139
- Wyckoff JB, Pinner SE, Gschmeissner S, Condeelis JS, Sahai E (2006) ROCK- and myosin-dependent matrix deformation enables protease-independent tumor-cell invasion in vivo. *Curr Biol* 16(15): 1515-1523

- Yang EJ, Yoon JH, Min do S, Chung KC (2004a) LIM kinase 1 activates cAMP-responsive element-binding protein during the neuronal differentiation of immortalized hippocampal progenitor cells. *J Biol Chem* 279(10): 8903-8910
- Yang N, Higuchi O, Mizuno K (1998a) Cytoplasmic localization of LIM-kinase 1 is directed by a short sequence within the PDZ domain. *Exp Cell Res* 241(1): 242-252
- Yang N, Higuchi O, Ohashi K, Nagata K, Wada A, Kangawa K, Nishida E, Mizuno K (1998b) Cofilin phosphorylation by LIM-kinase 1 and its role in Rac-mediated actin reorganization. *Nature* 393(6687): 809-812.
- Yang N, Mizuno K (1999) Nuclear export of LIM-kinase 1, mediated by two leucine-rich nuclear-export signals within the PDZ domain. *Biochem J* 338 ( Pt 3): 793-798
- Yang X, Yu K, Hao Y, Li DM, Stewart R, Insogna KL, Xu T (2004b) LATS1 tumour suppressor affects cytokinesis by inhibiting LIMK1. *Nat Cell Biol* 6(7): 609-617
- Yap CT, Simpson TI, Pratt T, Price DJ, Maciver SK (2005) The motility of glioblastoma tumour cells is modulated by intracellular cofilin expression in a concentration-dependent manner. *Cell Motil Cytoskeleton* 60(3): 153-165
- Yilmaz M, Christofori G (2009) EMT, the cytoskeleton, and cancer cell invasion. *Cancer Metastasis Rev* 28(1-2): 15-33
- Yokoo T, Toyoshima H, Miura M, Wang Y, Iida KT, Suzuki H, Sone H, Shimano H, Gotoda T, Nishimori S, Tanaka K, Yamada N (2003) p57Kip2 regulates actin dynamics by binding and translocating LIM-kinase 1 to the nucleus. *J Biol Chem* 278(52): 52919-52923
- Yoshioka K, Foletta V, Bernard O, Itoh K (2003) A role for LIM kinase in cancer invasion. *Proceedings of the National Academy of Sciences of the United States of America* 100(12): 7247-7252
- Zebda N, Bernard O, Bailly M, Welte S, Lawrence DS, Condeelis JS (2000) Phosphorylation of ADF/Cofilin Abolishes EGF-induced Actin Nucleation at the Leading Edge and Subsequent Lamellipod Extension. *J Cell Biol* 151(5): 1119-1128